WASM: Minerals, Energy and Chemical Engineering

Integration of Instrumentation and Computer Modelling to Understand and therefore Better Design and Represent the Rock bolt Support Behaviour

Prasoon Singh

0000-0001-5765-584X

This thesis is presented for the Degree of
Doctor of Philosophy
of
Curtin University

January 2022

Declaration

To the best of my knowledge and belief this thesis contains no material previously published by any other person except where due acknowledgment has been made.

This thesis contains no material which has been accepted for the award of any other degree or diploma in any university.

Signed:

Date: January 2022

Abstract

Fully grouted rock bolts are the most common type of primary roof reinforcement used in underground mines as they are efficient and relatively easy to install. Proper design of rock bolt reinforcement in underground mines is critical to avoid incidents, accidents and loss of production. In an underground mine the rock bolt is subjected to a combination of axial and shear loads. Traditionally, analytical and empirical models have been used in rock bolt support design. The currently available methods used in support design have rockbolt models which are oversimplified and therefore can be inaccurate. The rockbolt's response is limited to only axial loading disregarding the effect of shear loading. Therefore, there is a need to improve the understanding of the rock bolt response under shear loading and its effect on rock bolt reinforcement. In a fully grouted rock bolt, the load generated by differential rock movement in the surrounding rock mass is transferred to the rock bolt through a column of grout surrounding it. Therefore, to understand the rock bolt's response to different loading conditions, understanding the mechanical characteristics of all three materials and their interfaces is required.

Numerical modelling has become an important tool in the underground rock bolt reinforcement design process. Numerical modelling provides the advantage of easy and quick simulation of complex underground geometries and mechanisms. Rock bolts in geotechnical modelling software are represented by simplified structural elements. These models cannot accurately capture the rock bolt's response under lateral loading. The model also needs to be calibrated with in-situ measurements before they can be used for reinforcement design. In this work laboratory and numerical modelling of rock bolt shear tests have been used to analyse and understand the rock bolt behaviour under lateral loading. In-situ monitoring of the rock bolt has been conducted to validate the proposed models and procedures. All tests have been conducted using latest instrumentation technology to record the strain profile of the rock bolt.

In the first phase of the work physical and numerical modelling of an excavation with laminated roof was conducted to analyse the effect of combined axial and shear loading on roof reinforcement. Modelling of suspension and beam building methods of reinforcement was done and reduction in the safety factor due to combined loading was determined. In the second phase laboratory double shear tests and calibrated numerical models were used to study the loading regime of a rock bolt under lateral loading. The shortcomings of the current analytical model and pile structural element in FLAC3D were analysed by comparing the estimated loads with calibrated numerical model's results. The findings were then used to suggest a procedure for modifying the pile element to accurately model the rock bolt behaviour under combined loading.

In the third phase of the work an improved analytical model for lateral loading of rock bolt was proposed. In the new model rock bolts post-yield strain hardening behaviour was incorporated. The predictions of the improved analytical model were then compared with existing analytical model and laboratory results to demonstrate the importance of considering strain-hardening effect. In the fourth phase in-situ testing was conducted in a hard rock mine using instrumented rock bolts. The rock bolt strain data from the in-situ tests was then analysed with the new analytical model to identify the shear loading zones and measure the discontinuity orientations. A procedure to calculate the load-deformation relationship of the rock bolt from the in-situ strain data was also presented. The discontinuity and rock-bolt load-deformation data was then used to calibrate an in-situ rock bolt model. A flowchart was created to incorporate the above findings in the process of rock bolt reinforcement design using instrumented rock bolts and numerical modelling.

Acknowledgements

Firstly, I would like to thank my supervisors Dr. A.J.S. (Sam) Spearing, Dr. Hyong Doo Jang and Dr. Erkan Topal for their guidance and support throughout this PhD. I would also like to thank Karsten Hoehn (Mining3) for providing key support in conducting this research.

Finally, I would like to thank my family and friends for their continuous encouragement and support.

Funding for this dissertation was provided by the Minerals Research Institute of Western Australia (MRIWA); Mining3 (CSIRO); Peabody Energy and Curtin University.

Copyright statement

I have obtained permission from the copyright owners to use any third-party copyright material reproduced in the thesis (e.g. questionnaires, artwork, unpublished letters), or to use any of my own published work (e.g. journal articles) in which the copyright is held by another party (e.g. publisher, co-author).

Author's peer reviewed papers

Papers published or accepted for publication:

Singh, P., Spearing, A. S., Jessu, K. V., & da Silva Ribeiro, P. C. P. (2020). Establishing the need to model the actual state of stress along rock bolts. International Journal of Mining Science and Technology, 30(3), 279-286.

Singh, P., Spearing, A. J. S., & Jessu, K. (2020). Analysis of the combined load behaviour of rock bolt installed across discontinuity and its modelling using FLAC3D. Geotechnical and Geological Engineering, 38, 5867-5883.

Singh, P., & Spearing, A. J. S. (2021). An Improved Analytical Model for the Elastic and Plastic Strain-hardening Shear Behaviour of Fully Grouted Rockbolts. Rock Mechanics and Rock Engineering, 1-17.

Singh, P., Jang, H., & Spearing, A. J. S. (2022). Improving the Numerical Modelling of In-Situ Rock Bolts Using Axial and Bending Strain Data from Instrumented Bolts. Geotechnical and Geological Engineering, 1-25.

Table of Contents

Abstract……ii
Acknowledgements iv
Copyright statement v
Author's peer reviewed papers vi
List of Figures..... xi
List of Tables…….xvi
Chapter 1. Introduction.....1
1.1 Introduction..... 2
1.2 Problem Summary 5
1.3 Thesis Objectives..... 6
1.4 Outline of the thesis 6
Chapter 2. Rock bolt reinforcement mechanisms and design methods 12
2.1 Introduction..... 13
2.2 Rock bolt reinforcement methods..... 14
2.3 Numerical Methods..... 17
2.3.1 Explicit model of rock bolt 17
2.3.2 Implicit model of rock bolt 18
2.4 Instrumented rock bolts..... 21
2.5 Rock bolt loading mechanisms 24
2.6 Axial load transfer mechanism 25
2.6.1 Pull-out test..... 26
2.6.2 Analytical models 29
2.7 Shear load transfer mechanism 31
2.7.1 Single/Double shear tests..... 33
2.7.2 Analytical models 34
2.8 Discussion..... 37
Chapter 3. Establishing the Need to Model the Actual State of Stress along Rock Bolts……49
3.1 Introduction..... 50
3.1.1 Suspension 51
3.1.2 Beam building..... 53
3.2 Shear Displacement in Bedded roof..... 58
3.2.1 Physical modelling of shear displacement in bedded roof..... 58
3.2.2 Results of Physical Modelling 59
3.2.3 Numerical modelling of shear displacement in bedded roof..... 62

3.2.4 Results of numerical modelling of shear displacement in bedded roof 62
3.2.5 Analytical analysis of shear stress in beams 64
3.3 Effect of combined loading on rock bolt support design 66
3.3.1 Suspension 67
3.3.2 Beam building 71
3.4 Conclusion 75
Chapter 4. Analysis of the Combined Load Behaviour of Rock Bolt Installed across Discontinuity and its Modelling using FLAC3D 80
4.1 Introduction 82
4.2 Background 82
4.2.1 Experimental Studies 82
4.2.2 Analytical models 83
4.2.3 Numerical modelling 86
4.3 Experimental study – Double shear test 88
4.3.1 Experimental Setup 88
4.4 Numerical Modelling – Double Shear Test 89
4.4.1 ANSYS Model 89
4.4.2 ANSYS Model calibration results 92
4.4.3 Effect of concrete strength on stress profile in the rock bolt 94
4.5 Comparison of Numerical model with Analytical Model 95
4.5.1 Bending strain and Rock reaction 95
4.5.2 Modified analytical model 98
4.6 Numerical modelling of double shear test using FLAC3D 101
4.6.1 Model calibration 103
4.6.2 Modelling combined load yielding/failure of pile element 106
4.7 Results of modified pile element model 109
4.7.1 Verification of the model and comparison of shear response pile with un-modified pile 109
4.8 Conclusions 111
Chapter 5. An Improved Analytical Model for the Elastic and Plastic Strain-hardening Shear Behaviour of Fully Grouted Rockbolts 117
5.1 Introduction 121
5.2 Background 122
5.2.1 Rock bolts under shear load 122
5.2.2 Analytical Models 123
5.2.3 Rock bolt mechanics under shear 123
5.2.4 Current Analytical Models 125
5.3 Analytical Formulation 126

5.3.1 Elastic Deformation 127
5.3.2 Plastic Deformation 130
5.4 Bolt Yield and Failure Limit 133
5.4.1 Yield Limit 133
5.4.2 Failure Limit 134
5.5 Evaluation of the Analytical Model 135
5.5.1 Comparison with experimental data 135
5.5.2 Single shear test 135
5.5.3 Double-shear test 137
5.6 Discussion 139
5.6.1 Bending modulus after yield 139
5.6.2 Effect of strain-hardening on rock bolt shear behaviour 142
5.6.3 Variation in strain-hardening effect due to host media strength 143
5.7 Conclusions 144
Chapter 6. Improving the Numerical Modelling of In-situ Rock Bolts Using Axial and Bending Strain Data from Instrumented Bolts 153
6.1 Introduction 154
6.2 Background 156
6.2.1 Instrumented bolts 156
6.2.2 Numerical modelling 158
6.3 Discontinuity-bolt angle 160
6.3.1 Calculating the discontinuity-bolt angle. 161
6.3.2 Validation of discontinuity-bolt angle calculation 164
6.3.3 Double shear test 164
6.3.4 Angled shear test 167
6.3.5 Numerical modelling 170
6.3.6 Validation with laboratory and numerical modelling results 172
6.4 Calibration of pile element parameters 174
6.4.1 Load vs Displacement plot 175
6.4.2 Validation with laboratory double shear test 175
6.5 In-situ modelling 177
6.5.1 In-situ instrumented rock bolt study 177
6.5.2 Calibration of the numerical model with in-situ data 181
6.6 Conclusions 192
Chapter 7. Discussion and Conclusion 210
7.1 Discussion 211
7.2 Conclusions 221
7.3 Limitations and Future Work 226

Appendix A…….228
Appendix B……..……232

List of Figures

Figure 2.1 - Stress redistribution due to excavation in rock. 13

Figure 2.2 - Rock bolt loading modes. 15

Figure 2.3 - Explicit modelling of rock bolt. 18

Figure 2.4 - Pile element. 19

Figure 2.5 - Short resistive strain gauge instrumented rock bolt. 22

Figure 2.6 - Long base length inductive sensor instrumented rock bolts. 22

Figure 2.7 - Optical instrumented rock bolt. 24

Figure 2.8 - Fully-grouted rock bolt 25

Figure 2.9 - Load profile of fully grouted rock bolt. (Modified after Freeman (1978)) 26

Figure 2.10 - Pull out test setup. 27

Figure 2.11 - Rock bolt resisting shear displacement at the discontinuity. 32

Figure 2.12 – Rock bolt shear test setup. 33

Figure 2.13 - Rock bolt mechanics under lateral loading. (Modified after Pellet and Egger (1996)) 35

Figure 3.1 – a) Suspension support method b) Beam Building support method (modified from Luo (1994)) 52

Figure 3.2– Dowel action of rock bolt. 55

Figure 3.3 - Axial load on rock bolt due to axial stress in the rock and joint opening. 56

Figure 3.4 - a) Physical model setup (12mm beds). b) Model undergoing increasing vertical displacement (10mm to 60mm). 59

Figure 3.5 - a) Plot lines position in model b) Shear Displacement (12 mm above roof) vs vertical displacement of roof. 60

Figure 3.6 – a) Location of Plot lines in the model. Comparison of shear displacement in beds with different thickness at b) 100 mm line at 2 cm roof vertical displacement c) 200 mm line at 2 cm roof vertical displacement d) 100 mm line at 3 cm roof vertical displacement e) 200 mm line at 3 cm roof vertical displacement. 61

Figure 3.7 – Numerical model of bedded roof. 62
Figure 3.8 – Shear displacement in roof at 30mm vertical displacement with a) 12 mm bed thickness b) 19 mm bed thickness c) 30 mm bed thickness. 64
Figure 3.9 – a) Individual beams of thickness ‘d’ b) Composite beam of effective thickness ‘2d’. 64
Figure 3.10 – Shear stress in a vertical cross-section of beam (Stimpson, 1987). 65
Figure 3.11 – Uniformly loaded clamped beam. 66
Figure 3.12 – Two-dimensional model of suspension roof a) without joint b) with joint. 68
Figure 3.13 – Axial stress in bolt with and without joints. 70
Figure 3.14 – Shear displacement at rockbolt-joint intersection. 70
Figure 3.15 – Effect of shear load on axial capacity of rock bolt (Pellet and Egger (1996) [8]). 71
Figure 3.16 – Two-dimensional model of beam building roof. 73
Figure 3.17 – Axial Stress along the corner bolt in beam building. 74
Figure 3.18 – Shear displacement along the corner bolt at bolt-joint intersections in beam building. 74
Figure 4.1 – Rock bolt under shear load (modified from Pellet and Egger, (1996)). 84
Figure 4.2 – Double shear test setup (modified from Kostecki, 2019). 89
Figure 4.3 - FEM model of the double shear test. 91
Figure 4.4 - Strain measured along the lines A-1 and B-1 on the rock bolt. 91
Figure 4.5 - Bending strain in bolt at 1.25 tonnes load. 93
Figure 4.6 - Bending strain in bolt at 5.00 tonnes load. 93
Figure 4.7 – Double shear joint response laboratory results vs Ansys model. 94
Figure 4.8 - Shear stress in the rock bolt for different concrete strengths. 95
Figure 4.9 - Maximum moment in the rock bolt for different concrete strengths. 95
Figure 4.10 - Comparison of the numerical model with the analytical model. 98
Figure 4.11 - Shear force in rock bolt analytical vs. numerical model. 98
Figure 4.12 – Comparison of hinge point location at different concrete strengths. 100

Figure 4.13 - Comparison of shear force in rock bolt between analytical and numerical model. 101
Figure 4.14 – Double shear model in FLAC3D. 102
Figure 4.15 – Bending strain calibration plot. 105
Figure 4.16 - Double shear joint response laboratory results vs FLAC3D model. 106
Figure 4.17 - Piece-wise linear estimation of shear stress-strain graph for steel. 107
Figure 4.18 - Model geometry. 109
Figure 4.19 - Comparison of shear response of modified pile with laboratory test data. 111
Figure 5.1- Rock bolt undergoing shear deformation (Haas, 1976). 123
Figure 5.2- Forces on a rock bolt under shear (Pellet and Egger, 1996). 124
Figure 5.3- Rock bolt mechanical system (Pellet and Egger, 1996). 127
Figure 5.4- Displacement compatibility condition at point O for a deformed bolt (Li et al. ,2015). 130
Figure 5.5 - Bolt geometry after plastic deformation. 133
Figure 5.6- Single shear setup (modified from McHugh and Signer, 1999). 136
Figure 5.7 - Analytical model validation with single shear lab test data. 137
Figure 5.8 - Double shear test setup (Jalalifar, 2006). 138
Figure 5.9 - Analytical model validation with double shear lab test data. 138
Figure 5.10 - Bending modulus vs bending moment. 140
Figure 5.11 - Bending modulus curve for different diameter bolts. 141
Figure 5.12 - Effect of E_P on bending modulus curve. 142
Figure 5.13 – McHugh and Signer lab test analytical model strain hardening effect. 143
Figure 5.14 - Jalalifar lab test analytical model strain hardening effect. 143
Figure 5.15 - Variation in strain hardening effect due to host media strength. 144
Figure 5.16 - Tension-compression test diagram for steel. 149
Fig. 6.1 - Comparison of the three types of instrumentation technology 158
Fig. 6.2 Pile structural element (modified from Tulu, Esterhuizen, and Heasley (2012)) ... 160
Fig. 6.3 Rock bolt mechanical system (Singh et al., 2020) 162

Fig. 6.4 Double shear test schematic..... 165
Fig. 6.5 Double shear test – a) Experiment setup b) Instrumented bolt..... 166
Fig. 6.6 Strain profile 90^0 a) Bending strain b) Axial Strain..... 169
Fig. 6.7 Strain profile 80^0 a) Bending strain b) Axial Strain..... 170
Fig. 6.8 Angled double shear model 171
Fig. 6.9 Calibration of angled double shear test a) Bending strain b) Axial Strain 172
Fig. 6.10 Validation of bolt angle calculation..... 174
Fig. 6.11 Strain plots 80^0 angled bolt a) Bending strain b) Axial strain 176
Fig. 6.12 Load - Displacement: Actual vs Calculated 177
Fig. 6.13 Rock bolt installation location..... 178
Fig. 6.14 Instrumented rock bolt installation a) position and direction of inclination b) orientation with roof 178
Fig 6.15 Excavation stages with significant strain increases in instrumented rock bolts 179
Fig. 6.16 Strain profile bolt 7 a) Bending strain b) Axial strain 180
Fig 6.17 Strain profile bolt 10 a) Bending strain b) Axial strain 181
Fig. 6.18 FLAC3D in-situ model..... 182
Fig. 6.19 Model showing the instrumented rock bolts and the structure 185
Fig. 6.20 Calibrated bolt 7 model vs in-situ a) Bending strain b) Axial strain 189
Fig. 6.21 Calibrated bolt 10 model vs in-situ a) Bending strain b) Axial strain 192
Figure 7.1 - Effect of discontinuity on rock bolt loading..... 212
Figure 7.2 - a) Plot lines position in model b) Shear Displacement (12 mm above roof) vs vertical displacement of roof..... 213
Figure 7.3 - a) Location of Plot lines in the model. Comparison of shear displacement in beds with different thicknesses at b) 100 mm line at 2 cm roof vertical displacement c) 200 mm line at 2 cm roof vertical displacement d) 100 mm line at 3 cm roof vertical displacement. 213
Figure 7.4 – a) Shear stress in the rock bolt for different concrete strengths. b) Bending moment in the rock bolt for different concrete strengths. 215

Figure 7.5 -Change in hinge point location at different concrete strengths. 216

Figure 7.6 - Shear force in rock bolt analytical vs. numerical model. 217

Figure 7.7 - Comparison of shear response of modified pile with laboratory test data. 217

Figure 7.8 - Shear lab test vs analytical model with strain hardening. 219

Figure 7.9 - Calculated discontinuity orientation w.r.t rock bolt compared to actual orientation. 220

Figure 7.10 - Shear Load vs Displacement plot: Actual vs Calculated..... 221

Figure 7.11 - Rock bolt reinforcement modelling procedure..... 224

Figure 7.12 - Instrumented rock bolt strain plot with localised loading. 224

List of Tables

Table 3.1 – Material Properties (Zingano et al. 2009) 67

Table 3.2 – Rock bolt Properties (ASTM 2014) 67

Table 4.1 – Material details (Kostecki, 2019). 89

Table 4.2 - Material properties (Kostecki 2019). 92

Table 4.3 - Contact properties (Li et al. 2016a). 92

Table 4.4 – Material Properties (Kostecki 2019). 103

Table 4.5 – Pile Properties (Kostecki 2019). 103

Table 4.6 – Material Properties (McHugh and Signer 1999). 110

Table 4.7 – Pile Properties (Pammela Caroline Pinazzi 2020; Tulu et al. 2012). 110

Table 5.1 – Material properties for shear test (McHugh and Signer 1999). 136

Table 5.2- Bolt properties (McHugh and Signer 1999). 136

Table 5.3 - Material properties (Jalalifar 2006). 138

Table 5.4- Bolt properties (Jalalifar 2006). 138

Table 5.5 - Rock bolt properties 139

Table 5.6 - Rock bolt and steel properties (ASTM 2018). 141

Table 5.7 - Bolt properties. 144

Table 6.1 - Concrete and grout properties 166

Table 6.2 - Rock bolt properties 167

Table 6.3 - Concrete and rock bolt properties (Kostecki 2019). 168

Table 6.4 - Calibrated material properties for the angled shear test. 172

Table 6.5 - Parameters calculated from strain plots of shear tests and numerical models 173

Table 6.6 - Instrumented rock bolt properties. 178

Table 6.7 - Rock properties. 182

Table 6.8 - Major structures. 183

Table 6.9 - In-situ stress state 183

Table 6.10 - In-situ discontinuity orientation calculation. 184

Table 6.11 - Structure interface properties..... 185

Table 6.12 - Calibrated Pile element parameter..... 186

Chapter 1. Introduction

1.1 Introduction

A safe and efficient ground control system is one of the most vital components of an underground mine's operations. It ensures that all mining operations can proceed as planned and in a safe environment. An inadequate ground control system, whether it is due to its insufficient rock reinforcement leading to ground failure or due to inefficient design leading to a loss of money and operational time, can have a significant effect on the productivity of the mine. The International Council of Mining and Metals reported that the fall of ground resulted in the highest percentage of fatalities (26%) in the 28 member companies in 2020 (ICMM, 2021). In Western Australia 14 injuries and 180 incidents caused by ground movement were reported to DMIRS in the year 2019-20. Falls of ground in underground mines constituted 20% of major incidents in Western Australia between 2011 and 2017 (DMP, 2021).

Rock bolts have been used for reinforcing tunnels and excavations since 1930 (Tully, 1987). A rock bolt usually consists of a metal rod or hollow cylinder embedded into the rock mass. It reinforces the rock by resisting the deformations of the rock or by transferring the load from the outer exposed unstable rock to the stable inner layers or by forming a reinforced rock arch. The method of transfer of load from rock to the rock bolt depends on the type of rock bolt and how it is coupled to the rocks. The rock bolts based on their coupling method can be categorized into three types - Continuously Mechanically Coupled, Continuously Frictionally Coupled and Discretely Mechanically or Frictionally Coupled (Thompson et al., 2012). Fully grouted rock bolts fall under the continuously mechanically coupled category and are a common type of rock bolt used in underground mines for rock reinforcement. The work done in this thesis focuses only on fully grouted rock bolts. A fully grouted rock bolt consists of a solid bar of steel which is coupled to the surrounding rock using a grout. The load is transferred from the rock to the bolt through a complex interaction at the rock-grout and bolt-grout interfaces. Understanding this load transfer mechanism is important for designing a good rock reinforcement design. Rock bolting design methods are used to calculate the number of rock bolts that will be required to stabilize a particular area of the excavation. Rock bolt

reinforcement design methods used currently in underground mines are based on experiential, analytical, empirical, or numerical modelling. Most of the current methods for rock reinforcement design consider a simplified rock bolt behaviour to predict required support capacity (Obert and Duvall, 1967; Potvin, 1988; Mark, 2000). This combined with the complex excavation geometry and rock properties, lead to a support design that is either insufficient or inefficient. Rock reinforcement design needs to take into consideration the actual in-situ behaviour of the rock bolt in order to deliver a suitable reinforcement system.

Designing an appropriate rock bolt reinforcement system requires identifying the loads that the rock bolt will be subjected to in-situ. There are many factors that influence the loading of the rock bolts in an underground mine. Excavation depth, in-situ stress state, excavation size and geometry, rock condition, rock structures such as joints, nearby excavations, required life of excavation, etc. are some of the factors that should be considered while designing rock bolt reinforcement (Barton et al., 1974; Tully, 1987; Hoek et al., 2000; Villaescusa, 2014; Li, 2017). A combination of these factors leads to a complex stress distribution along the length of a rock bolt. A rock bolt in-situ can be subjected to axial, shear, bending or a combination of these loads along its length. Current rock bolt reinforcement design methods simplify the stress state by identifying the largest load on the bolt (axial load being considered in most common methods (Mark, 2000) and using it to design the required reinforcement. This leads to an insufficient rock reinforcement design. Empirical methods for rock bolt reinforcement design are based on predicting rock behaviour based on observation and measurements from existing underground structures. The recorded data from mines with similar rock and stress conditions can be interpolated to predict the stability of new underground excavations (Merritt, 1972; Barton, 1978; Potvin, 1988; Pakalnis, 2015). A shortcoming of such methods is the unavailability of a suitable database for a particular set of underground conditions. In the absence of a good database, the empirical models are often extrapolated resulting in support design not being accurate enough and a large factor of safety has to be selected (Dunn, 2013; Pakalnis, 2015; Potvin & Hadjigeorgiou, 2015). This can lead to over-designed rock

reinforcement with high cost and installation time. Empirical rock reinforcement design approaches calculate required rock bolt capacity by simplifying the loading mechanism of the rock bolt in order to make the calculations easier (Panek, 1956; Panek, 1964; Obert & Duvall, 1967; Cox, 1974; Fairhurst & Singh, 1974). In-situ conditions are seldom simple for the empirical approaches to provide a good prediction for reinforcement requirements. The most common approach for rock bolt support design is based on the suspension, beam building and key block concept (Mark, 2000). These methods consider a single mode of loading on the rock bolt when calculating the ultimate load capacity. The rock bolt loads are calculated based on supporting the dead-weight of the disturbed rock mass above the excavation. These methods do not consider the effect of lateral loading on the rock bolt which can lead to underestimation of the required rock bolt capacity.

Numerical modelling methods involves the simulation of the in-situ conditions and rock bolt's response on being subjected to those conditions. There are various numerical modelling techniques developed over the years such as finite element method, finite difference method, finite volume method, boundary element method, discrete element method etc. The advantage of using numerical modelling is that the method can be applied to any set of complex underground conditions. The accuracy of the simulation results depends on the underlying governing equations, the accuracy of the model geometry, and the reliability of material properties. Good numerical models with a high level of detail can simulate in-situ conditions with a high degree of accuracy. However, this is often at the expense of processing time which increases exponentially with model size and detail. Once a model with sufficient detail is created the next task is to initialize the material properties and forces in the model. This presents a problem as often the exact values of these parameters are not known. Before the model's results can be used for support design the numerical model parameters need to be calibrated with observation and measurements from in-situ. Numerical modelling of in-situ rock bolt reinforcement simulates the rock bolt using linear elements with nodes linking it to the rock grid elements. The linear element is used to simulate the rock bolt, and the grout and

interface being simulated by the links between the linear element and rock. The interface link parameters need to be calibrated with in-situ observation and measurements. Instrumented rock bolts can be used to measure the strains along the length of the rock bolt in-situ. This data can then be analyzed to obtain the loads or stress at different points on the rock bolt and calibrate the interface link parameters of the rock bolt model. Instrumented rock bolt data from pull tests can be used to calibrate the interface link parameters controlling the axial load transfer (Tulu et al., 2012). No procedure exists for calibrating the parameters of the links controlling lateral load transfer.

To create a rock bolt model, knowledge of the rock bolt's response to different loads, behaviour of the grout and interface under shear and normal loads are required. The response of the linear element is based on a mathematical model describing the response of a rock bolt under different loading conditions. This is the major shortcoming of an implicit model; it is only as accurate as the mathematical model used. These mathematical equations are based on numerous analytical models proposed by past researchers for describing the rock bolt behaviour. Analytical models for lateral loading behaviour of fully grouted rock bolts have been proposed by Pellet & Egger (1996), Ma et al. (2019), Liu & Li (2020). Existing analytical models need further improvement to accurately predict the post-yield behaviour of rock bolt under lateral loading.

In this work rock bolt instrumentation is used to analyze the response of a fully grouted rock bolt through laboratory and in-situ testing. The resulting understanding of the rock bolt response is then used to improve the numerical modelling of rock bolt.

1.2 Problem Summary

Rock bolt reinforcement design methods used in underground mines are based on a simplistic understanding of the rock bolt loading. Often a single mode of loading (most commonly axial) is considered when determining the reinforcement design. This leads to an inefficient or unsafe ground control design. Better instrumentation technology can be used to understand the actual

load behaviour of rock bolts and combined with improved numerical modelling procedures serve as an appropriate tool for rock bolt reinforcement design.

Optical sensors-based instrumentation can provide a real-time data of the deformations along the whole length of a rock bolt. Using such high-resolution monitoring technique, the true rock bolt behaviour can be analysed. This data can then be used to improve the available numerical modelling techniques for simulating rock bolts.

1.3 Thesis Objectives

The objective of this thesis is to gain a better understanding of the rock bolt loading in-situ and the actual rock bolt behaviour under such loading using laboratory and in-situ tests with instrumented rock bolts. The insight gained will then be used to improve existing rock bolt numerical modelling techniques. The objectives identified are:

1. Investigate the loading profile on a rock bolt using physical and numerical modelling. Demonstrate the need for considering the complete loading profile of rock bolt in rock bolt reinforcement design and the drawback of using reinforcement design methods based on single mode of loading.
2. Analyze rock bolt behaviour under combined loading using laboratory tests and calibrated numerical models. Identify the limitations of currently available implicit rock bolt numerical models.
3. Improve the currently available analytical models used in implicit modelling of rock bolts to simulate the actual rock bolt behaviour.
4. Analyze the results from laboratory tests and in-situ tests using instrumented rock bolts to devise techniques for improving numerical modelling of rock bolts for in-situ ground support design.

1.4 Outline of the thesis

i. **Chapter 2:** Rock bolt reinforcement mechanisms and design methods.

Chapter 2 provides an overview of the current design methodologies for rock bolt reinforcement with emphasising numerical modelling methods. An overview of the rock

bolt monitoring systems and their evolution with time is also presented. The chapter goes into the in-depth background of load transfer mechanisms in fully grouted rock bolts and the analytical models describing rock bolt behaviour under different load mechanisms.

ii. **Chapter 3:** Establishing the actual state of stress along the rock bolts.

Singh, P., Spearing, A. S., Jessu, K. V., & da Silva Ribeiro, P. C. P. (2020). Establishing the need to model the actual state of stress along rock bolts. International Journal of Mining Science and Technology, 30(3), 279-286.

A rock bolt is subjected to a combination of axial and shear loading. The current method of rock bolt reinforcement design only considers the axial load demand on the rock bolt. When a rock bolt is subjected to shear loading in addition to axial load the ultimate axial load capacity of the rock bolt decreases (Pellet and Egger, 1996). A scaled-down physical model of an underground excavation with a bedded roof was created to analyze the shear displacement between the roof layers. The shear displacement between the roof layers was measured at different levels of roof deformation. Models with different thickness roof layers were created to analyze the effect of bed thickness. Numerical models were created and calibrated with the observations from the physical model. To analyze the effect of combined axial and shear loading on rock bolt reinforcement, numerical models for suspension and beam building reinforcement were simulated and the loads on the rock bolt were measured. A procedure to calculate the reduction in the safety factor of the rock bolt due to combined loading was presented.

iii. **Chapter 4:** Analysis of the combined load behaviour of rock bolt installed across discontinuity and its modelling using FLAC3D.

Singh, P., Spearing, A. J. S., & Jessu, K. (2020). Analysis of the combined load behaviour of rock bolt installed across discontinuity and its modelling using FLAC3D. Geotechnical and Geological Engineering, 38, 5867-5883.

Numerical models use structural elements to simulate rock bolts for underground reinforcement design. Currently, available rock bolt numerical models cannot simulate the true

response of rock bolt under lateral loading. For accurate modelling of rock bolt response under lateral loading understanding the shear behaviour of rock bolt is important. Numerical models of rock bolt shear tests were calibrated with results from laboratory double shear tests of instrumented rock bolts. The stress distribution on the rock bolt under lateral loading was analyzed and compared with analytical model predictions. Shortcomings of the currently available analytical and numerical models for rock bolt were established. The understanding of the rock bolt's shear behaviour and shortcomings of current rock bolt models were then used to prepare a procedure for modifying the pile structural element in FLAC3D software to accurately simulate the rock bolt response under lateral loading.

iv. **Chapter 5:** An improved analytical model for the elastic and plastic strain-hardening shear behaviour of fully grouted rock bolts.

    Singh, P., & Spearing, A. J. S. (2021). An Improved Analytical Model for the Elastic and Plastic Strain-hardening Shear Behaviour of Fully Grouted Rock bolts. Rock Mechanics and Rock Engineering, 1-17.

Analytical models are constitutive equations describing the load-deformation behaviour of rock bolt. Current analytical model for lateral load response of fully grouted rock bolt does not consider the post-yield strain hardening of steel. The models assume that when the bending moment in the rock bolt reach yield point plastic hinges are formed and the rock bolt behaves like a truss for any further deformation. As the rock bolt deforms laterally without any increase in shear load the models predict the lower shear load on the rock bolt after yield point. A new analytical model for lateral loading of the rock bolt was developed which incorporates the strain-hardening effect of steel in calculating the post-yield response of rock bolt. The analytical model predictions were then verified with laboratory shear tests.

v. **Chapter 6:** Improving the numerical modelling of in-situ rock bolts using axial and bending strain data from instrumented rock bolts.

Numerical modelling can be used for optimizing rock bolt reinforcement in underground excavations. The rock bolt model requires calibration with actual in-situ measurements in

order to make quantifiable predictions. A rock bolt can undergo a combination of axial and lateral loads in-situ. Therefore, the rock bolt response needs to be calibrated for both axial and lateral loading. The axial response of rock bolt can be calibrated using in-situ pull tests. No such method is available for calibration of rock bolt's in-situ shear behaviour. Optical instrumented rock bolts can be used to monitor strains on rock bolts in-situ. The high-resolution strain measurement of optical instrumented rock bolts can accurately capture the localized shear loading on the rock bolt caused by discontinuities. The strain profiles of instrumented rock bolts installed in an underground excavation were analyzed and a procedure for calculating the discontinuity orientation and calibrating rock bolt shear behaviour was presented. The procedures were verified with laboratory shear tests.

vi. **Chapter 7:** Conclusions

Chapter 7 provides an overview of the significant findings of this work. A step-by-step procedure for the calibration of numerical model and optimization of rock bolt reinforcement for the effect of combined loading is presented. The limitations of current work and potential future work are also discussed.

References

Barton, N. I. C. K. (1978). Recent experiences with the Q-system of tunnel support design (No. Publication No. 119 Proceeding).

Barton, N., Lien, R., & Lunde, J. (1974). Engineering classification of rock masses for the design of tunnel support. Rock mechanics, 6(4), 189-236.

Cox, R. (1974). Why some bolted mine roofs fail: 11F, 14R. TRANS. SOC. MIN. ENGRS. AIME, V256, N2, JUNE, 1974, P167–171. Paper presented at the International Journal of Rock Mechanics and Mining Sciences & Geomechanics Abstracts.

DMP. (2021). Hazard register for serious injury or other serious incidents investigations from January 2011 to December 2017. Retrieved from -

https://www.dmp.wa.gov.au/Documents/Safety/MSH_Data_SeriousHazardRegister.xlsx

Dunn, M. (2013). Uncertainty in ground support design and implementation in underground mining. Paper presented at the Proceedings of the Seventh International Symposium on Ground Support in Mining and Underground Construction.

Fairhurst, C., & Singh, B. (1974). Roof bolting in horizontally laminated rock. Engineering and Mining Journal, 175(2), 80-88.

Hoek, E., Kaiser, P. K., & Bawden, W. F. (2000). Support of underground excavations in hard rock: CRC Press.

ICMM. (2021). SAFETY PERFORMANCE, Benchmarking progress of ICMM company members in 2020. Retrieved from https://www.icmm.com/website/publications/pdfs/health-and-safety/2021/benchmarking-safety-data-2020.pdf

Li, C. C. (2017). Principles of rockbolting design. Journal of Rock Mechanics and Geotechnical Engineering, 9(3), 396-414. doi:10.1016/j.jrmge.2017.04.002

Liu, C., & Li, Y. (2020). Predicting the shear resistance contribution of passive fully grouted bolts to jointed rock. International Journal of Geomechanics, 20(2), 04019174.

Ma, S., Zhao, Z., & Shang, J. (2019). An analytical model for shear behaviour of bolted rock joints. International Journal of Rock Mechanics and Mining Sciences, 121, 104019.

Mark, C. (2000). Design of roof bolt systems. Paper presented at the New Technology for Coal Mine Roof Support, Proceedings, NIOSH Open Industry Briefing, NIOSH IC.

Merritt, A. H. (1972). Geologic prediction for underground excavations. Paper presented at the N Am Rapid Excav & Tunnelling Conf Proc.

Obert, L., & Duvall, W. I. (1967). Rock mechanics and the design of structures in rock (Vol. 650): Wiley New York.

Pakalnis, R. (2015). Empirical design methods in practice. Paper presented at the Proceedings of the International Seminar on Design Methods in Underground Mining.

Panek, L. (1964). Design for bolting stratified roof. TRANSACTIONS OF THE SOCIETY OF MINING ENGINEERS OF AIME, 229(2), 113-119.

Panek, L. A. (1956). Principles of reinforcing bedded mine roof with bolts (Vol. 5156): US Department of the Interior, Bureau of Mines.

Pellet, F., & Egger, P. (1996). Analytical model for the mechanical behaviour of bolted rock joints subjected to shearing. Rock mechanics and rock engineering, 29(2), 73-97.

Potvin, Y. (1988). Empirical open stope design in Canada. University of British Columbia.

Potvin, Y., & Hadjigeorgiou, J. (2015). Empirical ground support design of mine drives. Paper presented at the Proceedings of the International Seminar on Design Methods in Underground Mining.

Thompson, A., Villaescusa, E., & Windsor, C. (2012). Ground Support Terminology and Classification: An Update. Geotechnical and Geological Engineering, 30. doi:10.1007/s10706-012-9495-4

Tully, D. M. (1987). Rock bolt reinforcement systems for coal mine roadways. Newcastle University.

Tulu, I. B., Esterhuizen, G. S., & Heasley, K. A. (2012, June). Calibration of FLAC3D to simulate the shear resistance of fully grouted rock bolts. In 46th US rock mechanics/geomechanics symposium. OnePetro.

Villaescusa, E. (2014). Geotechnical design for sublevel open stoping: CRC Press.

Chapter 2. Rock bolt reinforcement mechanisms and design methods

2.1 Introduction

The undisturbed rock below the surface remains under a state of equilibrium with its surrounding rock mass. When an excavation is created, the equilibrium state of the rock near the excavation boundary is disturbed (Goodman, 1989). The rock deforms, and the near field stresses are changed to regain the equilibrium Figure 2.1.

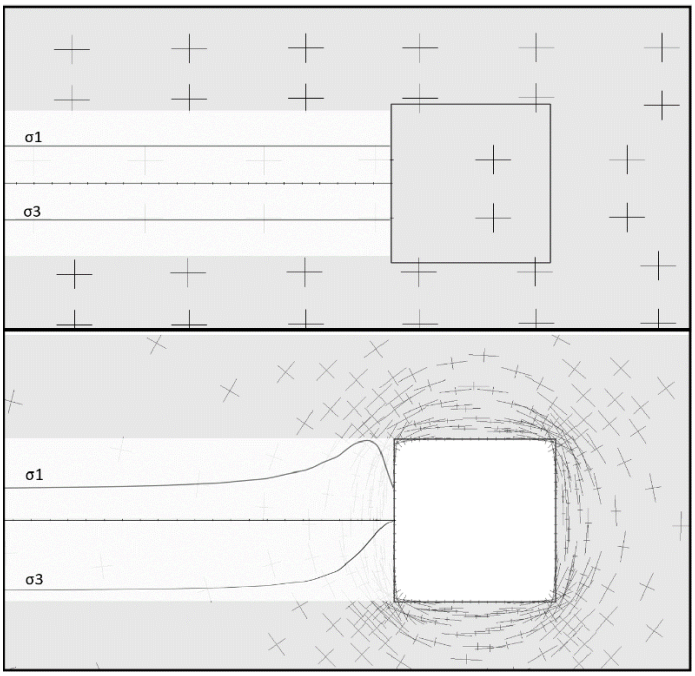

Figure 2.1 - Stress redistribution due to excavation in rock.

This deformation, if not restrained, can keep increasing until ground failure occurs. Rock reinforcements are installed to limit the amount of rock deformation by building ground arch and strengthening the rock. Rock bolts are one of the primary means of rock reinforcement used in underground mines. There are various types of rock bolts used in underground mines. Based on their mechanical model, the rock bolts can be categorised as mechanical rock bolts, fully encapsulated rock bolts, frictional rock bolts, and energy-absorbing rock bolts. Fully grout encapsulated rock bolts are the focus of this study.

Current rock bolt reinforcement design approaches have been discussed briefly, with emphasis on numerical modelling methods. The use of instrumentation to aid in the design of rock bolt reinforcement is also presented in this study. The chapter goes into the in-depth background

of the mechanisms by which fully encapsulated rock bolts reinforce rock and the different techniques used to study rock bolt mechanisms and rock interactions. It also aims to establish the shortcomings of current rock bolting design approaches and the need to improve the understanding and design of rock bolt loading. The literature review is presented in three sections - Rock bolt reinforcement methods, rock bolt instrumentation and rock bolt loading mechanisms.

2.2 Rock bolt reinforcement methods

The first step in designing rock bolt reinforcement is to determine all the loading mechanisms that the rock bolt will be subjected to in-situ and calculate the magnitude of these loads. Once these parameters are specified, a suitable rock bolt design is developed by determining the pattern, the rock bolt type, the performance and the number of rock bolts required. The loading mechanism and magnitude that the rock bolt will be subjected to can be determined by analysing all the possible failure mechanisms of the rock mass. The failure mechanism of the rock depends on various factors like the stress regime around the excavation, adjacent excavations, the geological structures in the rock mass and excavation geometry (Spearing, 1995). As the excavation is made, the stresses from the excavated rock are transferred to the adjacent rock. The rock strata near the roof and floor become destressed, bend and delaminate, resulting in tensile and shear stresses. As the rock deforms into the excavation, the rock bolt is loaded in tension. These stresses can also cause failure in the rock near the excavation surface or cause the rock to fail along the geological discontinuities (Thompson et al., 2012). In low-stress conditions, the failure mechanism is usually controlled by geological discontinuities. The low-stress state cannot provide enough confinement to the discontinuity to prevent displacement. In this case, the primary task of a rock bolt is to prevent the movement of rock along these discontinuities. In higher stress conditions, the discontinuities are usually closed due to the confinement from the surrounding rock. The increased stress can cause excessive rock deformation in stress concentration zones like the excavation's shoulder and toe, leading to new cracks forming, which can connect with pre-existing discontinuities and

destabilise them. In stratified rock mass, the high stress can lead to bending of the beams creating tensile forces at the centre and abutments leading to cracks developing perpendicular to the rock layers. This creates smaller beams of rock that can fall under gravity (Li, 2017; Thompson et al., 2012). All the failure mechanisms mentioned above subject the rock bolts to different loading mechanisms depending on the discontinuity orientation relative to the excavation, as shown in Figure 2.2.

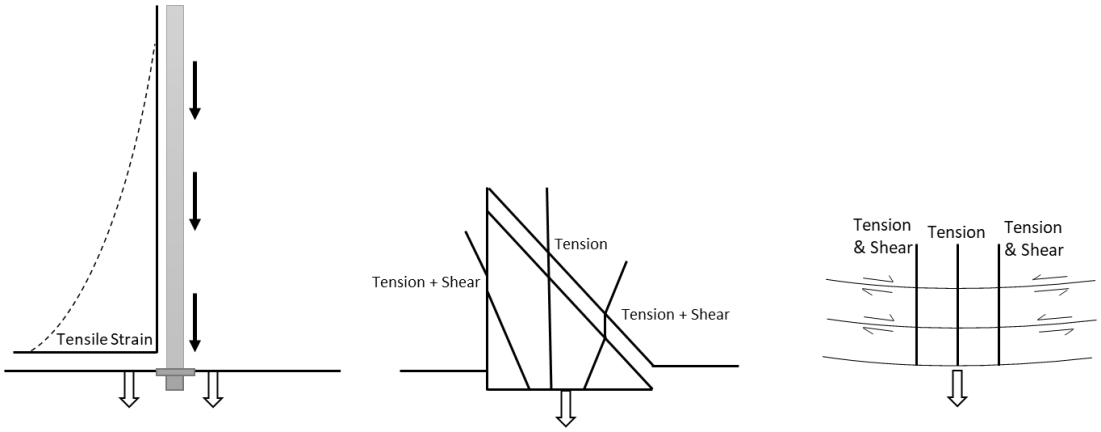

Figure 2.2 - Rock bolt loading modes.

As shown in Figure 2.2, a rock bolt can be subjected to axial, bending and shear loading in-situ. The load demand on the rock bolts in a tunnel with beam-like layers of rock can be calculated by Obert & Duvall (1967) as:

$$L_b = \frac{\gamma t w L}{(n1+1)(n2+1)} \tag{2.1}$$

Where, L_b is the load per bolt γ is the unit weight of the rock, t is the height of the unstable roof, w is the width of the tunnel, L is the length of the tunnel to be supported, $n1$ is the number of bolts along the length, $n2$ is the number of bolts along the width. The method assumes that all the load of the rock layers was supported only by the rock bolts, and the support from abutment was not considered. The equation also does not take into account the effect of in-situ stress on rock bolt load or the effect of shear stress. Cording & Mahar (1978) also calculated the support pressure for rock loaded only by gravity as:

$$P = nB\gamma \tag{2.2}$$

Where, P is the support pressure, n is a constant whose value varies from 0.1 to 0.3 depending upon the width of tunnel and shear strength of discontinuities., B is the width of the tunnel, γ is the unit weight of the rock.

Stimpson (1987) proposed an equation for calculating the required bolt spacing in a beam building rock bolt reinforcement design:

$$b = \frac{-F + \sqrt{F^2 + 1.5\gamma L^3 F}}{0.75\beta\gamma L^2} \tag{2.3}$$

$$F = \frac{D_b^2}{4}\sqrt{1.7\sigma_y \pi P_u \left(1 - \left(T / T_y\right)^2\right)} \tag{2.4}$$

Where, b is the bolt spacing, L is the width of excavation, F is the ultimate shear load of the bolt, γ is the rock density, β is the load multiplier at the abutment, D_b is the diameter of the bolt, σ_y is the yield stress of bolt, P_u is the bearing capacity of rock or grout, T_y is the yield load of the bolt, T is the axial load in bolt at the plastic moment.

Grimstad & Barton (1993) proposed calculating the roof pressure using the Q system of rock mass classification.

$$P_{roof} = \frac{2\sqrt{Jn}Q^{-\frac{1}{3}}}{3Jr} \tag{2.5}$$

Where, P_{roof} is the roof pressure-demand, Q is the rock mass quality, Jn and Jr are the joint number and roughness (Barton et al., 1974).

Underground wedges can be formed when three or more joints (and bedding planes) intersect, forming an unstable wedge of rock at the face of the excavation, which can fall under the force of gravity. The simplest method of calculating support load for such a failure mode is to

calculate the unstable wedge's deadweight and design the rock bolt reinforcement with an ultimate capacity greater than the deadweight. This method does not take into account the effect of the in-situ stresses and joint's cohesion and frictional properties. Pratama et al. (2014) proposed a wedge viability index to consider the effect of joint properties, in-situ stresses and wedge orientation in calculating the support requirement.

The above-mentioned rock bolt reinforcement design methods only calculate the axial load demand of the rock bolt. However, geological discontinuities in the rock mass can lead to a combination of axial and shear loading of the rock bolt, as shown in Figure 2.2. These methods also do not take into consideration the load transfer mechanism between the rock and rock bolt.

2.3 Numerical Methods

Numerical methods can be used for modelling rock reinforcement using rock bolts. Various numerical modelling methods such as finite element, finite difference, and boundary element methods have been used to design rock bolt reinforcement in past research. Numerical methods can be used to simulate the complex in-situ conditions to include the effect of in-situ stresses and geological discontinuities on rock bolt loading. To design rock bolt reinforcement, a model of the excavation needs to be created which can reproduce the in-situ rock behaviour, including the effect of in-situ stresses and geological discontinuities. The constitutive and failure properties of the rock and discontinuities are defined to replicate all the failure mechanisms in-situ. Another essential part of the numerical model are the analytical models used to implement rock bolts numerically. The rock bolt model should replicate the load transfer mechanism and the rock bolt's response to the loads accurately. The model is then validated with measurements and observations of the in-situ rock deformation, rock bolt load etc.

2.3.1 Explicit model of rock bolt

Explicit modelling of rock bolts in the context of this work refers to the direct representation of each component of rock bolt in the model using grid elements. The bolt, grout and the contact between the bolt-grout and rock-grout are implemented using grid elements (Figure

2.3). As all the rock bolt components are explicitly created in the model, the rock bolt model can accurately replicate the actual rock bolt behaviour if the material and contact properties are calibrated with laboratory or field results. The internal stress state of each component can also be known, resulting in better simulation of plastic deformation and failure behaviour of rock bolt (Kostecki, 2019). Since in this approach of modelling rock bolt each component consists of multiple grid elements, the computational overhead becomes too large for simulation of large scale in-situ models. This makes the approach unsuitable for in-situ rock bolt reinforcement design. However, the advantage of being able to analyse the internal stress state make this approach useful in analysing rock bolt behaviour in laboratory testing. Several researchers have used this approach to study the rock bolt behaviour under different loading conditions (Cao et al., 2010; 2011; Ghadimi et al., 2014; Ho et al., 2019; Li et al., 2016; Yokota et al., 2019). These studies will be covered in the next section, discussing rock bolt loading mechanisms.

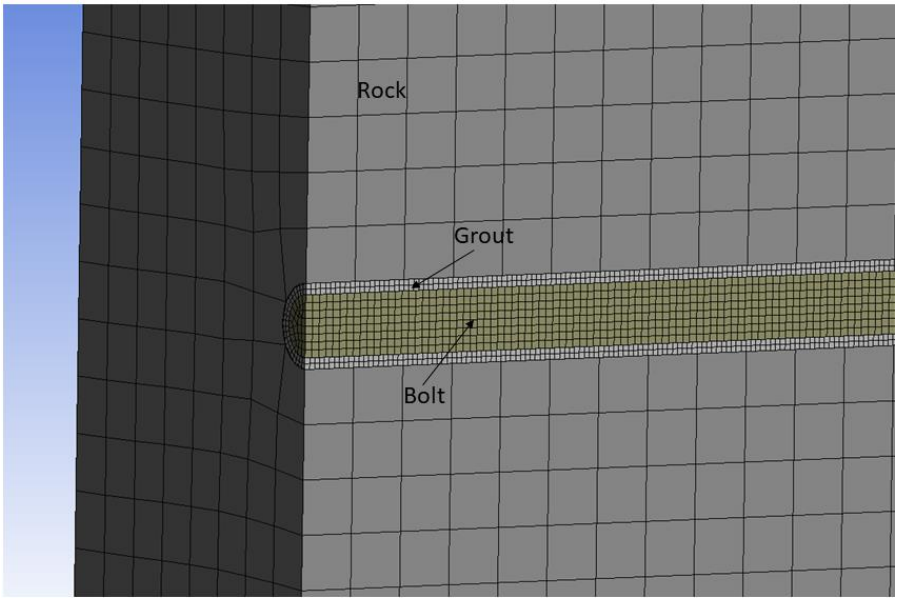

Figure 2.3 - Explicit modelling of rock bolt.

2.3.2 Implicit model of rock bolt

A rock bolt can be represented by a simplified one-dimensional linear element in a numerical model. The constitutive equations governing the deformation of the linear elements are based on analytical models which predict the rock bolt behaviour under different loading conditions.

The element is connected to the rock grid at nodes using a spring and slider system. The spring and slider properties control the load transfer mechanism from the rock to bolt (FLAC3D, 2017) Figure 2.4. The finite difference software FLAC is one of the most common software used for ground control modelling (Mark et al., 2007).

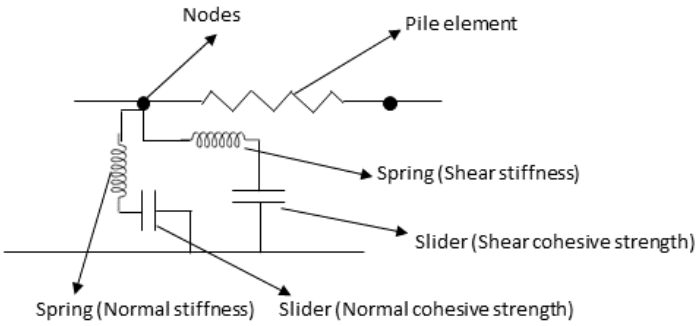

Figure 2.4 - Pile element.

FLAC software has an inbuilt structural support element pile for modelling rock bolts. Gale et al. (2004) used FLAC to analyse the rock bolt design performance in high horizontal stress conditions in a coal mine. Measurements from roof extensometers were used for calibrating the model. Different bolting patterns were analysed for their effect on roadway stability. It was concluded that numerical models could be used for rock bolt design analysis if the geology and properties of the rock are determined accurately. Zipf (2006) presented a procedure for creating numerical models in FLAC software for ground control design in underground coal mines. Laboratory pull-out tests were used to calculate the rock bolt anchorage stiffness parameter. Rock bolt anchorage failure parameter was calculated for different types of rocks using pull-out tests. It was noted that the correct linkage properties of the rock bolt element were significant for a realistic model. Zhang et al. (2015) conducted a similar study using FLAC3D to conduct a parametric analysis of rock bolting pattern, rock bolt length and anchorage length on ground support in a coal mine roadway. Bolt load measured in-situ using load cells were used to calibrate the model.

The constitutive properties of the pile structural element in FLAC3D are based on an anisotropic bi-symmetrical prismatic straight beam. The node linkages to the rock grid are simulated using a spring-slider system that replicates the grout's stiffness and strength, connecting the rock to the bolt. The pile element is not capable of accurately simulating the actual rock bolt behaviour in-situ. Tulu et al. (2012) calibrated the shear and normal spring parameters using laboratory tests. For calibration of the shear, spring parameters pull-out test results were used. The normal spring parameters were calibrated using laboratory rock bolt shear test results. The yielding and failure criteria for the pile element was modified using Fish programming language. The pile element's plastic moment and normal cohesion limits were adjusted to match the yield point of the rock bolt in the experiment. This resulted in unrealistic values for the plastic moment of the rock bolt. The shear response of the pile element was calibrated with laboratory tests data which might not represent the actual in-situ rock bolt behaviour.

Nemcik et al. (2014) modified the shear spring properties of the pile element in FLAC2D and implemented the non-linear bond-slip behaviour under tensile load. The complete debonding process of the rock bolt was also implemented. Ma et al. (2016) further improved the non-linear bond-slip behaviour of the pile element by implementing the behaviour of a fully grouted rock bolt reaching free end slip under tensile load.

The research works detailed above show that the calibration of the rock bolt parameters, particularly those controlling the rock bolt anchorage behaviour, is essential to accurately simulate rock bolt loading. The axial behaviour of the rock bolt can be calibrated using in-situ pull tests. No research work has been done for calibrating the shear behaviour of rock bolts using in-situ measurements. There is extensive research work on improving the pile element behaviour under tensile loads. However, the work on improving the pile element's shear behaviour is limited and needs further research.

2.4 Instrumented rock bolts

Instrumentation has been used in rock bolts to study the rock bolt behaviour in laboratory and in-situ tests since the 1970s. This section outlines how the technology of instrumented rock bolts has progressed to the present time, and the advantages of new technology over the older ones are also discussed. The first type of instrumentation technology for monitoring rock bolt strain was resistive strain gauges. These strain gauges were attached along the length of the rock bolt and could measure the strain in the rock bolt at their location Figure 2.5. Farmer (1975) used resistive gauges to measure shear stress at the grout-bolt interface under axial load. A procedure was proposed to estimate the shear stress at the rock bolt-grout interface using the strains measured from the strain gauges. Freeman (1978) used similar instrumented rock bolts to study the axial load transfer mechanism between the rock and bolt. The load along the bolt was divide into three sections – pick-up length, neutral point, and anchorage length. Serbousek & Signer (1987) used rock bolts instrumented with strain gauges to study the load transfer mechanism under axial tests using laboratory pull-out tests. Six pairs of strain gauges were used along the length of the rock bolt. It was noted that the wires connecting the strain gauges were the limiting factor in the number of strain gauges that can be attached. Signer (1990) & Signer (2000) used similar instrumented rock bolts to study the load transfer mechanism of fully grouted rock bolts in-situ. The instrumented rock bolts in these studies used the twin groove configuration in order to be able to measure the bending of the rock bolt. The instrumentation technology was limited by the small resistive strain gauges, which provided discrete strain measurements along the rock bolt length. The instrumentation was unable to measure localised loading on the rock bolt. The twin groove arrangement also limited the ability to measure bending if the direction of loading was not aligned with the grooves.

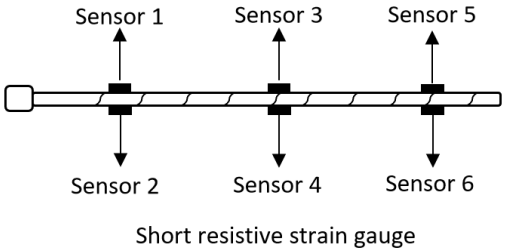

Figure 2.5 - Short resistive strain gauge instrumented rock bolt.

Inductive sensor technology was used by Spearing and Gadde (2011); Spearing et al. (2011); Spearing et al. (2013) to improve the rock bolt monitoring in underground mines. This new instrumentation technology used long base length inductive sensors to provide greater rock bolt length coverage than small resistive strain gauges. The sensors were installed in the twin-slot configuration like in previous studies. Two configurations of the sensors – stacked and staggered (Figure 2.6) were tested, and the staggered configuration was found to provide better coverage of the rock bolt. The instrumentation still had the drawback of twin-sensor configuration, but the better coverage provided some success in measuring the bending loads on the rock bolt. The longer length of the sensors provided more measurement points, but they measured the average load over their length instead of discrete measurements like strain gauge. This averaging of the loads would mean that the peak loads were often underestimated.

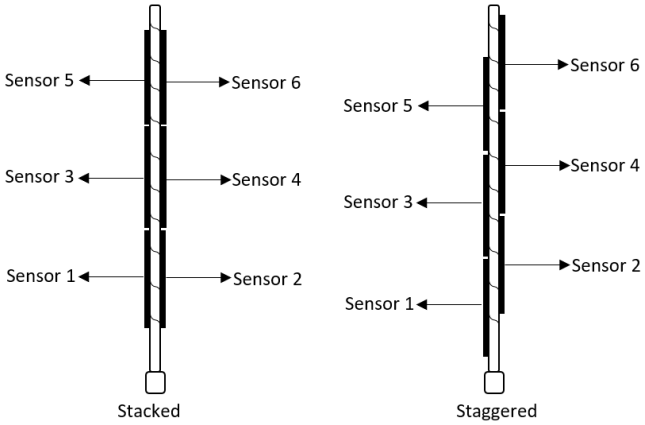

Figure 2.6 - Long base length inductive sensor instrumented rock bolts.

The development of optical fibre strain sensors improved the instrumentation technology for rock bolt. Hyett et al. (2013) first used the optical fibre instrumented rock bolt for studying the strain profile of a fully grouted rock bolt. The technology used in the instrumentation was Distributed optical sensors (DOS). An optical fibre cable is attached along the whole length of the rock bolt, and the fibre is capable of making discrete measurements of strain in the rock bolt every 5mm along its length. This technology overcame the drawbacks of previous sensors by providing complete coverage of the rock bolt length. The fibres were installed in a twin-slot arrangement and used to study the strain profile of rock bolts under axial and bending loads in laboratory testing. The DOS instrumentation could capture the strains within 10% of theoretical approximations with very high resolution. The sensor was also capable of capturing rib details of the rock bolt under the axial pull test. To capture the true bending strain of rock bolt, especially in field conditions where the sensor slots cannot be aligned with the direction of loading, the design of the instrumentation needed to be improved. Kostecki et al. (2015) used the DOS fibres in a three-slot configuration to capture the bending strain of a fully grouted rock bolt in laboratory shear testing. The three-slot arrangement was capable of capturing the actual bending strain profile of the rock bolt. It was shown that the twin-slot configuration could not capture the bending if the slots are not aligned with the lateral loads. Figure 2.7 shows the twin-slot and three-slot configurations for optical instrumented rock bolts. Subsequent studies by researchers using optical instrumented rock bolts to measure the rock bolt strain under laboratory and in-situ testing have established the optical sensors as key to understanding the load transfer mechanism and rock bolt response (Jessu et al., 2016; Vlachopoulos et al., 2018; Forbes et al., 2018; Kostecki, 2019; Forbes et al., 2020). Hoehn et al. (2020) proposed an improved design of optical instrumented rock bolts using a new technology All-Grating Fibre (AGF). AGF provided more robustness and easier data recording capability compared to previous technologies. A procedure was described for implementing the optical instrumentation for monitoring rock bolts in harsh underground conditions. The slot configuration was increased from three to four-slot to improve the tooling of slots and increase the redundancy.

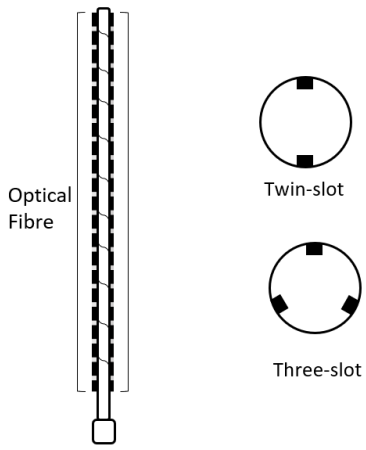

Figure 2.7 - Optical instrumented rock bolt.

The new optical instrumentation technology provides a valuable tool for analysing the rock bolt behaviour along its entire length and under different loading conditions. The optical instrumented bolts can also be used to monitor strains in rock bolt in-situ. This presents the possibility of using the technology to improve the understanding of rock bolt loading mechanisms and improve the numerical modelling procedures for rock bolts.

2.5 Rock bolt loading mechanisms

Under in-situ conditions, a rock bolt can be subjected to a range of different and changing loads. Analysing the deformation or loads along the rock bolt's length can help understand the load transfer mechanism between the rock bolt, grout and rock mass. A fully encapsulated rock bolt usually consists of a solid cylindrical metal bar called a bolt with ribs along its length. The bolt is placed inside a drill hole slightly larger than the bolt's diameter on the excavation boundary. The gap between the bolt and rock is filled with a cement, grout or resin mixture, which hardens and attaches the bolt to the rock Figure 2.8. The metal bolt usually made from structural steel has a stiffness many magnitudes higher than rock. As the rock deforms, the load is transferred through the encapsulating material to the bolt. As the steel bolt has very high stiffness, it undergoes very small deformation even at high loads, which effectively restrains rock deformation. As the load transfer between the rock and bolt takes place through the encapsulating material, there are two interfaces, rock-grout and grout-bolt, which governs

the load transfer mechanism. This makes the loading mechanism of a fully grouted rock bolt much more complex than other types of rock bolts.

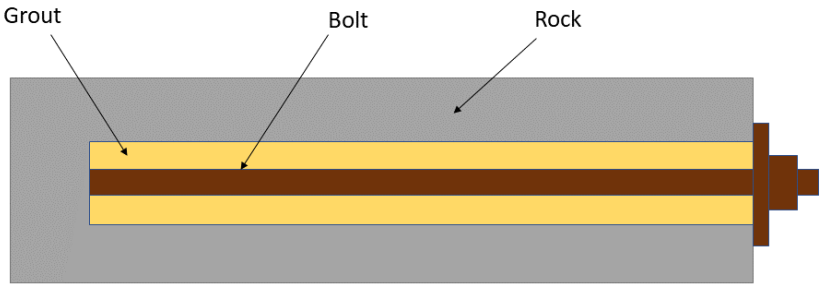

Figure 2.8 - Fully-grouted rock bolt.

2.6 Axial load transfer mechanism

The axial loading of a rock bolt has been extensively researched through both laboratory and in-situ testing. Tensile loading is one of the most common modes of loading found in underground mines. When a rock bolt is installed on the face of underground excavation, it experiences an axial load as the rock deforms or displaces into the void.

One of the first in-situ studies into the axial load transfer mechanism of a fully encapsulated rock bolt was done by Freeman (1978). In the study, instrumented fully grouted rock bolts were installed in a soft-sedimentary rock tunnel. The loading profile along the length of the rock bolt was observed. Freeman came up with three distinct loading regions along the rock bolt length. The pick-up length region starts from the bolt head near the excavation boundary Figure 2.9. This is the region of the rock bolt which supports the load of the rock. The axial load in the pick-up length increases away from the bolt head, reaching a maximum at a point defined as the neutral point. The shear stress in the grout at a neutral point is zero. The region beyond the neutral point is called the anchor length, where the axial load decreases gradually towards the end of the bolt. The anchor length is the part of the rock bolt that is anchored in the stable rock region.

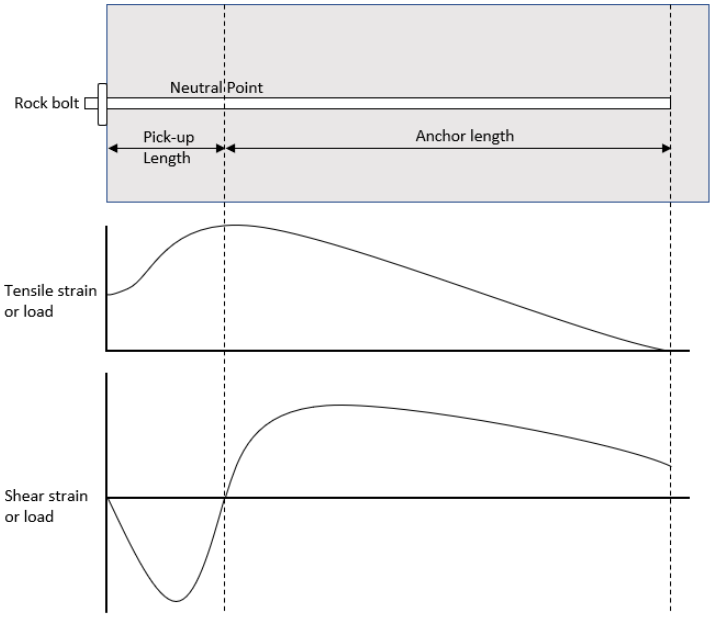

Figure 2.9 - Load profile of fully grouted rock bolt. (Modified after Freeman (1978))

Snyder et al. (1979) reported that the primary failure mode of fully grouted rock bolts in weak rock mines was a failure at the grout-rock interface. A field study was done by Signer (1990) using strain gauge instrumented fully grouted rock bolts installed in shale roofs in mines. It was found that the shear resistance at the grout interface was mainly due to the mechanical interlocking and in the later stages of the pull-out test due to frictional resistance. Giot et al. (2019) conducted pull-out tests in a soft rock underground mine, and several neutral points were observed over the length of rock bolts. The observation was attributed to the highly fractured rock condition near the excavation, which caused debonding near the bolt head.

In-situ observations and measurements of tensile loading of rock bolts have been conducted by researchers as early as 1970. Comprehensive studies have been done using instrumented rock bolts to analyse the tensile load profile of rock bolts using in-situ and laboratory pull tests.

2.6.1 Pull-out test

One of the most popular tests for evaluating the axial performance of a fully grouted rock bolt is the short encapsulation pull-out test (SEPT). The only internationally accepted standardised test for evaluating rock bolt load transfer capacity is ASTM F432 pull test (ASTM, 2013). In a pull test, an axial tensile load is applied to the head of a fully encapsulated rock bolt installed

either in a rock or concrete block or in-situ Figure 2.10. The load is slowly increased until either the bolt fails, or it loses anchorage. Often the rock bolt is instrumented to measure the loads along the length of the rock bolt. Past researchers have performed numerous such tests to analyse rock bolt load transfer and failure mechanism and propose mathematical models defining the load distribution on a rock bolt under axial loads.

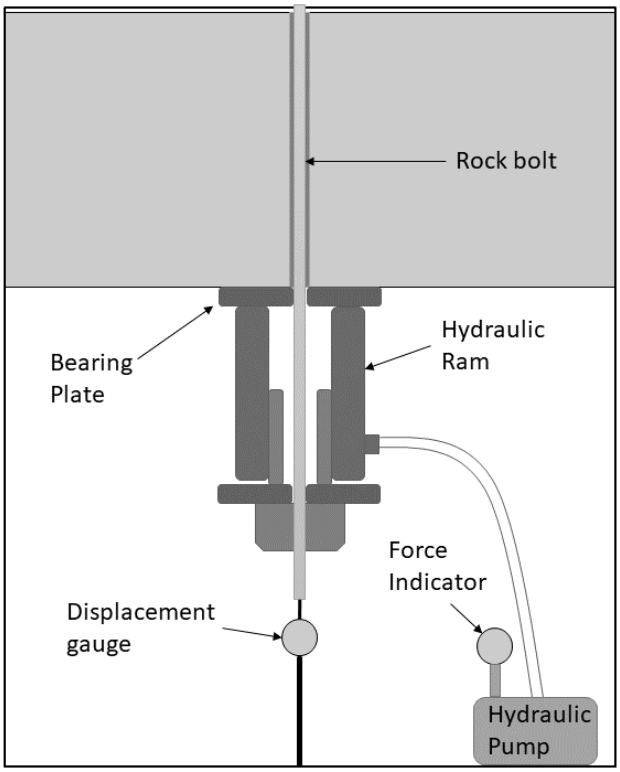

Figure 2.10 - Pull out test setup.

Failure in fully grouted rock bolts can take place in several different ways. The bolt is made of steel and therefore has a very high stiffness compared to rock and grout. It can take up a lot more load with very small deformations. The load from the rock is transferred to the bolt across the grout through shear stress. If enough load transfer length (anchor length) is available, then the failure occurs in the bolt when the ultimate capacity of the steel is reached. However, in a case where anchor length is not enough, failure can occur at either the grout-bolt or grout-rock interfaces. Where the failure will occur depends on the properties of grout and rock. If the grout and rock have similar strengths, failure will occur at the interface with smaller area that is the bolt-grout boundary (Serbousek & Signer, 1987). This is the most commonly

experienced failure (Stillborg, 1986; Kaiser et al., 1992; Martín et al., 2013) in rock bolts under tensile load. In the case of very weak rock, failure can occur at the rock-grout interface (Gerdeen et al., 1979; Aydan et al., 1987).

Farmer (1975) conducted axial pull tests on anchors installed in weak and hard rocks. Shear stress distribution in the grout at low axial loads in hard rocks implied elastic deformation at the interface. However, at higher axial loads, significant debonding was observed between the grout and rock. In soft rocks, this debonding occurred even at lower axial loads. Once the grout has completely debonded, the shear stress is reduced to a residual level held only by the frictional resistance. Serbousek & Signer (1987) had similar observations in pull-out tests of fully grouted rock bolts. The observation from the tests suggested that the bonding mechanism in the elastic stage was due to mechanical interlocking, which reduced to just frictional resistance after debonding. The bond strength depends on the compressive strength and shear strength of the grout, the embedment length and confining pressure (Benmokrane et al., 1995; Kılıc et al., 2002; Moosavi et al., 2005). Martín et al. (2013) conducted laboratory pull-out tests on fully grouted rock bolts and concluded that the initial shear response is due to chemical adhesion and mechanical interlocking. Bolt profile was found to have a significant effect on the peak pull-out load as well as on the axial load-displacement response of the rock bolt after the peak load point. Thenevin et al. (2017) conducted pull-out tests and confirmed the findings of Martín et al. (2013). Vlachopoulos et al. (2018); Yu et al. (2019) conducted pull-out tests on rock bolts embedded in concrete cylinders. They reported three failure modes depending upon the embedment length and confining pressure. At low embedment length and low confining pressure, the system failed due to the radial cracking of the concrete. At higher confinement, the failure occurred due to the debonding of the bolt-ground interface. The third failure occurred by bolt failure at high embedment length. Researchers have proposed analytical models attempting to mathematically predict the rock bolt's response under tensile loads based on these observations of the rock bolt's tensile behaviour.

2.6.2 Analytical models

One of the first mathematical models for axial stress distribution on a fully grouted rock bolt was proposed by Farmer (1975). Pull-out tests were conducted on fully grouted rock bolts instrumented with strain gauges. The shear stress at the grout-bolt and grout-rock interface was calculated from the test results. A mathematical model was proposed for shear stress distribution along with the grout interface with the assumption of a rigid rock-grout boundary. The model's results agreed with test results at low axial loads. However, the results didn't match at higher axial loads when debonding occurred at the grout-rock interface. Serbousek and Signer (1987) conducted laboratory pull out tests on fully grouted rock bolts installed in concrete blocks. They compared the bolt displacement observed in laboratory testing to existing analytical models. The results from a FEM model was also compared to the test data. It was found that the results from both FEM and analytical model disagreed with test data. It was concluded that further research on load transfer mechanisms in fully grouted rock bolts was required. Signer (1990) conducted field pull-out tests on fully grouted rock bolts in coal mines to understand the load transfer mechanism. The tests were first conducted to the elastic limit and then extended to the yielding of the rock bolt. It was found that the grout still retained some residual anchorage strength past the yield limit of steel. The results from the test matched with existing numerical and analytical models only until the elastic limit. These research studies showed that even in the cases where the anchorage length of the rock bolt was enough to overcome the strength of steel, there was still some slippage between the grout-rock interface. Therefore, the assumption of a rigid rock-grout interface was not correct. A new mathematical model which considered the effect of grout debonding was needed.

Earlier bond strength models were based on frictional coupling between the grout, bolt and rock. Laboratory studies evaluating the effect of confining pressure on the bond strength were done by Kaiser et al. (1992) and Hyett et al. (1995). Hyett et al. (1995) conducted pull tests on fully grouted cable bolts confined using a modified Hoek cell. A frictional dilation based mathematical model for cable bolt failure was proposed. The model displayed two distinct stages of debonding – first with a high shear stiffness under 1 mm of bolt displacement, the

second stage involved a significant drop in stiffness due to splitting of the grout annulus. The value of shear stiffness and transition from the first to the second stage was controlled by the confining pressure, hole size, cable and grout properties. Hyett et al. (1996) used this constitutive model for cable bolt failure to explain the difference of performance of fully grouted cable bolts in weak and hard rock. Although non-linear behaviour was considered in these mathematical models for cable bolt failure, the models still did not consider the effect of grout decoupling on the shear load distribution and its effect on the location of the neutral point.

A newer analytical model for axial loading of fully coupled rock bolts was proposed by Li (2000); Li & Stillborg (1999). The proposed mathematical model considered the bond between the rock bolt and coupling medium to consist of three components – adhesion, mechanical interlock and friction. A model for shear stress distribution along fully grouted rock bolts was proposed based on the experimental results. The proposed model consisted of three distinct regions of coupling in a fully grouted rock bolt under axial load. The grout near the loading end of the bolt is considered to be completely decoupled. The shear stress in this region remains constant at the residual shear strength value. Beyond this region, the grout is only partially decoupled, and the shear stress value increases linearly to peak shear strength. After this point, the grout undergoes elastic deformation, and the shear stress values decrease exponentially toward the end of the bolt. Li & Stillborg (1999) used this constitutive model to develop analytical models describing the axial loading behaviour of fully coupled rock bolts in uniform rock and jointed rock. Cai et al. (2004) proposed a similar analytical model for axial loading of a fully coupled rock bolt using a modified shear-lag theory to define the decoupling behaviour of grout. The proposed model could be used to calculate the neutral point position along the rock bolt's length and quantify the supporting effect of the rock bolt on the rock.

Martín et al. (2011) proposed a new analytical model that used the tri-linear bond slip model (Benmokrane et al., 1995) and can analyse the axial load distribution in a pull-out test using

only the displacement value at the loading point of the rock bolt. Ma et al. (2013); Ma et al. (2014) further extended the analytical model based on tri-linear bond-slip to predict the complete decoupling behaviour of rock bolts under axial load. The tri-linear slip model was modified into a non-linear slip model. Two models were proposed with free-end slip (in soft rocks) and no free-end slip (in hard rocks) of the rock bolt. The proposed model could predict the shear stress in the grout up to the point where the bolt becomes completely decoupled, and the shear stress reaches zero. The effect of plastic yielding of the rock bolt material on the pull-out behaviour of fully coupled rock bolt was also included in the model by Ma et al. (2017). Jin-feng & Peng-hao (2019) proposed an improved analytical model based on the dynamic bond-slip model based on the dynamic broken line model of Si et al. (2014). The model considered the bond-slip relationship to be dependent on the location along the rock bolt length instead of an idealised constant relationship of earlier models.

The above mentioned analytical models defining the axial behaviour of rock bolts can be used to modify the rock bolt structural elements in modelling software (Nemcik et al., 2014; Ma et al., 2016; Wang et al., 2020; Chen et al., 2021).

2.7 Shear load transfer mechanism

Rock mass in-situ is not a continuous media. Instead, it contains a lot of anisotropicity in the form of discontinuities like fractures, joints, slips and shear zones. When a fully encapsulated rock bolt is installed across such a discontinuity, it will resist the shear movement of the rock at that discontinuity Figure 2.11. Kwitowski et al. (1979) used a resistive strain gauge instrumented rock bolts in a coal mine to identify and measure the type of loads on the rock bolts. The rock bolts were found to be under both axial and transverse loading. Two to three discrete shearing locations were identified along the length of the rock bolts. However, there was uncertainty in the location and magnitude of the lateral loading due to the poor coverage of rock bolts using resistive strain gauges. Radcliffe et al. (1980) conducted a similar study with instrumented rock bolts in a coal mine. Localised bending was observed in some of the rock bolts, but the direction of lateral loading could not be correlated between different bolts.

Most of the loading on rock bolts was found to be concentrated in the shear line failures. Li (2010) conducted field observation of the failure mechanisms of fully grouted rock bolts in a cut and fill mine. The rock bolts were observed to have undergone a significant amount of shear loading in addition to tensile loads.

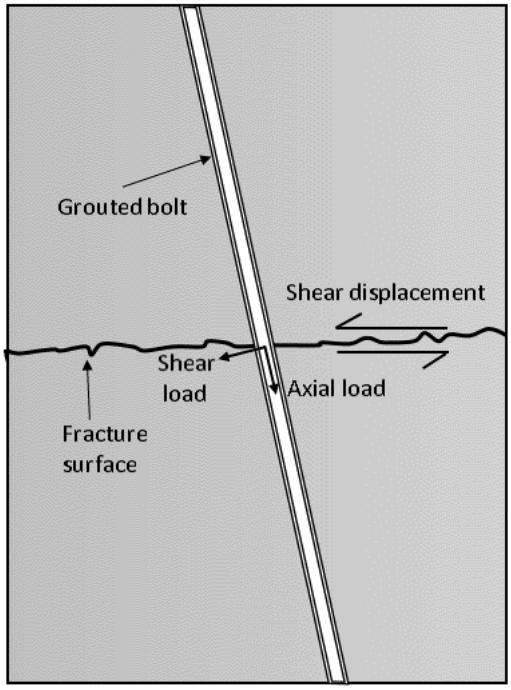

Figure 2.11 - Rock bolt resisting shear displacement at the discontinuity.

Snell (2021) used DOS instrumented rock bolts to study the effect of shear in potash mines. Shear planes were identified in the roof of the drifts, and the shear planes were correlated to known clay seams in the roof. Shear loading of rock bolts was found to be a significant factor in ground support stability. The development of new instrumentation technology has made the measurement of shear loading in in-situ conditions possible. This has led to many research works to understand the shear behaviour of rock bolts. Researchers have done laboratory tests to understand the load transfer mechanism in a fully encapsulated rock bolt resisting shear movement across a rock discontinuity. A standard method to test the rock bolts under shear load is conducting a single/double shear test laboratory.

2.7.1 Single/Double shear tests

Although there is no standardised method to conducting this type of test, most of the shear tests reported in various research works follow a more or less similar approach. At its most basic form, the shear test consists of a rock bolt installed in a hole through the centre of two or three separate blocks made of either concrete or rock. The adjacent edges of the blocks form the surfaces of the shearing discontinuity Figure 2.12. The rock bolt is subjected to a shear load by keeping one/two blocks fixed and displacing the second/third block parallel to the shear surface by applying a load. The load is increased gradually until either the blocks or the bolt fails. Researchers have used these laboratory tests to analyse the effects of different parameters on the shear behaviour of rock bolts.

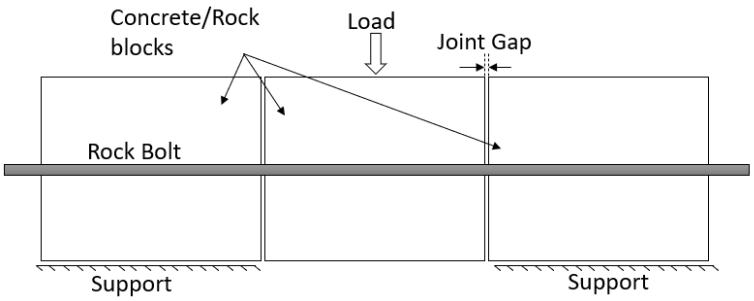

Figure 2.12 – Rock bolt shear test setup.

One of the first reported shear testings of fully encapsulated rock bolts was done by Haas (1976). Full-scale bolts were installed across a fracture in cubical blocks of limestone and shale. A load was applied normal to the fracture surface, and a shear load was applied such as to shear half of the block. The effect of bolt angle to discontinuity and normal pressure on the joint was analysed. It was reported that the bolts increased the strength of the fracture when oriented such that the bolts tensioned with the shear movement of the fracture. Similar results were reported by Dight (1982) and McHugh and Signer (1999), who analysed the shear resistance of joints reinforced with rock bolts. No effect of normal pressure on the strength of bolted joints was observed in both studies. Rock bolts contribution to the shear strength of the joint was found to be higher when it was installed at an angle to the joint. Li et al. (2016) reported an increase in stiffness of the joint with angled bolts, but the ultimate shear load was

less than perpendicular bolts. Li & Liu (2019) reported that the bolt contribution to joint strength followed a parabolic relationship with bolt angle. The bolt contribution increased with the initial decrease of bolt angle, reaching a maximum of around 40-50^0 and then started to decrease.

Ferrero (1995) and Jalalifar et al. (2006) reported an increase in joint shear strength due to normal stress on the joint as it induced tensile stress in the rock bolt. Ferrero (1995), McHugh and Signer (1999), Jalalifar et al. (2005), Jalalifar et al. (2006) reported higher shear strength of rock bolt in weak rock compared to a high strength rock. Weak rock was found to fail near the joint resulting in higher bending of rock bolt and mobilising the tensile strength. In hard rock, the rock bolt showed higher shear loads and tended to fail under shear. Ferrero (1995) and McHugh and Signer (1999) reported that pre-tensioning the rock bolt only affected the joint's stiffness while the ultimate strength remained the same in both studies.

Jalalifar et al. (2005), Aziz and Jalalifar (2007) reported an increase in the yield shear load of rock bolt with increasing pretension. Snell et al. (2017) tested rock bolts under shear loads to analyse the effect of joint gaps (Figure 2.12). Increasing the gap size resulted in a reduction of the ultimate failure load of the rock bolt. The stiffness of the joint was found to reduce with increasing gap size while the ultimate displacement increased substantially. Pinazzi et al. (2020) conducted shear tests with a gap on un-grouted rock bolts and reported no effect of gap on the ultimate shear capacity of rock bolt.

Shear loading of rock bolts involves a complex load transfer interaction between the rock, grout, and bolt. The shear test studies done by past researchers show that the rock bolt's response under lateral loading depends on factors like bolt angle to discontinuity, normal load on joint, host media strength and joint gap. Analytical models must incorporate the effect of all these parameters to accurately describe the shear behaviour of rock bolts.

2.7.2 Analytical models

Haas (1976) calculated the bolt contribution to the shear strength by considering only the tensile force generated in the rock bolt due to the shear movement of the joint. Dight (1982)

proposed an analytical model for the shear loading behaviour of fully grouted rock bolt. The analytical model calculated the dowel force and the tensile force generated in the rock bolt under lateral loading. The failure criteria for the rock bolt was based on the Tresca criterion taking into account the effect of shear and tensile loading. Pellet & Egger (1996) proposed a model for the shear behaviour of rock bolt by describing the mechanics of bolt under lateral loading using the beam on elastic foundation theory (BEF). The relationship between the loads and displacements were calculated using the minimum energy principle. The bolt was assumed to be a semi-infinite beam with one end replaced with shear and tensile loads to make the system statically determinate Figure 2.13.

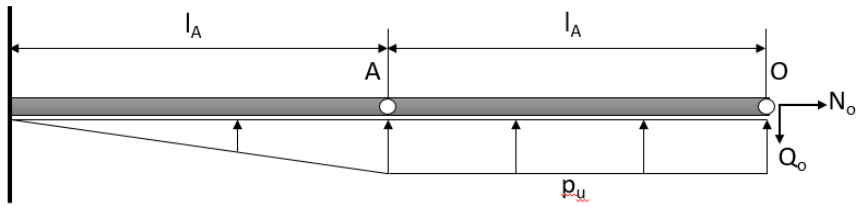

Figure 2.13 - Rock bolt mechanics under lateral loading. (Modified after Pellet and Egger (1996))

When shear displacement takes place at the joint, the bolt is displaced, and a reaction p_u is applied by the host material on the rock bolt. As the bolt bends, it is subjected to a shear load Q_0 and tensile load N_0 at point O at the bolt-joint intersection. The bending moment at this point is zero. The maximum bending occurs at point A, and the distance between points O and A is denoted by l_A. The relationship between elastic displacement and shear load was given as (Pellet & Egger, 1996):

$$U_{oe} = \frac{8192 Q_{oe}^4 b}{E\pi^4 D_b^4 p_u^3 \sin\beta} \tag{2.6}$$

Where, U_{oe} is the total elastic displacement at point O, D_b is the bolt diameter , Q_{oe} is the shear force at O at yield point, b is the a constant (0.27), p_u is the bearing capacity of rock or grout = $K\sigma_c D_b$, K is the load factor (K>=1), σ_c is the unconfined compressive strength of

rock or grout, E is the elastic modulus of rock bolt, β is the angle between rock bolt and discontinuity.

The yield and failure criteria were based on Tresca failure criteria -

$$Q_{oe} = \frac{1}{2}\sqrt{p_u D_b \left(\frac{\pi D_b^2 \sigma_{el}}{4} - N_{oe} \right)} \tag{2.7}$$

$$Q_{of} = \frac{\pi D_b^2}{8}\sigma_{ec}\sqrt{1-16\left(\frac{N_{of}}{\pi D_b^2 \sigma_{ec}} \right)^2} \tag{2.8}$$

Where, Q_{oe}, Q_{of} are the shear forces at O, at yield point and failure point, N_{oe}, N_{of} are the axial forces at O at yield point and failure point, σ_{el} is the yield stress and σ_{ec} is the failure stress.

At the yield limit, plastic hinges were assumed to form at point A, and the section OA of the bolt behaved like a truss. As the shear displacement increases, the section OA elongates axially, increasing the tensile force at point O. The plastic displacement of the bolt was given as (Pellet & Egger, 1996):

$$\Delta U_{op} = \frac{Q_{oe}\sin\Delta w_{op}}{p_u \sin\left(\beta - \Delta w_{op}\right)} \tag{2.9}$$

$$\Delta w_{op} = \arccos\left[\frac{l_e}{l_f}\sin^2\beta \pm \sqrt{\cos^2\beta\left(1-\left(\frac{l_e}{l_f}\right)^2\sin^2\beta\right)} \right] \tag{2.10}$$

$$l_f = l_e\left(1+\varepsilon_f\right) \tag{2.11}$$

Where, ΔU_{op} is the plastic displacement, Δw_{op} is the plastic rotation, l_e is the length of OA at yield point, l_f is the length of OA at the failure point, ε_f is the bolt strain at failure.

The analytical model was reasonable at predicting rock bolt behaviour for perpendicular bolts but was not very accurate for inclined bolts. For bolt inclination of 60^0 the model underestimated the bolt contribution to joint strength after the yield point. The model assumed a perfectly plastic behaviour at the maximum bending point in rock bolt after yield, which underestimated the rock bolt shear load. Jalalifar & Aziz (2010) used a similar analytical model of rock bolt under lateral loads to analyse the hinge point location. A semi-empirical relationship was used for calculating the host material reaction on the rock bolt. It was assumed that the hinge point location remained constant during the elastic phase of rock bolt deformation. Liu & Li (2017) used infinitesimal stress analysis to calculate the rock bolt displacements under the lateral loading conditions. The BEF model was used for lateral shear loading, and the tri-linear slip model was used for tensile loading of the rock bolt. Ma et al. (2018) and (2019) improved the analytical model by modifying the host material reaction using the curvature influence zone method. The new method included the effect of bolt lateral deformation, bolt properties and pretension load. Tri-linear bond-slip model was also included to calculate the axial deformation of rock bolt under shear loading. Liu & Li (2020) proposed a procedure for calculating the length of the rock bolt section deforming laterally under the shear load.

2.8 Discussion

The current rock bolt reinforcement design practices were reviewed, outlining the critical factors in the design process. Based on the review of the current practices it is apparent that most of the current methods for rock bolt reinforcement focus only on the axial loading of the rock bolt. From the past research work done on observation of rock bolt loading mechanism in-situ, it can be seen that lateral (shear and bending) loading is common in underground mines. Therefore, there is a need to highlight the importance of considering the effect of lateral loading on rock bolt reinforcement.

The current understanding of the rock bolt reinforcement mechanism was discussed through past researchers' laboratory and in-situ tests. A review of the analytical models for rock bolts

proposed in the past literature was also presented. The analysis of the past literature shows that the proposed analytical models for lateral loading of rock bolts need further development to accurately predict rock bolt response. The rock bolt models underestimate the shear load in the rock bolt after the yield point. Therefore, the post-yield strain hardening behaviour of the rock bolt needs to be incorporated in the analytical model.

A new, improved fibre-optic instrumentation technology has been used in this research. Past researchers have used the optical instrumented bolts to successfully measure the shear strain on the rock bolt in the laboratory and in-situ tests. However, there is a lack of research on analysing the recorded strain and using the data to calibrate the rock bolt model properties.

Numerical modelling as a tool for rock bolt reinforcement design was reviewed with examples of past research done in the field. Different approaches to modelling rock bolts in numerical models were also discussed. Substantial work has been done in modelling the axial behaviour and calibrating the axial response of rock bolts. The lack of research work in modelling shear behaviour and calibrating the shear response of rock bolts indicates the need for further improvement in the area.

References

ASTM. (2013). Standard Test Method for Rock Bolt Anchor Pull Test. In. West Conshohocken, PA: International ASTM.

Aydan, O., Kyoya, T., Ichikawa, Y., & Kawamoto, T. (1987). Anchorage Performance And Reinforcement Effect of Fully Grouted Rockbolts On Rock Excavations. Paper presented at the 6th ISRM Congress, Montreal, Canada. https://doi.org/

Aziz, N., & Jalalifar, H. (2007). Experimental and numerical study of double shearing of bolt under confinement.

Barton, N., Lien, R., & Lunde, J. (1974). Engineering classification of rock masses for the design of tunnel support. Rock mechanics, 6(4), 189-236.

Benmokrane, B., Chennouf, A., & Mitri, H. (1995). Laboratory evaluation of cement-based grouts and grouted rock anchors. Paper presented at the International Journal of Rock Mechanics and Mining Sciences & Geomechanics Abstracts.

Benmokrane, B., Chennouf, A., & Mitri, H. S. (1995). Laboratory evaluation of cement-based grouts and grouted rock anchors. International Journal of Rock Mechanics and Mining Sciences & Geomechanics Abstracts, 32(7), 633-642. doi:https://doi.org/10.1016/0148-9062(95)00021-8

Blanco Martín, L., Tijani, M., & Hadj-Hassen, F. (2011). A new analytical solution to the mechanical behaviour of fully grouted rockbolts subjected to pull-out tests. Construction and Building Materials, 25(2), 749-755. doi:10.1016/j.conbuildmat.2010.07.011

Blanco Martín, L., Tijani, M., Hadj-Hassen, F., & Noiret, A. (2013). Assessment of the bolt-grout interface behaviour of fully grouted rockbolts from laboratory experiments under axial loads. International Journal of Rock Mechanics and Mining Sciences, 63, 50-61. doi:10.1016/j.ijrmms.2013.06.007

Cai, Y., Esaki, T., & Jiang, Y. (2004). A rock bolt and rock mass interaction model. International Journal of Rock Mechanics and Mining Sciences, 41(7), 1055-1067. doi:https://doi.org/10.1016/j.ijrmms.2004.04.005

Cao, C., Nemcik, J., & Aziz, N. (2010). Advanced numerical modelling methods of rock bolt performance in underground mines. 2010 Underground Coal Operators' Conference, 326-329.

Cao, C., Nemcik, J., & Aziz, N. (2011). Improvement of rock bolt profiles using analytical and numerical methods.

Chen, J., Zhao, H., He, F., Zhang, J., & Tao, K. (2021). Studying the performance of fully encapsulated rock bolts with modified structural elements. International Journal of Coal Science & Technology, 8(1), 64-76. doi:10.1007/s40789-020-00388-z

Cording, E. J., & Mahar, J. W. (1978). Index properties and observations for design of chambers in rock. Engineering Geology, 12, 113-142. doi:https://doi.org/10.1016/0013-7952(78)90007-8

Dight, P. M. (1982). Improvements to the Stability of Rock Walls in Open Pit Mines: By Phillip M. Dight. Monash University,

Farmer, I. W. (1975). Stress distribution along a resin grouted rock anchor. International Journal of Rock Mechanics and Mining Sciences and, 12(11), 347-351. doi:10.1016/0148-9062(75)90168-0

Ferrero, A. M. (1995). The shear strength of reinforced rock joints. Paper presented at the International Journal of Rock Mechanics and Mining Sciences & Geomechanics Abstracts.

. FLAC3D — Fast Lagrangian Analysis of Continua in Three-Dimensions (Version 6.0). (2017). Minneapolis: Itasca: Itasca Consulting Group, Inc.

Forbes, B., Vlachopoulos, N., Diederichs, M. S., & Aubertin, J. (2020). Augmenting the in-situ rock bolt pull test with distributed optical fiber strain sensing. International Journal of Rock Mechanics and Mining Sciences, 126, 104202. doi:https://doi.org/10.1016/j.ijrmms.2019.104202

Forbes, B., Vlachopoulos, N., Hyett, A. J., & Valsangkar, A. (2018). The application of distributed optical strain sensing to measure the strain distribution of ground support members. FACETS, 3(1), 195-226. doi:10.1139/facets-2017-0093

Freeman, T. (1978). The behaviour of fully-bonded rock bolts in the Kielder experimental tunnel. Tunnels & Tunnelling International, 10(5).

Gale, W. J., Mark, C., Oyler, D. C., & Chen, J. (2004). Computer Simulation of Ground Behaviour and Rock Bolt Interaction at Emerald Mine. 21st International Conference on Ground Control in Mining, 27-34.

Gerdeen, J., Snyder, V., Viegelahn, G., & Parker, J. (1979). Design criteria for roof bolting plans using fully resin-grouted nontensioned bolts to reinforce bedded mine roof. Volume III: Experimental model studies; Volume IV: Theoretical analysis. In: Houghton, MI: Michigan Technological University. US Bureau of Mines contract.

Ghadimi, M., Shahriar, K., & Jalalifar, H. (2014). Analysis profile of the fully grouted rock bolt in jointed rock using analytical and numerical methods. International Journal of Mining Science and Technology, 24(5), 609-615. doi:https://doi.org/10.1016/j.ijmst.2014.07.009

Giot, R., Auvray, C., Raude, S., & Giraud, A. (2019). Experimental and numerical analysis of in situ pull-out tests on rock bolts in claystones. European Journal of Environmental and Civil Engineering, 1-24. doi:10.1080/19648189.2019.1626288

Grimstad, E., & Barton, N. (1993). Updating the Q-system for NMT. Proc. Int. Symp. on Sprayed Concrete, Fagernes, Norway 1993.

Goodman, R. E. (1989). Introduction to rock mechanics (Vol. 2, pp. 221-388). New York: Wiley.

Haas, C. J. (1976). Shear resistance of rock bolts. Trans. Soc. Min. Eng. AIME;(United States), 260(1).

Ho, D. A., Bost, M., & Rajot, J. P. (2019). Numerical study of the bolt-grout interface for fully grouted rockbolt under different confining conditions. International Journal of Rock Mechanics and Mining Sciences, 119, 168-179. doi:https://doi.org/10.1016/j.ijrmms.2019.04.017

Hoehn, K., Spearing, A. J. S., Jessu, K. V., Singh, P., & Pinazzi, P. C. (2020). The Design of Improved Optical Fibre Instrumented Rockbolts. Geotechnical and Geological Engineering, 38(4), 4349-4359. doi:10.1007/s10706-020-01246-0

Hyett, A., Forbes, B., & Spearing, S. (2013). Enlightening bolts: using distributed optical sensing to measure the strain profile along fully grouted rock bolts. Paper presented at the Proceedings of the 32nd international conference on ground control in mining.

Hyett, A., Moosavi, M., & Bawden, W. (1996). Load distribution along fully grouted bolts, with emphasis on cable bolt reinforcement. International Journal for Numerical and Analytical Methods in Geomechanics, 20(7), 517-544.

Hyett, A. J., Bawden, W. F., Macsporran, G. R., & Moosavi, M. (1995). A constitutive law for bond failure of fully-grouted cable bolts using a modified hoek cell. International Journal of Rock Mechanics and Mining Sciences & Geomechanics Abstracts, 32(1), 11-36. doi:https://doi.org/10.1016/0148-9062(94)00018-X

Jalalifar, H., & Aziz, N. (2010). Analytical behaviour of bolt–joint intersection under lateral loading conditions. Rock Mechanics and Rock Engineering, 43(1), 89-94.

Jalalifar, H., Aziz, N., & Hadi, M. (2006). The effect of surface profile, rock strength and pretension load on bending behaviour of fully grouted bolts. Geotechnical and Geological Engineering, 24, 1203-1227. doi:10.1007/s10706-005-1340-6

Jalalifar, H., Aziz, N. I., & Hadi, M. N. (2005). Rock and bolt properties and load transfer mechanism in ground reinforcement.

Jessu, K. V., Kostecki, T., & Spearing, S. (2016). Measuring roof-bolt response to axial and shear stresses: Laboratory and first in-situ analyses. The CIM Journal, 7(1), 62-70.

Jin-feng, Z., & Peng-hao, Z. (2019). Analytical model of fully grouted bolts in pull-out tests and in situ rock masses. International Journal of Rock Mechanics and Mining Sciences, 113, 278-294. doi:https://doi.org/10.1016/j.ijrmms.2018.11.015

Kaiser, P. K., Yazici, S., & Nosé, J. (1992). Effect of stress change on the bond strength of fully grouted cables. International Journal of Rock Mechanics and Mining Sciences & Geomechanics Abstracts, 29(3), 293-306. doi:https://doi.org/10.1016/0148-9062(92)93662-4

Kılıc, A., Yasar, E., & Celik, A. G. (2002). Effect of grout properties on the pull-out load capacity of fully grouted rock bolt. Tunnelling and Underground Space Technology, 17(4), 355-362. doi:https://doi.org/10.1016/S0886-7798(02)00038-X

Kostecki, T., Spearing, A., Forbes, B., & Hyett, A. (2015). New instrumented method to measure the true loading profile along grouted rockbolts.

Kostecki, T. R. (2019). Design Methods For Rock Bolts Using In-Situ Measurement From Underground Coal Mines. (Doctor of Philosophy Degree). Southern Illinois University Carbondale, Carbondale, Southern Illinois. Available from ProQuest

Kwitowski, A. J., Wade, L. V., & Mines, U. S. B. o. (1979). Reinforcement Mechanisms of Untensioned Full-column Resin Bolt: Department of the Interior, Bureau of Mines.

Li, C. (2000). Analytical study of the behavior of rock bolts. Paper presented at the 4th North American Rock Mechanics Symposium.

Li, C., & Stillborg, B. (1999). Analytical models for rock bolts. International Journal of Rock Mechanics and Mining Sciences, 36(8), 1013-1029.

Li, C. C. (2010). Field observations of rock bolts in high stress rock masses. Rock Mechanics and Rock Engineering, 43(4), 491-496.

Li, C. C. (2017). Principles of rockbolting design. Journal of Rock Mechanics and Geotechnical Engineering, 9(3), 396-414. doi:10.1016/j.jrmge.2017.04.002

Li, L., Hagan, P., Saydam, S., Hebblewhite, B., & Li, Y. (2016). Parametric study of rockbolt shear behaviour by double shear test. Rock Mechanics and Rock Engineering, 49(12), 4787-4797.

Li, Y., & Liu, C. (2019). Experimental study on the shear behavior of fully grouted bolts. Construction and Building Materials, 223, 1123-1134. doi:https://doi.org/10.1016/j.conbuildmat.2019.06.207

Liu, C., & Li, Y. (2020). Predicting the Shear Resistance Contribution of Passive Fully Grouted Bolts to Jointed Rock. International Journal of Geomechanics, 20(2), 04019174. doi:doi:10.1061/(ASCE)GM.1943-5622.0001581

Liu, C. H., & Li, Y. Z. (2017). Analytical Study of the Mechanical Behavior of Fully Grouted Bolts in Bedding Rock Slopes. Rock Mechanics and Rock Engineering, 50(9), 2413-2423. doi:10.1007/s00603-017-1244-9

Ma, S., Nemcik, J., & Aziz, N. (2013). An analytical model of fully grouted rock bolts subjected to tensile load. Construction and Building Materials, 49, 519-526. doi:10.1016/j.conbuildmat.2013.08.084

Ma, S., Nemcik, J., Aziz, N., & Zhang, Z. (2014). Analytical model for rock bolts reaching free end slip. Construction and Building Materials, 57, 30-37. doi:https://doi.org/10.1016/j.conbuildmat.2014.01.057

Ma, S., Nemcik, J., Aziz, N., & Zhang, Z. (2016). Numerical Modeling of Fully Grouted Rockbolts Reaching Free-End Slip. International Journal of Geomechanics, 16(1), 04015020. doi:doi:10.1061/(ASCE)GM.1943-5622.0000484

Ma, S., Zhao, Z., Nie, W., & Zhu, X. (2017). An Analytical Model for Fully Grouted Rockbolts with Consideration of the Pre- and Post-yielding Behavior. Rock Mechanics and Rock Engineering, 50(11), 3019-3028. doi:10.1007/s00603-017-1272-5

Ma, S., Zhao, Z., Peng, J., & Gui, Y. (2018). Analytical modeling of shear behaviors of rockbolts perpendicular to joints. Construction and Building Materials, 175. doi:10.1016/j.conbuildmat.2018.04.175

Ma, S., Zhao, Z., & Shang, J. (2019). An analytical model for shear behaviour of bolted rock joints. International Journal of Rock Mechanics and Mining Sciences, 121, 104019.

Mark, C., Pakalnis, R. T., & Tuchman, R. J. (2007). Proceedings of the International Workshop on Rock Mass Classification in Underground Mining.

McHugh, E., & Signer, S. (1999). Roof bolt response to shear stress: laboratory analysis. Paper presented at the Proceedings 18th international conference on ground control in mining, Morgantown, WV.

Moosavi, M., Jafari, A., & Khosravi, A. (2005). Bond of cement grouted reinforcing bars under constant radial pressure. Cement and Concrete Composites, 27(1), 103-109. doi:https://doi.org/10.1016/j.cemconcomp.2003.12.002

Nemcik, J., Ma, S., Aziz, N., Ren, T., & Geng, X. (2014). Numerical modelling of failure propagation in fully grouted rock bolts subjected to tensile load. International Journal of Rock Mechanics and Mining Sciences, 71, 293-300. doi:10.1016/j.ijrmms.2014.07.007

Obert, L., & Duvall, W. I. (1967). Rock mechanics and the design of structures in rock (Vol. 650): Wiley New York.

Pellet, F., & Egger, P. (1996). Analytical model for the mechanical behaviour of bolted rock joints subjected to shearing. Rock Mechanics and Rock Engineering, 29(2), 73-97.

Pinazzi, P., Spearing, A. S., Jessu, K., Singh, P., & Hawker, R. (2020). Mechanical performance of rock bolts under combined load conditions. International Journal of Mining Science and Technology.

Pratama, R., Bisri, T., & Fauziyyah, F. (2014). Wedge analysis for determining ground support demand in Pongkor GMBU Underground Mine PT. Antam (Persero) Tbk. In Mine Planning and Equipment Selection (pp. 431-445): Springer.

Radcliffe, D. E., Stateham, R. M., & Mines, U. S. B. o. (1980). Stress Distribution Around Resin Grouted Bolts: Department of the Interior, Bureau of Mines.

Serbousek, M. O., & Signer, S. P. (1987). Linear load-transfer mechanics of fully grouted roof bolts (Vol. 9135): US Department of the Interior, Bureau of Mines.

Si-si, L., Ming-hua, Z., & Liang, L. (2014). Analysis of dynamic broken line model based on experimental data of anchor anti-pullout. Rock and Soil Mechanics, 35(12), 3389-3395.

Signer, S. P. (1990). Field verification of load transfer mechanics of fully grouted roof bolts (Vol. 9301): Bureau of Mines, US Department of the Interior.

Signer, S. P. (2000). Load Behavior Of Grouted Bolts In Sedimentary Rock. Paper presented at the Proceedings: new technology for coal mine roof support. Mark C, Dolinar DR, Tuchman RJ, Barczak TM, Signer SP, Wopat PF, eds. Cincinnati, OH: U.S. Department of Health and Human Services, Public Health Service, Centers for Disease Control and Prevention, National Institute for Occupational Safety and Health, DHHS (NIOSH) Publication No. 2000-151; (IC 9453), 2000 Oct; :99-109, Cincinnati, OH.

Snell, G. (2021). The Effect of Shearing on Fully-grouted Rebar Rock Bolts in Saskatchewan Potash Mines. University of Saskatchewan,

Snell, G., Kuley, E., & Milne, D. (2017). A laboratory-based approach to assess rockbolt behaviour in shear. Paper presented at the Proceedings of the First International Conference on Underground Mining Technology.

Snyder, V., Gerdeen, J., & Viegelahn, G. (1979). Factors governing the effectiveness of roof bolting systems using fully resin-grouted nontensioned bolts. Paper presented at the 20th US Symposium on Rock Mechanics (USRMS).

Spearing, A. (1995). Handbook on hard-rock strata control: South African Institute of Mining and Metallurgy.

Spearing, A., & Gadde, M. (2011). Final report on NISOH funded project Improving underground safety by understanding the interaction between primary rock bolts and the immediate roof strata. NIOSH Project, BAA(2008-N), 10989.

Spearing, A., Gadde, M., Ray, A., Reisterer, J., & Lee, S. (2011). The initial performance of commonly used primary support on US coal mines. Paper presented at the Proceedings, 30th International Conference on Ground Control in Mining.

Spearing, A. J. S., Hyett, A. J., Kostecki, T., & Gadde, M. (2013). New technology for measuring the in situ performance of rock bolts. International Journal of Rock Mechanics and Mining Sciences, 57, 153-166. doi:10.1016/j.ijrmms.2012.07.027

Stillborg, B. (1986). Professional users handbook for rock bolting.

Stimpson, B. (1987). Estimating the degree of reinforcement of horizontally bedded roofs strengthened by non-tensioned, full-column grouted bolts. International Journal of Mining and Geological Engineering, 5(3), 273-284.

Thenevin, I., Blanco-Martín, L., Hadj-Hassen, F., Schleifer, J., Lubosik, Z., & Wrana, A. (2017). Laboratory pull-out tests on fully grouted rock bolts and cable bolts: Results and lessons learned. Journal of Rock Mechanics and Geotechnical Engineering, 9(5), 843-855. doi:10.1016/j.jrmge.2017.04.005

Thompson, A., Villaescusa, E., & Windsor, C. (2012). Ground Support Terminology and Classification: An Update. Geotechnical and Geological Engineering, 30. doi:10.1007/s10706-012-9495-4

Tulu, I., Esterhuizen, G., & Heasley, K. (2012). Calibration of FLAC3D to simulate the shear resistance of fully grouted rock bolts. Paper presented at the 46th US Rock Mechanics/Geomechanics Symposium.

Vlachopoulos, N., Cruz, D., & Forbes, B. (2018). Utilising a novel fiber optic technology to capture the axial responses of fully grouted rock bolts. Journal of Rock Mechanics and Geotechnical Engineering, 10(2), 222-235. doi:https://doi.org/10.1016/j.jrmge.2017.11.007

Wang, R., Bai, J.-b., Yan, S., Song, Y.-b., & Wang, G.-d. (2020). An Improved Numerical Simulation Approach for the Failure of Rock Bolts Subjected to Tensile Load in Deep Roadway. Geofluids, 2020, 8888390. doi:10.1155/2020/8888390

Yokota, Y., Zhao, Z., Nie, W., Date, K., Iwano, K., & Okada, Y. (2019). Experimental and Numerical Study on the Interface Behaviour Between the Rock Bolt and Bond Material. Rock Mechanics and Rock Engineering, 52(3), 869-879. doi:10.1007/s00603-018-1629-4

Yu, S., Zhu, W., Niu, L., Zhou, S., & Kang, P. (2019). Experimental and numerical analysis of fully grouted long rockbolt load-transfer behavior. Tunnelling and Underground Space Technology, 85, 56-66. doi:https://doi.org/10.1016/j.tust.2018.12.001

Zhang, K., Zhang, G., Hou, R., Wu, Y.-S., & Zhou, H. (2015). Stress Evolution in Roadway Rock Bolts During Mining in a Fully Mechanized Longwall Face, and an Evaluation of Rock Bolt Support Design. Rock Mechanics and Rock Engineering, 48. doi:10.1007/s00603-014-0546-4

Zipf, K. (2006). Numerical modeling procedures for practical coal mine design. Paper presented at the Golden Rocks 2006, The 41st US Symposium on Rock Mechanics (USRMS).

Chapter 3. Establishing the Need to Model the Actual State of Stress along Rock Bolts

This chapter has been accepted and published in International Journal of Mining Science and Technology as:

Singh, P., Spearing, A. S., Jessu, K. V., & da Silva Ribeiro, P. C. P. (2020). Establishing the need to model the actual state of stress along rock bolts. International Journal of Mining Science and Technology, 30(3), 279-286.

Abstract

Proper design of rock bolt support in underground mines is critical to avoid incidents, accidents and loss of production. The traditional design approach only considers the axial (tensile) capacity and this is clearly not the situation in situ, where a rock bolt is subjected to both axial and shear/bending loads which determines its overall performance and failure behaviour. To demonstrate and analyse the shear displacement in bedded roof, scaled physical models of underground excavation were created. From the models it was found that the shear displacement between the layers depends on the vertical roof deformation and thickness of beds. To analyse the effect of combined loading on rock bolt design for suspension and beam building models, analytical methods were used to calculate the required spacing of rock bolt for a given safety factor. Numerical models were then created using Rocscience RS2 software to establish the stresses on the rock bolt. The results show a significant reduction in safety factor for suspension as demonstrated in an example (reduced from 3.5 to 2.0) and beam building (2.0 to 1.36) when the rock bolt capacities are calculated considering the effect of combined loading as opposed to just the axial or shear loads.

Keywords – Combined loading; rock bolt; suspension model; beam building model; numerical modelling; analytical methods.

3.1 Introduction

Fully grouted rock bolts are the most common type of supports used in underground mines (Windsor, 1997). For a reliable rock bolt support design, it is important to understand the effect of different loads acting along the rock bolt length. All of the rock bolt support design methodologies currently used in underground mines only take into account the axial or shear loading of the rock bolt (Mark, 2000; Tang & Peng, 1984). However, a rock bolt installed across a discontinuity such as a joint or a bedding plane undergoes combined axial and shear

loading. If the effect of combined loading on the rock bolt failure behaviour is not considered and the rock bolt support is designed only for single mode of loading such as axial, it might fail in shear or combined axial and shear load. This study aims to show why knowing the actual loading capacity is important when designing support and how combined axial and shear loading effects the overall capacity of the rock bolt.

In a multi bedded or a laminated roof, the mechanism of roof failure is usually considered through the pressure arch theory (Luo, 1994). Due to the excavation, the zone above the roof is de-stressed which causes the underlying bedding layers to sag and separate from the main roof. The bedded layers sag under their weight and horizontal stress, leading to inter layer movement causing both tension and shear in the bedded roof. This could lead to roof failure if the roof convergence and inter layer shear is not controlled and restricted. Depending on the local geology, the rock bolt design methodologies used for bedded roof are modifications of either suspension or beam building concept (Luo, 1994). Suspension and beam building method consider only single mode of loading axial and shear respectively (Obert & Duvall, 1967; Stimpson, 1987) to calculate the required rock bolt support and therefore lead to insufficient reinforcement.

3.1.1 Suspension

Support design in suspension method is based on supporting the deadweight of the weak layers. This assumes axial loading which is clearly incorrect as the beams bend under loading and reach a maximum in the centre of the roof span and almost zero on the pillar (or intact rock) sides. The rock bolts are anchored in the overlying intact roof and therefore are designed to carry the weight of the weaker layers below (Figure 3.1a).

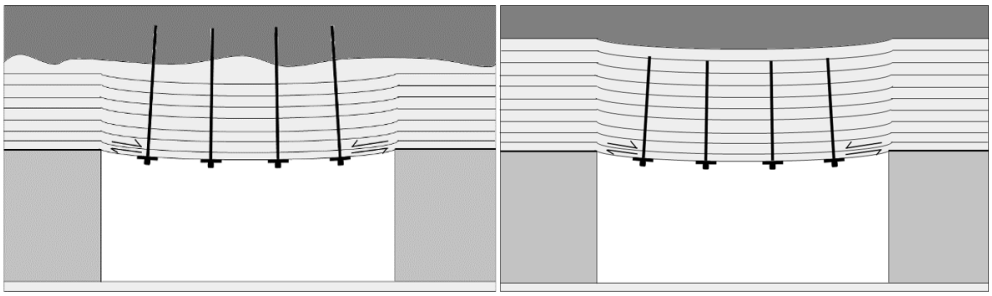

a) b)

Figure 3.1 – a) Suspension support method b) Beam Building support method (modified from Luo (1994))

Obert & Duvall (1967) proposed a simple equation to calculate the load carried by each bolt based on the weight of the weak layers. It was assumed that the weak layers completely separate from intact roof and the load of layers carried by pillars was ignored. The minimum required bolt spacing can be calculated from the Obert & Duvall equation as:

$$b = \left(\frac{P}{U * t}\right) * \frac{1}{SF} \tag{3.1}$$

Where, b is bolt spacing, P is the bolt capacity, U is the unit weight of rock, t is thickness of roof and SF is the safety factor.

Tang & Peng (1984) gave a similar equation to calculate the load on the rock bolts. Unal (1984) calculated the thickness of roof to be supported using the excavation width and rock quality (RMR). These methods are still commonly used for rock bolt support design in underground mines. In these studies only the axial capacity of the rock bolt required to hold the weight of the rock is considered. However, inter-layer shear caused by bending in the bedded roof will cause a shear load in a rock bolt. The rock bolt will therefore be under a combined axial and shear load at various positions along its length and this effectively reduces its axial capacity (Pellet & Egger, 1996).

3.1.2 Beam building

The presence of an intact strong zone so near the immediate roof is not always the case and therefore another concept called beam building is used to stabilise the roof (Gerdeen et al., 1977). In beam building, the individual thin layers of bedded roof are bolted together to form a composite beam of greater thickness (Figure 3.1b) which increases the strength and stiffness of the roof (Panek, 1956). In this method the rock bolt support design is based on the shear capacity of the rock bolt to stop the inter layer movement by the dowel action.

Panek (1956) conducted theoretical and experimental studies on the beam building mechanism and on the effect of bolt spacing, bolt tension, number of layers and roof span on beam building. He found the normal force provided by the tensioned bolts increases the friction between the bedding layers to be the main mechanism producing beam building. Jeffery & Daemen (1983) concluded that in a bedded roof it is not possible to completely eliminate bed separation and slip. The roof is reinforced by the resistance of fully grouted rock bolt to both shear and normal displacement. Stimpson (1987) developed an analytical analysis of the rock bolt support required to reinforce a horizontally bedded or laminated roof. The rock bolt spacing was established by calculating the maximum shear in a clamped beam of thickness equal to the thickness of roof and the maximum shear resistance of the rock bolt. The bolt spacing for beam building was calculated assuming uniform loading over the beds and rock bolt row spacing equal to bolt column spacing. The equation for calculating bolt spacing, assuming uniform loading over beds and bolt row spacing equal to bolt column spacing is (Stimpson, 1987):

$$b = \frac{-F + (F^2 + 1.5\gamma L^3 F)^{1/2}}{0.75\beta\gamma L^2} \tag{3.2}$$

Where, b is the bolt spacing, L is span of opening, F is maximum shear resistance of a single bolt, γ is rock density and β is the load multiplier at abutment. The maximum shear resistance or dowel force (F) of the rock bolt is calculated by:

$$F = \frac{D_b^2}{4}(1.7\sigma_y \pi P_u(1 - (T/T_y)^2))^{1/2} \tag{3.3}$$

Where, D_b is the diameter of bolt, σ_y is the yield strength of bolt material, P_u is the bearing capacity of rock or grout, T_y is the yield strength of bolt and T is the tension in bar at plastic moment. The dowel effect of the rock bolt for providing resistance to the bed slippage is considered in the equation 3.2. However, the axial load on the rock bolt is not taken into account. The combined axial and shear load on the rock bolt changes the shear capacity of the rock bolt and therefore should be considered while designing rock bolt support.

Rock bolt behaviour only under axial load is simple and generally well understood (although clearly not accurate). Studies done by Farmer (1975), Freeman (1978), Li (1999) and Martin et al. (2011) describe the rock bolt behaviour under axial loading. Shear behaviour of a fully grouted rock bolt under in-situ conditions is much more complex and many studies (Dulacska, 1972; Bjurstrom, 1974; Dight, 1983; Pellet & Egger, 1996) have been done to describe the rock bolt's response to shear. One of the most commonly used analytical model for shear response of rock bolt was proposed by Dight (1983). The dowel force (F) in a rock bolt installed across a joint was calculated as:

$$F = \frac{D^2}{4}\sqrt{1.7\sigma_y P_u \pi[1 - \left(\frac{T}{T_y}\right)^2]} \tag{3.4}$$

$$P_u = \sigma_c \left[\frac{\delta}{K(\pi D + 2\delta)}\right]^{A/2} \tag{3.5}$$

$$A = \frac{2sin\emptyset}{1 + sin\emptyset} \tag{3.6}$$

$$K = \sigma_c \left(\frac{1 - \vartheta^2}{E}\right) \ln\left(\frac{\sigma_c}{2P_0 - \sigma_t}\right) + \frac{\sigma_c}{2P_0 - \sigma_t}[\frac{2\vartheta(P_0 - \sigma_t) - \sigma_t}{E} \tag{3.7}$$

Where, σ_y and T_y are the yield stress and yield force in the bolt respectively, σ_c is the unconfined compressive strength of rock, σ_t is the tensile strength of rock, ϕ is the internal friction angle of rock, υ and E are Poisson's ratio and elastic modulus of rock respectively, P_0 is the initial stress in the rock in the plane of the joint, δ is the shear displacement of the joint and T is the initial bolt pretension.

A rock bolt installed across a joint resists joint shear by dowel action (Figure 3.2). The rock bolt bends and forms hinge near the joint. As the rock bolt is symmetric around the dotted line, the forces acting only on the bolt section 'AO' is shown. The Dowel force (F) acting on the bolt at point 'O' is the resistance provided by the rock bolt to joint shearing. Rocscience RS2 software uses a modified form of Dight's model for shear response of rock bolt. The model considers dowel force only due to the shear load S in the rock bolt. However, in a fully grouted rock bolt dowel force (F) will be resultant of both the shear (S) and axial (N) loads in the rock bolt. The failure of the rock bolt will also be determined by the combined effect of axial and shear load.

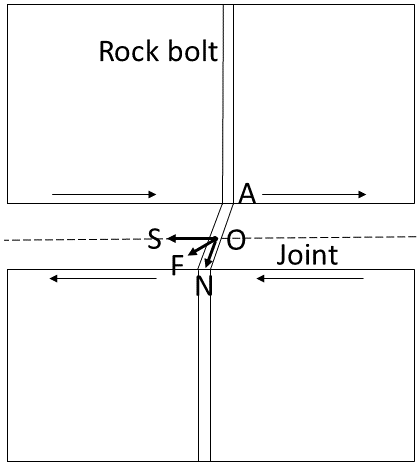

Figure 3.2– Dowel action of rock bolt.

Pellet & Egger (1996), proposed a new analytical model for shear resistance of a joint due to a rock bolt. The dowel force of the rock bolt was calculated using both axial and shear load in the rock bolt generated due to joint shearing caused by sliding across the joints or beds. The bolt was considered to fail in combined axial and shear loading. The relationship for axial and shear load at failure in a rock bolt is given by Pellet & Egger (1996):

$$S_f = \frac{\pi D_b^2}{8}\sigma_{ec}\sqrt{1 - 16\left(\frac{T_f}{\pi D_b^2 \sigma_{ec}}\right)^2} \tag{3.8}$$

Where, T_f is the axial load at failure, D_b is bolt diameter, S_f is shear load at yield and σ_{ec} is failure stress for bolt material.

To calculate the shear load in the bolt at the bolt-joint intersection when the bolt is in elastic state, the following relationship is used (Pellet & Egger, 1996):

$$U_e = \frac{8192 S_e^4 b}{E\pi^4 D_b^4 p_u^3 sin\beta} \qquad (In\ elastic\ stage) \qquad (3.9)$$

Where, S_e is the elastic shear load, b is the constant (value = 0.27), D_b is the diameter of bolt, E is the elastic modulus of bolt, p_u is the bearing capacity of rock, β is the angle between bolt and joint and U_e is the shear displacement. The model considered that after yield point only the axial load in the rock bolt increases with further joint displacement. Following relationship was given to calculate shear load at yield point (Pellet & Egger, 1996) –

$$S_e = \frac{1}{2}\sqrt{p_u D_b \left(\frac{\pi D_b^2 \sigma_{el}}{4} - T_e\right)} \qquad (At\ yield\ point) \qquad (3.10)$$

Where, T_e is the axial load in bolt at yield and σ_{el} is the yield stress for bolt material.

Their model considered the effect of axial and shear loads on rock bolt failure caused due to the shear loading of the bolt. However, such models do not consider the effect of axial load on rock bolts generated due to axial stress in the rock or joint opening (Figure 3.3).

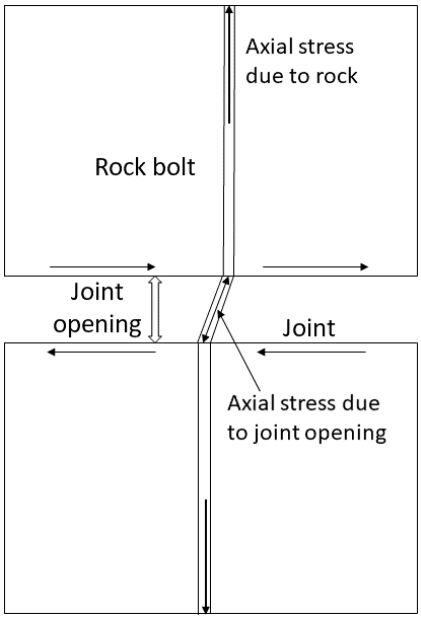

Figure 3.3 - Axial load on rock bolt due to axial stress in the rock and joint opening.

Instrumented rock bolts can be used to better understand the effect of combined loading on rock bolts. Distributed optical sensing instrument are found to be advantageous over discrete measurement instruments like foil resistance strain gauges as they provide strain profile over the complete length of rock bolt. Hyett and Spearing (2013) used distributed optical sensing technology based on Rayleigh backscattering to measure strain on rock bolts under different loading conditions. Kostecki et al., (2016) showed that at least three slots were essential for correct measurement of bending and shear loads. It was shown that optical sensors combine the advantages of both long base-length and short-base length strain gauges. Jessu et al., (2016) used distributed optical sensing instrument to conduct shear loading test with rock bolts installed perpendicular, and at an angle of 80^0 to the discontinuity. Li et al., (2016) conducted double shear tests on different types of bolts to test their behaviour under combined axial and shear loading. Pretension in bolt increased the shear strength of bolted joints while reducing the shear displacement at failure. The elastic modulus of rock bolt and the normal tension in bolts were found to have a considerable effect on shear stiffness of the joint after the yield point of bolt. Snell et al., (2017) investigated the effect of gap size on failure behaviour of rock bolts grouted in steel pipes and undergoing double shear. It was found that increasing gap size reduced the stiffness, yield strength and ultimate strength of the bolt. A more significant effect was observed in magnitude of displacement (increasing) at failure with increasing gap size. These studies demonstrate the effect of axial, shear and combined axial and shear loading on the rock bolt behaviour by changing its ultimate strength, stiffness and failure process. Therefore, rock bolt designs based solely on the axial strength of the rock bolt are insufficient.

A rock bolt installed in a bedded roof is subjected to shear loading due to inter layer movement, and an axial load due to roof convergence. The shear between the beddings is analysed using physical models of underground excavation with bedded roof. Numerical models are then calibrated to the results of physical models to further analyse the shear in bedded roofs and validate the results.

The effect of combined loading on rock bolt support design is analysed with an example of an underground excavation in a coal mine with bedded roof. The analysis is undertaken for rock bolt design in suspension and beam building. Analytical methods are used to calculate the required bolt spacing. Then numerical models of the rock bolt support is made for both suspension and beam building using Rocscience RS2. The axial and shear stresses on the rock bolts in the numerical models are analysed and compared with analytical results. The results of the numerical model are used to analyse the effect of combined loading on rock bolt support and hence the factor of safety.

3.2 Shear Displacement in Bedded roof

3.2.1 Physical modelling of shear displacement in bedded roof

Physical models of bedded roof above an underground excavation were created and loaded vertically to simulate roof convergence. The shear displacement between the layers due to inter layer slip and roof convergence was measured and analysed.

The physical model was undertaken using wooden slats with an excavation width and height of about 500 mm and 156 mm respectively (Figure 3.4a) in order to have similar width to height ratio as in an underground opening of 6 m width and 2 m height. Wood was used to simulate the bedded roof considering the low cost and ease of constructing the model. Wood also having large elastic limit and therefore will be able to undergo high deformation without breaking. Wood has relatively consistent properties if there are no characteristics like knots, cross grains, checks, and splits. The wooden slats were chosen such that no such characteristics were present. The physical models were developed with three bed thickness of 12 mm, 19 mm and 30 mm for a total roof height of 168 mm, 228 mm and 210 mm respectively. Straps and bolts were used to hold the model from buckling and slippage. Load was applied using the hydraulic cylinder (Figure 3.4a) at the top of model above the centre of an excavation. The shear measurements were taken after every 10 mm vertical displacement of the roof as shown in Figure 3.4b. To analyse the shear between the layers in the roof, straight vertical lines were drawn across the roof at five positions before the test: -200 mm, -100 mm, 0 mm, 100 mm and

200 mm, where 0 mm denotes the centre of the roof. The space between the lines is further marked at intervals of 10 mm to measure shear along the joints (Figure 3.4). As the layers sheared across one another the lines became staggered clearly depicting the shear displacement between the layers.

a) b)

Figure 3.4 - a) Physical model setup (12mm beds). b) Model undergoing increasing vertical displacement (10mm to 60mm).

3.2.2 Results of Physical Modelling

Shear displacements along the roof at a height of 12 mm is plotted at the points shown in Figure 3.5a. Figure 3.5b shows the change in shear displacement at these points with increasing vertical deformation of roof for the model with 12mm thick beds. It was observed that the shear displacement between the roof layers increased with the increase in vertical displacement of roof. It can also be observed that there is minimal shear displacement at the centre of the excavation and increasing shear displacement towards the pillar (Figure 3.5b).

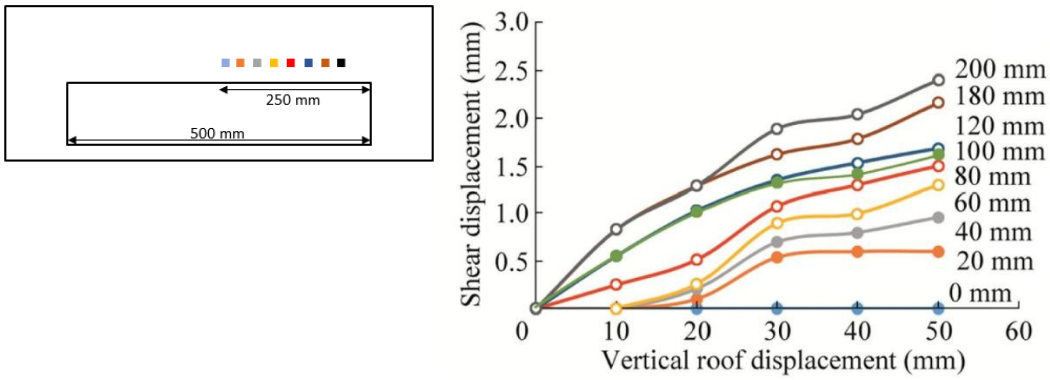

a) b)

Figure 3.5 - a) Plot lines position in model b) Shear Displacement (12 mm above roof) vs vertical displacement of roof.

Shear displacements at 20 mm and 30mm vertical roof displacement were plotted for all three different bed thickness. The shear displacements are plotted along the lines shown in Figure 3.6a. For both 20 mm and 30 mm roof vertical displacement, shear displacement was found to increase with bed thickness. This shows that the shear displacement in bedded roof is dependent on the bed thickness. Shear displacement between layers decreases with height above the roof up to a height of 40 mm for 12 mm and 19 mm thick beds, and up to 60 mm for 30 mm thick beds, after which the shear displacement remains constant with height.

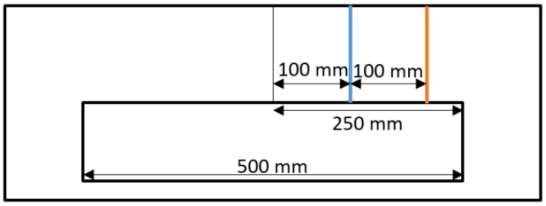

a)

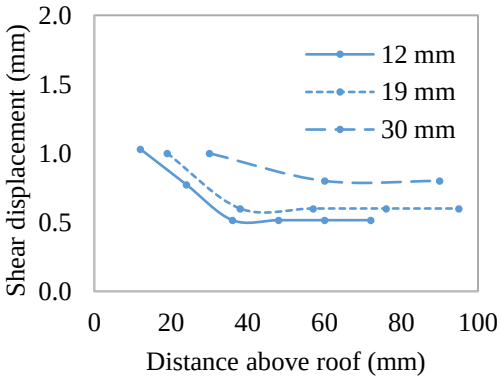

b)

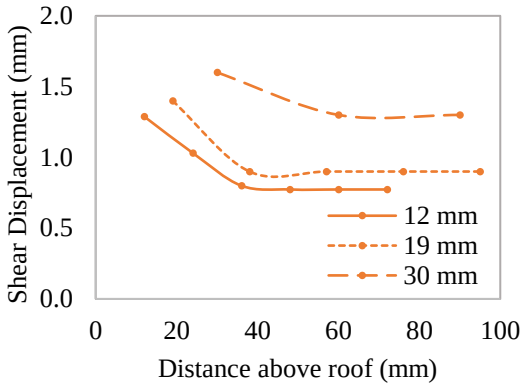

c)

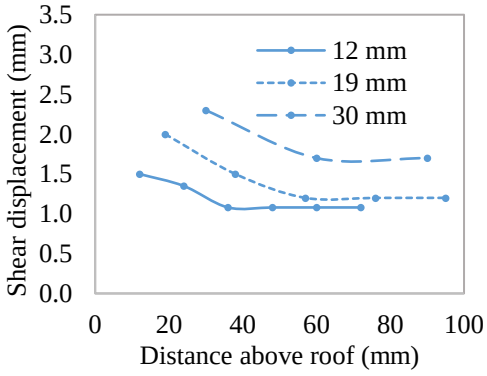

d)

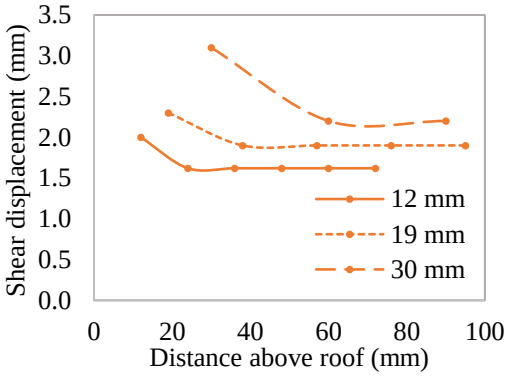

e)

Figure 3.6 – a) Location of Plot lines in the model. Comparison of shear displacement in beds with different thickness at b) 100 mm line at 2 cm roof vertical displacement c) 200 mm line at 2 cm roof vertical displacement d) 100 mm line at 3 cm roof vertical displacement e) 200 mm line at 3 cm roof vertical displacement.

3.2.3 Numerical modelling of shear displacement in bedded roof

Numerical models were developed and calibrated to the physical models so that further analysis can be conducted to study the shear in bedded roof. The results from the physical model were used to calibrate the numerical models using RS2 (Rocscience, 2018) software. The numerical model was constructed with the same dimensions as the physical model (Fig 7). The numerical model was unconstrained on the sides while at the bottom it was bounded in both x and y directions. The joints were made with similar spacing as in the physical model; that is 12 mm, 19 mm and 30 mm. The model was loaded at the top with a uniform force and the magnitude of the force was adjusted so that the immediate roof of the excavation shows similar vertical deformation as the physical model. As it was not possible to measure the mechanical properties of wood easily the calibration of the numerical model was done by varying the load and matching the roof displacement with that of physical model.

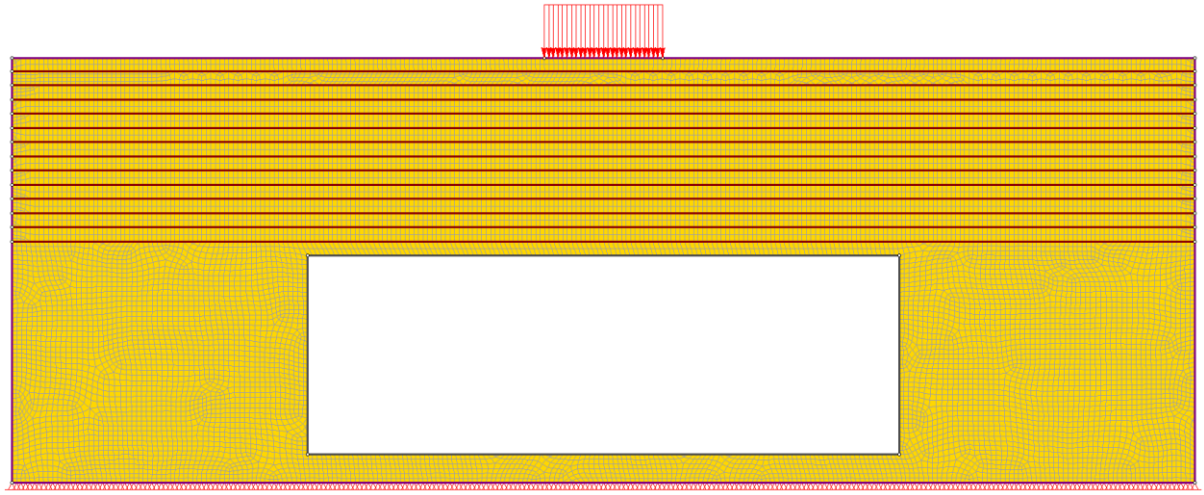

Figure 3.7 – Numerical model of bedded roof.

3.2.4 Results of numerical modelling of shear displacement in bedded roof

The results of the physical model and numerical models for different bed thickness with 30mm of vertical roof deformation are shown in Figure 3.8a, 3.8b and 3.8c. The shear displacements shown in the plots are at the first and second simulated joints from the roof of the excavation. From the plots, it can be seen that the behaviour of shear displacement in all three physical models is the same. The shear displacement at the centre of the excavation is zero in all three cases which is logical and to be expected. The shear displacement increases towards the corner

and is highest at approximately 60 to 80 mm from the corner. The shear displacement then again starts to decrease towards the corner of the excavation. This behaviour is similar to the bending behaviour in clamped beams. The shear displacement in clamped beams is zero at centre and then increases towards the corners. It reaches a maximum and then becomes zero at the corner. The shear displacement in the physical model and the numerical model decreases but does not become zero at corners. This is because the layers are not perfectly clamped and some inter-layer shear occurs at the ends of the layers clamped above the pillars.

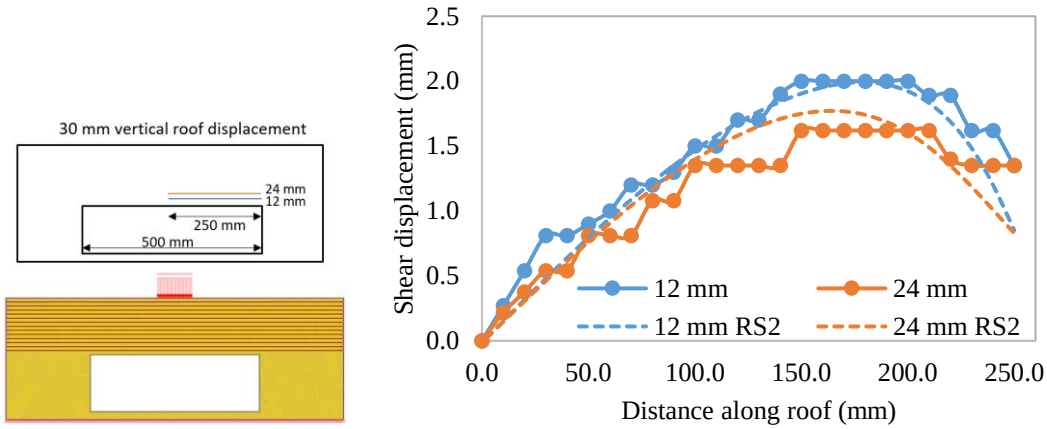

a)

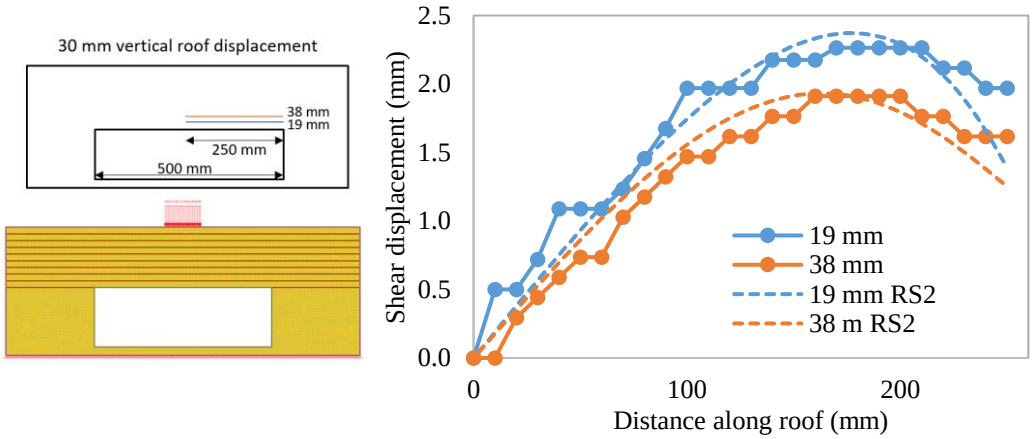

b)

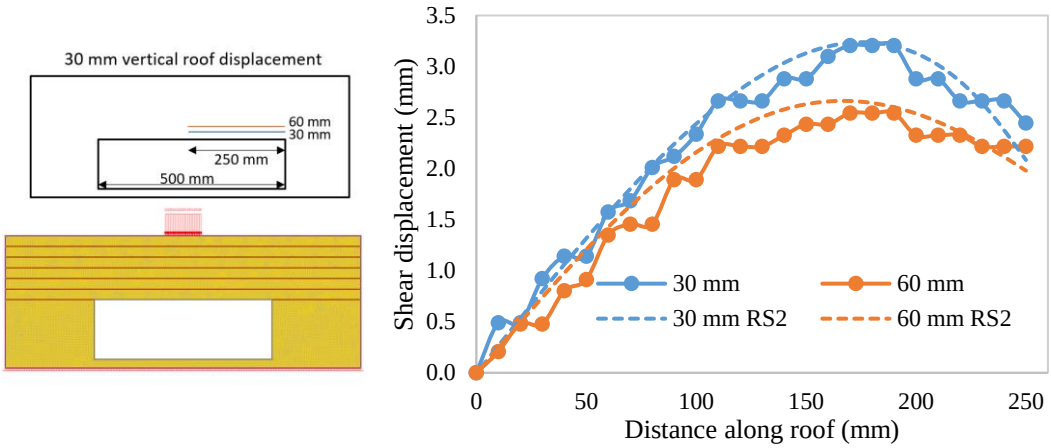

c)

Figure 3.8 – Shear displacement in roof at 30mm vertical displacement with a) 12 mm bed thickness b) 19 mm bed thickness c) 30 mm bed thickness.

3.2.5 Analytical analysis of shear stress in beams

When two beams undergo bending, shear displacement takes place between them (Figure 3.9a). In beam building, the individual thin layers of bedded roof are bolted together to form a composite beam of greater thickness (Figure 3.9b) which increases the strength and stiffness of the roof (Stimpson, 1987).

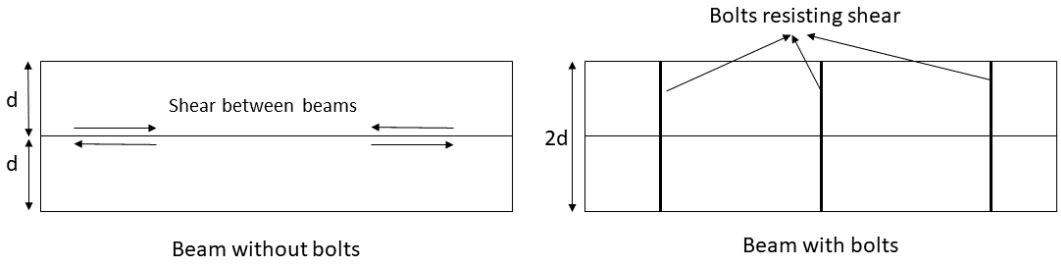

a) b)

Figure 3.9 – a) Individual beams of thickness ‘d’ b) Composite beam of effective thickness ‘2d’.

In an effective composite beam there should not be any shear displacement between the layers (Figure 3.9b). Therefore, the shear stress between the layers will be equal to the shear stress in a single beam of equal thickness to the composite beam. The rock bolts should be able to

provide this shear stress to resist the shear movement. In a beam the shear stress is distributed parabolically along its section, with the highest shear at the neutral axis (Figure 3.10).

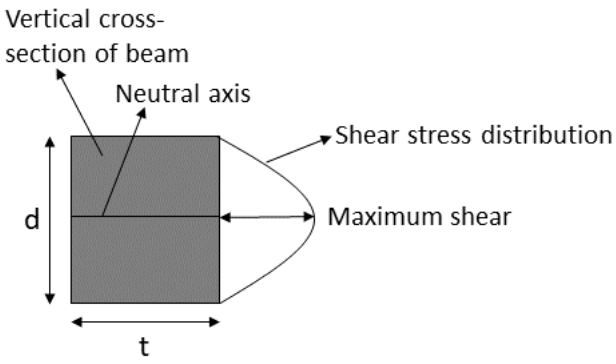

Figure 3.10 – Shear stress in a vertical cross-section of beam (Stimpson, 1987).

Therefore, the shear resistance of the rock bolt should be equal to the shear stress at the neutral axis of the composite beam. As the bedded layers in an underground excavation act like a clamped beam the shear stress in the beam can be calculated using the classical beam theory (Stimpson, 1987). According to the classical beam theory (Timoshenko, 1983) the transverse shear stress in a uniformly loaded clamped beam (Figure 3.11) is calculated using the equation:

$$\tau = \frac{VQ}{It} \tag{3.11}$$

$$V = W\left(\frac{L}{2} - x\right) \tag{3.12}$$

$$Q = \frac{td^2}{8} \tag{3.13}$$

$$I = \frac{td^3}{12} \tag{3.14}$$

Where, τ is the shear stress, V is the shear load, Q is the first moment of cross-sectional area, I is the second moment of inertia, t is the beam width, W is the load on beam and d is the beam thickness.

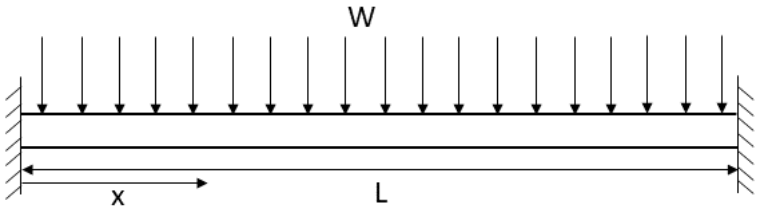

Figure 3.11 – Uniformly loaded clamped beam.

Equation 3.11 shows that the shear stress in the beam is inversely proportional to the thickness of the beam ‘d’ and directly proportional to the load ‘W’. Therefore, a thick beam will be stiffer than a thin beam. In the physical models the thicker beds showed higher shear displacement than thinner beds. This was because the shear displacement in the layers was compared at equal vertical deformation of the roof, not at equal vertical loads. The thicker layers required higher load to achieve the same vertical deformation as thinner layers. Therefore, in an excavation, an immediate roof with thick beds will show less vertical deformation and shear than a roof with thin beds under the same stress conditions. However, if the roof vertical deformation is same in both case, the roof with thicker beds will have a higher shear generated across the beds than a roof with thinner beds.

3.3 Effect of combined loading on rock bolt support design

The effect of combined loading as opposed to just considering axial loading on rock bolt support design is compared with an example of an underground excavation in a coal mine. The excavation width and height is assumed to be 6m and 2m respectively. The excavation depth is taken as 200m and horizontal to vertical stress ratio is taken as 3:1. The excavation is made in a coal seam with the immediate roof of bedded siltstone. It is assumed that separation of the weak layers will occur as is common in bedded roofs in coal mines and therefore the shear stiffness of the joints is considered to be zero (Stimpson, 1987). The normal stiffness of the joints is taken as 50 GPa/m (Barbato et al.,2016). The siltstone layer is overlaid by sandstone that acts as the competent roof. The mechanical properties of the rocks are based on Zingano

et al., 2009. The mechanical properties of the rocks is given in Table 3.1. General properties of the structural steel are used for rock bolt. Rock bolt properties are given in Table 3.2.

Table 3.1 – Material Properties (Zingano et al., 2009)

Material	**Elastic modulus (GPa)**	**Poisson's ratio**	**Tensile strength (MPa)**	**Friction angle**	**Cohesion (MPa)**	**Unit weight (MN/m^3)**
Sandstone	9	0.18	5	30	4.33	0.025
Siltstone	3.5	0.25	2.4	30	2.11	0.025
Coal	3.25	0.3	2.6	25	2.07	0.019

Table 3.2 – Rock bolt Properties (ASTM, 2014)

Rock bolt	**Elastic modulus (GPa)**	**Yield strength (kN)**	**Length (m)**	**Diameter (mm)**
Fully –grouted	200	125	1.8	19

3.3.1 Suspension

The suspension method is assumed where a competent rock is present above a thin layer of bedded immediate roof. For analysing the effect of combined loading on suspension rock bolt design, the thickness of immediate siltstone layer above the excavation is kept as 1.5m. The rock bolt spacing is first calculated using analytical method and then the loads on the rock bolt is analysed using numerical models.

Analytical method for suspension rock bolt support

The bolt spacing for suspension roof is calculated using Equation 3.1 (Obert & Duvall, 1967). In this calculation the row spacing is taken as 1 m to simplify the calculation. Using a desired safety factor of 3.5, bolt tensile strength (P) of 125 kN, rock unit weight (U) of 0.025 MN/m^3

and roof thickness (t) of 1.5m, the bolt spacing is calculated as 0.95 ≈ 1 m. As a safety factor value of 3.5 is considered in rock bolt design, each rock bolt will have an axial load 3.5 times less than its tensile strength i.e. 35.7 kN or 125.7 MPa.

Numerical modelling of suspension rock bolt support

Two-dimensional models of the excavation were created using Rocscience RS2 software. Firstly, a model with immediate roof thickness of 1.5m without joints in the immediate roof was simulated to understand the loads on rock bolt (Figure 3.12a). Then joints were added to the immediate roof to analyse and calculate the combined loading on rock bolt (Figure 3.12b). Joint spacing in the immediate siltstone roof is 0.5m. The parameters of the numerical model are kept the same as previously described. The sides of the model are bounded in x-direction while the bottom of the model is bounded in both x and y directions. A load equal to the weight of overburden is applied at the top of the model. Fully grouted rock bolts are installed in the roof of the excavation. The numerical model was made with bolt spacing of 1m as calculated using Equation 3.1. As the excavation width is 6m there are total 5 rock bolts installed with 1m spacing. The model is calibrated by changing the overburden depth and matching the bolt stress with analytical result.

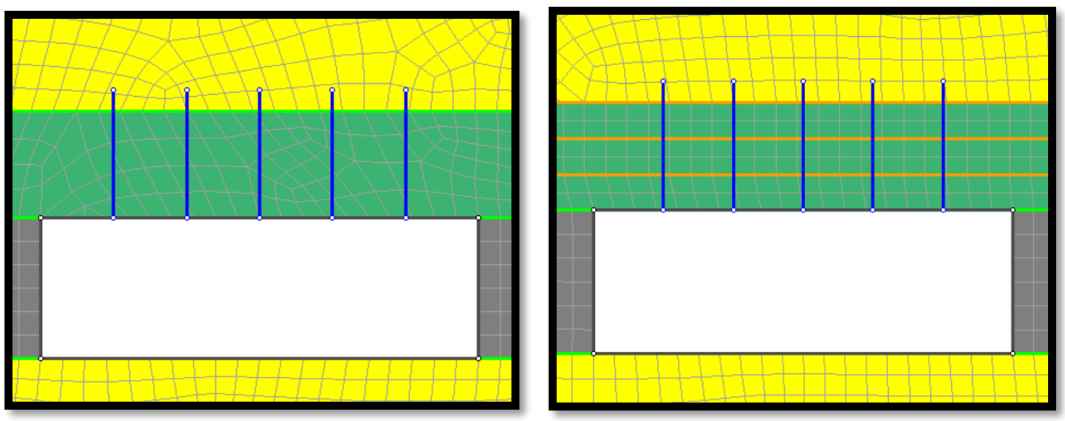

a) b)

Figure 3.12 – Two-dimensional model of suspension roof a) without joint b) with joint.

Analysis of the effect of shear load on axial capacity of rock bolt

The axial stress on the corner bolt (2m from center) in the models with and without the joint is shown in Figure 3.13. The axial stress on the rock bolt in the model without the joint matched with the axial stress calculated using Equation 3.1. The stress in the bolt is highest near roof surface and decreases away from it. The sudden drop near the end is due to presence of material boundary. In the model with joints, the axial load on the rock bolt at the intersection of rock bolt and joint at 0.5m from roof is 212 MPa or 60 kN. The axial load is higher than the load predicted by equation 3.1 (Obert & Duvall, 1967) due to the shear induced axial load in the bolt at the joint intersection. This increase in axial load can be seen in Figure 3.13 at 0.5, 1 and 1.5m points (rock bolt-joint intersections) along the rock bolt. Figure 3.14 shows the shear displacement in the rock bolt at the bolt-joint intersections. The shear displacement is highest in the joint near the roof and decreases with height. The behaviour is similar to the shear displacement observed in the physical model. The increase in shear displacement in the joint 1.5 m above roof is due to the joint being in between two different materials. The weaker siltstone deforms more than the overlying sandstone leading to higher relative movement between the layers. Figure 3.13 and 3.14 shows that the bolt is under a combined axial and shear loading. To analyse the effect of shear load on axial capacity, loads on the corner most bolt (2m from centre) in the model with joints are analysed.

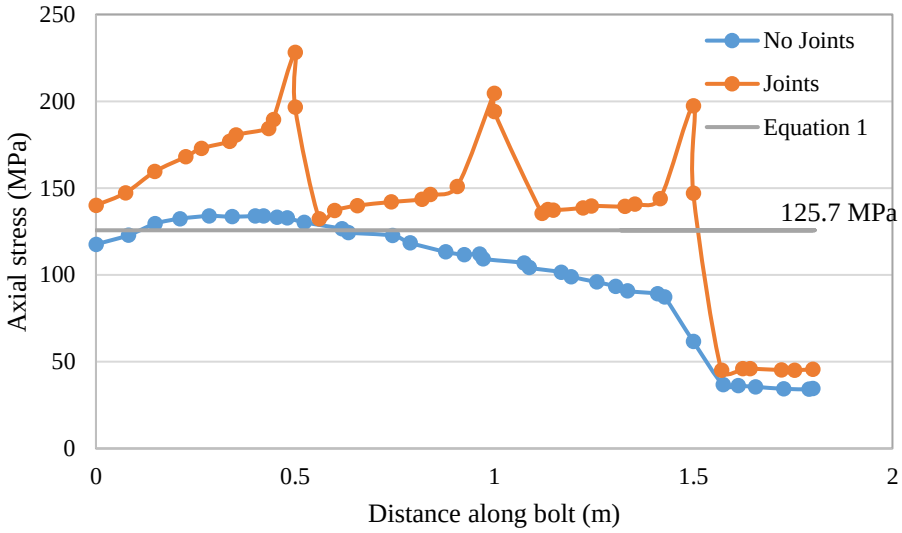

Figure 3.13 – Axial stress in bolt with and without joints.

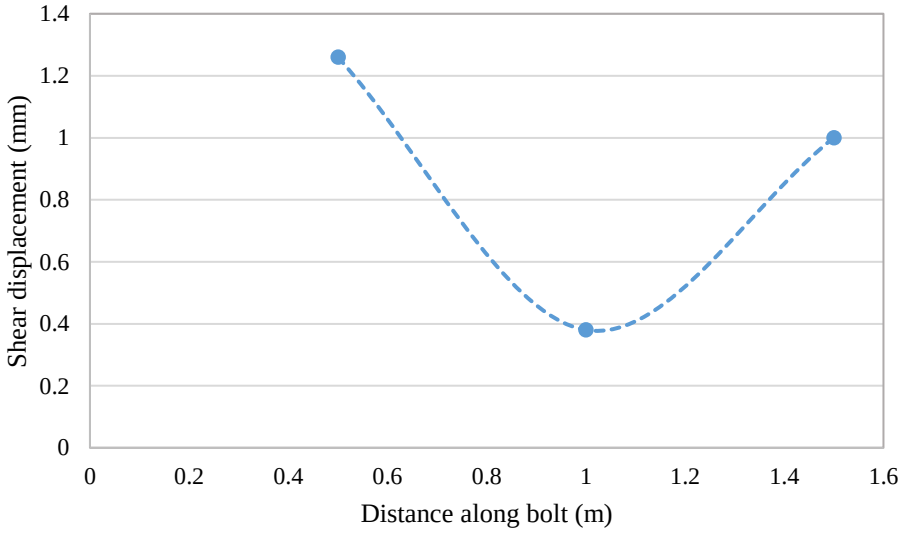

Figure 3.14 – Shear displacement at rockbolt-joint intersection.

In addition to the extra axial load on the rock bolt due to joint opening, shear stress on the rock bolt also decreases the axial capacity of the rock bolt (Pellet & Egger, 1996). The shear load in the bolt at the bolt-joint intersection is calculated using Equation 3.9 (Pellet & Egger, 1996). For shear displacement of 1.26mm (Figure 3.14), equation 3.9 gives the shear load on the rock bolt as 29.8 kN. The shear load at yield point is calculated using equation 3.10 (Pellet &

Egger, 1996) as 15.8 kN. Equation 9 gives a higher value of shear load than that at the yield point (equation 3.10). As after yield point shear load remains constant in the rock bolt (Pellet & Egger, 1996), the shear load in the rock bolt will be equal to shear load at yield point i.e. 15.8 kN. Equation 3.8 (Pellet & Egger, 1996), is then used to calculate the effect of shear load on axial strength of rock bolt (Figure 3.15).

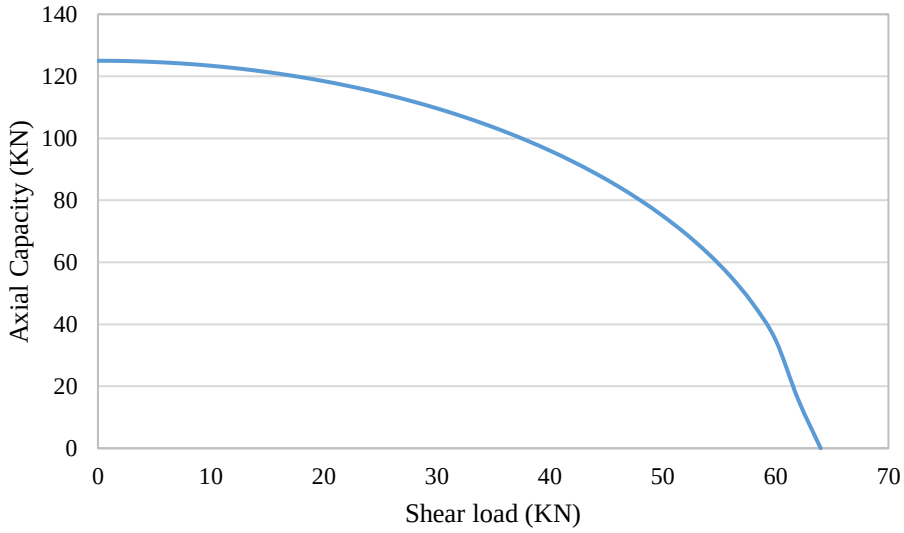

Figure 3.15 – Effect of shear load on axial capacity of rock bolt (Pellet and Egger (1996) [8]).

Figure 3.15 shows that the effective tensile yield limit of rock bolt for shear load of 15.8 kN decreases to 120 kN. The safety factor is now calculated using the increased axial load due to joints and decrease in axial capacity due to combined loading, decreases from 3.5 to 2. This shows that the combined loading of the rock bolt can significantly decrease the actual safety factor from the designed one.

3.3.2 Beam building

The beam building method is used where a competent rock is present above a thick layer of bedded roof. For analysing the effect of combined loading on beam building rock bolt design, the thickness of immediate siltstone layer above the excavation is kept as 3m. The rock bolt spacing is first calculated using analytical method and then the loads on the rock bolt is analysed using numerical models.

Analytical method for beam building rock bolt support

In beam building the rock bolts are designed to resist the shear displacement between the layers in the bedded roof. The maximum shear resistance of the bolt (Equation 3.3) is calculated as 62.9 kN or 222 MPa for zero pretension load (Stimpson, 1987). For uniform loading over the beds and rock bolt row spacing equal column spacing, the bolt spacing is calculated as 2.5m (Equation 3.2). Using a safety factor of 2 for maximum shear resistance of single bolt, the required spacing reduces to 2m and the shear load on bolt reduces to 31.5 kN or 111 MPa. For the sake of this example, a safety factor 2 is chosen instead of 3.5 because at safety factor of 2 the bolt spacing is 2 m while safety factor of 3.5 gives bolt spacing of 1.5 m. As the bolt pattern is such that the bolts are placed symmetrically around a central bolt and corner bolts at half spacing distance from pillars (Stimpson, 1987), bolt spacing of 2 m is more suitable for such bolting pattern.

Numerical model for beam building

Two-dimensional models of the excavation is created using Rocscience RS2 software (Figure 3.16). The parameters of the numerical model are kept the same as described earlier. The thickness of immediate siltstone layer above the excavation is 3m. Joint spacing in the immediate siltstone roof is 0.5m. The sides of the model are bounded in x-direction while the bottom of the model is bounded in both x and y directions. A load equal to the weight of overburden is applied at the top of the model. Fully grouted rock bolts are installed in the roof of the excavation. The numerical model is made with bolt spacing of 2m as calculated with safety factor of 2. According to Stimpson (1987), the bolts are installed at equal spacing on both sides of the roof's centre with corner bolts at half spacing distance from pillars. The model

is calibrated by changing the overburden depth and matching the bolt stress with analytical result.

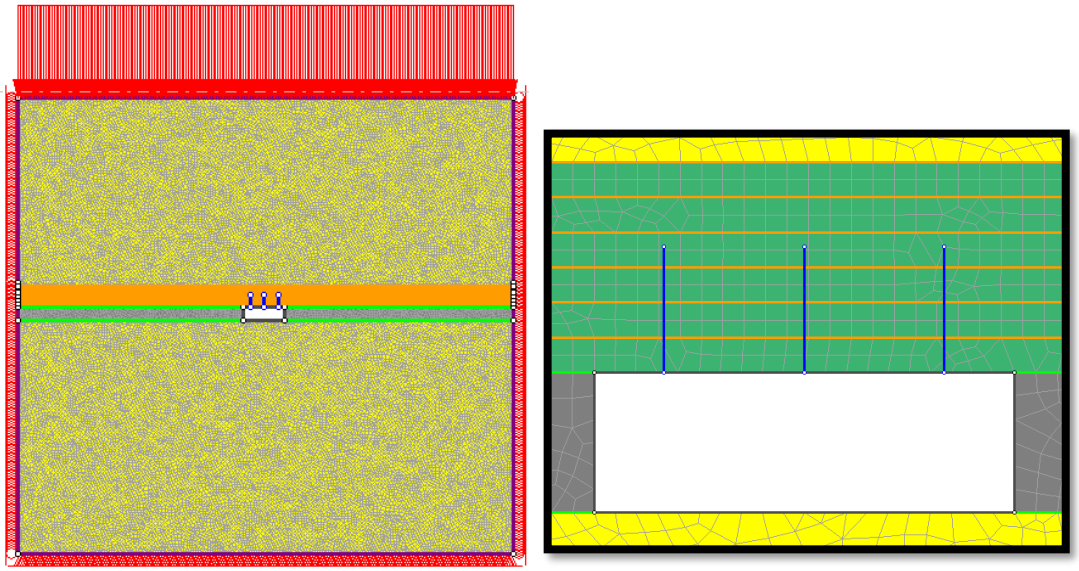

Figure 3.16 – Two-dimensional model of beam building roof.

Analysis of effect of axial load on shear capacity of rock bolt

For analysis of the effect of axial on shear capacity, the rock bolt in the corner (2m from centre) will be analysed as the highest shear occurs towards the corner of the roof. The axial stress and shear displacement in the corner rock bolt as obtained from numerical model are shown in Figure 3.17 and 3.18.

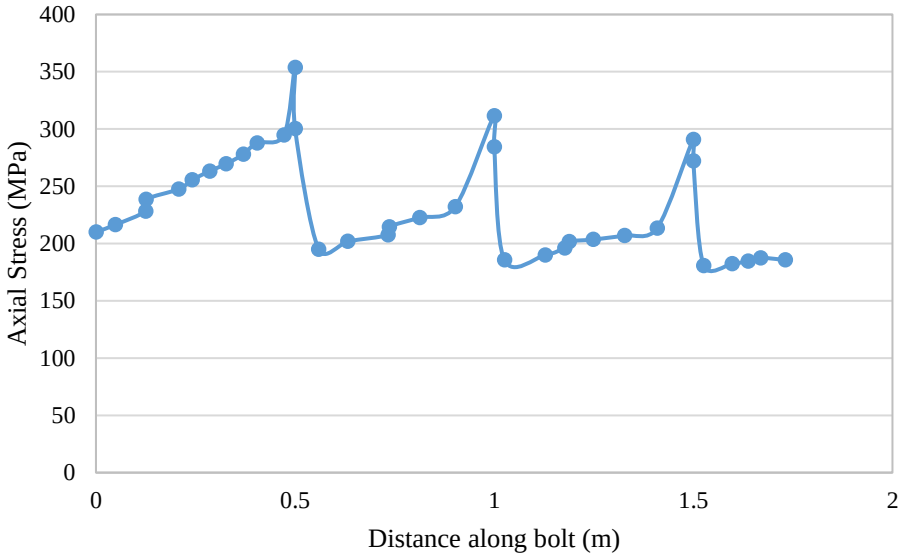

Figure 3.17 – Axial Stress along the corner bolt in beam building.

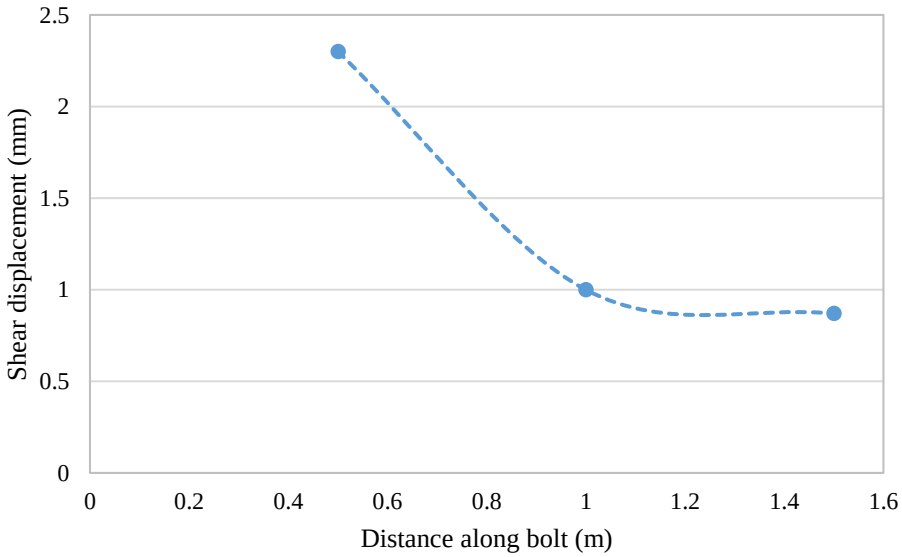

Figure 3.18 – Shear displacement along the corner bolt at bolt-joint intersections in beam building.

In Figure 3.17, the jumps in the axial stress at 0.5, 1 and 1.5m points is due to increase in axial stress due to joint opening and shearing. The behaviour of shear displacement in the rock bolt (Figure 3.18) matches with observations in physical model. Figures 3.3.17 and 3.18 show that

the rock bolt is under a combined axial and shear load. From Figure 3.18, the shear load on the rock bolt at 0.5m from the roof is calculated as 31 kN using Equation 3.4 (Dight, 1983). The shear load in the bolt matches with the shear resistance of 31.5 kN calculated using equation 3.2 (Stimpson, 1987) with safety factor of 2. From Figure 3.17, it can be seen that the rock bolt is also under an axial load of 326.5 MPa at the bolt-joint intersection. This axial load is due to the axial stress in the rock and the additional axial load due to joint opening. According to Equation 3.3 (Stimpson, 1987) for maximum shear load of a rock bolt, any initial axial load in the bolt (326.5 MPa) will reduce the bolt's maximum shear capacity. The maximum shear capacity of the rock bolt is then calculated as 42.16 kN (Equation 3.3). The safety factor, now calculated using the decreased shear capacity of the rock bolt, is reduced from 2 to 1.36.

Most of the commonly used rock bolt design methods whether analytical or numerical, do not take into consideration the effect of combined load; leading to over-estimation of safety factors as illustrated from the earlier examples. In the analytical and numerical methods used earlier, the shear and axial behaviour of the rock bolt are evaluated separately from one another. However, in a combined loading conditions, it is necessary to evaluate the rock bolt's axial and shear behaviour together as they are dependent on one another. This interdependence changes the failure characteristics and mechanical response of the rock bolt. In order to model the effect of combined load on rock bolt, a good understanding of the rock bolt's response to combined loading is required.

3.4 Conclusion

Based on the physical, analytical and numerical analysis of combined loading on rock bolt support, the following conclusions are made:

1. Underground excavations with bedded (or jointed) roof undergo interlayer shear and its magnitude depends upon the amount of the roof deformation and the thickness of bedding layers.

2. A rock bolt installed in a jointed rock mass would undergo a combined axial and shear loading. The normal stress in the rock and the joint opening subjects the rock bolt to axial loads while the joint shear movement causes shear loads on the rock bolt.
3. Rock bolt design in roof suspension method only considers the dead weight of the weak roof in order to calculate the axial capacity of bolts. However, rock bolts installed across jointed rock also undergo shear loading. The shear load if not considered in rock bolt design can reduce the designed safety factor. The rock bolt safety factor in the analysis of suspension rock bolt support design decreased from 3.5 to 2.0 due to combined load.
4. In beam building only the required shear resistance of the bolts is calculated. However, the bolts are also under axial loading due to weight of layers. This axial load reduces the shear capacity of the rock bolt and consequently the designed safety factor. The rock bolt safety factor in the analysis of beam building rock bolt support design decreased from 2.0 to 1.36 due to combined load.

Acknowledgements

Funding: This work was supported by the Minerals Research Institute of Western Australia (MRIWA); Mining3 and Peabody Energy.

References

Standard, A. S. T. M. (2014). B209M-14: Standard Specification for Aluminum and Aluminum Alloy Sheet and Plate. ASTM Int, 1-26.

Barbato, J., Hebblewhite, B., Mitra, R., & Mills, K. (2016). Review of horizontal surface movements due to longwall coal mining using numerical modelling.

Bjurstrom, S. (1974). Shear strength of hard rock joints reinforced by grouted untensioned bolts. Proc. 3rd Cong. ISRM, Denver, 2, 1194-1199.

Blanco Martín, L., Tijani, M., & Hadj-Hassen, F. (2011). A new analytical solution to the mechanical behaviour of fully grouted rockbolts subjected to pull-out tests. Construction and Building Materials, 25(2), 749-755. doi:10.1016/j.conbuildmat.2010.07.011

Dight, P. M. (1982). Improvements to the stability of rock walls in open pit mines: by Phillip M. Dight (Doctoral dissertation, Monash University).

Dulacska, H. (1972, December). Dowel action of reinforcement crossing cracks in concrete. In Journal Proceedings (Vol. 69, No. 12, pp. 754-757).

Farmer, I. W. (1975). Stress distribution along a resin grouted rock anchor. International Journal of Rock Mechanics and Mining Sciences and, 12(11), 347-351. doi:10.1016/0148-9062(75)90168-0

Freeman, T. (1978). The behaviour of fully-bonded rock bolts in the Kielder experimental tunnel. Tunnels & Tunnelling International, 10(5).

Gerdeen, J. C. (1977). Design criteria for roof bolting plans using fully resin-grouted nontensioned bolts to reinforce bedded mine roof. National Technical Information Service.

Hyett, A., Forbes, B., & Spearing, S. (2013). Enlightening bolts: using distributed optical sensing to measure the strain profile along fully grouted rock bolts. Paper presented at the Proceedings of the 32nd international conference on ground control in mining.

Jeffrey, R. G., & Daemen, J. J. (2021). Analysis of rockbolt reinforcement of layered rock using beam equations. In Rock Bolting (pp. 173-185). Routledge.

Jessu, K. V., Kostecki, T., & Spearing, S. (2016). Measuring roof-bolt response to axial and shear stresses: Laboratory and first in-situ analyses. The CIM Journal, 7(1), 62-70.

Kostecki, T. R., Spearing, A. J. S., Forbes, B., & Hyett, A. (2016). New instrumented method to measure the true loading profile along grouted rockbolts. SME transactions, January.

Li, C., & Stillborg, B. (1999). Analytical models for rock bolts. International Journal of Rock Mechanics and Mining Sciences, 36(8), 1013-1029.

Li, X., Aziz, N., Mirzaghorbanali, A., & Nemcik, J. (2016). Behavior of fiber glass bolts, rock bolts and cable bolts in shear. Rock Mechanics and Rock Engineering, 49(7), 2723-2735.

Luo, J. (1999). A new rock bolt design criterion and knowledge-based expert system for stratified roof. Virginia Polytechnic Institute and State University.

Mark, C. (2000). Design of roof bolt systems. Paper presented at the New Technology for Coal Mine Roof Support, Proceedings, NIOSH Open Industry Briefing, NIOSH IC.

Obert, L., & Duvall, W. I. (1967). Rock mechanics and the design of structures in rock (Vol. 650): Wiley New York.

Panek, L. A. (1956). Principles of reinforcing bedded mine roof with bolts (Vol. 5156): US Department of the Interior, Bureau of Mines.

Pellet, F., & Egger, P. (1996). Analytical model for the mechanical behaviour of bolted rock joints subjected to shearing. Rock Mechanics and Rock Engineering, 29(2), 73-97.

Snell, G., Kuley, E., & Milne, D. (2017). A laboratory-based approach to assess rockbolt behaviour in shear. Paper presented at the Proceedings of the First International Conference on Underground Mining Technology.

Stimpson, B. (1987). Estimating the degree of reinforcement of horizontally bedded roofs strengthened by non-tensioned, full-column grouted bolts. International Journal of Mining and Geological Engineering, 5(3), 273-284.

Tang, D. H., & Peng, S. S. (1984, June). Methods of designing mechanical roof bolting in horizontally bedded strata. In The 25th US Symposium on Rock Mechanics (USRMS). OnePetro.

Timoshenko, S. (1983). Strength of Materials, Pt. 2: Advanced Theory and Problems: Krieger Publishing Company.

Unal, E. (1983). Development of design guidelines and roof-control standards for coal-mine roofs. The Pennsylvania State University.

Windsor, C. R. (1997). Rock reinforcement systems. International journal of rock mechanics and mining sciences, 34(6), 919-951.

Zingano, A., Gomes, C., Koppe, J., Costa, J. F., Valentini, N., Schneider, C. H., & Silveira, C. A. Calibrating Numerical Model for Room-And-Pillar Coal Mining Simulation in Weak Immediate Roof Based on In-Situ Tests.

Chapter 4. Analysis of the Combined Load Behaviour of Rock Bolt Installed across Discontinuity and its Modelling using FLAC3D

This chapter has been accepted and published in Geotechnical and Geological Engineering as:

Singh, P., Spearing, A. J. S., & Jessu, K. (2020). Analysis of the combined load behaviour of rock bolt installed across discontinuity and its modelling using FLAC3D. Geotechnical and Geological Engineering, 38, 5867-5883.

Abstract –

Determining the rock bolt response under the typical in situ loading conditions of tension, shear and bending is an important part of the support design process. Calibrated numerical modelling can be an important tool for simulating the rock bolt response under in situ loads. However, currently available structural support models do not accurately model the rock bolt behaviour under shear loads. These models need to be modified to simulate the actual rock bolt response as determined under laboratory testing. Results from double shear laboratory tests by Kostecki (2019) have been used to calibrate the numerical models in ANSYS (ANSYS® Academic Research Mechanical, 2019). The calibrated numerical models were used to study the state of stress along the rock bolt under different concrete strength. These numerical models are compared with the analytical model proposed by Pellet and Egger (1996). The results show that the rock reaction and consequently the shear load on rock bolt in the analytical model is underestimated (by up to 50% in case of high strength concrete). In high strength concrete, the yield and failure behaviour is determined by the shear stress rather than the bending and tensile stress as predicted by the analytical models. The analytical model is modified to better predict the shear forces in high strength concrete. The pile structural element available in FLAC3D (FLAC3D — Fast Lagrangian Analysis of Continua in Three-Dimensions, 2017) finite difference method neglects the transverse shear strain in the element. In this paper, the pile structural element is modified to simulate the correct response of rock bolt under shear. The FLAC3D code is also modified to simulate the bolt yielding and failure under combined axial, bending and shear load. The modified model is validated with laboratory results from Mchugh and Signer (McHugh and Signer, 1999) and is shown to be better at simulating the shear response and failure of rock bolt under shear compared to the original pile model.

4.1 Introduction

Fully grouted rock bolts are used in underground excavations to reinforce the rock mass. The rock bolt provides reinforcement to the rock by resisting the loads transferred to it by strata movement. The rock bolts load capacity should be designed according to the magnitude and nature of typical in situ loads. When an excavation is made underground, the stresses in the rock gets redistributed around the excavation. This leads to deformation in the roof of the excavation, which, if left unchecked, leads to failure. The deformation in the roof of the excavation can be both vertical (sagging or bending) and horizontal (shearing across beds, joints, or fractures). The vertical deformation of the roof loads the fully grouted rock bolt with an axial load while horizontal movement leads to shear loading on the rock bolt. Rock bolt behaviour under axial loads is generally well understood (Blanco Martín et al., 2011; Farmer, 1975; Freeman, 1978; Li and Stillborg, 1999). Therefore, most common rock bolt support methodologies only consider the axial capacity of rock bolt (Frith, 2011). A rock bolt is subjected to both axial and shear loads (Li, 2010; McHugh and Signer, 1999), therefore a rock bolt support design should also consider the shear behaviour of the rock bolt.

4.2 Background

4.2.1 Experimental Studies

Shear tests of fully grouted rock bolts have been reported in the literature. Bjurstrom (1974); Dight (1982); Haas (1976); Spang and Egger (1990) reported on the effect of parameters like normal stress, bolt inclination, joint roughness, and rock strength on the shear resistance of a bolted joint. Different failure mechanisms of rock bolt under shear load have been reported in the literature. Ferrero (1995) discussed two types of failure mechanisms – one at the shear plane and the other at the plastic hinge point. Pellet and Egger (1996) discussed failure at the shear plane due to a combination of shear and tensile stress. McHugh and Signer (1999) tested fully grouted rock bolts with strain gauges in direct shear to measure the strains on the bolt. They proposed the formation of plastic hinge points on bolts when sheared and then ultimate failure due to tensile strain.

Chen (2014); Chen and Li (2015) tested the effect of combined axial and shear loads on fully grouted rock bolts and D-bolt by loading the bolts at different angles to the bolt axis. Ultimate displacement at failure was found to increase slightly with an increase in displacing angle. Li et al. (2016b) tested different bolts under combined axial and shear loading by pre-tensioning the bolts in the double shear test. Pre-tensioning was found to increase the shear stiffness of the joint in the elastic stage. Jessu et al. (2016) tested instrumented bolts under double shear installed perpendicular and at 80^0 to the discontinuity. Perpendicular bolts to the discontinuity were found to be stiffer than inclined bolts. Snell et al. (2017) investigated the effect of gap size on fully grouted rock bolts under shear. Stiffness, yield strength, and ultimate strength of the bolted joint was found to be reduced with gap size. A more significant effect was observed in the magnitude of displacement (increasing) at failure with increasing gap size. Pinazzi et al. (2020) tested un-grouted rock bolts under different loading conditions to understand the effect of combined load on the rock bolt mechanical response. Shear performance of un-grouted rock bolts under combined loads and shear gap was analysed. Combined load was found to reduce the axial and shear capacity of the rock bolts by up to 18% and 30%, respectively. These studies show that combined loading has a significant effect on the shear behaviour of the rock bolt.

4.2.2 Analytical models

Analytical models have been used to predict the rock bolt response under shear load. Gerdeen et al. (1979) proposed a model for shear behaviour of rock bolts, assuming that they behaved as a beam on an elastic foundation. Dight (1982) proposed a relationship between the maximum load on the bolt and the shear displacement. He considered the effect of bolt inclination, grout response, and failure under combined load.

Pellet and Egger (1996) proposed an analytical model to describe the behaviour of a fully grouted rock bolt installed across a discontinuity. The model predicts the relationship between the loads on the rock bolt and shear displacement. Bolt response is calculated for both elastic and large plastic deformations. Bolt yielding and failure under combined loading is also

predicted. It is assumed that due to joint displacement, the host material nearby becomes unconfined and the reaction of the host material can be assumed to be rigid perfectly plastic.

Pellet and Egger (1996) proposed that the loads on the bolt at the discontinuity point O can be resolved into axial N_o and shear loads Q_o (Figure 4.1). The bending moment is zero at this point and highest at point A. The distance between these two points is l_A and the host material reaction is shown as p_u.

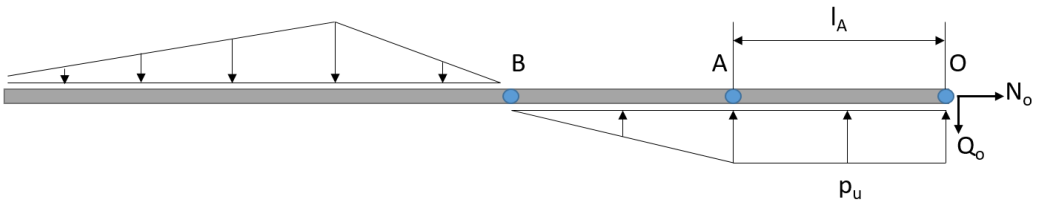

Figure 4.1 – Rock bolt under shear load (modified from Pellet and Egger, (1996)).

The following relationships are proposed by Pellet and Egger (1996) –

$$p_u = K\sigma_c D_b \tag{4.1}$$

$$Q_{oe} = \frac{1}{2}\sqrt{p_u D_b \left(\frac{\pi D_b^2 \sigma_{el}}{4} - N_{oe}\right)} \tag{4.2}$$

$$Q_{of} = \frac{\pi D_b^2}{8}\sigma_{ec}\sqrt{1-16\left(\frac{N_{of}}{\pi D_b^2 \sigma_{ec}}\right)^2} \tag{4.3}$$

$$U_o = \frac{24 N_o Q_o}{E p_u \pi D_b^2} \tag{4.4}$$

$$V_o = \frac{8192 Q_o^4 b}{E\pi^4 p_u^3 D_b^4} \tag{4.5}$$

Where:

p_u : bearing capacity of rock or grout

K : load factor (K>=1)

σ_c : unconfined compressive strength of rock or grout

D_b : bolt diameter

$Q_{o,} Q_{oe}, Q_{of}$: shear force at O, at yield point and failure point

N_o, N_{oe}, N_{of} : axial force at O, at yield point and failure point

D_b : bolt diameter

σ_{el}, σ_{ec} : yield stress and failure stress

U_o, V_o : horizontal and vertical elastic displacement at point O

b : constant (0.27)

E : Elastic modulus of rock bolt

β : angle between rock bolt and discontinuity

Equation 4.1 can be used to calculate the ultimate bearing capacity of the host material. Equations 4.2 and 4.3 define the relationship between axial and shear load at yielding and failure of bolt, respectively. Equations 4.4 and 4.5 give the relationship between the shear force, axial force, and the bolt displacements at point O.

Chen et al. (2018) used the model developed by Pellet and Egger (1996) to derive and study the relationship between the displacing angle and loading angle of a bolt subjected to shear. Ma et al. (2019) proposed a model for shear behaviour of rock bolt considering the pre-tension loads and grout-bolt interface shear stress. They used the beam on elastic foundation theory to predict the shear loads on the bolt.

As can be seen from these studies, that although the analytical models can be used to calculate the rock bolt response under shear loads, they are limited by the assumptions that the host material behaves elastically or as an unconfined rigid perfectly plastic material.

4.2.3 Numerical modelling

In recent times as the computational power is increasing significantly, numerical modelling is gaining popularity as a tool for designing rock bolt supports. Spang and Egger (1990) modelled fully grouted rock bolts installed across rough joints using the Finite Element Method (FEM). They used Von-Mises failure criteria for rock, grout and steel. The bolt-grout de-bonding behaviour was simulated by using a low Young's Modulus. Grasselli (2005) used FEM software to simulate the double shear test. The material behaviour was assumed to be elastic while the interfaces were simulated as elastic-perfectly plastic. Jalalifar et al. (2004) used 3D numerical models to study the stresses in rock bolt under shear load. Pre-tension was found to decrease the shear stress in bolt, increasing the shear resistance. Aziz et al. (2005) investigated the effect of resin thickness on shear behaviour of rock bolt using FEM models. Resin thickness was found to affect the shear displacement however, it was found that under lateral loads strength of host media was more important. Jalalifar et al. (2005) studied the stresses and strains at the shear interface of grouted rock bolts under pull and push tests using FEM numerical simulation. Aziz and Jalalifar (2007) conducted double shear tests and numerical modelling to study the effect of pre-tension and host media strength on shear behaviour of rock bolt. Pre-tension was found to significantly affect the bolt deflection and stresses. Shear load in bolt was higher in higher strength surrounding media. Li et al. (2016a) used FLAC3D software to conduct a parametric study of the shear behaviour of rock bolt under double shear. All these studies explicitly modelled the fully grouted rock bolt. The bolt, grout, rock, and their interfaces are modelled using grid elements. This is advantageous when the internal stress state of the bolt is to be analysed (Kostecki, 2019) such as while studying rock bolt behaviour in a laboratory test. However, these models are computationally costly and result in long solution times which makes them impractical for modelling in-situ rock bolt support where a large number of support elements need to be modelled simultaneously. For this purpose,

implicit rock bolt models are used as they are simple to implement and require less solution time. Implicit rock bolt models are one dimensional structural element which are linked to the grid elements through nodes. The properties of the one-dimensional elements determine the bolt response and the links determine the interface behaviour. FLAC3D is one of the most commonly used software for rock bolt support modelling (Mark et al., 2007) and it develops the rock bolt model using an inbuilt structural element called Pile.

Tulu et al. (2012) presented the procedure to calibrate the pile element in FLAC3D software to simulate the rock bolt response in shearing. Laboratory shear test results were used to calibrate the normal spring and shear spring properties. The model was calibrated to show failure under combined axial and shear loads using the Tresca criterion. The failure was calculated using only elastic tensile and shear loads in the bolt and plastic yielding was not considered. Kostecki (2019) conducted double shear tests on rock bolts installed perpendicular and at an inclination to the shear plane. The shear tests were modelled both explicitly and also using the implicit rock bolt element in FLAC3D software. From the explicit models it was found that the rock bolt failed due to combined axial and shear load. The implicit models were simulated until the plastic yielding of bolt and not to failure.

A Pile in FLAC3D consists of a series of one-dimensional pile elements connected end to end. A pile element has bi-symmetrical uniform properties and six degrees of freedom per node. Its properties are similar to that of an isotropic bi-symmetrical prismatic straight beam. The element can simulate axial and flexural deformations; however, the transverse shear displacement is neglected to simplify the formulation (FLAC3D — Fast Lagrangian Analysis of Continua in Three-Dimensions, 2017). The pile structural element in FLAC3D, in its original form, cannot be used to simulate the shear failure of a bolt. In this paper, the stresses on a rock bolt under shear are analysed with an explicit numerical model. Then the pile element is modified to show the actual shear response of a rock bolt and failure due to combined axial and shear load.

4.3 Experimental study – Double shear test

Kostecki (2019) investigated the use of rock bolts instrumented with fibre-optics to measure strains in laboratory tests and for in-situ measurements. In this paper, the results from double shear tests of the work are used for calibrating the numerical models.

4.3.1 Experimental Setup

The instrumented bolts used Distributed Optical Sensing technology to measure strain along the length of the bolt. The strain measuring fibres were placed in two 3X3 mm slots made diametrically opposite to each other. The advantage of using optical technology over traditional strain gauges is the higher bolt coverage and also the higher spatial resolution of 1-2 mm. The instrumented rock bolts were grouted in the centre of the concrete blocks perpendicular to the shear interface as shown in Figure 4.2. The concrete blocks were cast with a 24 mm diameter hole in the centre. The resin grout was then poured into the holes and the rock bolt inserted into it, ensuring complete encapsulation of bolt. No pre-tension was applied to the rock bolt. The grout was allowed to set for at least 24 hours before the test. To simulate the double shear load on the rock bolt, the concrete blocks were loaded as shown in Figure 4.2. Force was applied on the central block while the corner blocks were supported at their base. The central block was loaded to 1.25 and 5.00 tonnes. The rate of loading was kept small (0.15 to 0.2 KN/sec) to keep the loading conditions under static loading. Strain from instrumented bolt and displacement at the top of the central block were recorded. Details of the material used are given in Table 4.1**.**

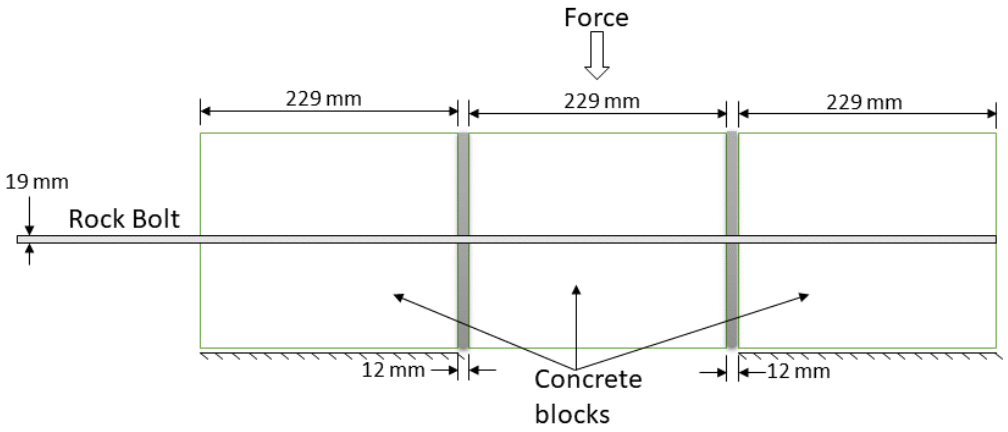

Figure 4.2 – Double shear test setup (modified from Kostecki, 2019).

Table 4.1 – Material details (Kostecki, 2019).

Bolt						
Bolt Diameter (mm)	**Bolt Grade**	**Bolt length (mm)**	**Number of slots**	**Rebar design**	**Yield strength (MPa)**	**Tensile strength (MPa)**
19	60	1198.5±7.5	2	Double Threaded Ends	420	620
Concrete						
Average Compressive strength (MPa)			**Average Modulus of Elasticity (GPa)**			
31			28			

4.4 Numerical Modelling – Double Shear Test

4.4.1 ANSYS Model

Finite Element Method (FEM) software ANSYS was used to simulate the rock bolt under double shear test. The numerical model was made to the same dimensions as the laboratory

test (Figure 4.3a). The rock bolt, grout, and concrete were explicitly modelled. Only half of the setup was needed to be modelled as it is symmetric across the bolt's vertical centre plane. A fixed displacement boundary condition was applied to the top surface of the centre block and displacements at bottom surfaces of the corner blocks were fixed. The mesh near the bolt and shear plane was densified to better capture the plastic deformation. Two different bolt designs – with rib and without rib were analysed (Figure 4.3b and c).

The concrete and grout were modelled using isotropic elastic properties and Mohr-Coulomb failure criteria with perfectly plastic post-yield behaviour (Li et al., 2016a). For steel, bi-linear isotropic hardening using Von-Mises yield criteria was used. The properties for all materials were taken from Kostecki (2019) and are given in Table 4.2**.**

Frictionless contact was assumed between the concrete blocks and wood partitions as they have very low friction and no cohesion. The concrete-grout and grout-bolt contact is modelled as a Mohr-Coulomb contact i.e. a frictional contact with cohesion. The contact properties were taken from Li et al. (2016a). The values used for contact are given in Table 4.3.

The strains on the rock bolt were measured along the lines A1 and B1, which coincides with the location of strain measurement in the double shear laboratory tests, as shown in Figure 4.4. Displacement at the top of the centre block for each applied load was measured during the laboratory test. In the numerical model, displacement corresponding to the desired load was applied at the top of the centre block, and the reaction load was measured. The model was calibrated to the laboratory test results using the bending moment recorded by the instrumented bolts, reaction load, and displacement at two loads - 1.25 tonnes and 5.00 tonnes.

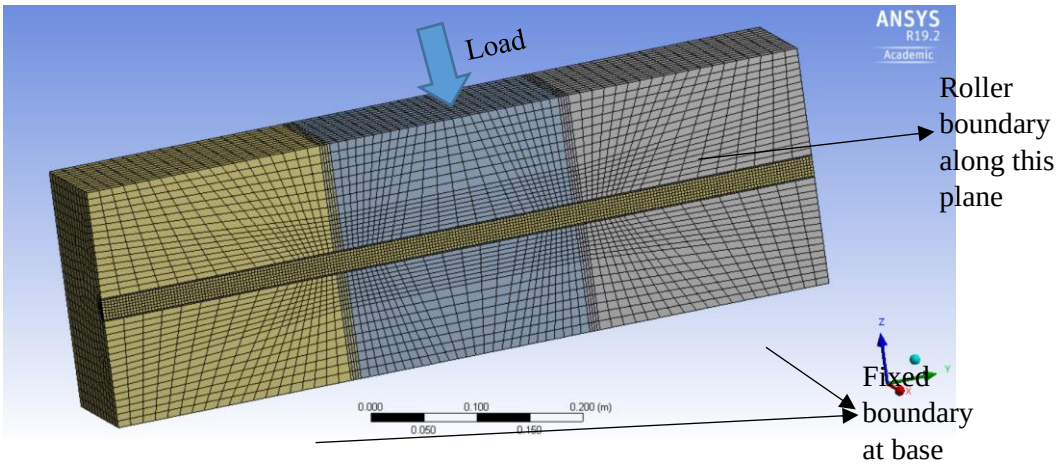

a) Model geometry showing the rock bolt installed in three concrete blocks separated by wooden spacers.

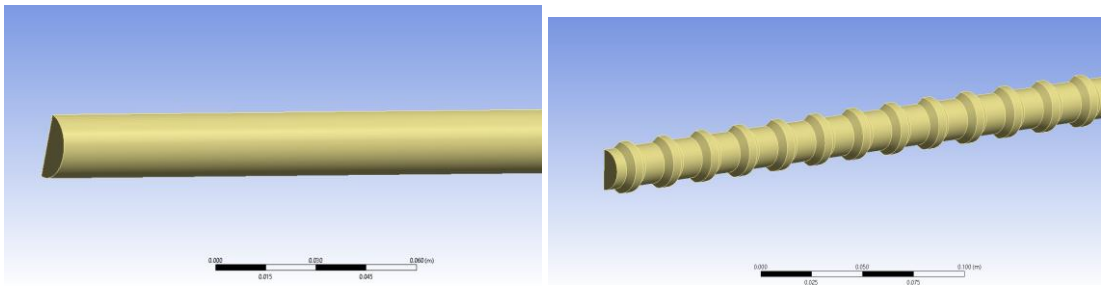

b) Smooth bolt

c) Bolt with ribs

Figure 4.3 - FEM model of the double shear test.

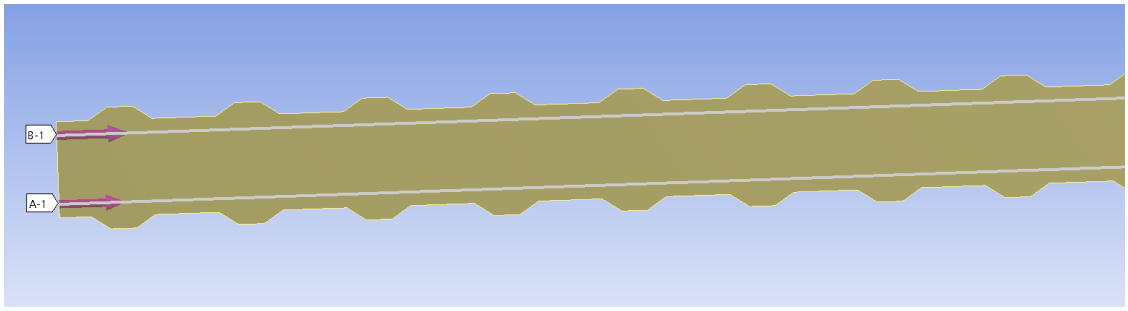

Figure 4.4 - Strain measured along the lines A-1 and B-1 on the rock bolt.

Table 4.2 - Material properties (Kostecki, 2019).

Material	**Elastic Modulus (GPa)**	**Poisson's Ratio**	**Cohesion (MPa)**	**Friction Angle (degrees)**	**Tensile Strength (MPa)**
Concrete	14	0.2	9	30	3.1
Grout	3	0.2	53.1	30	13.8
Wood	8	0.3			
			Yield Strength (MPa)	**Tangent Modulus (MPa)**	
Steel	200	0.3	415	300	

Table 4.3 - Contact properties (Li et al., 2016a).

Contact	**Type**	**Friction Angle Degrees**	**Cohesion (MPa)**	**Normal Stiffness (GPa)**
Grout-Steel	Mohr-Coulomb	32	10	500
Grout-Concrete	Mohr-Coulomb	30	1	500
Concrete-Wood	Frictionless	0	0	2000

4.4.2 ANSYS Model calibration results

The model was calibrated using the bending strains, load, and displacements measured in the laboratory tests. It was found that the contact properties between the grout, bolt, and concrete do not play a significant role in the shear response of the rock bolt as there is no appreciable axial strain on the rock bolt. Only the normal stiffness of the contact affected the bolt response.

The material properties of concrete and grout were adjusted to calibrate the model response to the laboratory test. Figures 4.5 and 4.6 show the bending strains of the bolt models compared with the laboratory results at 1.25t and 5.00t load, respectively. Two rock bolt models were compared, one with and one without ribs.

As seen from Figures 4.5 and 4.6, the rock bolt model with ribs has localised aberrations in the bending strain profile due to stress concentrations near rib edges. Small aberrations can also be seen in the laboratory test results. These aberrations in strain profile are small and can be ignored. To make analysis simpler in the rest of the paper results from only the smooth bolt model will be used. Along with calibrating the bending strain, the joint displacement and load were also calibrated with laboratory results. The calibration results are shown in Figure 4.**7.**

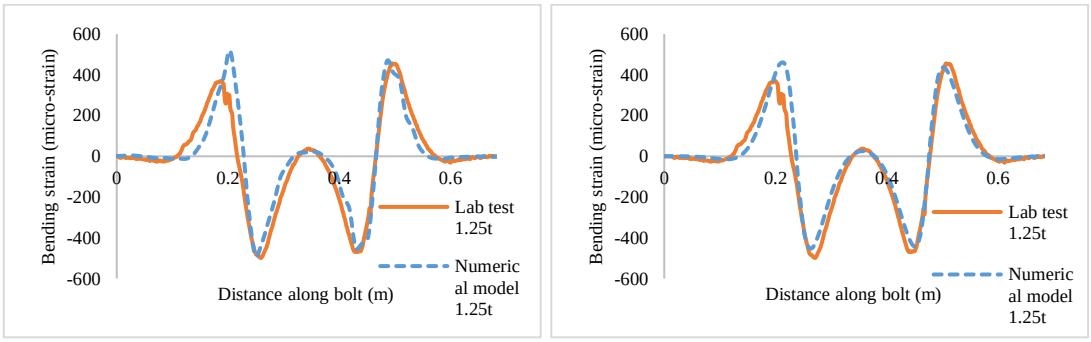

a) Bolt with ribs b) Bolt without ribs

Figure 4.5 - Bending strain in bolt at 1.25 tonnes load.

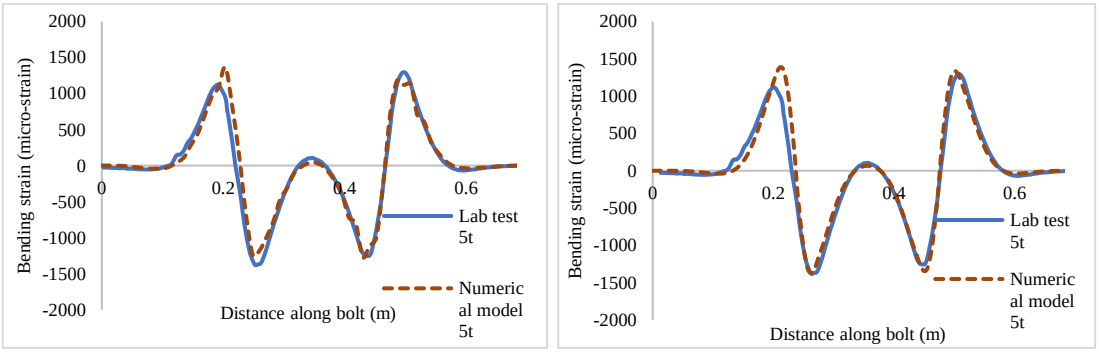

a) Bolt with ribs b) Bolt without ribs

Figure 4.6 - Bending strain in bolt at 5.00 tonnes load.

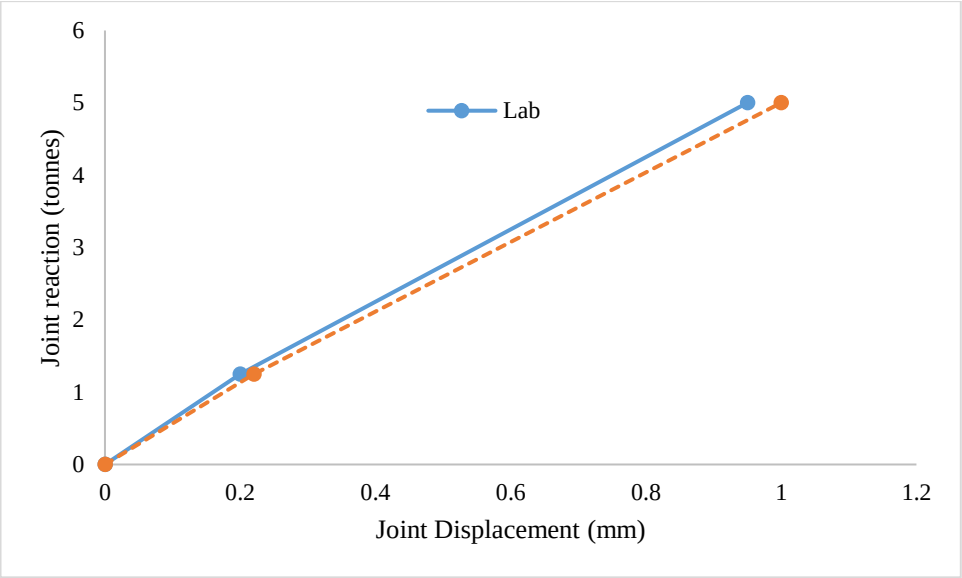

Figure 4.7 – Double shear joint response laboratory results vs Ansys model.

4.4.3 Effect of concrete strength on stress profile in the rock bolt

The calibrated numerical model of the double shear test was used to investigate the effect of concrete strength on the stress profile in the rock bolt. When a rock bolt is loaded in shear, there are two stress concentration points – the location of the maximum bending stress and the shear plane. The double shear test models were simulated for six different concrete strengths 10, 20, 30, 50, 70, and 90 MPa. The models were subjected to 10 mm of joint shear displacement. The shear stress and the maximum bending moment in the rock bolt was plotted relative to the applied displacement in Figures 4.8 and 4.9, respectively. Shear stress in the rock bolt increased with the increase in concrete strength. As seen from Figure 4.8, the shear stress in the rock bolt reached the yield point in concrete with strength 30 MPa and above. The maximum bending moment in the rock bolt also increased with the increase in concrete strength. Bending moment in all the rock bolts reached the plastic moment point. The shear stress in higher strength concretes (50, 70 and 90 MPa) reached the shear yield strength of the bolt as the bending moment value reaches the plastic limit (around 4-4.5 mm shear displacement).

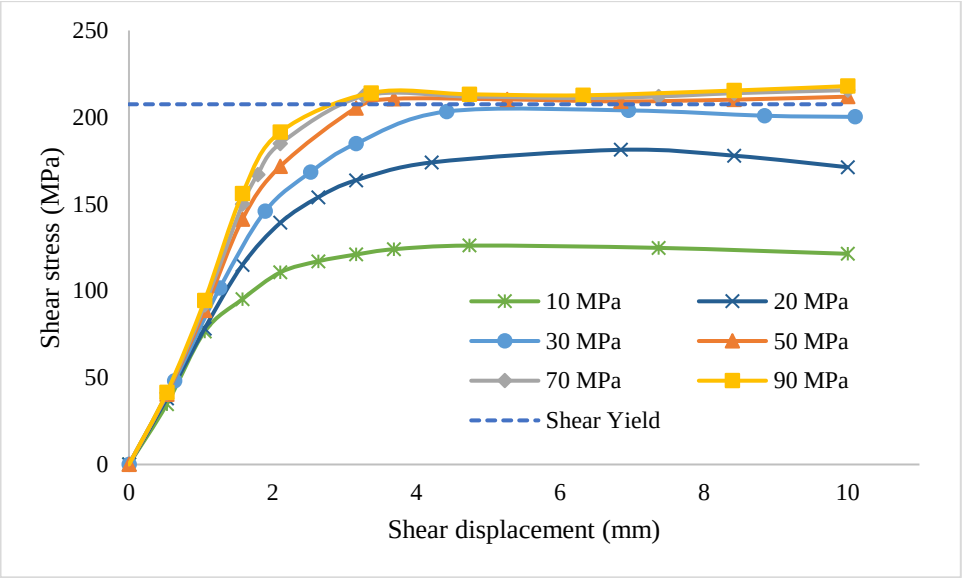

Figure 4.8 - Shear stress in the rock bolt for different concrete strengths.

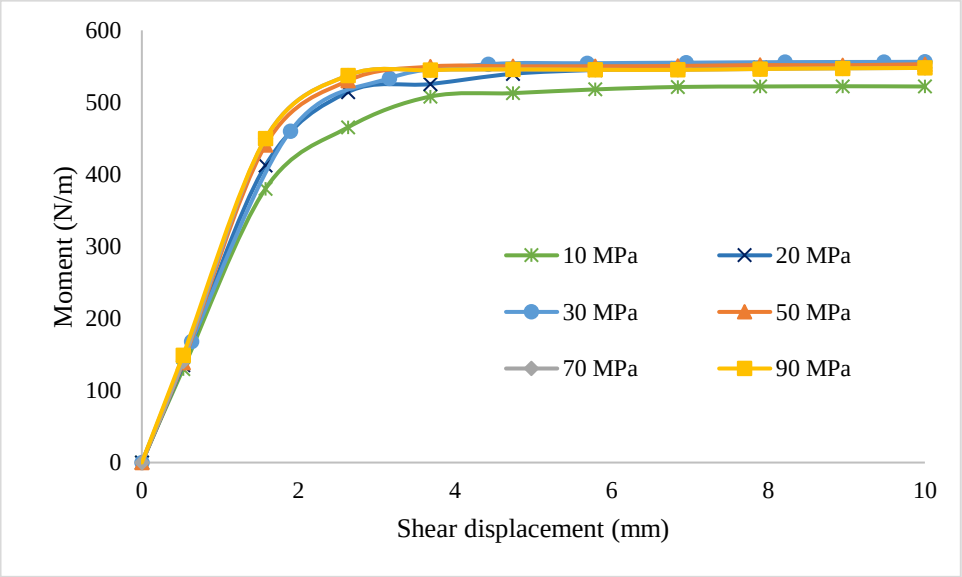

Figure 4.9 - Maximum moment in the rock bolt for different concrete strengths.

4.5 Comparison of Numerical model with Analytical Model

4.5.1 Bending strain and Rock reaction

Analytical models (Chen et al., 2018; Dight, 1982; Ma et al., 2019; Pellet and Egger, 1996) for the shear response of rock bolt divide the loading stage of rock bolt into two parts. First, when the bending moment in the rock bolt is below the plastic moment limit. In this stage, the shear stress in the rock bolt depends on the rock reaction and maximum bending moment. The

second loading stage starts after maximum bending moment reaches the plastic limit and plastic hinges are formed. After this point, the shear stress stops increasing as the maximum bending moment and the rock reaction remains constant. The rock bolt ultimately fails due to increasing tensile or bending strain. Pellet and Egger (1996) determined the bearing capacity of the rock or grout based on the assumption that the grout or rock near the joint becomes unconfined. The rock or grout response is assumed to be plastic from the start as the elastic part of the response is very small. Therefore, the bearing capacity of the rock or grout, assuming a perfectly plastic response, can be given by equation 4.1 (Pellet and Egger, 1996).

Equation 4.1 predicts a constant normal reaction from the grout or rock as the joint displacement increases. The model predicted the bending moment at the shear plane to be zero and increasing to a maximum value at a distance from the shear plane. The rock response and bending strain are measured in the calibrated 5 tonnes shear load numerical model. The bending strain in the rock bolt is directly proportional to the bending moment. The bending strain and rock response measured from the numerical model is shown in Figures 4.10a and b, respectively. The point O in the plot is the location of the wooden spacers at the shear plane. The rock bolt intersects the shear plane at point 0.23 m. The maximum bending strain point A and the shear discontinuity point O at which the rock reaction is maximum are shown on the plots for reference. In the numerical model, the bending strain at point O is not zero because of the presence of wooden spacers which shift the shear plane left. The general trend of the bending strain in the rock bolt is the same as that predicted by the analytical model.

In Figure 4.10b, the rock response is maximum near the shear plane and gradually decreases to zero away from point O. However, the numerical model shows a considerably higher rock reaction due to the confinement effect when compared to the analytical model. From the plot, it can be seen that the assumption in the analytical model of unconfined perfectly plastic behaviour of host media is incorrect. The analytical models also under-estimates the shear stress in the rock bolt as the shear stress depends only on the rock reaction and maximum bending moment. A comparison of shear stress at the yield point predicted by the analytical

model using equation 4.2 is done with the shear stress in the numerical models and shown in Figure 4.11. As can be seen from the plot, the analytical model underestimates the shear stress by more than 50% for higher strength concretes. This underestimation of the shear force in analytical models results in the incorrect shear response of the rock bolt, which is dominated by only bending and tensile stresses. As seen from the shear stress plot in Figure 4.8, the shear stress in the rock bolt, particularly in the case of high strength concretes, reached the yield point before the formation of plastic hinges. The yield behaviour of the rock bolt was actually dominated by shear stress. As the shear strength of a rock bolt is about 50% to 70% of its tensile strength, it becomes even more important to consider the shear stress and strain in the rock bolt to model the actual response of a bolted rock joint. Therefore, the analytical model needs to be modified to better predict the shear load on the rock bolt in high strength concrete and most rock materials.

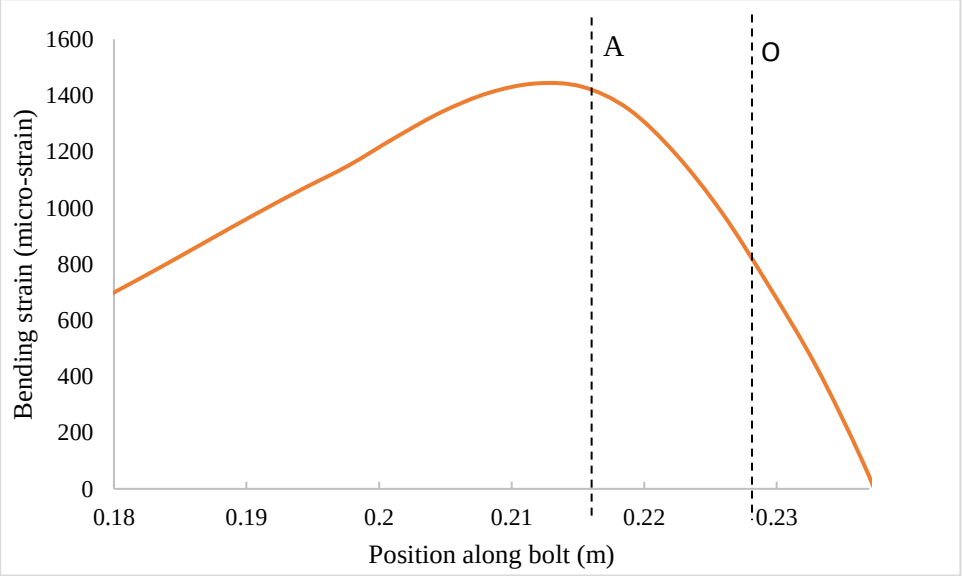

a) Bending strain in numerical model.

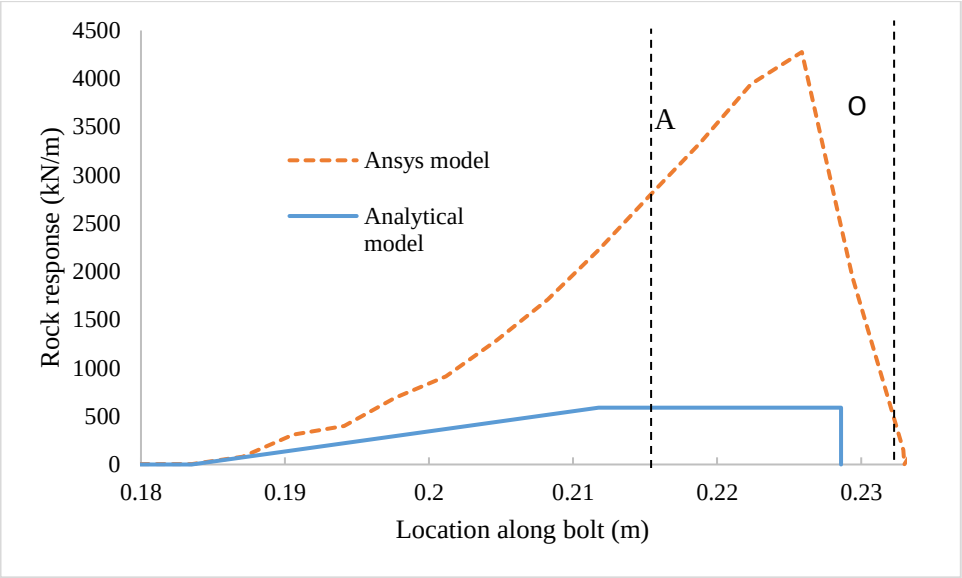

b) Rock response

Figure 4.10 - Comparison of the numerical model with the analytical model.

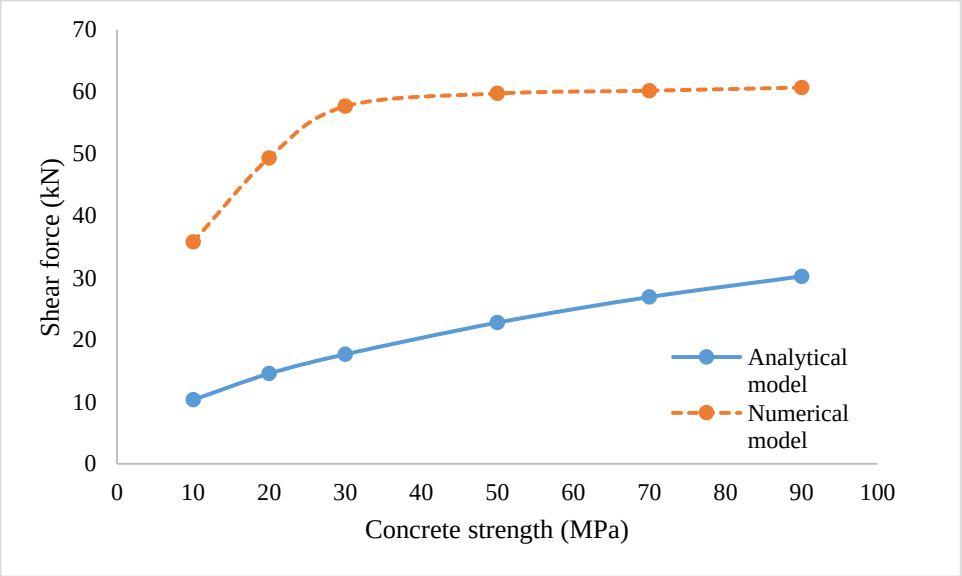

Figure 4.11 - Shear force in rock bolt analytical vs. numerical model.

4.5.2 Modified analytical model

From Figures 4.10 and 4.11, it can be seen that in case of high strength concretes, the rock reaction and shear force in the bolt during shearing is underestimated by the analytical model when compared with the results from the numerical model. Pellet and Egger (1996) used equation 4.1 to calculate the maximum bearing capacity of the rock/grout. In order to predict

the actual shear load on the rock bolt under shear, the assumption of rock/grout reaction equal to the bearing capacity of unconfined rock/grout material needs to be modified.

Using force equilibrium rock reaction P_u can be written as –

$$P_u = \frac{Q_{oe}}{l_A} \tag{4.6}$$

Where, Q_{oe} is the shear force in the rock bolt near the joint and l_A is the distance between point O and point of maximum moment. The expression for hinge point location l_A according to beam on elastic foundation theory is –

$$l_A = \frac{\pi}{4}\sqrt[4]{\frac{4EI_b}{150 f_c^{0.85}}} \tag{4.7}$$

Where, E is the bolt's elastic modulus, I_b is the moment of inertia of bolt and f_c is the compressive strength of concrete. Equation 4.7 only takes into account the concrete strength and bolt properties to calculate l_A. According to Jalalifar and Aziz (2010), the hinge point location also depends on the test setup. To include this effect a coefficient k is multiplied to the equation 4.7 -

$$l_A = k\frac{\pi}{4}\sqrt[4]{\frac{4EI_b}{150 f_c^{0.85}}} \tag{4.8}$$

To calculate k the value of l_A from equation 4.6 is compared with the l_A measured from the numerical model in Figure 4.12.

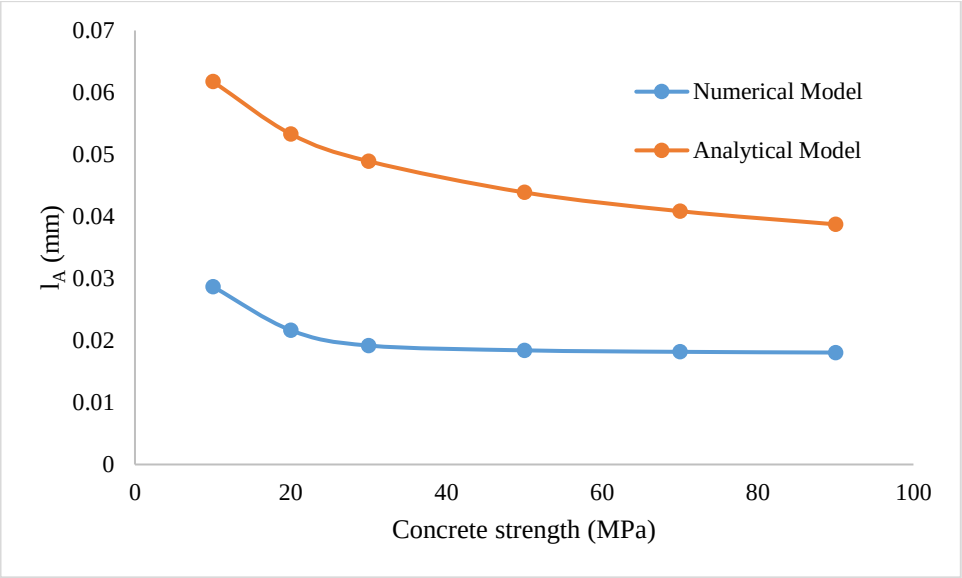

Figure 4.12 – Comparison of hinge point location at different concrete strengths.

As seen from Figure 4.12 the shape of the plot is same for equation 4.6 and l_A measured from the numerical models. The value of coefficient k is calculated as 0.4 from the difference in magnitude of l_A between the two plots. Equation 4.6 is then inserted into equation 4.4 and 4.5 to derive the relationship between the shear force, axial force, and displacements at point O –

$$Q_o = \frac{E\pi^4 D_b^4}{8192 b l_A^3} V_o \tag{4.9}$$

$$N_o = \frac{E\pi D_b^2}{24 l_A} U_o \tag{4.10}$$

Equation 4.9 and 4.10 are valid only in the elastic deformation region of bolt displacement. The bolt yield criteria are given by –

$$\frac{M_A}{M_P} + \left(\frac{N_o}{N_y}\right)^2 = 1 \tag{4.11}$$

$$\left(\frac{Q_o}{Q_y}\right)^2+\left(\frac{N_o}{N_y}\right)^2=1 \tag{4.12}$$

Where, M_A, M_P are moment at point A and plastic moment limit, respectively and Q_y, N_y are the shear and normal yield force limit, respectively. A comparison of the shear force estimated using equation 4.4, equation 4.9, and the numerical model of 90 MPa concrete blocks is shown in Figure 4.13. The value of maximum shear force calculated using the modified analytical equation has a better match with the shear force measured from the numerical model.

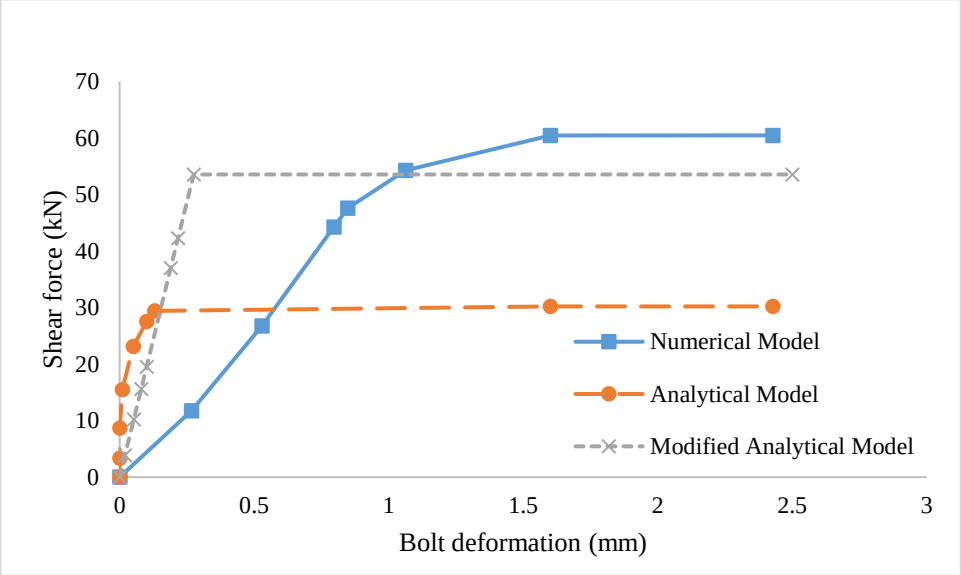

Figure 4.13 - Comparison of shear force in rock bolt between analytical and numerical model.

4.6 Numerical modelling of double shear test using FLAC3D

The double shear test was modelled using FLAC3D software. The model consists of a rock bolt element, wood partings, and three concrete blocks, as shown in Figure 4.14**.** The dimensions of the model are kept same as the laboratory test. Cubic structured mesh is used as it gives the most accurate results for plastic deformations. The displacements in x, y, and z direction are restricted for the end blocks while the load was applied on the central block. The concrete is modelled as isotropic elastic and Mohr-Coulomb perfectly plastic material. The

wood partitions have the same properties as the ANSYS model. The material properties are given in Table 4.4 (Kostecki, 2019).

In FLAC3D, supports are modelled using structural elements. To simulate a rock bolt, FLAC3D provides the pile structural element with an additional rock bolt option. A pile consists of linear elements connected end to end, and the pile-rock interaction is simulated using a spring-slider system. The number of nodes in a pile should be at least one per zone. The size of the pile is 70cm, with a total of 200 elements making up one pile. The pile structural element's normal and shear spring properties need to be calibrated to the test results. The shear spring properties (longitudinal) do not have any effect on the transverse shear behaviour of the pile. The pile properties are given in Table 4.5 (Kostecki, 2019).

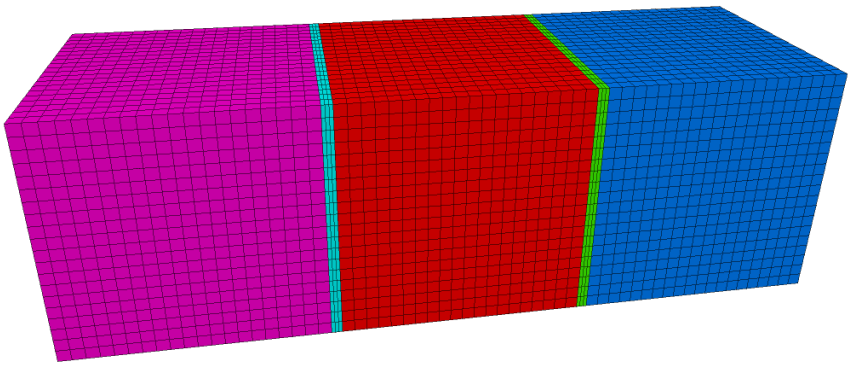

a) Model geometry showing the concrete blocks and spacers.

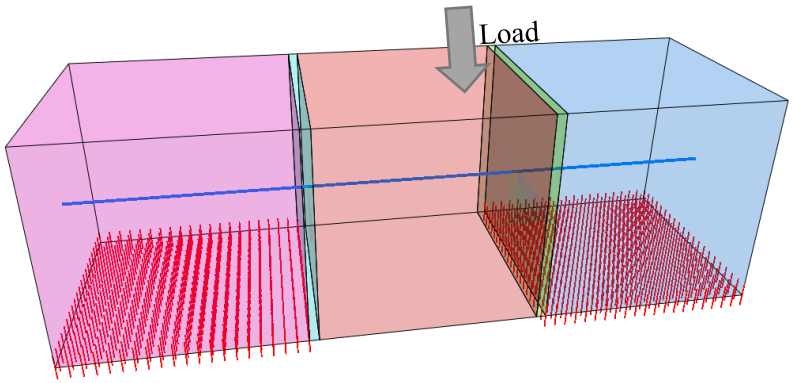

b) Model showing the pile element going through the centre of concrete blocks and fixed boundary at bottom of corner blocks.

Figure 4.14 – Double shear model in FLAC3D.

Table 4.4 – Material Properties (Kostecki, 2019).

Material	**Elastic Modulus (GPa)**	**Poisson's Ratio**	**Cohesion MPa**	**Friction Angle**	**Tensile Strength MPa**
Concrete	14	0.20	9	30	3.10

Table 4.5 – Pile Properties (Kostecki, 2019).

Diameter (mm)	**Young's Modulus (GPa)**	**Poisson's Ratio**	**Normal spring stiffness (GPa)**	**Normal spring cohesion (N/m)**	**Shear spring stiffness (GPa)**
19	200	0.30	31.30	2.10e6	1.52
Shear spring cohesion (N/m)	**Plastic Moment (Nm)**	**Failure strain**	**Normal spring friction angle**	**Shear spring friction angle**	**Axial yield load (kN)**
2.9e5	572	0.18	25	23	117.91

The results from the double shear tests with 1.25 and 5 tonnes of load on the central block were used to calibrate the pile's normal spring properties.

4.6.1 Model calibration

As the pile structural element in FLAC3D does not provide an inbuilt option for bending strain it is calculated using the bending moment of the pile. The double shear tests were conducted with a load of 1.25 tonnes and 5.00 tonnes applied on the central block. The strain profiles obtained on the two slots were derived into bending strains**.** Figure 4.15 shows the bending

strains of the bolt in the laboratory test conditions and from the simulated model. Figure 4.16 compares the joint reaction in FLAC3D and laboratory tests. The bending strain and the joint reaction in the model match closely with the laboratory test results. This shows that the FLAC3D pile element can model the shear response of rock bolt for low shear loads or before the bolt yielding starts. The pile element needs to be modified to model the combined shear and tensile yielding and failure of rock bolt.

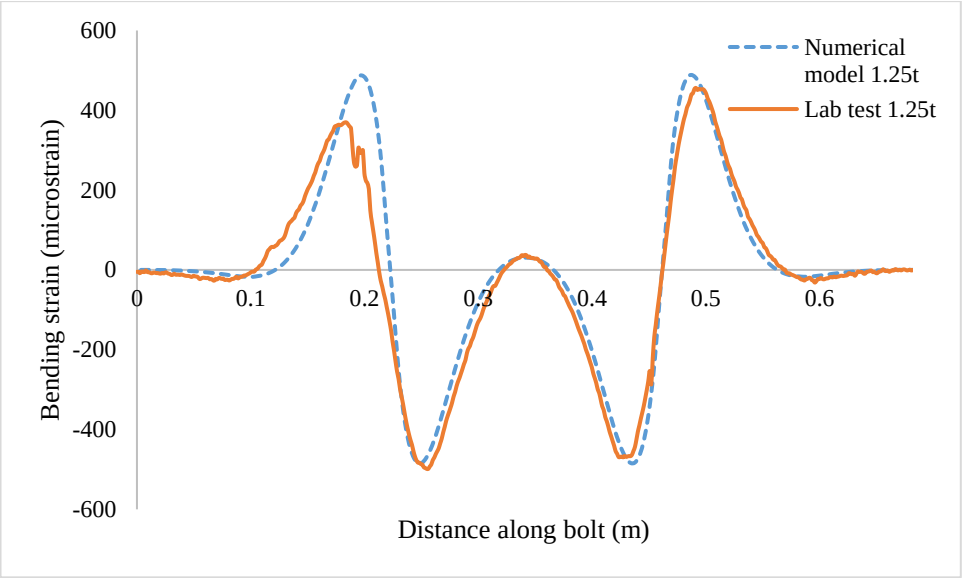

a) 1.25 tonnes

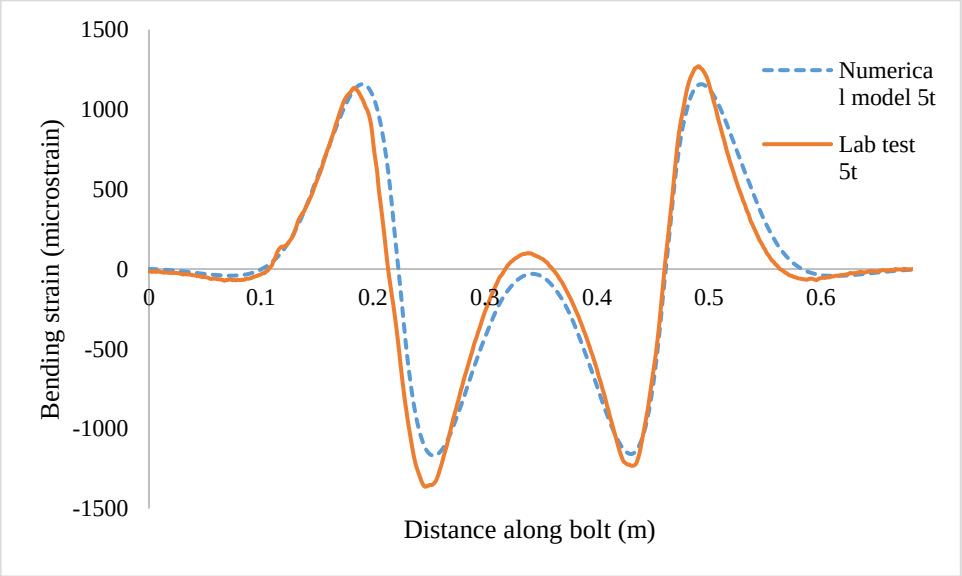

b) 5.00 tonnes

Figure 4.15 – Bending strain calibration plot.

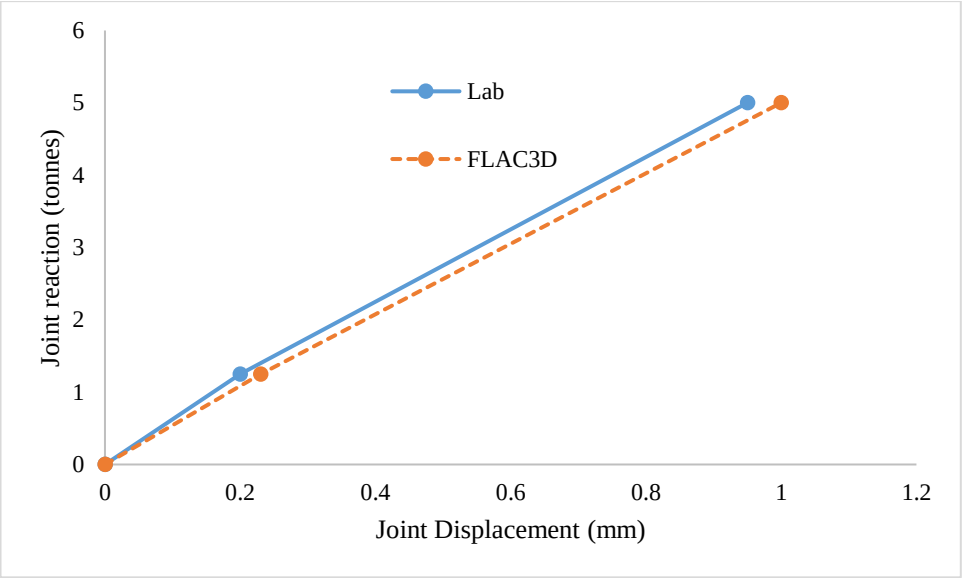

Figure 4.16 - Double shear joint response laboratory results vs FLAC3D model.

4.6.2 Modelling combined load yielding/failure of pile element

The pile element in FLAC3D provides three limiting variables to simulate the yielding/failure of rock bolt. A limiting moment value, after which the bolt deforms without any increase in bending moment. A tensile yield force value at which the bolt starts perfectly plastic yielding. A tensile rupture strain value at which the bolt fails in tension and bending. There is no option to simulate the rock bolts yielding/failure under combined axial and shear load.

As seen from the numerical models of double shear test, a rock bolt under shear load can yield by two mechanisms depending on the strength of the host media. If the host media is weak, bending deformation dominates and plastic hinges form at a distance from the shear plane. If the host media is strong, then the rock bolt will start yielding due to shear stress at the shear plane. After the bolt has yielded, failure can occur at either the plastic hinges due to a combination of tensile and bending loads or the rock bolt can fail at the shear plane under pure shear or a combination of tensile and shear loads.

Combined load yield and failure criteria for rock bolt have been proposed by Pellet and Egger (1996) using equations 4.2 and 4.3, respectively. Equation 4.2 can be used to determine the yielding at plastic hinges. For determining shear yield, equation 4.3 can be used by replacing the failure stress with the yield stress of bolt material.

For determining the failure point of the bolt, equation 4.3 cannot be used directly, as it uses a relationship based on ultimate failure loads. The pile element in FLAC3D behaves perfectly plastic after yielding. The load in the pile after yielding remains constant and failure load is never achieved. Therefore, to determine the failure point in the pile, it is proposed that instead of ultimate failure load, the total strain is calculated and when it reaches the failure strain value, the pile fails.

Total strain in the pile element at a node is calculated by adding up the axial, bending, and shear strain. The axial strain and bending strain can be calculated at the pile nodes using the displacement of the nodes. Transverse shear strain cannot be directly calculated from the node displacement as the pile element ignores the displacement caused by transverse shear. The shear stress-strain curve can be estimated using a simple piece-wise linear graph as shown in Figure 4.17.

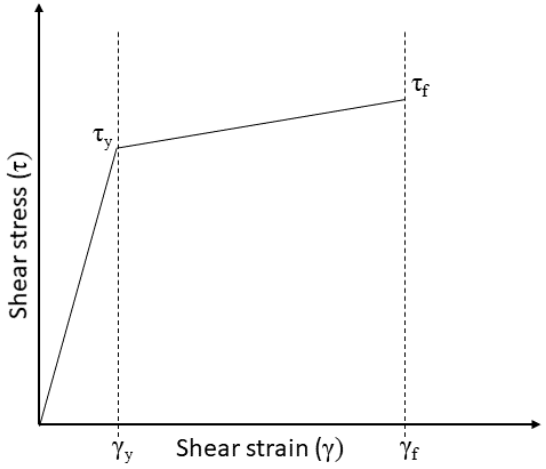

Figure 4.17 - Piece-wise linear estimation of shear stress-strain graph for steel.

The shear strain up to the yield point can be estimated by –

$$\gamma_e = \frac{4 f_s}{\pi D_b^2} \times \frac{\gamma_y}{\tau_y} \tag{4.13}$$

Where:

γ_e : elastic shear strain

f_s : shear force in pile

D_b : pile diameter

γ_y : shear yield strain of bolt material

τ_y : shear yield stress of bolt material

FLAC3D does not have the option to simulate the shear yielding of the pile. To simulate the shear response of rock bolt, the normal spring stiffness is calibrated to the rock bolt response before yield. After shear yield point, the normal spring stiffness is reduced to simulate the strain hardening. The value of normal spring stiffness after yield can be obtained by calibrating the model with the laboratory test data. The shear strain after shear yielding can then be calculated by –

$$\gamma_{ay} = \gamma_y + \frac{(4 f_s - \pi D_b^2 \tau_y)(\gamma_f - \gamma_y)}{\pi D_b^2 (\tau_f - \tau_y)} \tag{4.14}$$

Where:

γ_{ay} : shear strain after yield

γ_y : shear yield strain of bolt material

γ_f : shear failure strain of bolt material

τ_y : shear yield stress of bolt material

τ_f : shear failure stress of bolt material

4.7 Results of modified pile element model

4.7.1 Verification of the model and comparison of shear response pile with un-modified pile

To verify the shear response of the modified pile element, the model is calibrated with the data from the laboratory shear test of a fully grouted rock bolt done by McHugh and Signer (1999). These test results have been selected as the bolts were tested to failure under shear load. The shear test is conducted by installing a fully grouted rock bolt in two concrete blocks placed inside the steel shear test frames. The numerical model consists of 29 cm concrete blocks like the laboratory test. The rock bolt is modelled using the pile elements and placed perpendicular to the interface between the two blocks. The pile is fixed at the two ends points and no pre-tension is applied. The steel shear test frame around the concrete blocks is simulated using shell structural elements. To shear the rock bolt, one concrete block is fixed in place while the other one is displaced parallel to the interface. The free block is confined to displace only in the vertical direction. The model geometry is shown in Figure 4.18. The material properties and pile properties are shown in Table 4.6 and Table 4.7, respectively.

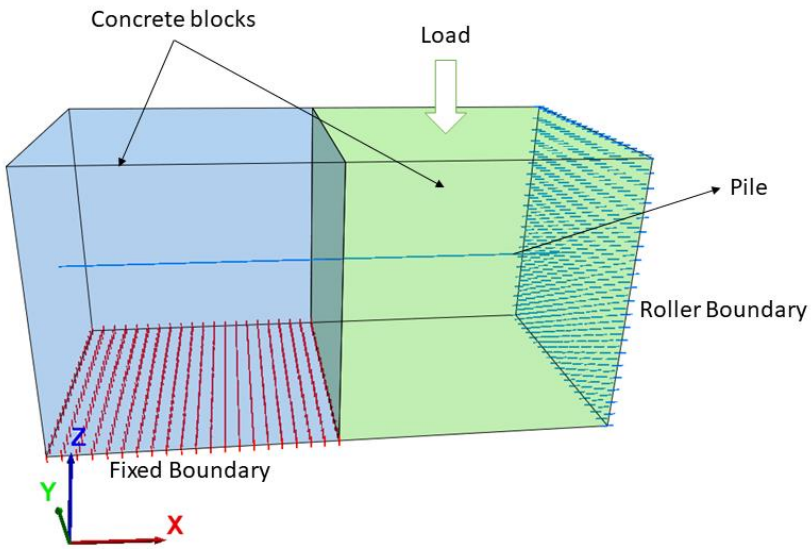

Figure 4.18 - Model geometry.

Table 4.6 – Material Properties (McHugh and Signer, 1999).

Material	**Elastic Modulus (GPa)**	**Poisson's Ratio**	**Cohesion MPa**	**Friction Angle**	**Tensile Strength MPa**
Concrete	33.8	0.18	22.3	35	8.55

Table 4.7 – Pile Properties (Pammela Caroline Pinazzi et al., 2020; Tulu et al., 2012).

Diameter (mm)	**Young's Modulus (GPa)**	**Poisson's Ratio**	**Normal spring stiffness (GPa)**	**Normal spring cohesion (N/m)**	**Shear spring stiffness (GPa)**
22	200	0.30	1.5	2.75e6	1.52
Shear spring cohesion (N/m)	**Plastic Moment (Nm)**	**Failure strain**	**Normal spring friction angle**	**Shear spring friction angle**	**Axial yield load (kN)**
8e5	2000	0.175	25	23	160
Shear yield stress (MPa)	**Shear yield strain**	**Shear failure stress (MPa)**	**Shear failure strain**		
252	0.1	312	0.4		

Figure 4.19 shows the shear response of the modified pile element compared with the laboratory test data and the un-modified pile. The shear response of the modified pile model matches closely with the laboratory test data from McHugh and Signer (McHugh and Signer

1999). The modified pile model has similar pre-yield behaviour as the un-modified pile model. After shear yielding, the modified pile model shows higher displacement due to the additional transverse shear deformation. The un-modified pile model is stiffer after yield point as transverse shear deformation in the pile is ignored. The modified pile fails under combined shear and axial load while the un-modified pile fails under only axial load. This leads to a higher predicted failure load for un-modified pile (30 tonnes) as compared to the modified pile (22.5 tonnes).

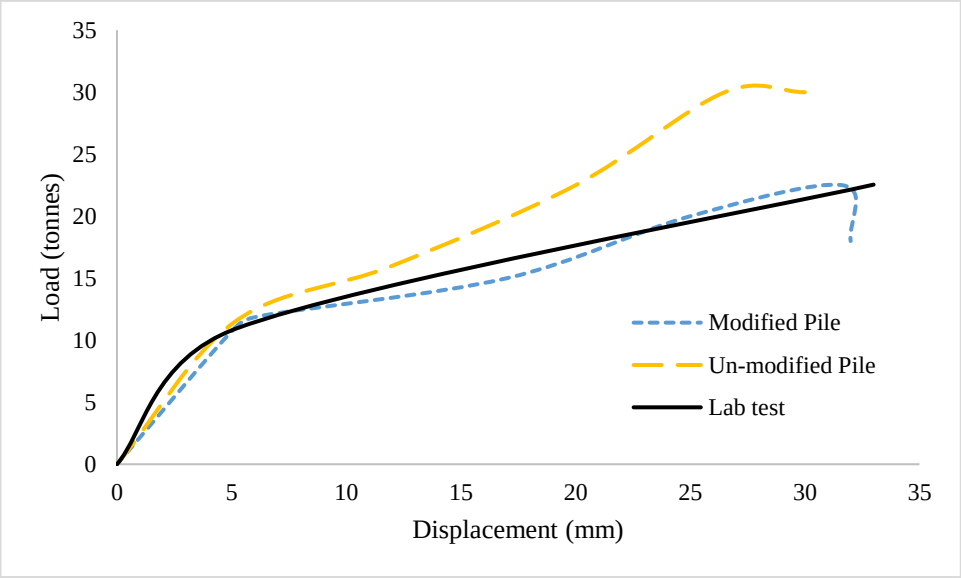

Figure 4.19 - Comparison of shear response of modified pile with laboratory test data.

4.8 Conclusions

The double shear laboratory tests undertaken by Kostecki (2019) were used to calibrate the numerical models. The calibrated model was used to study the effect of concrete strength on rock bolt stress profile. The maximum shear stress in the rock bolt increased with increasing concrete strength and stiffness. The results from the numerical model were also compared with the analytical model. The following conclusions were made based on the analysis –

1. As the strength and stiffness of the concrete increased, the dominant stress in the rock bolt at the yield point changed from bending stress to shear stress.

2. The analytical model proposed by Pellet and Egger (1996) can qualitatively predict the rock bolt behaviour under shear load. The analytical model, however, underestimates the rock response due to the assumption that the host material becomes unconfined near the shear interface. This leads to the underestimation of the shear force on the rock bolt. The analytical model was found to under-estimate the shear force by 50% compared to the numerical model.

3. Due to this underestimation of shear force, the rock bolt's post-yield behaviour in analytical models does not consider the shear plastic deformation. This leads to an underestimation of the total shear deformation at failure. Underestimation of shear load in rock bolt also leads to an overestimation of the failure load. The modified analytical model was found to be better at estimating shear force at yield point in rock bolt in high strength concrete.

To simulate the actual shear response of the rock bolt in FLAC3D, the pile structural element was modified to show actual shear load and deformation. The model was verified using laboratory tests data from McHugh and Signer (1999) and compared with the un-modified pile element. Following conclusions can be made based on the analysis:

4. FLAC3D pile elements underestimate shear deformation in the case of localised high shear stress, as found in a rock bolt installed across a joint.

5. The modified pile model can simulate the correct shear response of rock bolt and combined axial and shear load failure of the rock bolt at joints and discontinuities. The un-modified pile's shear response was stiffer, and it predicted a much higher (25% higher) failure load compared to test data. Therefore, the modified pile element can be used in numerical modelling of rock bolts installed across discontinuities where the shear response and combined load failure behaviour of rock bolt is important.

The results of this work show that the conventional models of rock bolt behaviour under shear underestimate the shear force and deformation in the rock bolt. Right estimation of the stress profile on the rock bolt is important to correctly determine the deformation and failure behaviour of the rock bolt. The modified FLAC3D pile element presented can be used in

designing rock bolt reinforcement for mines with a high degree of shear deformations in the rock excavations.

Acknowledgements

This work was supported by the Minerals Research Institute of Western Australia (MRIWA); Mining3 and Peabody Energy.

References

ANSYS® Academic Research Mechanical. (2019).

Bjurstrom, S. (1974). Shear strength of hard rock joints reinforced by grouted untensioned bolts. Proc. 3rd Cong. ISRM, Denver, 2, 1194-1199.

Blanco Martín, L., Tijani, M., & Hadj-Hassen, F. (2011). A new analytical solution to the mechanical behaviour of fully grouted rockbolts subjected to pull-out tests. Construction and Building Materials, 25(2), 749-755. doi:10.1016/j.conbuildmat.2010.07.011

Chen, Y. (2014). Experimental study and stress analysis of rock bolt anchorage performance. Journal of Rock Mechanics and Geotechnical Engineering, 6(5), 428-437. doi:10.1016/j.jrmge.2014.06.002

Chen, Y., Cao, P., Zhou, K., & Li, L. (2018). Analytical Study of Loading and Displacing Angles of Rock Bolt Subjected Shear Condition. Paper presented at the 52nd US Rock Mechanics/Geomechanics Symposium.

Chen, Y., & Li, C. C. (2015). Performance of fully encapsulated rebar bolts and D-Bolts under combined pull-and-shear loading. Tunnelling and Underground Space Technology, 45, 99-106. doi:10.1016/j.tust.2014.09.008

Dight, P. M. (1982). Improvements to the stability of rock walls in open pit mines: by Phillip M. Dight (Doctoral dissertation, Monash University).

Farmer, I. W. (1975). Stress distribution along a resin grouted rock anchor. International Journal of Rock Mechanics and Mining Sciences and, 12(11), 347-351. doi:10.1016/0148-9062(75)90168-0

Ferrero, A. M. (1995, September). The shear strength of reinforced rock joints. In International journal of rock mechanics and mining sciences & geomechanics abstracts (Vol. 32, No. 6, pp. 595-605). Pergamon.

FLAC3D — Fast Lagrangian Analysis of Continua in Three-Dimensions (Version 6.0). (2017). Minneapolis: Itasca: Itasca Consulting Group, Inc.

Freeman, T. (1978). The behaviour of fully-bonded rock bolts in the Kielder experimental tunnel. Tunnels & Tunnelling International, 10(5).

Frith, R. (2011). Why dead load suspension design for roadway roof support is fundamentally flawed within a pro-active strata management system.

Gerdeen, J., Snyder, V., Viegelahn, G., & Parker, J. (1979). Design criteria for roof bolting plans using fully resin-grouted nontensioned bolts to reinforce bedded mine roof. Volume III: Experimental model studies; Volume IV: Theoretical analysis. In: Houghton, MI: Michigan Technological University. US Bureau of Mines contract.

Grasselli, G. (2005). 3D behaviour of bolted rock joints: Experimental and numerical study. International Journal of Rock Mechanics and Mining Sciences, 42(1), 13-24. doi:10.1016/j.ijrmms.2004.06.003

Haas, C. J. (1976). Shear resistance of rock bolts. Trans. Soc. Min. Eng. AIME;(United States), 260(1).

Jalalifar, H., Aziz, N. I., & Hadi, M. N. (2005). Rock and bolt properties and load transfer mechanism in ground reinforcement.

Jessu, K. V., Kostecki, T., & Spearing, S. (2016). Measuring roof-bolt response to axial and shear stresses: Laboratory and first in-situ analyses. The CIM Journal, 7(1), 62-70.

Kostecki, T. R. (2019). Design Methods For Rock Bolts Using In-Situ Measurement From Underground Coal Mines. (Doctor of Philosophy Degree). Southern Illinois University Carbondale, Carbondale, Southern Illinois. Available from ProQuest

Li, C., & Stillborg, B. (1999). Analytical models for rock bolts. International Journal of Rock Mechanics and Mining Sciences, 36(8), 1013-1029.

Li, C. C. (2010). Field observations of rock bolts in high stress rock masses. Rock Mechanics and Rock Engineering, 43(4), 491-496.

Li, L., Hagan, P., Saydam, S., Hebblewhite, B., & Li, Y. (2016). Parametric study of rockbolt shear behaviour by double shear test. Rock Mechanics and Rock Engineering, 49(12), 4787-4797.

Li, X., Aziz, N., Mirzaghorbanali, A., & Nemcik, J. (2016). Behavior of fiber glass bolts, rock bolts and cable bolts in shear. Rock Mechanics and Rock Engineering, 49(7), 2723-2735.

Ma, S., Zhao, Z., & Shang, J. (2019). An analytical model for shear behaviour of bolted rock joints. International Journal of Rock Mechanics and Mining Sciences, 121, 104019.

Mark, C., Pakalnis, R. T., & Tuchman, R. J. (2007). Proceedings of the International Workshop on Rock Mass Classification in Underground Mining.

McHugh, E., & Signer, S. (1999). Roof bolt response to shear stress: laboratory analysis. Paper presented at the Proceedings 18th international conference on ground control in mining, Morgantown, WV.

Pinazzi, P. C., Spearing, A. S., Jessu, K. V., Singh, P., & Hawker, R. (2020). Mechanical performance of rock bolts under combined load conditions. International Journal of Mining Science and Technology, 30(2), 167-177.

Pellet, F., & Egger, P. (1996). Analytical model for the mechanical behaviour of bolted rock joints subjected to shearing. Rock Mechanics and Rock Engineering, 29(2), 73-97.

Snell, G., Kuley, E., & Milne, D. (2017). A laboratory-based approach to assess rockbolt behaviour in shear. Paper presented at the Proceedings of the First International Conference on Underground Mining Technology.

Spang, K., & Egger, P. (1990). Action of fully-grouted bolts in jointed rock and factors of influence. Rock Mechanics and Rock Engineering, 23(3), 201-229. doi:10.1007/BF01022954

Tulu, I. B., Esterhuizen, G. S., & Heasley, K. A. (2012, June). Calibration of FLAC3D to simulate the shear resistance of fully grouted rock bolts. In 46th US Rock Mechanics/Geomechanics Symposium. OnePetro.

Chapter 5. An Improved Analytical Model for the Elastic and Plastic Strain-hardening Shear Behaviour of Fully Grouted Rockbolts

This chapter has been accepted and published in Rock Mechanics and Rock Engineering as:

Singh, P., & Spearing, A. J. S. (2021). An Improved Analytical Model for the Elastic and Plastic Strain-hardening Shear Behaviour of Fully Grouted Rockbolts. Rock Mechanics and Rock Engineering, 1-17.

Abstract

Fully grouted rock bolts are one of the main forms of rock reinforcement used in underground mines, especially in coal mines. Analytical models describing the deformation behaviour of rock bolts under various loading conditions are used in numerical models for designing appropriate rock reinforcement. A reliable analytical model capable of accurately predicting rock bolts' responses under different loading conditions is, therefore, important for more realistic numerical models and effective reinforcement design. In this paper, a new analytical model for shear behaviour of rock bolts is proposed which can better predict rock bolt behaviour under large shear deformations. A method to consider the effect of post-elastic strain hardening on bending stiffness of rock bolt is presented. The analytical model is validated with results from laboratory shear tests and found to be consistent with the laboratory results. To analyse the effect of post-elastic strain hardening on shear behaviour of a rock bolt, results from the proposed analytical model is compared with analytical model without strain-hardening effect. Without strain hardening, the analytical models overestimate the ultimate shear displacement by up to 35% in the examples shown in the paper.

List of Symbols

l_A : Hinge length (m)

D_b : Bolt diameter (m)

c_r : Joint cohesion (N/m^2)

c_b : Additional cohesion from bolt (N/m^2)

σ_i : Initial joint confining stress (N/m^2)

σ_b : Additional joint confining stress from bolt (N/m^2)

ϕ : Joint friction angle (rad)

α : Angle between bolt axis and joint (rad)

p_u : Bearing capacity of rock or grout (N/m)

K : Load factor (K>=1) (Dimensionless)

σ_c : Unconfined compressive strength (UCS) of rock (N/m^2)

δW_{int} : Internal virtual work (Nm)

δW_{ext} : External virtual work (Nm)

$M_{O,A}, \delta M_{O,A}$: Real and virtual bending moment at point O or A (N/m)

$N_{O,A}, \delta N_{O,A}$: Real and virtual axial load at point O or A (N)

$Q_{O,A}, \delta Q_{O,A}$: Real and virtual shear load at point O or A (N)

F_Y, δF_Y : Real and virtual shear force in y-axis direction (N)

E : Young's Modulus of bolt (N/m^2)

I_z : Area moment of inertia along z-axis of bolt (m^4)

G : Shear modulus of bolt (N/m^2)

A_s : Equivalent shear area (m^2)

u_y : Bolt deformation at point O in y-axis direction (m)

u_x : Bolt deformation at point O in x-axis direction (m)

θ: Bolt deflection angle (rad)

Δ_{ext} : Axial extension of bolt at point O (m)

E_r : Reduced modulus (N/m^2)

$\varepsilon_1, \varepsilon_2$: Maximum elongation and contraction strain on the bolt (Dimensionless)

Δ : Sum of the absolute values of maximum elongation and contraction strain (Dimensionless)

r : Bolt curvature (m)

l_p : Length of plastic section of bolt (m)

$\Delta_{ext.e}$: Axial extension at yield point (m)

N_{oe} : Axial load at point O at yield point (N)

$\sigma_{y,f}$: Yield and ultimate strength of bolt (N/m^2)

$\varepsilon_{y,f}$: Yield and failure strain of bolt (Dimensionless)

M_P : Plastic bending moment (N/m)

N_p : Yield load of bolt (N)

Q_p : Shear yield load of bolt (N)

N_f : Ultimate load capacity of bolt (N)

σ_f : Ultimate strength of bolt (N/m^2)

Q_f : Ultimate shear load capacity of bolt (N/m^2)

5.1 Introduction

Rock bolts provide an effective method of ground reinforcement in underground mines. The low profile of rock bolts protruding from the excavation periphery provides an unobstructed path for equipment and personnel movement, and this combined with the quick, cost effective and easy installation has made rock bolts the most common form of rock reinforcement system used in mines. Among the different types of rock bolts available, fully grouted rock bolts are used for their high stiffness to both axial and shear loads, and for their inherent improved resistance to corrosion. Fully grouted rock bolts consist of a solid bar (usually a deformed bar, typically rebar) coupled to the surrounding rock around the drill hole through a grouting medium such as cement or resin. This bolt-grout and grout-rock coupling leads to a complex load transfer mechanism along the length of the grouted rock bolt and the surrounding rock. Any effective rock bolt reinforcement design method requires a full understanding of this load transfer mechanism which is complex and changes as mining progresses. Among the common rock reinforcement design methods, numerical modelling lends itself as most convenient to use under complex physical and geometrical rock conditions. The modelling is generally qualitative but when combined with model validation it becomes quantitative and more reliable than other design methods such as experiential and empirical methods.

In the context of this paper, a useful numerical model should be able to simulate the rock bolt behaviour under different and complex loading conditions. There are two primary ways of modelling a rock bolt in a geotechnical study either by modelling the bar and grout as grid elements or by simulating the bar and grout behaviour using a linear structural element (Kostecki 2019). Modelling the rock bolt using grid elements requires the knowledge of only the material and contact properties of the rock bolt. It also facilitates the analysis of the internal stress state of the rock bolt and therefore provides a better estimation of the plastic deformation and failure behaviour of the rock bolt. This is important from a rock related safety point of view. However, this method is computationally costly and is practical for only small scale laboratory test models. Linear structural elements overcome this problem by simulating the

rock bolt as a one-dimensional element that simulates the behaviour of a rock bolt and grout interface with the rock. The response of the structural element is usually derived from an analytical model describing the behaviour of a rock bolt under different loading conditions. The accuracy of the results of such a numerical model depends upon the underlying analytical model's ability to describe the actual response of a fully grouted rock bolt. A rock bolt installed in an underground excavation undergoes a combined axial and shear load. Analytical models should be able to describe both axial and shear behaviour of a rock bolt. Considerable research has been conducted in the past on analytical models describing rock bolt behaviour under different loads but the focus has been mainly on the tensile capacity and performance and this is not representative of the in situ loading. However, owing to the complex behaviour of the rock bolt, current analytical models are still inaccurate and tend to overestimate the effective rock bolt capacity which is not desirable. This paper focuses on the shear behaviour of the rock bolt and presents an improved analytical model for a rock bolt's response to shear loading.

5.2 Background

5.2.1 Rock bolts under shear load

Rock bolts installed in underground mines undergo shear deformation along with axial deformation (Li, 2010; McHugh and Signer, 1999; Simser, 2007). A rock bolt intersecting a discontinuity like a fracture or a joint plane undergoes shear deformation due to the shear movement of rock along the discontinuity (Figure 5.1).

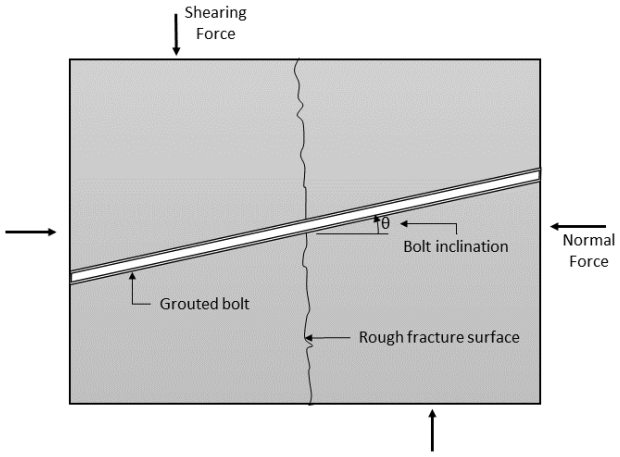

Figure 5.1- Rock bolt undergoing shear deformation (Haas, 1976).

Past studies have examined the shear behaviour of a fully grouted rock bolt through laboratory shear tests and in-situ observations (Chen, 2014; Chen and Li, 2015; Dight, 1982; Egger and Spang, 1987; Haas, 1976; Li, et al. 2016; Pammela Caroline Pinazzi et al., 2020; Snell et al., 2017). These studies investigated the effect of bolt inclination to a discontinuity, normal load on the joint, joint roughness, shear gap and combined loading on shear response of a fully grouted rock bolt. The data resulting from these studies has been used to formulate analytical models in order to better describe the rock bolt behaviour under shear.

5.2.2 Analytical Models

Analytical models are mathematical models which are used to approximately describe a physical system. These models consist of equations whose solutions govern the behaviour of the system. In this case, these equations give a relationship between the deformations along the bolt and the corresponding bolt loads.

5.2.3 Rock bolt mechanics under shear

A rock bolt installed across a rock joint or fracture when subjected to shearing, deforms with the joint displacement. The rock bolt is subjected to a combination of loads as shown in Figure 5.2 (Pellet and Egger, 1996). Point O on the rock bolt denotes the rock bolt intersection with joint. The figure shows forces on half of the rock bolt with reaction from the other half of bolt

represented by an axial load N_0 and a shear load Q_0 at point O. The reaction of the host media is represented by a distributed load P_u. Points A and B define the distribution of host media reaction on rock bolt. The bolt bends under the shear load with point A denoting the location of the maximum bending moment and the maximum shear load at point O. Rock reaction on the rock bolt decreases linearly from P_u at A to zero at point B. As the load on the rock bolt increases the bolt continues to deform in shear and at yield point a plastic hinge is formed at the point A (Spang and Egger, 1990) and the length l_A is called the hinge length.

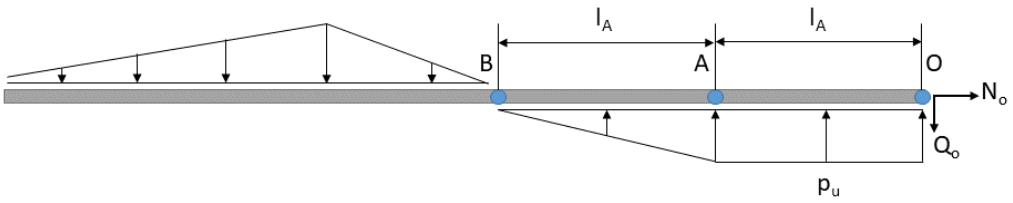

Figure 5.2- Forces on a rock bolt under shear (Pellet and Egger, 1996).

The rock bolt's contribution to the joint shear strength can be divided into two parts – the axial component N_0 increases the confining stress on the joint and the shear component Q_0 supplements the cohesion of the joint. The strength of the joint can be expressed using the Mohr-Coulomb criterion as (Pellet and Egger, 1996):

$$\tau = (c_j + c_b) + (\sigma_i + \sigma_b)\tan\phi \tag{5.1}$$

Where,

c_r - joint cohesion

c_b - additional cohesion from bolt

σ_i - initial joint confining stress

σ_b - additional joint confining stress from bolt

ϕ - joint friction angle

5.2.4 Current Analytical Models

Gerdeen et al. (1979) proposed a rock bolt shear model based on elastic foundation beam theory (BEF). Dight (1982) used BEF to propose a model for bolt deformation under shear load considering grout yield and bolt failure under combined axial and shear load. Pellet and Egger (1996) used the BEF theory with minimum energy principle to propose an analytical model for shear deformation of rock bolt. The proposed model predicted rock bolt behaviour under large shear deformation of the rock bolt. The model assumed an elastic, rigid perfectly plastic behaviour of the host media. The rock reaction was given by the following formula:

$$p_u = K\sigma_c D_b \tag{5.2}$$

p_u : bearing capacity of rock or grout

K : load factor (K>=1)

σ_c : unconfined compressive strength (UCS) of rock.

Jalalifar and Aziz (2010) investigated the effect of host media strength, axial loading and bolt diameter on the hinge length l_A and proposed a relationship for calculating it. Li et al. (2015) used statically indeterminate beam theory to derive two models for shear behaviour of cable bolt during the elastic and plastic stages of host material. Ma et al. (2018) used BEF theory to derive an analytical model with the host material stiffness calculated based on the curvature influence zone and bolt properties. Effect of pretension and plastic rock deformation on curvature influence zone was also included in the model. Ma et al. (2019) proposed a model combining the effect of pretension load, axial load due to shear and dowel shear load on the rock bolt. Effect of axial load on bolt-grout interface was considered using the trilinear bond slip model. Chen et al. (2020) used elastic theory for a semi-infinite length beam to derive an analytical model for rock bolt under shear and axial load. Deflection curves were proposed for elastic, elastic and plastic and fully plastic stages. Liu and Li (2020); Liu and Li (2017)

proposed an analytical model for rock bolt shear using force method. A method to derive the transverse deformation section length of rock bolt was proposed using the minimum potential energy principle. The model was only applicable to elastic deformation of the rock bolt.

Most of the analytical models (described above) proposed shear behaviour of rock bolt used the beam with elastic foundation theory. The differential equation for beam deflection used in BEF theory is valid only for small deflections of the beams. The models also assume the post yield behaviour of rock bolt to be perfectly plastic. This assumption leads to the conclusion that the shear load on the rock bolt remains constant once the plastic hinges forms at the maximum bending points on the rock bolt. However, the actual behaviour of rock bolt is not perfectly plastic (Timoshenko, 1983). Post-yield behaviour of steel shows a considerable amount of strain-hardening before failure. This leads to increase in shear load on the rock bolt even after the formation of plastic hinges. Analytical methods based on force methods consider both bending and transverse shear deformation in rock bolt (Li et al., 2015; Liu and Li, 2020; Liu and Li, 2017). The force method can also give better results for larger deflection of beam, however, these models were only derived for elastic deformation of the rock bolt. The analytical model presented in this paper focuses on the development of a rock bolt shear model by the principle of virtual work using a virtual force method, considering the actual loading profile of a rock bolt under shear. The analytical model also includes a method to consider the effect of the post-yield strain-hardening behaviour of steel, which results in better prediction of the post-yield shear response of a fully grouted rock bolt.

5.3 Analytical Formulation

The aim of an analytical formulation is to derive the actual relationships between the loads on the rock bolt and the corresponding rock bolt deformation produced by these forces. The analytical formulation presented here is based on the rock bolt mechanical system proposed by Pellet and Egger (1996) in their analytical model for rock bolt shear. As the joint deforms, the rock bolt deforms with the host media and a reaction from the host media acts on the rock bolt. This reaction increases elastically with the bolt deformation until the host media yields.

The maximum value for host media reaction was assumed by Pellet and Egger (1996) from equation (5.2).

The statically indeterminate problem of a rock bolt under shear is converted into a statically determinate problem by replacing the right half of the rock bolt by its reaction on the left half (Figure 5.3). As the rock bolt has almost zero deflection at point B (Pellet and Egger, 1996) the end is considered as fixed. As the rock bolt continues to bend, a plastic hinge will develop at the maximum bending point A given by the hinge length l_A. After this point where the hinge is formed, the rock bolt will deform plastically. The bolt will keep on deforming until it fails due to a combination of axial and bending stress at point O.

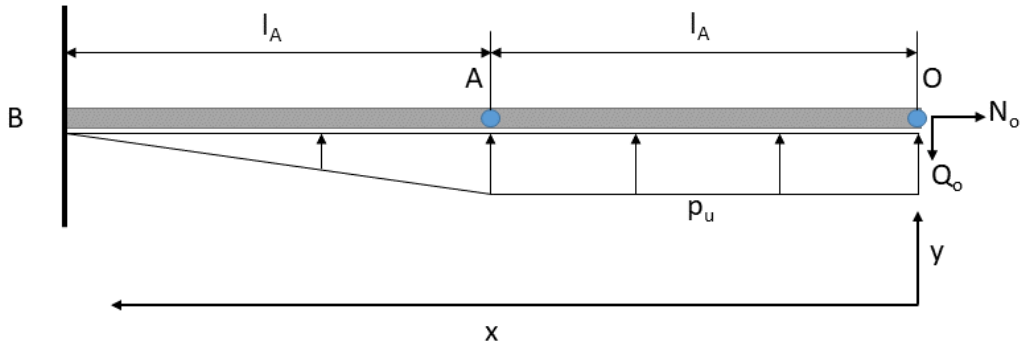

Figure 5.3- Rock bolt mechanical system (Pellet and Egger, 1996).

5.3.1 Elastic Deformation

Using static mechanics, the moment and shear force on the rock bolt section can be determined from the loads shown in Figure 5.3. The moment and shear load on the rock bolt within elastic limit is given by:

Shear force:

$$\begin{aligned} &Q_o - p_u x \qquad x < l_A \\ &Q_o - p_u l_A - \frac{p_u}{2}\left(x - l_A\right)\left(3 - \frac{x}{l_A}\right) \qquad l_A < x < 2l_A \end{aligned} \tag{5.3}$$

Bending Moment:

$$\begin{aligned} & Q_o x - \frac{p_u}{2} x^2 \qquad x < l_A \\ & Q_o x - p_u l_A \left(x - \frac{l_A}{2} \right) - \frac{p_u}{2} \left(x - l_A \right)^2 \left(2 - \frac{x}{l_A} \right) \\ & \qquad - \frac{p_u}{3} \left(x - l_A \right)^2 \left(\frac{x}{l_A} - 1 \right) \qquad l_A < x < 2l_A \end{aligned} \tag{5.4}$$

Using the principle of virtual work using the virtual force method (McGuire et al., 1999), the displacement of point O on the rock bolt can be calculated. The internal and external virtual work equations for displacement at point O can be written as:

$$\delta W_{\text{int}} = \int_0^{2l_A} \delta M_z . \frac{M_z}{EI_z} dx + \int_0^{2l_A} \delta F_y . \frac{F_y}{A_s G} dx \tag{5.5}$$

$$\delta W_{ext} = \delta Q_o u_y \tag{5.6}$$

Where,

M_Z is the bending moment about z-axis

F_Y is the shear force in y-axis direction

E is Young's Modulus of bolt

I_Z is area moment of inertia along z-axis of bolt

G is shear modulus of bolt

A_s is the equivalent shear area [3/4*(cross-sectional area of bolt)(McGuire et al., 1999)]

The first term on right hand side of equation (5.5) denotes the work done by bending and the second term denotes work done by shear. Equating the internal and external virtual work and solving the equations gives the expression for the deformation of bolt at point O in y-axis direction as (for details on solving the equations see Appendix 1):

$$u_y = \frac{1}{EI_Z}\left(\frac{8Q_O l_A^3}{3} - \frac{133 p_u l_A^4}{360}\right) + \frac{1}{A_s G}\left(2Q_O l_A - \frac{11 p_u l_A^2}{6}\right) \tag{5.7}$$

l_A is calculated using the following equation:

$$l_A = k\frac{\pi}{4}\sqrt[4]{\frac{EI_z}{150\sigma_c^{0.85}}} \tag{5.8}$$

Where, k is a constant whose value depends on the test setup. The value of P_u before host media yielding can be calculated as:

$$P_u = \frac{Q_O}{l_A} \tag{5.9}$$

The maximum value for P_u is given by equation (5.2). If the angle between bolt and joint is α and bolt deflection angle at O is θ then as shown in Figure 5.4, a kinematic condition can be written for axial extension of the bolt as (Li et al., 2015):

$$\Delta_{ext} = \frac{u_x \cos(\alpha - \theta)}{\cos(\alpha)} \tag{5.10}$$

Where, $u_x = u_y/\tan\alpha$ and the bolt deflection angle θ can be calculated from static mechanics as (see Appendix 2 for details):

$$\theta = \frac{1}{EI_Z}\left(\frac{19 p_u l_A^3}{24} - 2Q_O l_A^2\right) \tag{5.11}$$

As the bolt deforms the grout around the rock bolt gets crushed. It is assumed that the grout up to point A gets completely crushed (Pellet and Egger, 1996) and the axial load remains constant in the bolt section OA. As the bolt section near point A is undergoing plastic deformation, it can be assumed that majority of the axial elongation will occur in this section. The axial load at point O due to the extension of bolt section OA can then be calculated as:

$$N_o = \frac{\pi D_b^2}{4}\left(\frac{E\Delta_{ext}}{l_A}\right) \tag{5.12}$$

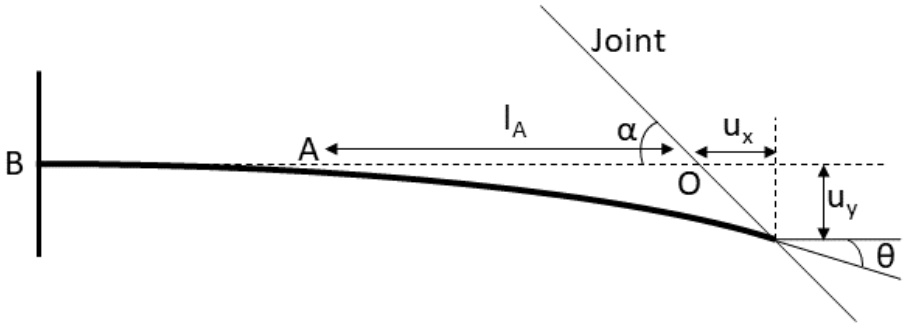

Figure 5.4- Displacement compatibility condition at point O for a deformed bolt (Li et al. ,2015).

5.3.2 Plastic Deformation

As the rock bolt deforms, the bending moment and shear force on the rock bolt increases. The bolt yields at point A by forming a plastic hinge. Once the plastic hinge is fully formed the rock bolt's bending stiffness reduces significantly at the hinge. Earlier research assumed that the bolt after this point starts behaving like a truss with hinge at point A and only the axial load in the bolt increases on further bolt deformation (Chen et al., 2020; Jalalifar and Aziz, 2010; Li et al., 2015; Liu and Li, 2020; Liu and Li, 2017; Ma et al., 2018; Ma et al., 2019; Pellet and Egger, 1996). However, as the steel yields it shows a considerable strain hardening before failing (Timoshenko, 1983). To include the effect of strain hardening of steel the concept of reduced modulus for bending deformation beyond the elastic limit (Timoshenko, 1983) is used. The flexural rigidity of a point in the bolt is calculated based on the bending moment at that point. The reduced modulus E_r for the bolt section over elastic limit is calculated as (Timoshenko, 1983):

$$E_r = \frac{256}{\pi D_b \Delta^3} \int_{\varepsilon_2}^{\varepsilon_1} \sigma\varepsilon \sqrt{\frac{D_b^2}{4} - \frac{D_b^2 \varepsilon^2}{\Delta^2}}\, d\varepsilon \tag{5.13}$$

Where,

Δ is the sum of the absolute values of maximum elongation and contraction strain on the bolt ε_1 and ε_2 respectively. The relationship between moment in the bar and the curvature is given by:

$$M = \frac{E_r I_z}{r} \tag{5.14}$$

Where, M is the moment at a point in the bolt and r is the curvature of the neutral axis at that location. The maximum strains on the bolt are equal on elongation and contraction sides and are related to curvature by:

$$\varepsilon_1 = \varepsilon_2 = \frac{D_b}{2r} \tag{5.15}$$

For a given value of bending moment beyond the plastic moment limit of the bolt, the value of the reduced modulus E_r at that location can be back calculated using equations (5.13) to (5.15) (for details see Appendix 3).

For calculating the bolt deformation beyond the elastic limit, the bending moment in the rock bolt is calculated with the increased shear force Q_o. An average value of moment is calculated for the rock bolt section with bending moment above the plastic moment limit. Then the value of the reduced modulus E_r is calculated using the average bending moment as detailed above (Timoshenko, 1983). The value of E_r will be less than the elastic modulus E where the bending moment is greater than the plastic moment limit. To calculate the deformation of the bar at point O in y-axis direction, equations (5.23) and (5.24) are integrated for elastic and plastic sections (where bending moment is greater than the plastic moment) separately, replacing the modulus E with reduced value E_r for the plastic section. The equations are solved for incremental increase in shear load. As the load increases further the value of E_r decreases rapidly creating a much larger curvature near the hinge points compared to rest of the beam which remains elastic.

To calculate axial load in rock bolt after yielding, kinematic relationships between shear displacement and axial extension of bolt can be established by assuming that the shape of bolt between the plastic hinges remains linear (Pellet and Egger, 1996) (Figure 5.5). The rotation, axial extension and axial load in bolt can be calculated as:

$$\tan\theta = \frac{u_y}{l_A + \frac{u_y}{\tan\alpha}} \tag{5.16}$$

$$\Delta_{ext.p} = \frac{l_A}{\cos\theta} + \frac{u_y}{\tan\alpha\cos\theta} - \left(l_A + \Delta_{ext.e}\right) \tag{5.17}$$

$$N_o = \frac{\pi D_b^2 E_P \Delta_{ext.p}}{4l_P} + N_{oe} \tag{5.18}$$

$$E_p = \left(\frac{\sigma_f - \sigma_y}{\varepsilon_f - \varepsilon_y}\right) \tag{5.19}$$

Where,

l_P is the length of plastic section (where bending moment is greater than the plastic moment) of bolt.

$\Delta_{ext.e}$ is the axial extension at yield point.

N_{oe} axial load at point O at yield point.

$\sigma_{y,f}$ are the yield and ultimate strength of bolt.

$\varepsilon_{y,f}$ are the yield and failure strain of bolt.

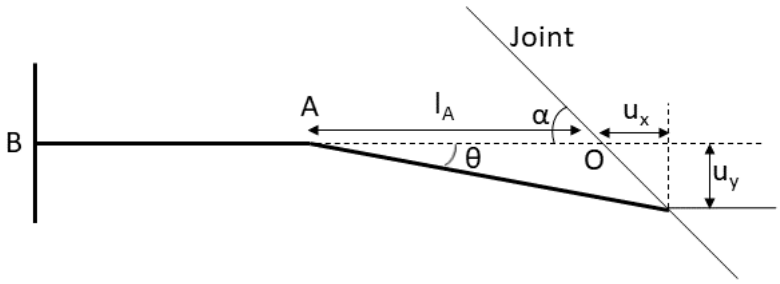

Figure 5.5 - Bolt geometry after plastic deformation.

5.4 Bolt Yield and Failure Limit

Now that the load-displacement relationship of the rock bolt under shear has been established for both the elastic and plastic conditions, to completely characterize the rock bolt behaviour, the yield and failure point of the bolt needs to be determined and defined.

5.4.1 Yield Limit

The bolt as it deforms is subjected to a combination of three forces – axial, bending moment and shear force. According to the mechanism of a fully grouted rock bolt under shear load (Figure 5.3) the bolt has two load concentration points – O and A. At point A the bending moment is maximum and the shear force is zero. At point O the shear force is maximum while the bending moment is zero. The axial load is assumed to be constant and equal to N_o along the length of the rock bolt in vicinity of the joint. This assumption is valid as the host media is considered to be crushed near the joint and therefore the bolt section near the joint is de-bonded from the host media. The bolt can yield at any one or both of these points. If the axial force, bending moment and shear force in the bolt is known then the yield condition can be checked with following expression (Maekawa and Qureshi, 1996):

$$\left(\frac{M_{O,A}}{M_p} + \left(\frac{N_{O,A}}{N_p} \right)^2 \right)^2 + \left(\frac{Q_{O,A}}{Q_p} \right)^2 = 1 \qquad (5.20)$$

Where,

$M_{O,A}$ is the bending moment at point O or A

$N_{O,A}$ is the axial load at point O or A

$Q_{O,A}$ is the shear load at point O or A

M_P is the plastic bending moment limit given by $M_p = \sigma_y D_b^3 / 6$

σ_y is the yield strength of bolt

N_p is the yield load of bolt ($\sigma_y * \pi D_b^2/4$)

Q_P is the shear yield load of bolt ($N_p/\sqrt{3}$)

5.4.2 Failure Limit

After the bolt yields, the bolt starts deforming plastically. The axial, shear and bending load on the bolt keeps increasing as the bolt deformation continues. Due to the formation of plastic hinges on the bolt, the flexural rigidity of the bolt decreases with further deformation. The rock bolt shows large deformation with small increase in bending and shear load. The axial load on the bolt keeps increasing and the bolt fails at point O by a combination of axial and shear loads (Dight, 1982). The condition for bolt failure at point O can be checked as:

$$\left(\frac{N_O}{N_f}\right)^2 + \left(\frac{Q_O}{Q_f}\right)^2 = 1 \qquad (5.21)$$

Where,

N_f is the ultimate load capacity of bolt ($\sigma_f * \pi D_b^2/4$)

D_b is the rock bolt diameter

σ_f is the ultimate strength of bolt

Q_f is the ultimate shear load capacity of bolt ($N_f/\sqrt{3}$)

5.5 Evaluation of the Analytical Model

5.5.1 Comparison with experimental data

To verify the analytical model developed, its predictions are compared with data from two sets of laboratory shear tests. A code is written in MATLAB to compute the bolt deformations using the proposed analytical model. Laboratory tests for shear behaviour of rock bolts can be done using either single shear or double shear test setup. The proposed analytical model is verified with two experiments, one with single shear setup and other with double shear setup, in both the rock bolt is sheared to failure.

5.5.2 Single shear test

McHugh and Signer (1999) conducted single shear tests on a fully grouted rock bolt to its failure limit. The rock bolts were grouted in two 29 cm cubic concrete blocks. The whole setup was enclosed in a steel shear box as shown in Figure 5.6. The top concrete block was kept fixed while the bottom block was displaced horizontally. A normal load of 8 kN was applied on the top block. Average pretension of 60 kN was applied on the rock bolts. A normal load of 10 kN was applied on the joint. The bottom block was displaced until the rock bolt failed. A total of 17 bolts were tested and shear load and displacements at yield and failure reported. The material and bolt properties are given in Table 5.1 and Table 5.2. Figure 5.7 shows the average test data compared with the analytical model results and it is evident that the analytical model fits well with the lab test data (Figure 5.7).

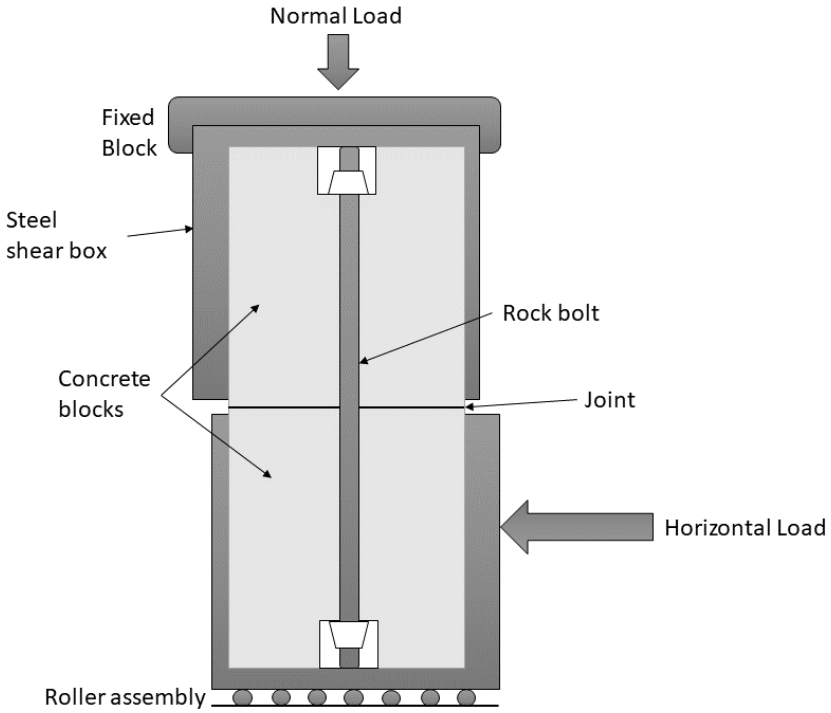

Figure 5.6- Single shear setup (modified from McHugh and Signer, 1999).

Table 5.1 – Material properties for shear test (McHugh and Signer, 1999).

Material	UCS (MPa)	Joint friction angle
Concrete	85.5	30^0

Table 5.2- Bolt properties (McHugh and Signer, 1999).

Diameter (mm)	Young's Modulus (GPa)	Shear Modulus (GPa)	Axial yield load (kN)	Ultimate Load (kN)	Yield Strain	Failure Strain
22	200	80	163	233	0.0021	0.16

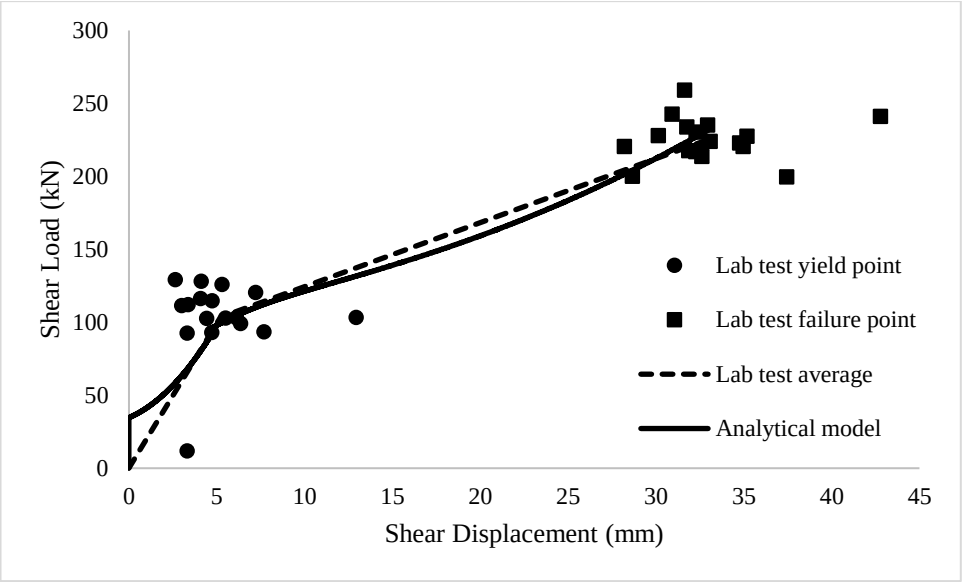

Figure 5.7 - Analytical model validation with single shear lab test data.

5.5.3 Double-shear test

Jalalifar (2006) conducted double shear tests on different types of rock bolts. Concrete of different strengths were used for the tests. Moulds of dimensions 600mm X 150mm X 150mm were used to cast the concrete blocks. The blocks were partitioned into three sections, a central section of 300mm and the other two sections of 150mm each. The rock bolt was installed in a hole in the centre of the concrete blocks. The blocks were enclosed in a steel shear box. The setup is shown in Figure 5.8. The side blocks were supported at the bottom and a load was applied to the top surface of central block until the bolt failed. To verify the proposed analytical model it was compared with results from double shear tests of rock bolt T1 in two different strength concrete 20 and 100 MPa. The material and bolt properties are given in Table 5.3 and Table *5.4*. A pretension of 20 kN is applied on the bolts. Figure 5.9 shows the double shear test data for rock bolt in concrete of different strengths and its comparison with analytical model results. The analytical model predictions are consistent with the lab test data.

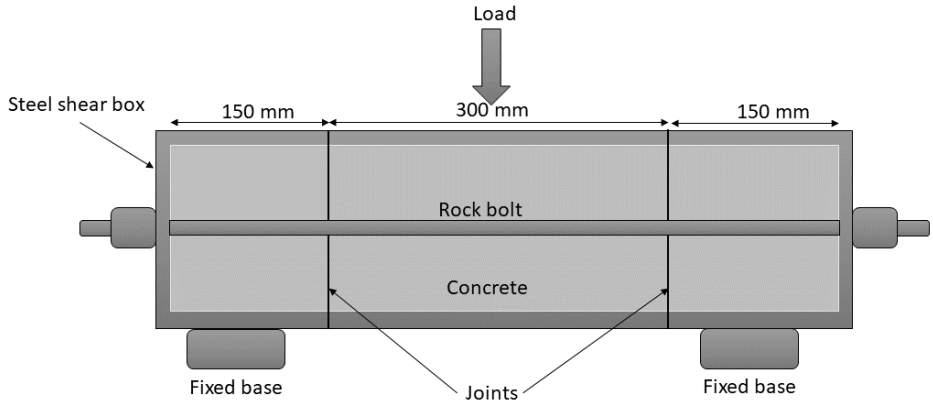

Figure 5.8 - Double shear test setup (Jalalifar, 2006).

Table 5.3 - Material properties (Jalalifar, 2006).

Material	UCS (MPa)	Joint friction angle
Concrete	20	25^0
	100	25^0

Table 5.4- Bolt properties (Jalalifar, 2006).

Diameter (mm)	Young's Modulus (GPa)	Shear Modulus (GPa)	Axial yield load (kN)	Ultimate Load (kN)	Yield Strain	Failure Strain
22	200	80	260	360	0.0034	0.22

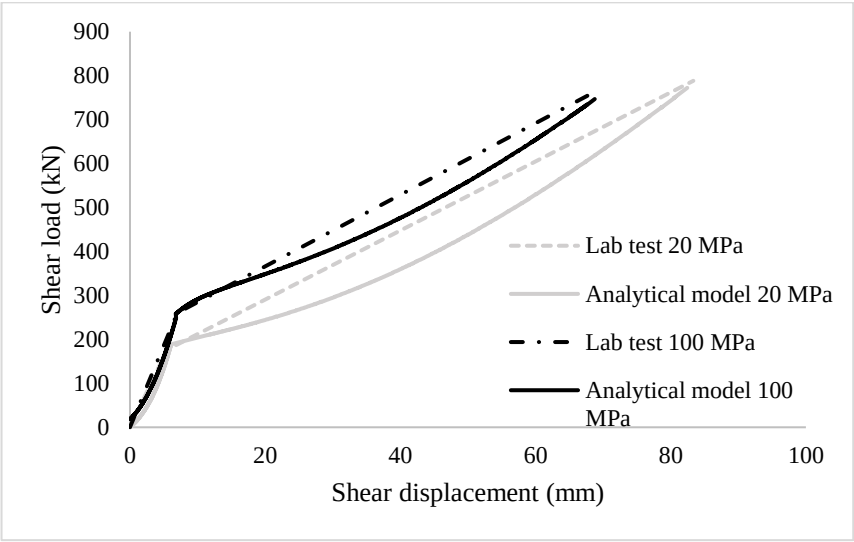

Figure 5.9 - Analytical model validation with double shear lab test data.

5.6 Discussion

The proposed analytical model improves on the existing models by incorporating the effect of strain-hardening in post-yield shear behaviour of rock bolt. As the rock bolt yields, plastic hinges are formed which reduces the flexural rigidity of the bolt. The modulus shows a gradual decrease with increase in bending of the rock bolt. This leads to an increase in the shear load on the rock bolt even after the formation of the plastic hinges. The effect of this process is discussed in this section along with comparison of the proposed model with some existing models.

5.6.1 Bending modulus after yield

The reduced value of bending modulus for a given bending moment can be calculated using equations (5.13) - (5.15) as discussed earlier. Figure 5.10 shows the plot between modulus and bending moment for the rock bolt properties given in Table 5.5. It can be seen from the plot that the reduction in flexural rigidity occurs gradually when the bending moment increases beyond yield point. The proposed model uses this plot to calculate the reduced bending modulus after bolt yields. At yield point the value of E_r is equal to the elastic modulus. As the bending moment increases E_r reduces and approaches the residual value equal to E_P from equation (5.19).

Table 5.5 - Rock bolt properties.

Diameter (mm)	Young's Modulus (GPa)	Axial yield strength (MPa)	Ultimate strength (MPa)	Yield Strain	Failure Strain
20	200	680	860	0.0034	0.16

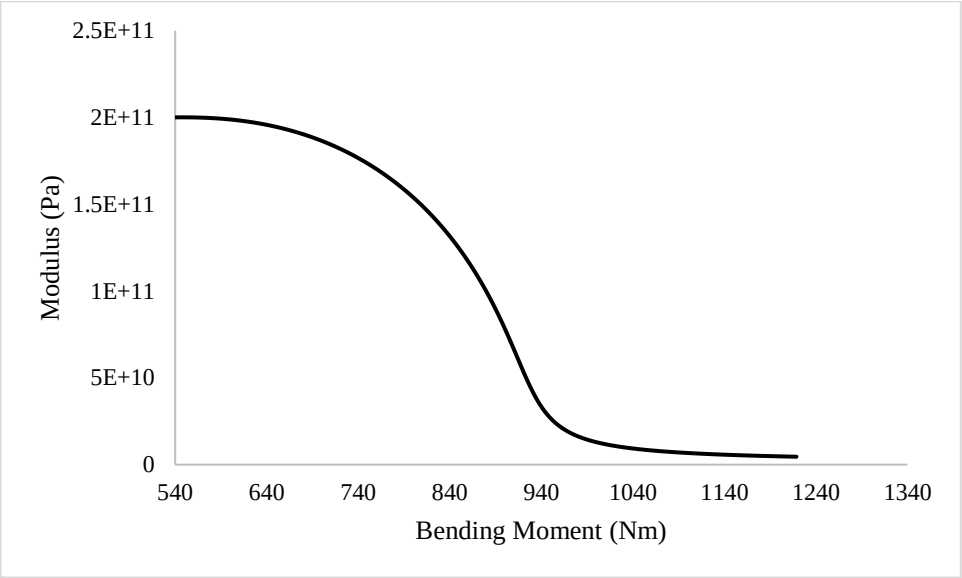

Figure 5.10 - Bending modulus vs bending moment.

To analyse how the curve shown in Figure 5.10 is influenced by different rock bolt properties it is plotted for different bolt diameters and E_P values. Figure 5.11 shows the reduced modulus vs bending moment plot for bolts with diameters 18, 20 and 22 mm. As the bolts with different diameter start yielding at different values of bending moment, for comparison the curves are plotted between the reduced modulus and bending moment – M_y, where M_y is the bending moment at which the bolt starts yielding. Rock bolt properties other than diameter are same for all three plots and given in Table 5.5. As seen from the figure as the diameter of the bolt increases the slope of the curves reduces. This is because bolt with bigger diameter can undergo higher bending before the inner fibres of the bolt reach plastic limit. Therefore, a larger diameter bolt will show higher resistance to bending than a smaller diameter bolt beyond the elastic limit.

Figure 5.12 shows the bending modulus vs bending moment– M_y curves for rock bolt with different post-yield strain hardening behaviour. For the analysis three types of structural steels Grade 50, 60 and 65 are compared. The properties of the three steel types are shown in Table 5.6. Higher E_P values corresponds to a higher slope of post-yield strain hardening curve. Steel

fibres at the bending point in a bolt with higher E_P will therefore show higher resistance to bending than fibres in a bolt with lower E_P for similar plastic deformations.

Table 5.6 - Rock bolt and steel properties (ASTM, 2018).

ASTM A572 Grade	Diameter (mm)	Young's Modulus (GPa)	Axial yield strength (MPa)	Ultimate strength (MPa)	Failure Strain	E_P (MPa)
50	20	200	345	450	0.21	500
60	20	200	415	520	0.18	580
65	20	200	450	550	0.17	596

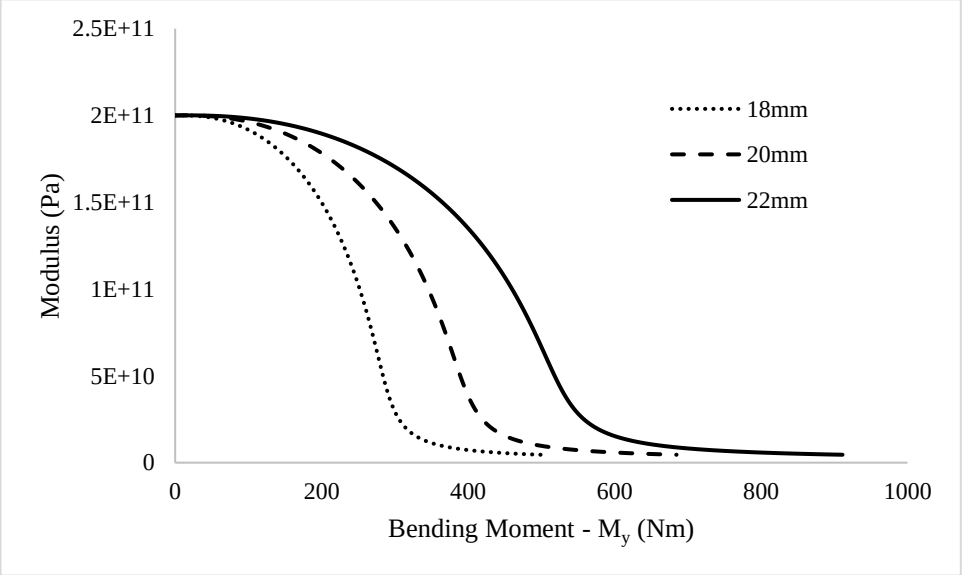

Figure 5.11 - Bending modulus curve for different diameter bolts.

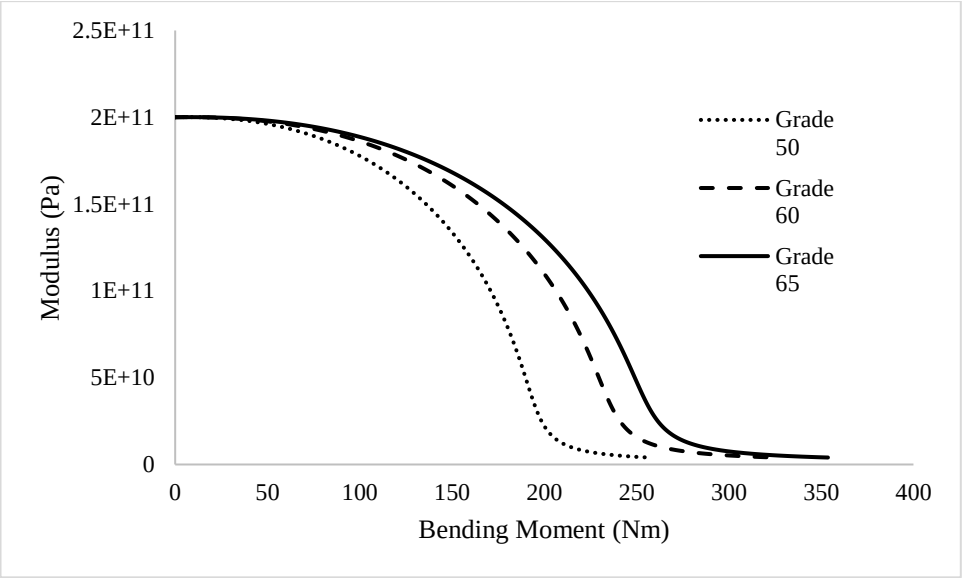

Figure 5.12 - Effect of E_P on bending modulus curve.

5.6.2 Effect of strain-hardening on rock bolt shear behaviour

In most conventional rock bolt shear analytical models the flexural rigidity of the bolt is reduced to zero after yielding. As the bolt then offers no resistance to bending the shear load on the bolt remains constant. However, as discussed before due to strain hardening the bolt's flexural rigidity instead of becoming zero, gradually decreases with increasing bending moment and approaches a residual value. To analyse the effect of strain hardening on rock bolt's shear behaviour, the lab shear test examples used in the validation of the model are compared with the shear behaviour of rock bolt without strain hardening effect. To remove the strain hardening effect the shear force in the rock bolt after yield point is considered constant and the bolt is considered to behave like a truss fixed at the hinge points. Figure 5.13 and Figure 5.14 show the shear loads vs shear displacement plots using the proposed model which considers effect of strain hardening and results without considering strain hardening. Analytical models which do not consider the effect of strain hardening on rock bolt shear response underestimate the shear load on the rock bolt. As the rock bolt fails under a combined axial and shear load, the model overestimates the shear displacement at which the rock bolt fails. In the examples shown in Figure 5.13 and Figure 5.14 the analytical model without strain

hardening overestimates the ultimate shear displacement by about 25% and 27% compared to proposed analytical model.

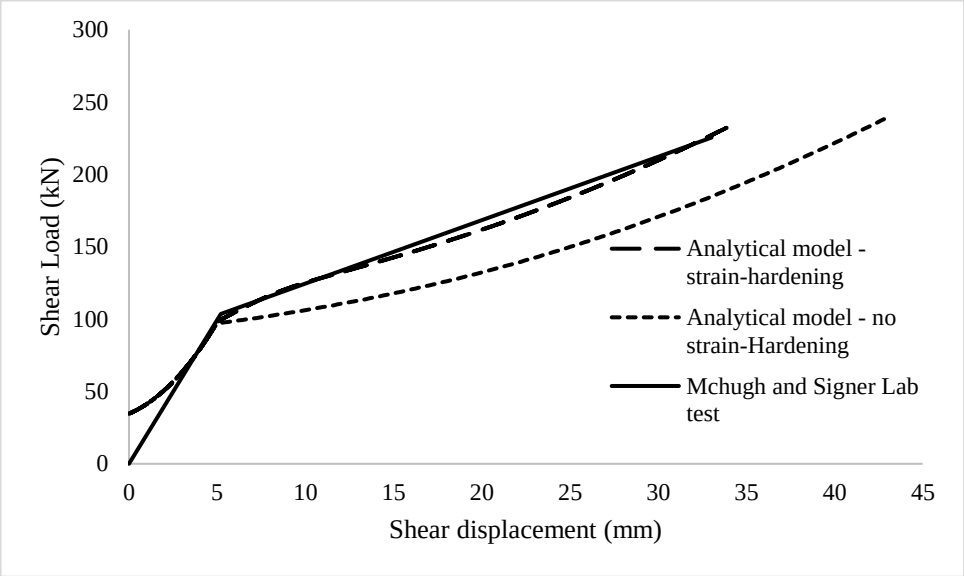

Figure 5.13 – McHugh and Signer lab test analytical model strain hardening effect.

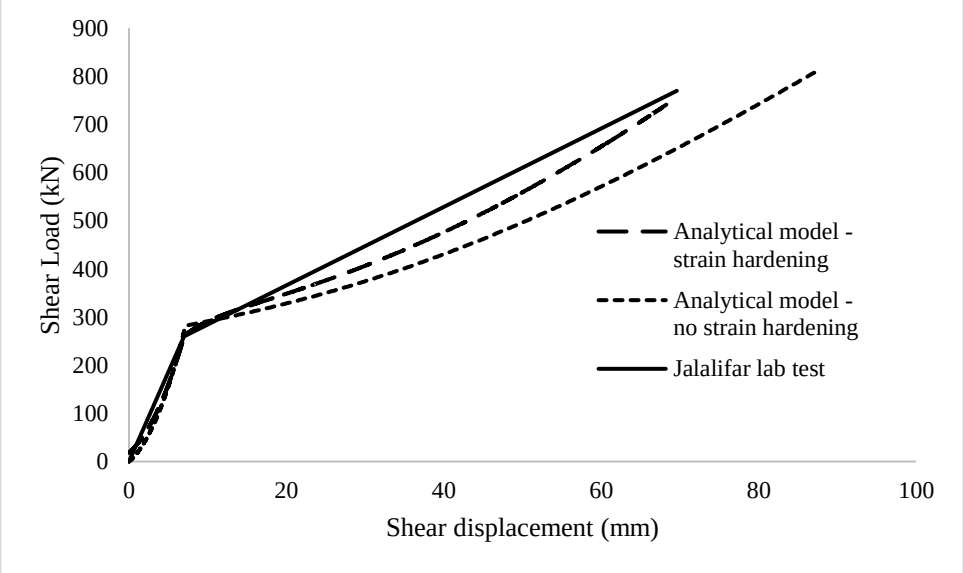

Figure 5.14 - Jalalifar lab test analytical model strain hardening effect.

5.6.3 Variation in strain-hardening effect due to host media strength

The change in rock bolt shear response due to strain hardening is caused by the extra shear load on the rock bolt. Therefore, it is expected that this effect will be higher in shear conditions where the rock bolt undergoes high shear loading. This will be the case in higher strength host

media. To analyse how the strain hardening effects changes with host media strength, ultimate shear load and displacement were calculated for different host media strength first using the proposed analytical model and then by removing effect of strain hardening. The rock bolt properties used are shown in Table 5.7. The effect of strain hardening in different strengths of host media is shown in Figure 5.15. As can be seen from the figure, the model with 20 MPa host media overestimates the shear displacement by about 27%. This value increases to almost 34% in 150 MPa host media.

Table 5.7 - Bolt properties.

Diameter (mm)	Young's Modulus (GPa)	Axial yield load (kN)	Ultimate Load (kN)	Yield Strain	Failure Strain
20	200	520	740	0.0026	0.16

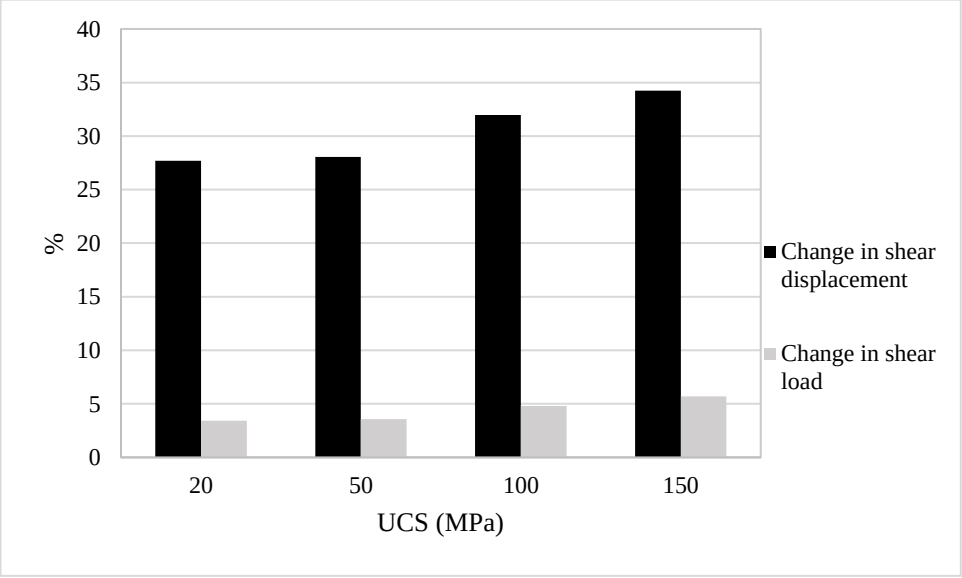

Figure 5.15 - Variation in strain hardening effect due to host media strength.

5.7 Conclusions

A new analytical model for shear response of fully grouted rock bolt using the virtual work principle is proposed. A method to consider the effect of plastic strain hardening of steel on

post elastic shear behaviour of rock bolt is presented. The analytical model has been validated with laboratory shear tests results. The following conclusions can be made from the work done in this paper:

1. The validation of the analytical model with lab test results have shown that it can more accurately predict large shear deformation behaviour of rock bolts.
2. Analytical models that do not consider effect of strain hardening, overestimate the ultimate shear displacement by up to 35% as shown by examples in the paper. Therefore, it is important to consider plastic strain hardening in post-elastic shear behaviour of rock bolt. The proposed analytical model outlines a method to do so.
3. The magnitude of the effect of strain hardening on shear behaviour of rock bolt depends on the host media properties. In the analysis the model with 20 MPa host media overestimated the ultimate shear displacement by about 27% while the 150 MPa host media model overestimated it by 34%.

Acknowledgements

This work was supported by the Minerals Research Institute of Western Australia (MRIWA); Mining3, Curtin University and Peabody Energy.

Appendix 1

The internal virtual work consists of two terms – bending and shear force work. The equation for total internal virtual work can be written as –

$$\delta W_{\text{int}} = \int_0^{2l_A} \delta M_z . \frac{M_z}{EI_z} dx + \int_0^{2l_A} \delta F_y . \frac{F_y}{A_s G} dx \qquad (5.22)$$

These terms can be calculated by replacing M_z and F_y by the moment and shear force in the bolt respectively as shown below –

$$\int_0^{2l_A} \delta M_z . \frac{M_z}{EI_z} dx = \frac{1}{EI_z} \int_0^{L_A} \delta Q_o x \left(Q_o x - \frac{P_u x^2}{2} \right) dx + \frac{1}{EI_z} \int_{L_A}^{2L_A} \delta Q_o x \begin{pmatrix} Q_o x - P_u L_A \left(x - \frac{L_A}{2} \right) - \frac{P_u}{2} (x - L_A)^2 \left(2 - \frac{x}{L_A} \right) \\ - \frac{P_u}{3} (x - L_A)^2 \left(\frac{x}{L_A} - 1 \right) \end{pmatrix} dx \tag{5.23}$$

$$\int_0^{2l_A} \delta F_y . \frac{F_y}{A_s G} dx = \frac{1}{A_s G} \int_0^{L_A} \delta Q_o \left(Q_o - P_u x \right) dx + \frac{1}{A_s G} \int_{L_A}^{2L_A} \delta Q_o \left(Q_o - P_u L_A - \frac{P_u}{2} (x - L_A) \left(3 - \frac{x}{L_A} \right) \right) dx \tag{5.24}$$

Integrating the equations (5.23) and (5.24), and the total internal virtual work can be written as –

$$\delta W_{\text{int}} = \delta Q_o \left(\frac{1}{EI_Z} \left(\frac{8 Q_O L_A^3}{3} - \frac{133 p_u L_A^4}{360} \right) + \frac{1}{A_s G} \left(2 Q_O L_A - \frac{11 p_u L_A^2}{6} \right) \right) \tag{5.25}$$

To find out the displacement at point O, the external work done by forces acting at point O is calculated as follows –

$$\delta W_{ext} = \delta Q_o u_y \tag{5.26}$$

Equating (5.24) and (5.25) gives the relationship for transverse displacement and shear force at point O –

$$u_y = \frac{1}{EI_Z} \left(\frac{8 Q_O L_A^3}{3} - \frac{133 p_u L_A^4}{360} \right) + \frac{1}{A_s G} \left(2 Q_O L_A - \frac{11 p_u L_A^2}{6} \right) \tag{5.27}$$

Appendix 2

According to static mechanics (McGuire et al., 1999) the deflection angle θ at a point in a beam can be written as –

$$\frac{d\theta}{dx} = \frac{M}{EI_z} \tag{5.28}$$

Inserting the expression for moment in the bolt from equation (5.4) and integrating both sides –

$$\begin{aligned}\int_{\theta_B}^{\theta_O} d\theta = \frac{1}{EI_z}\int_{2L_A}^{L_A}&\left(\begin{array}{l} Q_o x - P_u L_A\left(x-\frac{L_A}{2}\right) - \frac{P_u}{2}\left(x-L_A\right)^2\left(2-\frac{x}{L_A}\right) \\ -\frac{P_u}{3}\left(x-L_A\right)^2\left(\frac{x}{L_A}-1\right)\end{array}\right)dx \\ &+\frac{1}{EI_z}\int_{L_A}^{0}\left(Q_o x-\frac{P_u x^2}{2}\right)dx\end{aligned} \tag{5.29}$$

Solving equation (5.29) gives the equation for total deflection angle as –

$$\theta = \frac{1}{EI_Z}\left(\frac{19 p_u L_A^3}{24} - 2Q_O L_A^2\right) \tag{5.30}$$

Appendix 3

The equation for reduced modulus E_r is given by –

$$E_r = \frac{256}{\pi D_b \Delta^3}\int_{\varepsilon_2}^{\varepsilon_1} \sigma\varepsilon\sqrt{\frac{D_b^2}{4} - \frac{D_b^2\varepsilon^2}{\Delta^2}}\,d\varepsilon \tag{5.31}$$

Where Δ the sum of the absolute values of maximum elongation and contraction strain on the bolt can be calculated as –

$$\Delta = \frac{D_b}{r} \tag{5.32}$$

Where r is the radius of curvature of beam. For integrating equation (5.31) we also need an expression for stress-strain relationship for the bolt material. Such a relationship can be calculated from the tension-compression test diagram for the bolt material. For steel the diagram can be estimated by Figure 5.16. As can be seen the stress-strain diagram for steel in

compression and tension are symmetric of each other. Therefore the relationship for stress-strain can be written as –

For elastic region –

$$\sigma = \frac{\sigma_y}{\varepsilon_y}\varepsilon \tag{5.33}$$

For plastic region –

$$\sigma = \left(\frac{\sigma_f - \sigma_y}{\varepsilon_f - \varepsilon_y}\right)\left(\varepsilon - \varepsilon_y\right) + \sigma_y \tag{5.34}$$

Using equations (5.32) to (5.34) and noting that the tension-compression test diagram for steel is symmetric, equation (5.31) can be written as –

$$E_r = \frac{256r^3}{D_b^4\pi}\left(\int_0^{\varepsilon_y}\frac{\sigma_y}{\varepsilon_y}\varepsilon^2\sqrt{\frac{D_b^2}{4}-r^2\varepsilon^2}\,d\varepsilon + \int_{\varepsilon_y}^{\varepsilon_1}\left(\left(\left(\frac{\sigma_f-\sigma_y}{\varepsilon_f-\varepsilon_y}\right)\left(\varepsilon-\varepsilon_y\right)+\sigma_y\right)\varepsilon\sqrt{\frac{D_b^2}{4}-r^2\varepsilon^2}\right)d\varepsilon\right) \tag{5.35}$$

The relationship between moment and radius of curvature is given by –

$$M = \frac{I_z E_r}{r} \tag{5.36}$$

The equation (5.35) is used to calculate the value of E_r for various possible values of radius of curvature r. Then the corresponding value of moment for that curvature is calculated using equation (5.36). This gives a plot between moment M and E_r. The plot can then be used in the analytical model for calculating the value of E_r if the bending moment in the rock bolt is known.

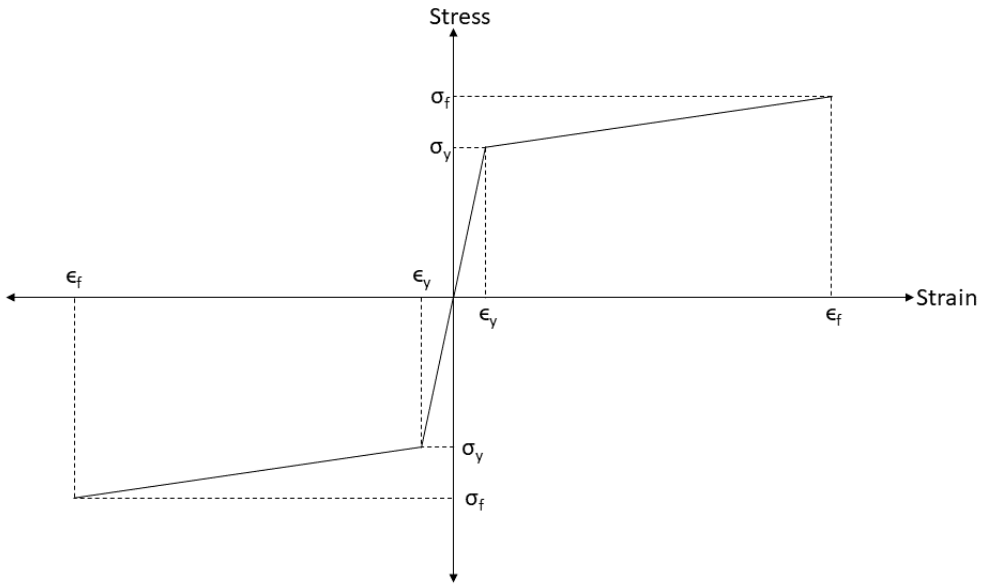

Figure 5.16 - Tension-compression test diagram for steel.

References

ASTM. (2018). ASTM A572 / A572M-18. In Standard Specification for High-Strength Low-Alloy Columbium-Vanadium Structural Steel. West Conshohocken, PA.

Chen, Y. (2014). Experimental study and stress analysis of rock bolt anchorage performance. Journal of Rock Mechanics and Geotechnical Engineering, 6(5), 428-437. doi:10.1016/j.jrmge.2014.06.002

Chen, Y., & Li, C. C. (2015). Performance of fully encapsulated rebar bolts and D-Bolts under combined pull-and-shear loading. Tunnelling and Underground Space Technology, 45, 99-106. doi:10.1016/j.tust.2014.09.008

Chen, Y., Wen, G., & Hu, J. (2020). Analysis of Deformation Characteristics of Fully Grouted Rock Bolts Under Pull-and-Shear Loading. Rock Mechanics and Rock Engineering, 53(7), 2981-2993. doi:10.1007/s00603-020-02108-0

Dight, P. M. (1982). Improvements to the stability of rock walls in open pit mines: by Phillip M. Dight (Doctoral dissertation, Monash University).

Egger, P., & Spang, K. (1987). Stability investigations for ground improvement by rock bolts at a large dam. Paper presented at the 6th ISRM Congress.

Gerdeen, J., Snyder, V., Viegelahn, G., & Parker, J. (1979). Design criteria for roof bolting plans using fully resin-grouted nontensioned bolts to reinforce bedded mine roof. Volume III: Experimental model studies; Volume IV: Theoretical analysis. In: Houghton, MI: Michigan Technological University. US Bureau of Mines contract.

Haas, C. J. (1976). Shear resistance of rock bolts. Trans. Soc. Min. Eng. AIME;(United States), 260(1).

Jalalifar, H. (2006). A new approach in determining the load transfer mechanism in fully grouted bolts. (Doctoral dissertation, University of Wollongong).

Jalalifar, H., & Aziz, N. (2010). Analytical behaviour of bolt–joint intersection under lateral loading conditions. Rock Mechanics and Rock Engineering, 43(1), 89-94.

Kostecki, T. R. (2019). Design Methods For Rock Bolts Using In-Situ Measurement From Underground Coal Mines. (Doctor of Philosophy Degree). Southern Illinois University Carbondale, Carbondale, Southern Illinois.

Li, C. C. (2010). Field observations of rock bolts in high stress rock masses. Rock Mechanics and Rock Engineering, 43(4), 491-496.

Li, X., Aziz, N., Mirzaghorbanali, A., & Nemcik, J. (2016). Behavior of fiber glass bolts, rock bolts and cable bolts in shear. Rock Mechanics and Rock Engineering, 49(7), 2723-2735.

Li, X., Nemcik, J., Mirzaghorbanali, A., Aziz, N., & Rasekh, H. (2015). Analytical model of shear behaviour of a fully grouted cable bolt subjected to shearing. International Journal of Rock Mechanics and Mining Sciences, 80, 31-39. doi:10.1016/j.ijrmms.2015.09.005

Liu, C., & Li, Y. (2020). Predicting the Shear Resistance Contribution of Passive Fully Grouted Bolts to Jointed Rock. International Journal of Geomechanics, 20(2), 04019174. doi:doi:10.1061/(ASCE)GM.1943-5622.0001581

Liu, C. H., & Li, Y. Z. (2017). Analytical Study of the Mechanical Behavior of Fully Grouted Bolts in Bedding Rock Slopes. Rock Mechanics and Rock Engineering, 50(9), 2413-2423. doi:10.1007/s00603-017-1244-9

Ma, S., Zhao, Z., Peng, J., & Gui, Y. (2018). Analytical modeling of shear behaviors of rockbolts perpendicular to joints. Construction and Building Materials, 175. doi:10.1016/j.conbuildmat.2018.04.175

Ma, S., Zhao, Z., & Shang, J. (2019). An analytical model for shear behaviour of bolted rock joints. International Journal of Rock Mechanics and Mining Sciences, 121, 104019.

Maekawa, K., & Qureshi, J. (1996). Computational model for reinforcing bar embedded in concrete under combined axial pullout and transverse displacement. Doboku Gakkai Ronbunshu, 1996(538), 227-239.

McGuire, W., Gallagher, R. H., & Ziemian, R. D. (1999). Matrix Structural Analysis: Wiley.

McHugh, E., & Signer, S. (1999). Roof bolt response to shear stress: laboratory analysis. Paper presented at the Proceedings 18th international conference on ground control in mining, Morgantown, WV.

Pinazzi, P. C., Spearing, A. S., Jessu, K. V., Singh, P., & Hawker, R. (2020). Mechanical performance of rock bolts under combined load conditions. International Journal of Mining Science and Technology, 30(2), 167-177.

Pellet, F., & Egger, P. (1996). Analytical model for the mechanical behaviour of bolted rock joints subjected to shearing. Rock Mechanics and Rock Engineering, 29(2), 73-97.

Simser, B. P. (2007, November). The Weakest Link-Ground Support Observations at Some Canadian Shield Hard Rock Mines. In Proceedings of the fourth international seminar on deep and high stress mining (pp. 335-348). Australian Centre for Geomechanics.

Snell, G., Kuley, E., & Milne, D. (2017). A laboratory-based approach to assess rockbolt behaviour in shear. Paper presented at the Proceedings of the First International Conference on Underground Mining Technology.

Spang, K., & Egger, P. (1990). Action of fully-grouted bolts in jointed rock and factors of influence. Rock Mechanics and Rock Engineering, 23(3), 201-229. doi:10.1007/BF01022954

Timoshenko, S. (1947). Strength of materials. Part 2: Advanced theory and problems. 9th printing. Van Nostrand.

Chapter 6. Improving the Numerical Modelling of In-situ Rock Bolts Using Axial and Bending Strain Data from Instrumented Bolts

This chapter has been accepted and published in Geotechnical and Geological Engineering as:

Singh, P., Jang, H., & Spearing, A. J. S. (2022). Improving the Numerical Modelling of In-Situ Rock Bolts Using Axial and Bending Strain Data from Instrumented Bolts. Geotechnical and Geological Engineering, 1-25.

Abstract

Numerical modelling has become an important tool in the underground rock bolt reinforcement designing process. Numerical modelling provides the advantage of easily and quickly simulating complex underground geometries and mechanisms with sensitivity analyses. However, a numerical model needs to be calibrated using mathematical solutions, lab testing or with actual in-situ observations and measurements (which is the preferred method) before its results can be quantitatively applied to reinforcement design. Instrumented rock bolts provide a useful data source for calibrating in-situ rock bolt models. In this work, procedures have been presented to identify and determine the orientation of structures in the rock mass based on the strains on the instrumented rock bolts. A method to calibrate the rock bolt model with in-situ data is also presented. The results of the presented procedures have been validated with laboratory tests and numerical modelling. The procedures have been applied to create and calibrate an in-situ rock bolt model in FLAC3D and the results are validated using in-situ data.

6.1 Introduction

A safe and cost-effective ground reinforcement design is an important aspect of any underground mining operation. These can prevent ground failure incidents which can lead to fatalities, injuries and loss of production. Among the different rock reinforcement methods in use currently, fully grouted rock bolts constitute the major form of reinforcement in underground mines. Rock bolts provide an easy, quick and efficient way of reinforcing the rock. Fully grouted rock bolts are a type of rock bolt in which a solid steel rebar is coupled to

the rock using a grout. These types of rock bolts are used for their high stiffness and corrosion resistance. The rock bolt provides reinforcement to the rock by resisting the deformations in the rock. This transfer of load from rock to bolt occurs through a complex interaction between rock, grout and steel bar. In order to design a safe and efficient rock reinforcement, it is important to understand this behaviour.

Different analytical and empirical methods have been proposed for rock reinforcement design. Most of these methods rely on a simplified model of the rock bolt to reduce the complexity of the calculation (Obert and Duvall 1967, Potvin 1988, Mark 2000). Numerical modelling as a tool for designing rock reinforcement has the advantage of easily modelling complex mechanisms and therefore its use in rock reinforcement design has become common in recent years.

Numerical modelling uses the fundamental mechanics of the materials and therefore can be used to analyse specific systems without the need for significant simplification to approximate the problem. However, a numerical model needs to be calibrated and validated before its results can be useful (Esterhuizen, 2014). This calibration of the numerical model is done using in-situ measurements and observations. Once a model is calibrated and produces verifiable results for a current in-situ excavation, it can be extrapolated and used for making reliable predictions for future excavations. The in-situ measurements used for calibrating numerical models are done using different types of instrumentation. The instrumentations used on rockbolts in underground mines have evolved from the use of resistive strain gauges to digital (inductive) gauges and now into the use of optical sensing (Kostecki, 2019). Each improvement in instrumentation technology provided more accurate measurements with higher resolution along more of the rockbolt length. This increase in the quality of data available has made it possible for new and better methods for the calibration of numerical models. The focus of this paper is to present a procedure for using the data obtained from optical instrumented bolts to calibrate in-situ rock bolt models under shear, tensile and combined loads.

6.2 Background

6.2.1 Instrumented bolts

The first type of instrumented rock bolts installed in underground mines used resistive strain gauges attached in several fixed positions along the length of the rock bolts to measure the strains. Freeman (1978) used instrumented fully grouted rock bolts in Kielder experimental tunnel to study the axial load transfer between rock and bolt. Similar studies were done by other researchers in the subsequent years using resistive strain gauge instrumented rock bolts to study the axial and bending loads on rock bolts installed in-situ (Serbousek and Signer, 1987; Signer, 1990; Signer and Cox et al., 1997; Johnson, Brady et al. 1999, Signer 2000). The shortcoming of these resistive strain gauges was their limited coverage of the rock bolt length. The measured strain depended on the positioning of the gauges on the rock bolt. The small resistive gauges were unable to reliably measure concentrated loads on the rock bolt. They were also only attached in 2 positions 180° apart so the results were not reliable.

The shortcoming of limited coverage of rock bolt length by small resistive strain gauges was overcome by the use of long base inductive sensors. Rock bolts instrumented with these long base inductive sensors were used by researchers to study the axial and bending loads on rock bolts (Spearing and Gadde 2011, Spearing, Gadde et al. 2011, Spearing, Hyett et al. 2013). The longer sensor provided better coverage of the rock bolt length and was used in staggered and stacked configurations. The studies were able to measure bending loads on the rock bolts in-situ. However, the longer inductive sensors averaged the strain measured over their length. This resulted in a significant underestimation of the peak loads measured on the rock bolts. The shortcomings of the short resistive strain gauge and long inductive sensors were overcome by the use of optical sensors.

Distributed optical sensors (DOS) consists of an optical fibre attached to the whole length of the rock bolt. The optical fibre can measure strain typically every 5mm along the length of the rock bolt. This provided a significant increase in the resolution and accuracy of the strain measured on the rock bolt. The use of optical fibres in instrumented rock bolts was first

described by Hyett, Forbes et al. (2013). The rock bolts were instrumented with optical fibres running along with two diametrically opposite slots along the length of the rock bolt. The instrumented bolt was used to measure axial and bending strain in laboratory tests. Kostecki, Spearing et al. (2015) used the DOS instrumented rock bolts with three slots along the rock bolt to demonstrate the need for a third slot to successfully capture the true strain of the rock bolt (axial and bending). It was concluded that instrumented bolts with two slots for measuring strain were not able to capture the bending of the rock bolt if the slots were not oriented parallel to the bending direction. Therefore, to capture the bending strain of a rock bolt in-situ a minimum of three slots are required. Fig. 6.1 shows a comparison of the three types of instrumentation technology described above and the rock bolt strain profile they are capable of capturing. Optical instrumented rock bolts have been used by researchers to measure strain on the rock bolts in a laboratory and in-situ (Jessu, Kostecki et al. 2016, Forbes, Vlachopoulos et al. 2018, Vlachopoulos, Forbes et al. 2018, Kostecki 2019). Hoehn, Spearing et al. (2020) improved the optical instrumented bolt technology using an All-Grating Fibre (AGF). Improvements were also made by increasing the number of sensing slots to four and better tooling of the slots. This improved instrumented rock bolt was used in this study for in-situ measurements.

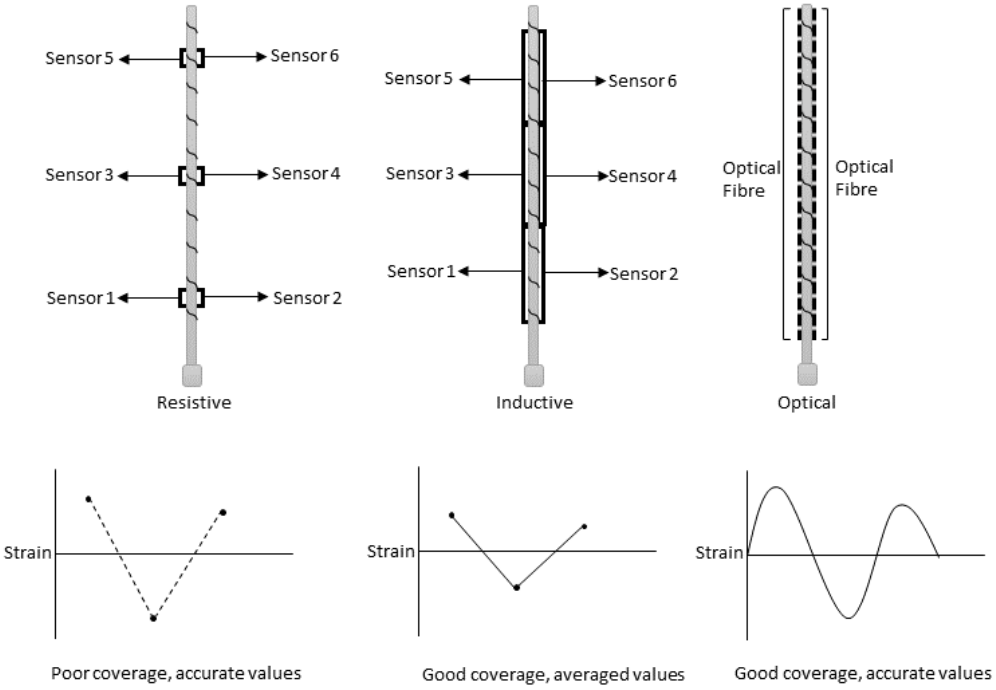

Fig. 6.1 - Comparison of the three types of instrumentation technology

6.2.2 Numerical modelling

Numerical modelling can be used for rock bolt reinforcement design by creating a detailed mathematical model for the specific case of an excavation. The model can then be used to analyse the response of the rock bolts to the stresses and deformations produced in the rock. As the basis of a numerical model are mathematical equations based on the basic mechanics of the material. These equations define the response of each element such as rock or rock bolt in the model. In the case of rock bolt support models, there are two ways of modelling the rock bolt. The rock bolt can be modelled using grid elements like the surrounding rock whose behaviour is based on the basic mechanics of the material or using linear structural elements based on analytical models. Several different analytical models have been proposed to describe the axial, bending and shear behaviour of the fully grouted rock bolt (Spang and Egger 1990, Hyett, Moosavi et al. 1996, Pellet and Egger 1996, Li and Stillborg 1999, Cai, Esaki et al. 2004, Jalalifar and Aziz 2010, Ren, Yang et al. 2010, Ma, Nemcik et al. 2013, Ghadimi, Shahriar et al. 2015, Zhang, Huang et al. 2020, Singh and Spearing 2021).

Although numerical models have great potential for use in rock bolt support design, the lack of a detailed geotechnical model of the rock mass presents a challenge in the wider adoption of numerical modelling. Uncertainty in the properties of the rock mass, the location, variation and properties of discontinuities create difficulties in creating a representative numerical model including rock bolt support. Therefore, once a model has been created it needs to be calibrated against in-situ measurements and observations; and the uncertain parameters adjusted (Esterhuizen 2014). Common sources of in-situ measurements for calibration of rock bolt numerical models are the instrumented rock bolts discussed in the previous section. Spearing and Gadde (2011), Spearing and Hyett (2014) used instrumented rock bolts to measure axial loads on the rock bolts during coal panel excavation. A numerical model of the excavation was created in FLAC3D and used structural elements to simulate rock bolts. The axial loads from in-situ measurements were used to calibrate the models. However, due to the unavailability of optical sensors, the instrumentation could not capture the true strain profile along the length of the rock bolt. This made it difficult to use the data to calibrate the rock bolt model for concentrated loads (axial and bending) such as caused by local discontinuities in the rock. Kostecki (2019) used DOS instrumented rock bolts with a three-slot configuration for in-situ rock bolt monitoring. Calibration of in-situ numerical models using the data from the instrumented rock bolts was discussed. It was found that the instrumentation was able to capture the strain on the rock bolt due to the local inhomogeneity of the rock mass such as the presence of discontinuities. This made it possible to create and calibrate rock bolt models to capture the localized rock strain.

In this study, the numerical modelling is done using the linear structural element as they are commonly used in most of the currently available geotechnical analysis software. The numerical modelling of in-situ rock bolt support is done using FLAC3D (2017) software with the inbuilt pile structural element. The pile element in FLAC3D simulates the behaviour of a fully grouted rock bolt using a linear two noded element. The linear element is connected to the surrounding rock grid with spring sliders which simulate the behaviour of rock-grout and

grout-bolt interface (Fig. 6.2). The properties of the linear element can be derived from the structural properties of the rock bolt. However, the parameters controlling the behaviour of the spring-slider system cannot be directly derived from the bolt or grout properties. The shear spring parameters which control the axial behaviour of the pile have been calibrated using data from in-situ pull tests (Bin, Taiyue et al. 2012, Nemcik, Ma et al. 2014). Calibration for normal spring parameters which control the bending and shear behaviour of piles has only been done using laboratory shear tests (Tulu, Esterhuizen et al. 2012). This is done by calibrating the shear-load vs displacement plot of the bolted interface in the model with the actual measured shear-load vs displacement from laboratory tests. No work has been done on calibrating the normal spring parameters using in-situ data as the shear-load vs displacement data is not available in an in-situ test. Also, the actual orientation of the discontinuity with the rock bolt in-situ is often not known. However, with the availability of new instrumentation technology which can provide a high-resolution plot of the in-situ strains on the rock bolt, it is possible to calibrate the rock bolt models to simulate the shear loading. In this work procedures for calculating the bolt-discontinuity angle and consequently calibrating the pile element in FLAC3D to simulate shear behaviour of rock bolt using in-situ data has been presented.

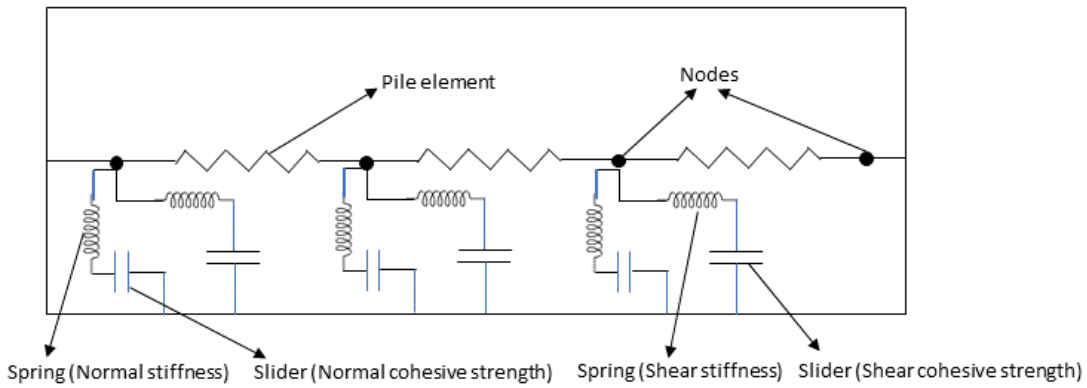

Fig. 6.2 Pile structural element (modified from Tulu, Esterhuizen, and Heasley (2012))

6.3 Discontinuity-bolt angle

The effect of bolt inclination angle on the shear behaviour of rock joints has been studied by many researchers (Bjurstrom 1974, Haas 1981, Dight 1982, Pellet and Egger 1996, Grasselli

2005). Haas (1976) studied the effect of bolt inclination on shear behaviour using laboratory shear tests and found that the shear resistance of the joint increased with an increase in bolt inclination. Similar results were presented by Dight (1982) where the inclined bolts were found to be stiffer than perpendicular ones. Spang and Egger (1990) conducted laboratory and in-situ shear testing of fully grouted rock bolts and found that the inclination of the rock bolt affects the maximum shear resistance and shear displacement of the joint. The maximum shear resistance was found to increase with bolt inclination while the shear displacement reduced. Based on the laboratory and in-situ observations analytical models for shear behaviour of rock bolt also include the effect of bolt inclination. Pellet and Egger (1996) described an analytical model which showed a good correlation with laboratory tests for the effect of bolt inclination on shear resistance and displacement. Since then, a lot of research has been done in improving the analytical models for shear behaviour of rock bolts (Jalalifar and Aziz 2010, Lin, Xiong et al. 2014, Li, Nemcik et al. 2015, Singh and Spearing 2021). Jessu, Kostecki et al. (2016) used optical instrumented rock bolts to compare the difference in strain profile of rock bolts at a different inclination to the discontinuity under shear loads. It was shown that the axial and bending strain profile of the rock bolt changes significantly with the inclination of the bolt. However, no method was proposed to calculate this inclination angle from the strain data. In this section, an analytical procedure is presented to determine the bolt-discontinuity angle from the instrumented rock bolt strain data based on the analytical model proposed by Singh and Spearing (2021).

6.3.1 Calculating the discontinuity-bolt angle.

A rock bolt undergoes a combination of axial, shear and bending load as shear displacement takes place at the discontinuity. Axial load is induced in the rock bolt parallel to its axis due to change in its length. The bending load is caused by the curving of rock bolt as a result of the shear load acting perpendicular to the axis of the rock bolt. The rock bolt mechanical system described in the analytical model in Singh and Spearing (2021) is shown in Fig. 6.3. Q_0 and N_0 are the shear load and axial load at point O. A is the point of maximum bending

strain and p_u is the rock/grout reaction. According to the analytical model, the elastic axial strain in the rock bolt is dependent on the angle between the rock bolt and the discontinuity and the shear displacement of the bolt. The shear displacement of the bolt can be calculated from using the bending strain and La (active length) obtained from the instrumented rock bolt strain data. Once the shear displacement is known the angle between the rock bolt and the discontinuity can be back calculated from the axial strain obtained from the instrumented rock bolt strain data.

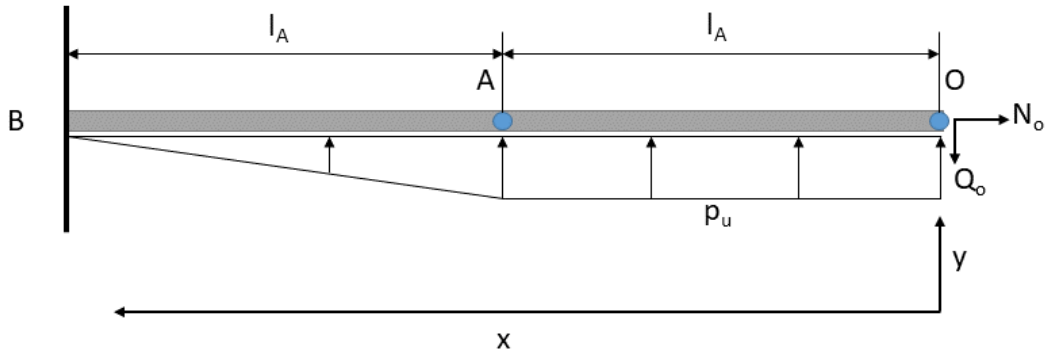

Fig. 6.3 Rock bolt mechanical system (Singh et al., 2020)

The shear load Q_o can be calculated as:

$$Q_0 = \frac{4\varepsilon_b EI_z}{D_b} \tag{6.1}$$

Where, ε_b is the maximum bending strain at point A (measured from instrumented rock bolt), E is the young's modulus of a bolt, I_z is the area moment of inertia along the z-axis of the bolt and D_b is the bolt diameter.

The shear displacement u_y is calculated as:

$$u_y = \frac{1}{EI_Z}\left(\frac{8Q_O l_A^3}{3} - \frac{133 p_u l_A^4}{360}\right) \tag{6.2}$$

Where, l_A is the length of section OA (measured from the instrumented rock bolt data), p_u is the bearing capacity per unit length of the soil.

The value of p_u before reaching maximum value is calculated as:

$$p_u = \frac{Q_O}{l_A} \tag{6.3}$$

The maximum value for p_u is given by:

$$p_u = K\sigma_c D_b \tag{6.4}$$

Where, K is a load factor (K≥ 1) and σ_c is the unconfined compressive strength (UCS) of rock.

The axial strain in the bolt at point O is given by (Ma, Zhao et al. 2019, Singh and Spearing 2021):

$$\varepsilon_A = \Delta_{ext} \frac{\left(1 + \frac{\pi D_b K_1 l_A^2}{2EA}\right)}{\left(2l_A + \frac{\pi D_b K_1 l_A^3}{2EA}\right)} \tag{6.5}$$

$$\Delta_{ext} = \frac{u_y \cos(\alpha - \theta)}{\sin(\alpha)} \tag{6.6}$$

$$\theta = \frac{1}{EI_Z}\left(\frac{19 p_u l_A^3}{24} - 2Q_O l_A^2\right) \tag{6.7}$$

Where, K_1 is the stiffness of the bond-slip model in the elastic stage (Ma, Zhao et al. 2019), θ is the bolt deflection angle, A is the area of the bolt cross-section, α is the angle between bolt and discontinuity, and Δ_{ext} is the axial extension in the bolt.

Using the equations (6.5), (6.6) and (6.7) if the axial strain in the bolt is known α (angle between bolt and discontinuity) can be back calculated.

6.3.2 Validation of discontinuity-bolt angle calculation

Measurements from double shear lab tests and double shear numerical models are used to validate the method outlined in the above section. Results from two sets of double shear lab tests are used in the validation. The first set of results were taken from series of double shear tests done in this study with the rock bolt perpendicular to the discontinuity in two different strength concretes. The second set of lab test results were taken from the double shear tests presented in Jessu, Kostecki et al. (2016) and Kostecki (2019). These tests consist of two double shear tests, one with bolt perpendicular to discontinuity and the other with rock bolt at 80^0 to discontinuity. Due to the difficulty in testing rock bolt in double shear at a lower angle with discontinuity in a lab test, a numerical model of the double shear test is created and calibrated with the lab test results. The numerical model is then used to simulate the double shear tests at angles of 60^0 and 45^0. The axial and bending strain profile of the rock bolt in each test is used to measure the parameters outlined in section 3.1 and then the bolt-discontinuity angle is calculated for each case.

The analytical model for shear behaviour of rock bolt used in calculation of the discontinuity-bolt angle and rock bolt shear response does not consider the effect of normal displacement of grout-bolt interface due to rock bolt rib profile. The effect of gap in discontinuity is also not taken into account in the model. As the effect of these factors cannot be directly measured from the strain profile of the rock bolt, they are not considered in this work.

6.3.3 Double shear test

Six double shear tests were conducted on instrumented rock bolts embedded in concrete blocks with two different strength concrete. The concrete blocks were casted in wooden moulds of 30cmX30cmX30cm and a steel rod of 30mm diameter was placed through the middle of the blocks to create the hole for grouting the bolt prior to pouring the concrete. The blocks were curing for 28 days before testing. After the concrete was completely set, the steel rod was removed, and the instrumented rock bolt was grouted in the hole through the middle of the blocks (Fig. 6.4). The ends of the rock bolt were kept unconstrained during the test. The grout

was cured for 24 hours, and the double shear test was conducted by applying a load on the middle block while the two side blocks were supported at their base. The instrumented bolt was connected to the interrogator and the strains on the rock bolt were recorded during the test (Fig. 6.5). The vertical displacement of the centre block and load applied on it was also recorded. An increasing load was applied until the concrete blocks failed. The properties of the concrete and rock bolt used in the test are given in Table 6.1 and Table 6.2.

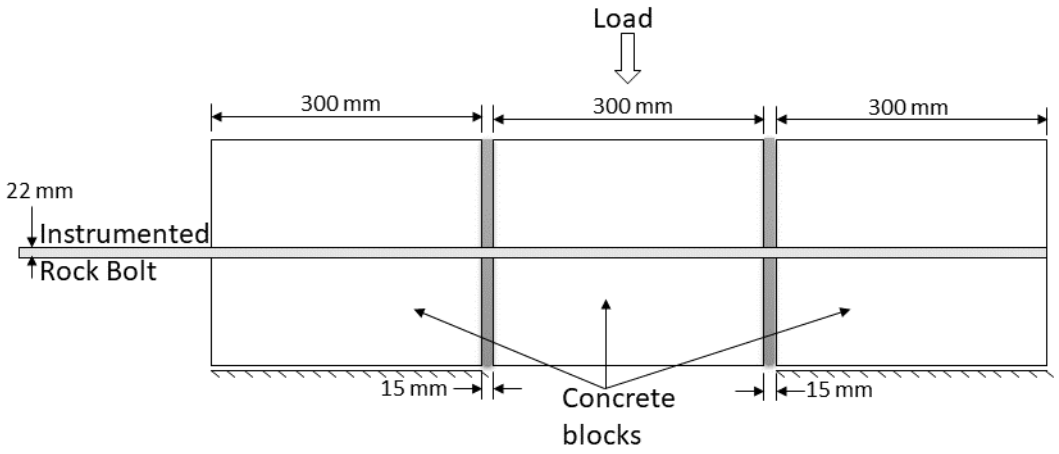

Fig. 6.4 Double shear test schematic

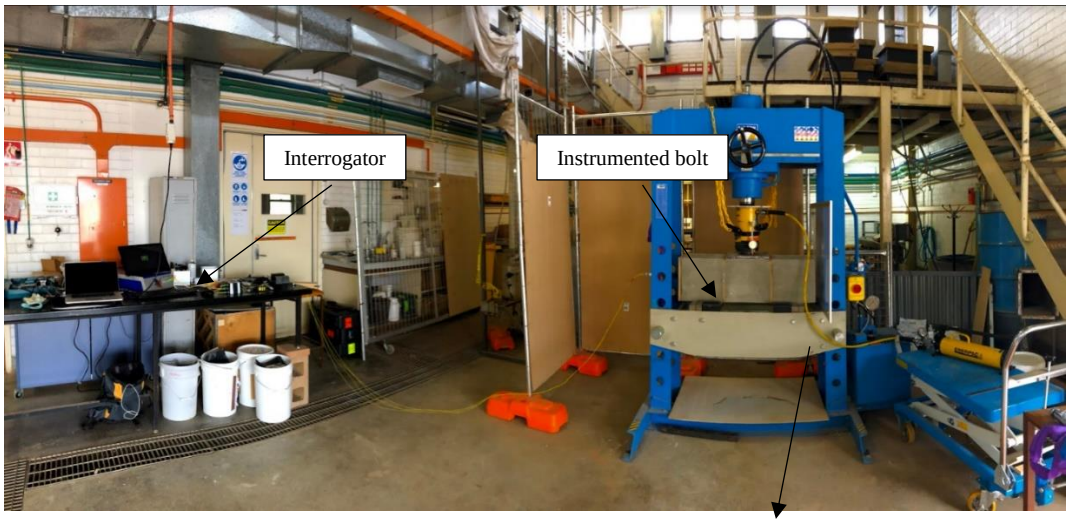

a)

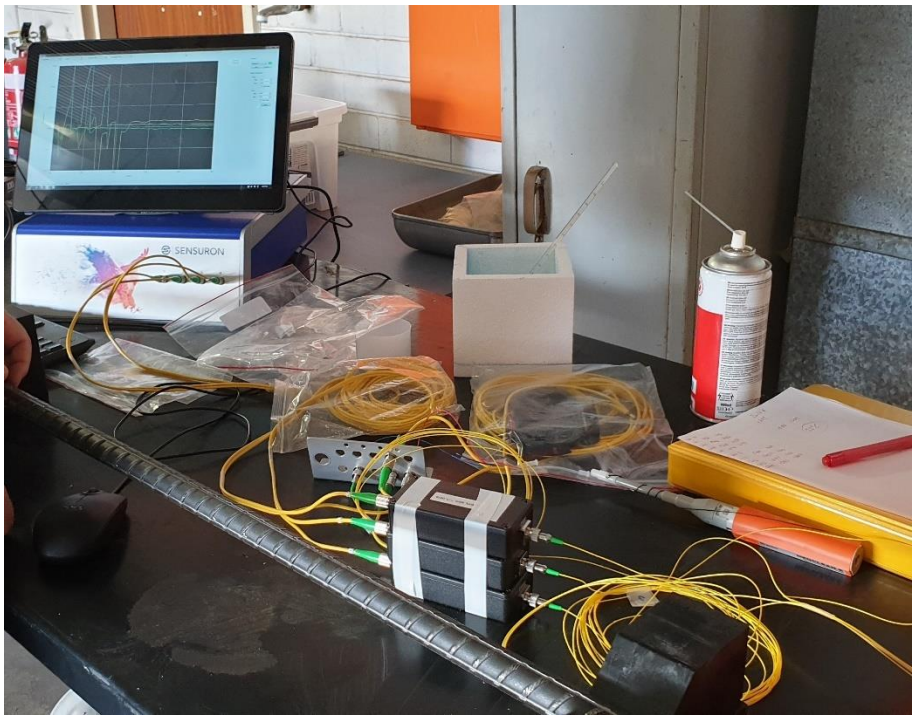

b)

Fig. 6.5 Double shear test – a) Experiment setup b) Instrumented bolt

Table 6.1 - Concrete and grout properties.

Test	Concrete	UCS (MPa)
1	Low strength	20.5
2	Low strength	18.5
3	Low strength	22.8
Average UCS		**20.6**
4	Medium strength	28.1
5	Medium strength	33.5
6	Medium strength	27
Average UCS		**29.5**

Table 6.2 - Rock bolt properties

Elastic Modulus (GPa)	200
Diameter (mm)	22
Yield Strength (MPa)	340
Ultimate Strength (MPa)	490

The axial and bending strain plot for all the tests can be found in the Appendix Figure A1 to A6.. The bending strain at point A, axial strain at point O and the length of the section OA can be measured from the strain plots.

6.3.4 Angled shear test

To increase the dataset for validation of bolt angle calculation, results from double shear tests conducted by Jessu, Kostecki et al. (2016) and Kostecki (2019) are also used. Jessu, Kostecki et al. (2016) and Kostecki (2019) conducted double shear tests on instrumented rock bolts installed at 90^0 and 80^0 to the discontinuity. The double shear tests were conducted in a similar manner to the test described in the previous section. The bolts were cast in concrete blocks and the centre block was loaded vertically keeping the side blocks fixed. The properties of concrete and rock-bolt used in the test are given in Table 6.3. The strain profiles of the bolt under double shear at 5 tonnes of load are shown in Fig. 6.6 and Fig. 6.7 for 90^0 and 80^0 bolt angles, respectively. A positive axial strain indicates extension and negative axial strain indicates compression. A positive bending strain indicates compression on the lower part of rock bolt and tension on top part and vice versa. From the strain plots it can be seen that the ratio of bending strain to the axial strain in the 90^0 bolt angle is higher than in the 80^0 bolt angle. This is consistent with the analytical model. The bending strain at point A, axial strain at point O and the length of the section OA are measured from the strain plots similar to the previous section.

Table 6.3 - Concrete and rock bolt properties (Kostecki, 2019).

Bolt				
Bolt Diameter (mm)	**Bolt Grade**	**Bolt length (mm)**	**Number of slots**	**Rebar design**
19	60	1198.5±7.5	2	Double Threaded Ends
Concrete				
Average Compressive strength (MPa)		**Average Modulus of Elasticity (GPa)**		
31		28		

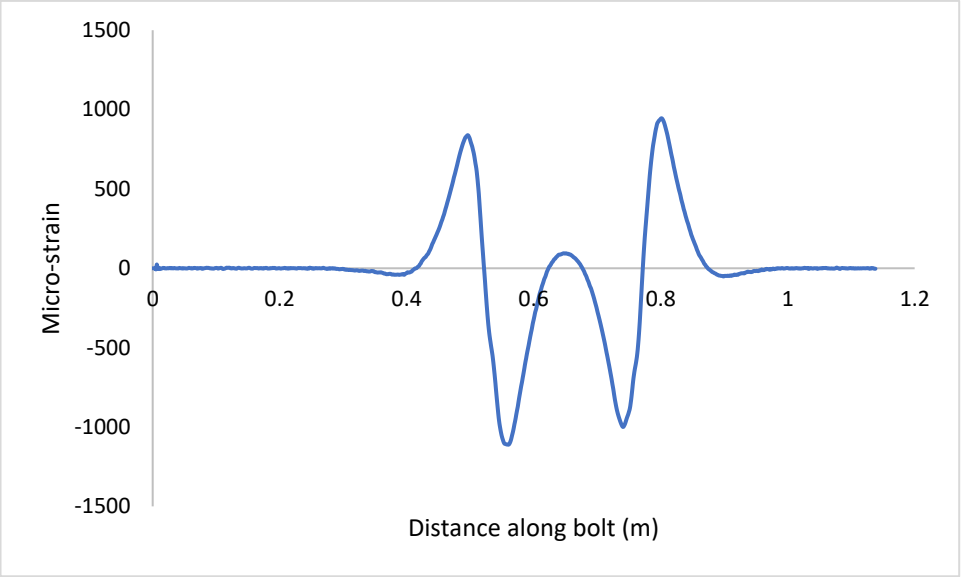

a)

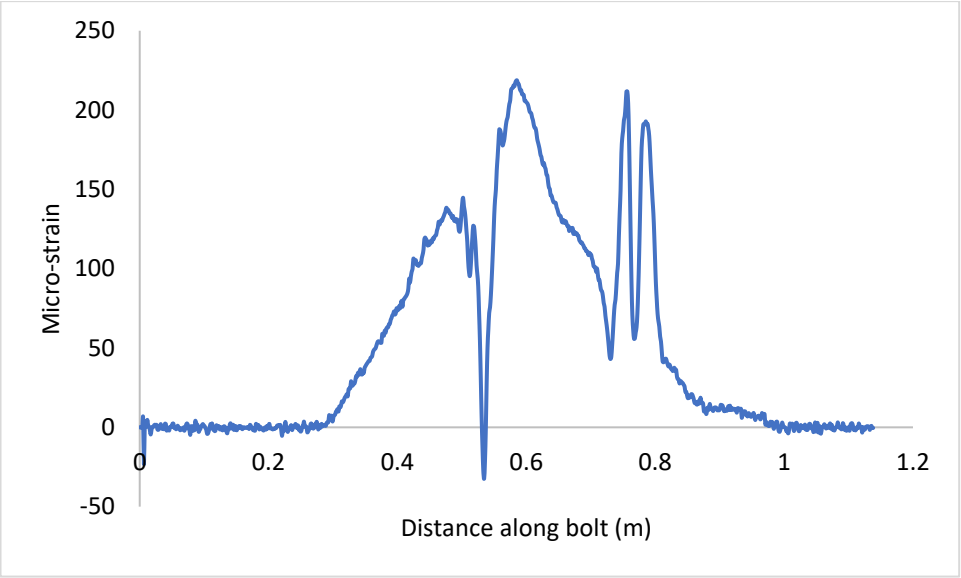

b)

Fig. 6.6 Strain profile 90^0 a) Bending strain b) Axial Strain

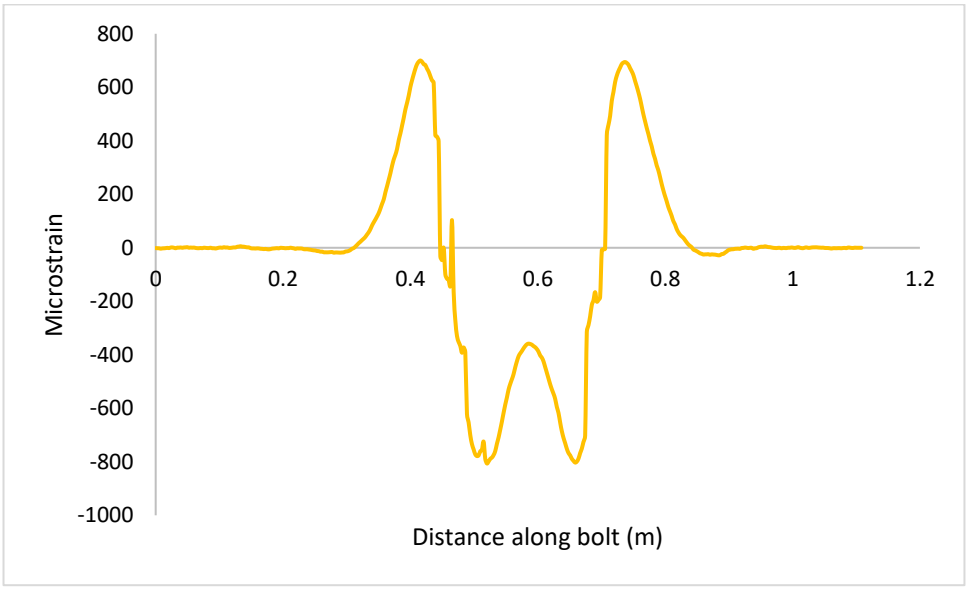

a)

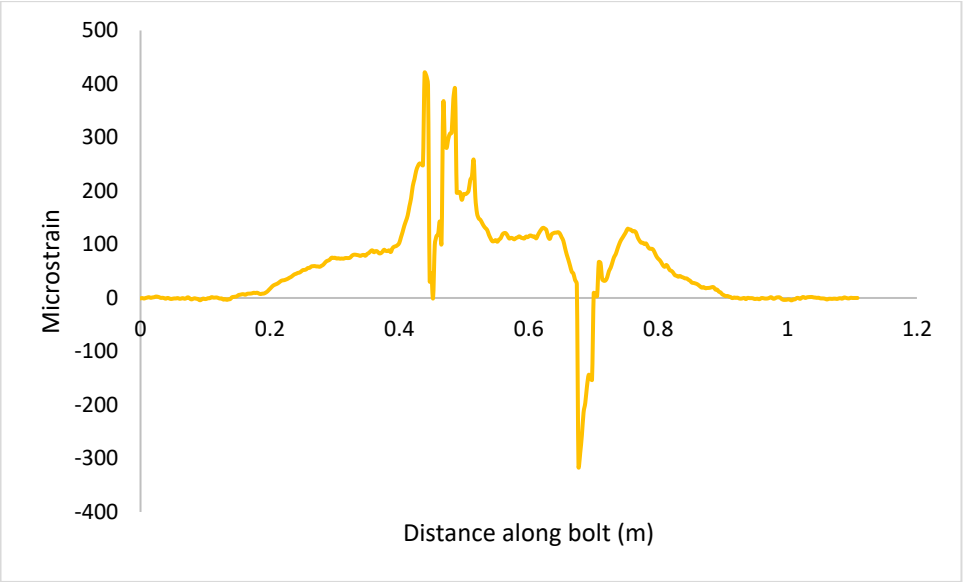

b)

Fig. 6.7 Strain profile 80^0 a) Bending strain b) Axial Strain

6.3.5 Numerical modelling

As double shear tests with lower bolt-discontinuity angles are very difficult to conduct in a lab, numerical modelling is used to analyse the bolt strains under shear tests with bolt-discontinuity angles of 60^0 and 45^0. A numerical model is created in Ansys (2019) with a bolt at 80^0 to the discontinuity (Fig. 6.8) and calibrated with the results of Jessu, Kostecki et al. (2016). The strain plots from the calibrated model compared with the lab results (at 2.5 tonnes load) are shown in Fig. 6.9. The calibrated material properties of the numerical model are shown in Table 6.4. Two new models were created with bolt-discontinuity angles of 60^0 and 45^0 using the calibrated material properties. The numerical models and the axial and bending strain plots for the two cases are shown in the Appendix Figure A7 to A10. The bending strain at point A, axial strain at point O and the length of the section OA are measured from the strain plots of the rock bolts.

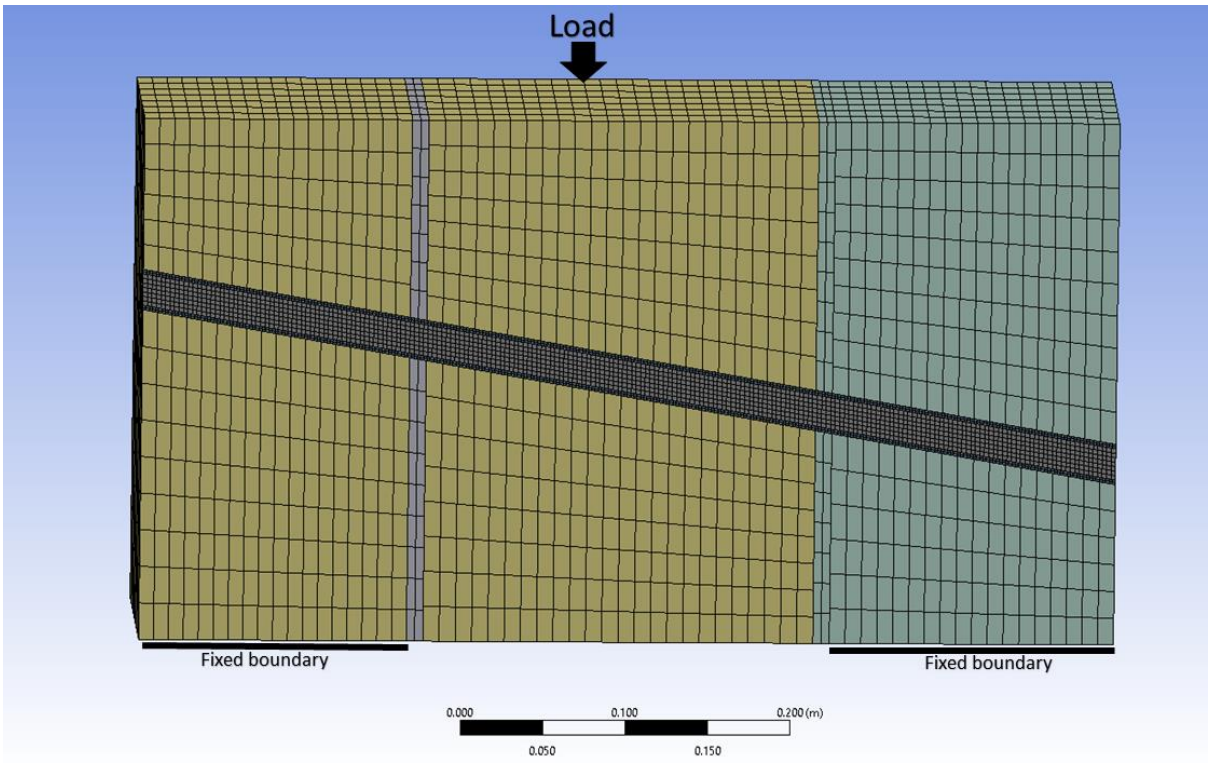

Fig. 6.8 Angled double shear model

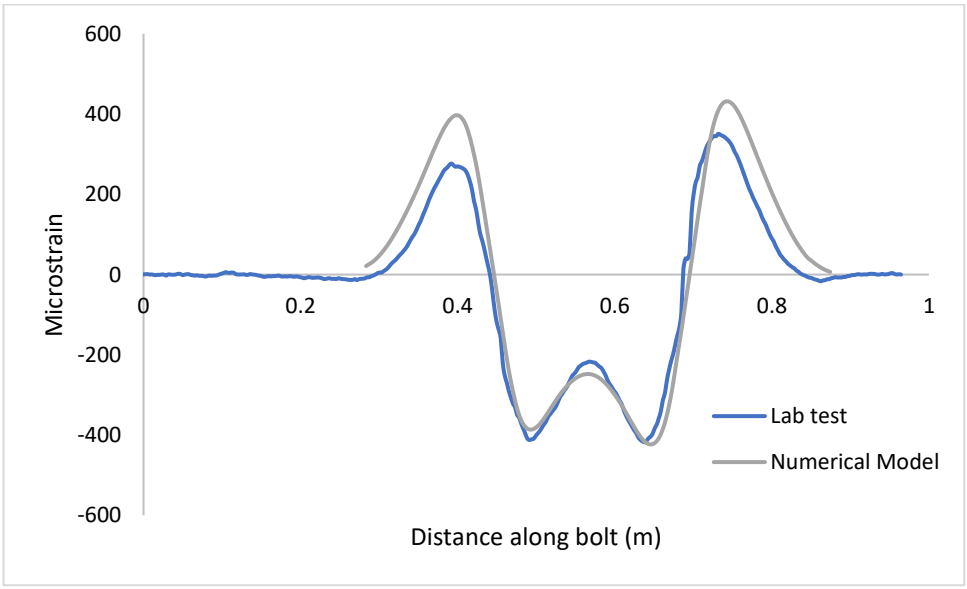

a)

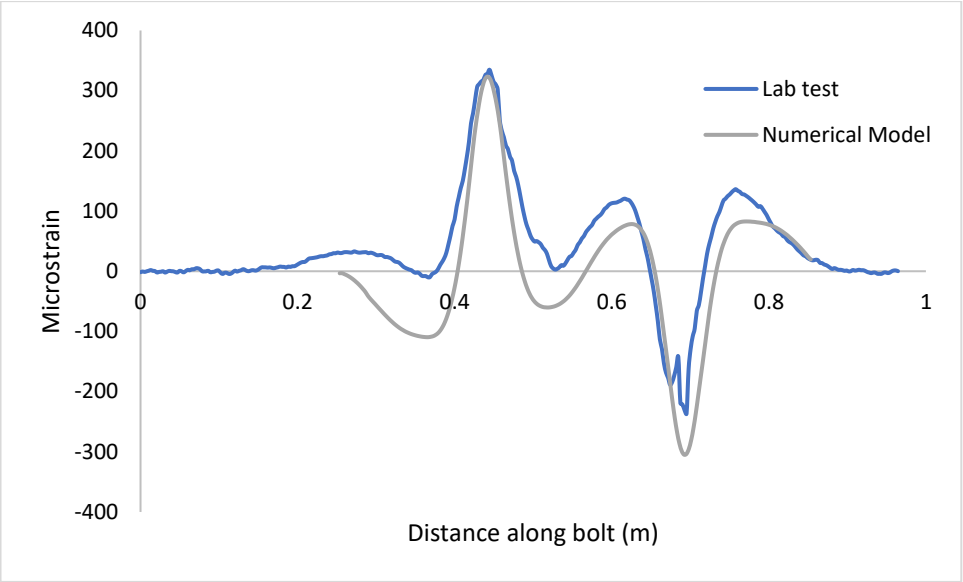

b)

Fig. 6.9 Calibration of angled double shear test a) Bending strain b) Axial Strain

Table 6.4 - Calibrated material properties for the angled shear test.

Concrete		
Elastic Modulus (MPa)	**UCS (MPa)**	**UTS (MPa)**
26,000	30	3
Grout		
Elastic Modulus (MPa)	**UCS (MPa)**	**UTS (MPa)**
3,000	184	13.8
Interface		
Normal stiffness (MPa)	**Friction coefficient**	**Cohesion (MPa)**
80,000	0.57	0

6.3.6 Validation with laboratory and numerical modelling results

Bolt-Discontinuity angles are calculated from the strain plots obtained from the laboratory and numerical models presented in the previous sections. The parameters calculated from the strain plots for each case are given in Table 6.5. Fig. 6.10 compares the bolt-discontinuity angles

calculated using equations (6.1) to (6.7) for each case with the actual bolt-discontinuity angle. As can be seen from Fig. 6.10 the values of the angles calculated analytically, matches with the actual bolt-discontinuity angle.

Table 6.5 - Parameters calculated from strain plots of shear tests and numerical models.

Test	E_b (bending strain at A)	E_a (bending strain at A)	L_A (Length of section OA)
DST 1	1772	246	0.0174
DST 2	3692	327.5	0.0312
DST 3	1635	168.5	0.0247
DST 4	717.5	103.5	0.0191
DST 5	1042	82.2	0.0386
DST 6	1110	266	0.0300
DST (Kostecki 2019)	970	80	0.0313
DST 80^0 (Jessu, Kostecki et al. 2016)	272	325	0.0300
60^0 Numerical Model	446	813	0.0160
45^0 Numerical Model	140	620	0.02

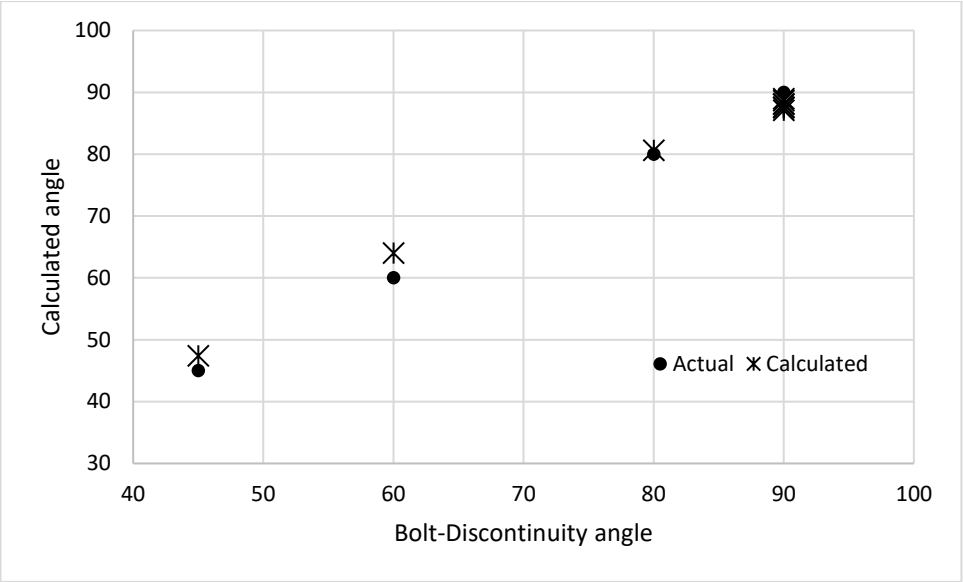

Fig. 6.10 Validation of bolt angle calculation

6.4 Calibration of pile element parameters

The pile element used in FLAC3D to model rockbolts as discussed earlier uses springs to combine the interface interactions in a fully grouted rock bolt between bolt-grout and grout-rock. The parameters which define the behaviour of these springs need to be calibrated to simulate the real rock bolt behaviour. There are two springs - shear and normal which control the axial and shear behaviours of the pile element, respectively. The three parameters that define the spring properties are stiffness, cohesion and friction angle. The stiffness of the spring represents the deformability of the interface and the cohesion and friction angle control the strength of the interface. The parameters for the shear spring can be obtained using the load-displacement plot from in-situ pull testing of the rock bolt (Bin, Taiyue et al. 2012, Nemcik, Ma et al. 2014). Calibration of the normal spring parameters which control the shear behaviour of the pile element requires load-displacement data from an in-situ shear test of the rock bolt. However, no method is currently available to directly obtain the load-displacement data from in-situ testing. In this study, a method is proposed to derive the load-displacement plot for the shear loading of rock bolt from in-situ instrumented rock bolt data. The load-displacement plot can then be used to calibrate a rock bolt shear model in FLAC3D to obtain the pile's normal spring parameters which can then be used in an in-situ model.

6.4.1 Load vs Displacement plot

The load and displacement values can be calculated from the strain plots using the analytical model proposed by Singh and Spearing (2021). The analytical model gives a relationship between the bolt displacement, load and strains. The shear load on the rock bolt Q_0 can be calculated using equation (6.1). The axial load N_0 can be calculated as:

$$N_o = \varepsilon_A EA \tag{6.8}$$

The displacement can be calculated using equation (6.2). The total displacement of the joint will be double the value obtained from equation (6.2). The total load can be calculated as:

$$L = (N_0 \cos(\alpha - \theta) + Q_0 \sin(\alpha - \theta)) + (N_0 \sin(\alpha - \theta) + Q_0 \cos(\alpha - \theta)) \tan\phi \tag{6.9}$$

Where, ϕ is the joint friction angle.

6.4.2 Validation with laboratory double shear test

The above procedure is used to calculate the load-displacement plot from the strain plots of a double shear laboratory test with inclined bolt (Jessu, Kostecki et al. 2016) and compared with the actual load-displacement plot from the test. The test has been described in section 3. The axial and bending strain plots at five different loads are shown in Fig. 6.11. The load and displacement are calculated using equation (6.2) and (6.9) as discussed in the previous section. The calculated load-displacement plot is compared with the measured load-displacement values in Fig. 6.12. As can be seen from the figure the calculated plot matches with the actual.

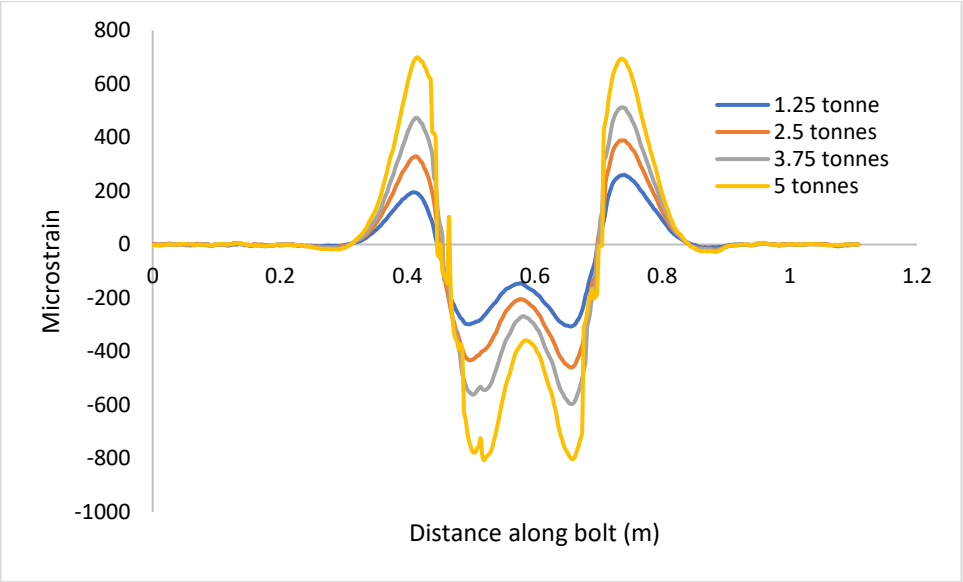

a)

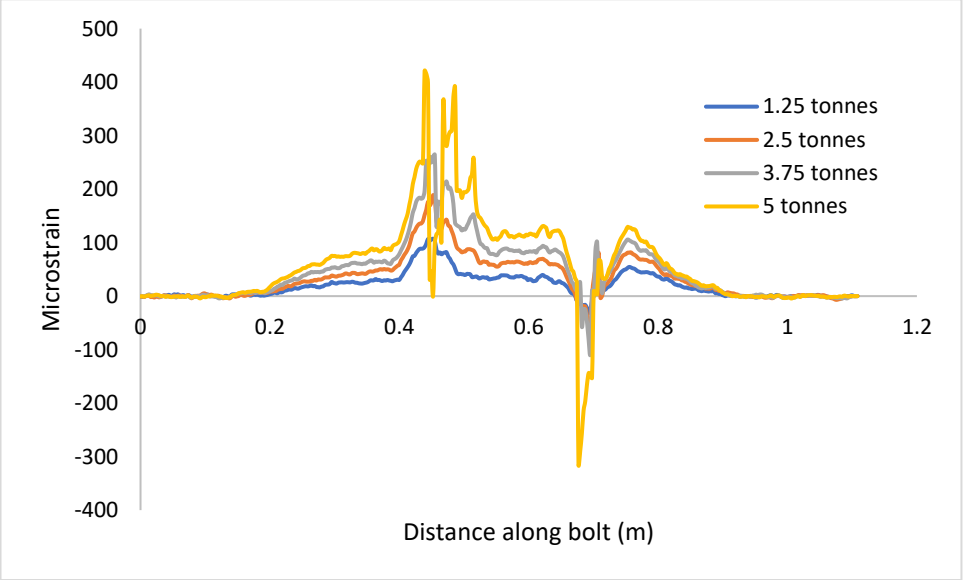

b)

Fig. 6.11 Strain plots 80^0 angled bolt a) Bending strain b) Axial strain

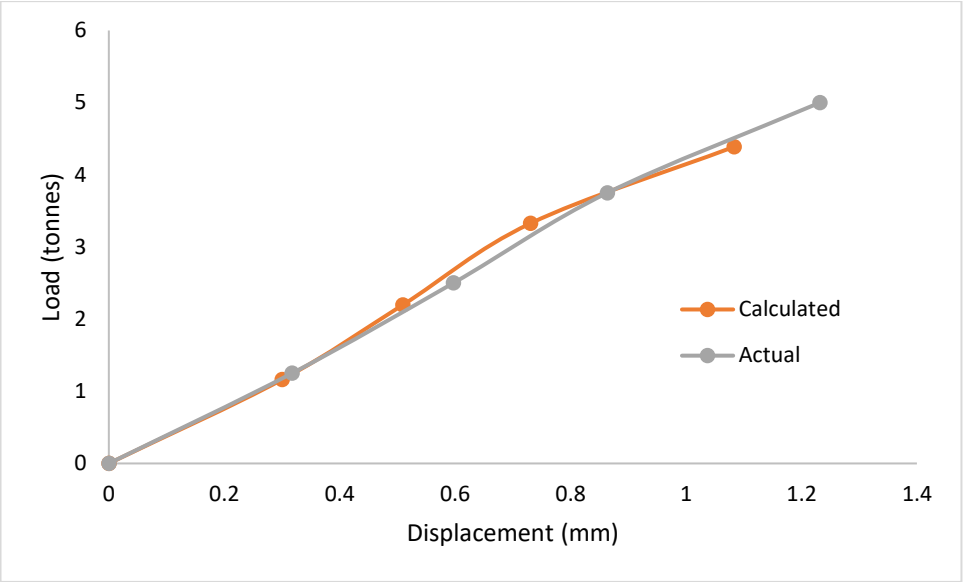

Fig. 6.12 Load - Displacement: Actual vs Calculated

6.5 In-situ modelling

In-situ rock bolt models need to be calibrated with actual in-situ observations before they can produce results useful for rock-bolt reinforcement design. In this study, optical instrumented rock bolts were installed in a hard rock mine and the recorded strain data from the instrumentation is used to calibrate an in-situ rock bolt model.

6.5.1 In-situ instrumented rock bolt study

Six instrumented rock bolts were installed in a hard rock gold mine and the rock bolt strains were recorded over a period of 2 months. The instrumented rock bolts used a newly developed continuous Fibre Bragg grating (FBG) technology and the strain data from the bolts were recorded at a fixed interval of 30 minutes (Hoehn, Spearing et al. 2020). The location chosen for the installation of the instrumented rock bolt was a development heading in an inclined Room and Pillar mining area at a depth of approximately 627m. The rock bolts were located adjacent to a pillar in an intersection as shown in Fig. 6.13. The instrumented rock bolts were installed as secondary supports. The specifications of the rock bolts used in the test are given in Table 6.6. The position of the rock bolts and their orientation is shown in Fig. 6.14.

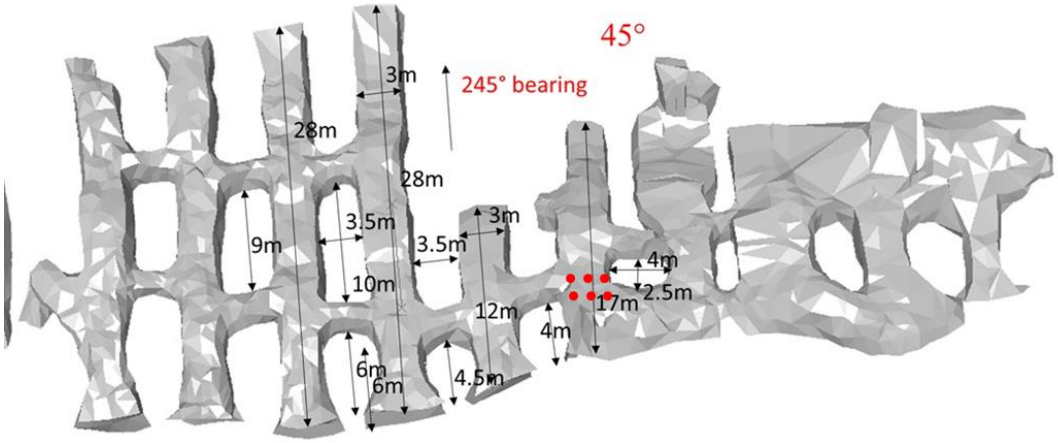

Fig. 6.13 Rock bolt installation location

Table 6.6 - Instrumented rock bolt properties.

Length (m)	2.4
Diameter (mm)	22
Young's Modulus (GPa)	200
Yield Strength(kN)	270
Failure strain	0.15

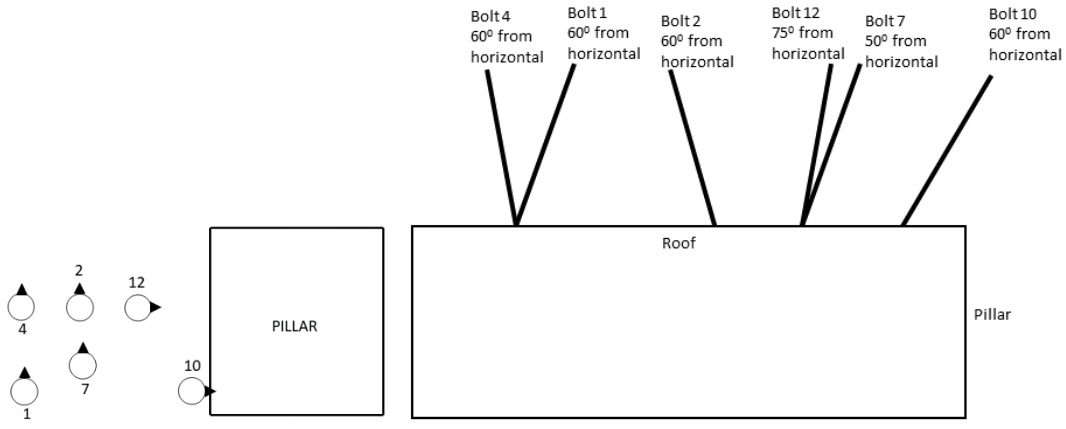

a) b)

Fig. 6.14 Instrumented rock bolt installation a) position and direction of inclination b) orientation with roof

As the instrumented rock bolts were un-tensioned it was expected that they will undergo an increasing load as the development proceeded in the adjacent headings. While the strain on the rock bolt was recorded continuously, the rock bolts only showed an increase in load when the excavation progressed. Therefore, in this study three mining stages have been identified where the rock bolts showed a significant change in strain magnitudes. The excavation stages are shown in Fig 6.15.

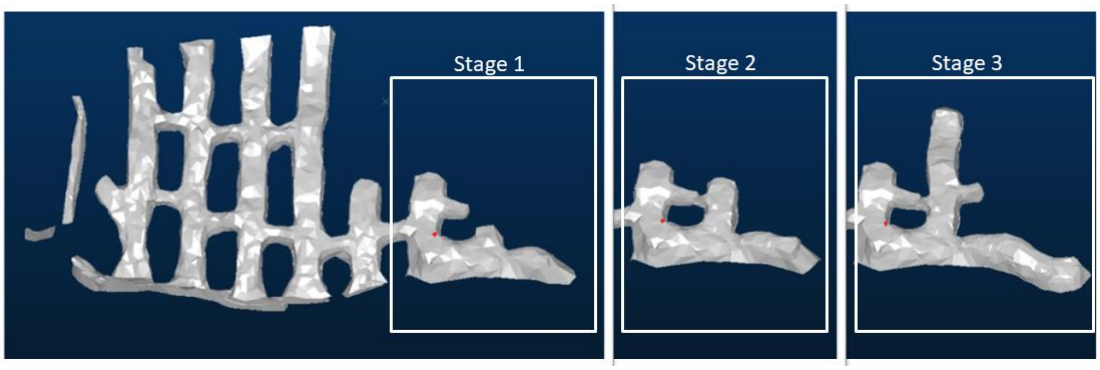

Fig 6.15 Excavation stages with significant strain increases in instrumented rock bolts

The strain data obtained from the rock bolts was processed to calculate the axial and bending strain plots at each of the three excavation stages. To calculate bending strain and directions on the rock bolt strain values from at least three of the four fibres are required. Due to installation errors and later due to mining activity some of the fibres were damaged on one of the rock bolts. Complete strain profiles from only five of the rock bolts were obtained at the end of the test. The axial and bending strain profile of the bolts at the three stages of excavation are given in Appendix Figure A11 and A12. The rock bolts do not show much increase in axial loading as the excavation progressed. This can be attributed to the fact that the bolts were installed as secondary supports and were un-tensioned. Also, the rock in the mine is very competent and has high strength and elastic modulus therefore the rock behaviour is mostly dominated by structures in the rock mass. Bolts 7 and 10 show a significant bending loading which increases with the mining progress Fig. 6.16 and Fig 6.17. In the axial and bending profile of the rock bolts, a bending point can be seen about 0.75 m from the bolt head. This strain profile indicates the presence of a discontinuity that intersects the bolts. The axial strains

on the rock bolts can also be attributed to the discontinuity as the load is concentrated at the bending point. As can be seen from the strain profiles in Fig. 6.16 and Fig 6.17, the new instrumented rock bolt technology can provide a very high-resolution detail of the strains on the complete length of the rock bolt. This data can be used to calibrate the numerical models for in-situ rock bolt reinforcement design as shown in the section below. Since bending was observed only in bolt 7 and 10, these two bolts will be used to calibrate the rock bolt model for shear loading.

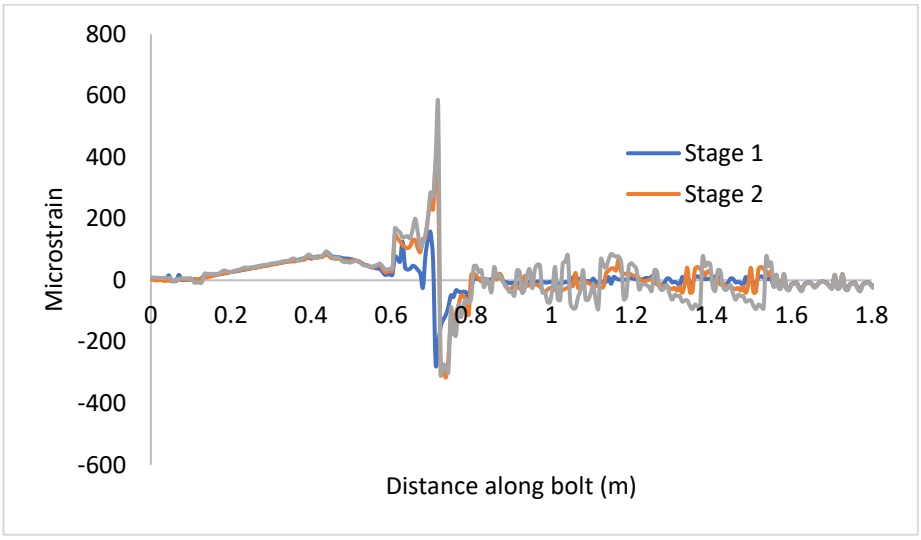

a)

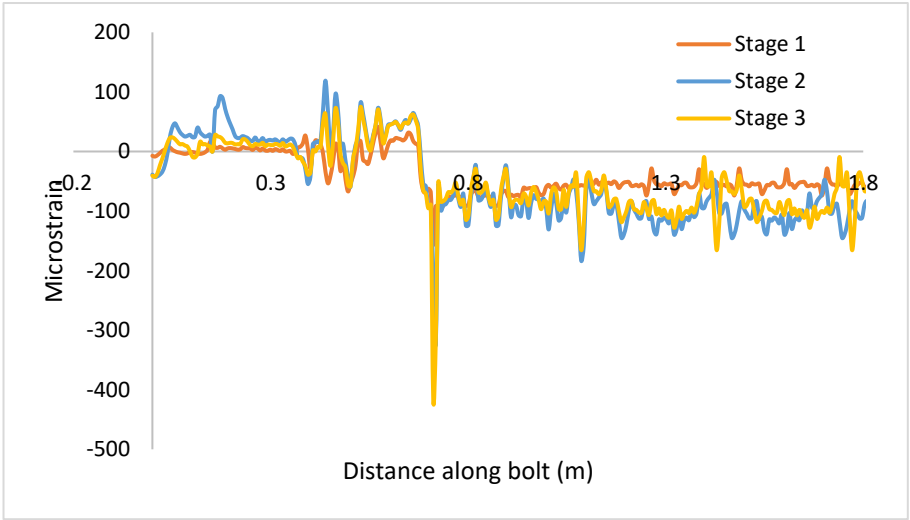

b)

Fig. 6.16 Strain profile bolt 7 a) Bending strain b) Axial strain

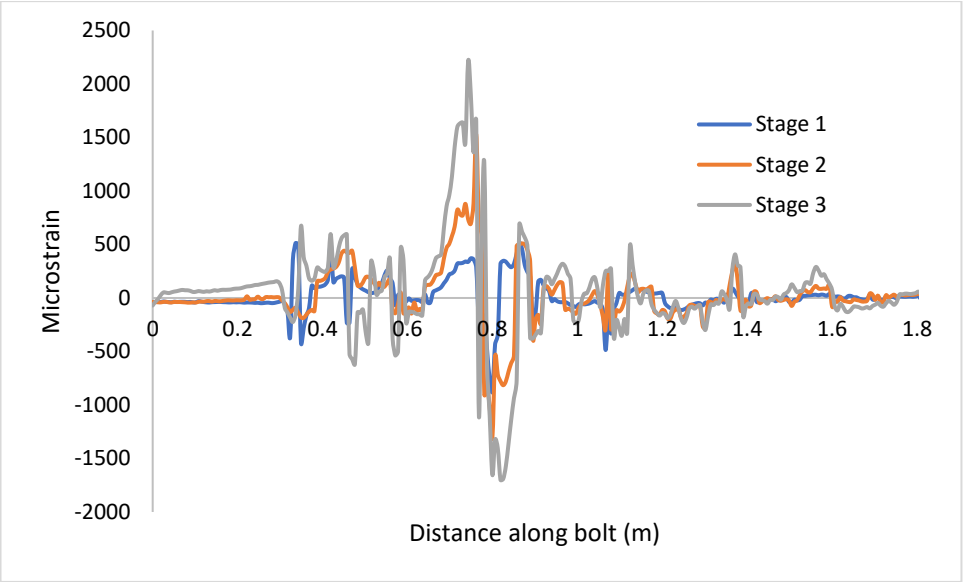

a)

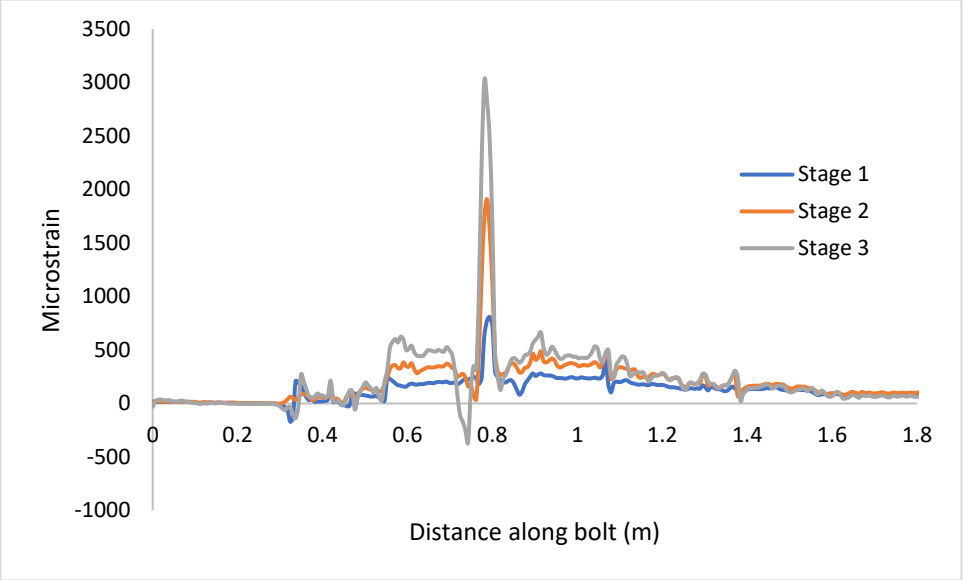

b)

Fig 6.17 Strain profile bolt 10 a) Bending strain b) Axial strain

6.5.2 Calibration of the numerical model with in-situ data

Numerical modelling of the in-situ rock bolt reinforcement was done using FLAC3D. A three-dimensional model of the excavation was created with the excavation stages progressing according to the actual mining progress. The model boundaries dimensions are 60mX60mX40m. The development headings are 3mX2m and the Pillars are 3.5mX2m. The

grid size is 0.5mX0.5mX0.5m in the pillars and 0.5mX0.5mX0.2m in the roof close to the excavation. The 3D model of the excavation is shown in Fig. 6.18. The model's sides were constrained using roller boundary and the base was constrained using a fixed boundary. A load equivalent to the vertical stress was applied at the top boundary of the model. The rock properties, the prominent discontinuity data and the in-situ stress data obtained from the mine are given in Table 6.7 to Table 6.9. The in-situ stresses were rotated to the direction of the coordinate system of the model and applied using the in-built stress initialization command of FLAC3D. The Mohr-Coulomb constitutive model was used for the rock because the rockmass in the area behaved basically elastically.

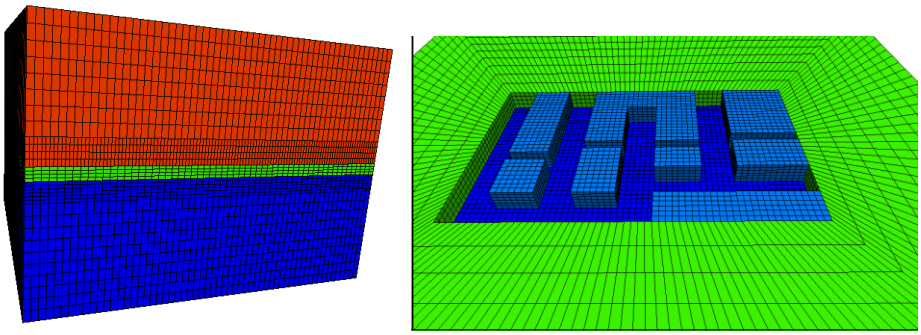

Fig. 6.18 FLAC3D in-situ model

Table 6.7 - Rock properties.

UCS (MPa)	181
Young's Modulus (GPa)	64.2
Poisson's Ratio	0.324
Cohesion (MPa)	27.5
Friction angle	35^{o}
Tensile Strength (MPa)	8.1

Table 6.8 - Major structures.

Defect Set	Dip/ Dip Direction (°)	Type	Trace Length	Planarity	Roughness
1	64°→110	Joints and quartz veins	1-7m	Planar and undulating	Rough and smooth
2	51°→259	Foliation and joints	1-10m	Planar and undulating	Rough and smooth
3	59°→020	Joints and quartz veins	1-5m	Planar	Rough
4	85°→179	Joints	>5m	Planar and Stepped	Rough to slightly rough

Table 6.9 - In-situ stress state.

Depth 627 m	Major (MPa)	54.3	13	313
	Intermediate (MPa)	24.1	54	204
	Minor (MPa)	8.0	32	52

As seen from the in-situ data the major strain identified on the rock bolts was bending due to the presence of a shearing discontinuity. Therefore, the focus was to calibrate the model to the shear behaviour of the rock bolts observed in-situ. The calibration process can be divided into two parts – discontinuity and rock bolt properties. The location and orientation of the discontinuity are calculated using the method detailed in section 3.1. The parameters calculated from the strain plots and angles calculated for Bolt 7 and 10 are given in Table 6.10.

From the bolt-discontinuity angle calculated in Table 6.10, the orientation of the discontinuity can be derived by considering the orientation of the rock bolts with respect to excavation. From the prominent structure data in Table 6.8, the joint set with 51^0 dip and 259^0 strike matches closest with the calculated discontinuity orientation (Fig. 6.19). The discontinuity properties are estimated from joint data in Table 6.8 and joint properties for similar rock type from Bandis, Lumsden et al. (1983), Hoek, Kaiser et al. (1995), Sitharam, Maji et al. (2007). The joint was modelled as an interface and the location was adjusted to match the location of the bending point on the rock bolts. Joint properties used in the model are given in Table 6.11.

Table 6.10 - In-situ discontinuity orientation calculation.

	Bolt 7	Bolt 10
Diameter (m)	0.022	0.022
L_A (m)	0.019	0.0127
E_b (Bending strain)	370e-6	1529e-6
E_a (Axial strain)	226e-6	1467e-6
Bolt-Discontinuity angle (°)	81.2	70
Bolt angle with horizontal (°)	50	60
Discontinuity orientation with rock (°)	48.8	50

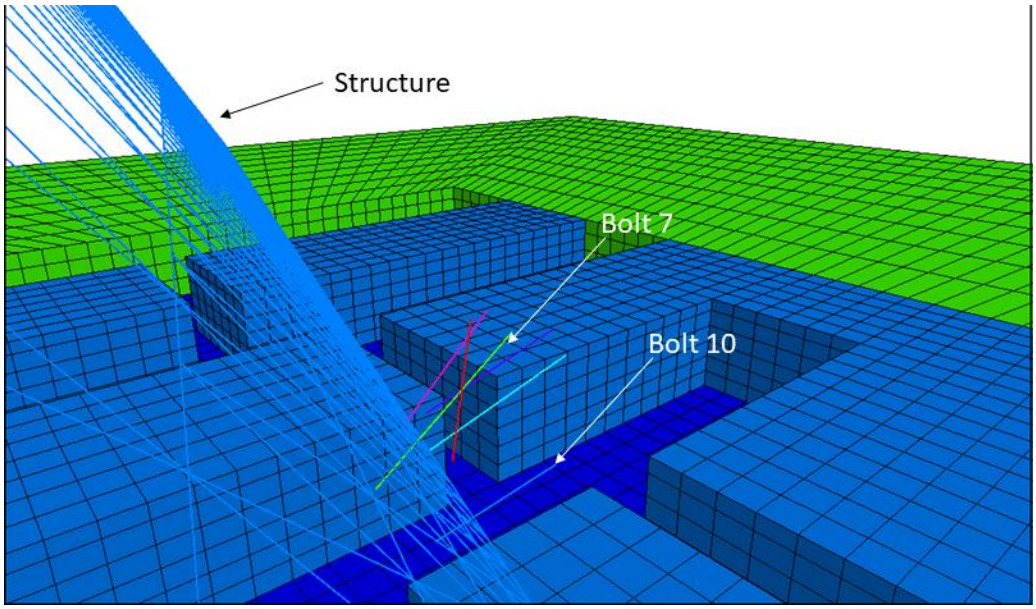

Fig. 6.19 Model showing the instrumented rock bolts and the structure

Table 6.11 - Structure interface properties.

Normal stiffness (MPa/m)	50000
Shear stiffness (MPa/m)	17000
Friction angle (°)	26.5

The model is first run without any excavations to initiate the in-situ stresses in the rocks. Then the excavation is made in stages as shown above in Fig 6.15. The primary rock bolt reinforcement in the mine consisted of 1.8m bolts installed at a 1mX1.5m spacing. These bolts are installed in the model as soon as the excavation stage is progressed. The instrumented bolts were installed as secondary supports. The strain developed on these bolts is measured at end of each excavation stage and the procedure outlined in section 4 is used to calibrate the pile element's parameters. The rock bolt properties and calibrated parameters are given in Table 6.12. The strain plots of bolts 7 and 10 in the numerical model are compared with the strain plots measured from in-situ instrumented bolts in Fig. 6.20 and Fig. 6.21. As can be seen from the plots the strain in the rock bolt numerical model matches closely with the in-situ measured strains.

Table 6.12 - Calibrated Pile element parameter.

Length (m)	2.4
Diameter (mm)	22
Young's Modulus (GPa)	200
Yield Strength(kN)	270
Failure strain	0.15
Normal spring stiffness (GPa)	20
Normal spring cohesion (Nm)	2.75e6
Normal spring friction angle	25
Shear spring stiffness (GPa)	20
Shear spring cohesion (Nm)	8e5
Shear spring friction angle	23

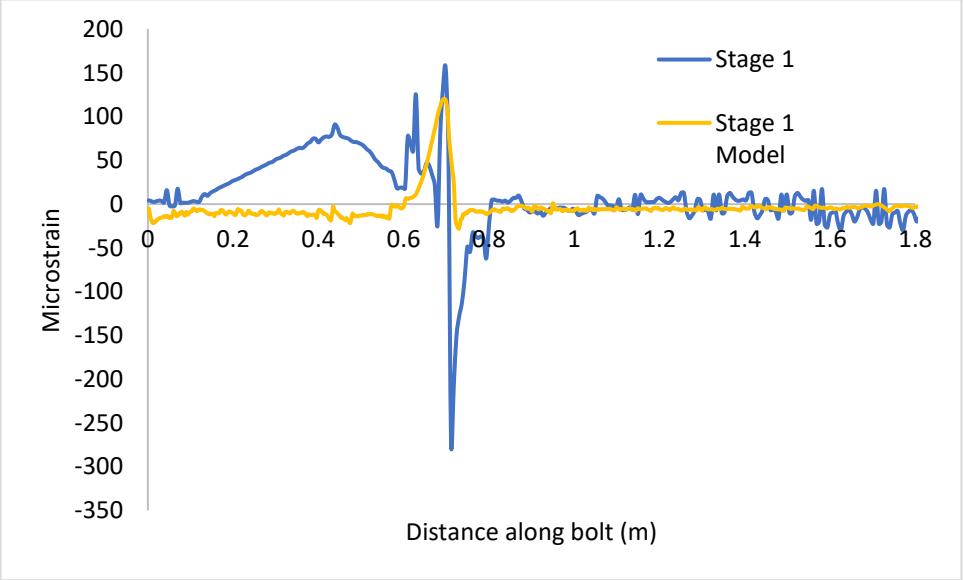

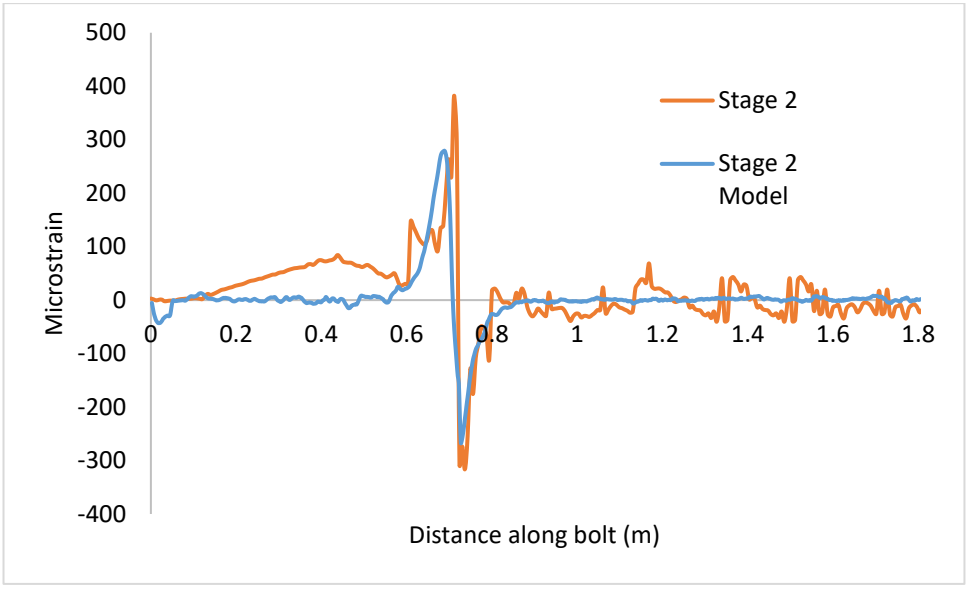
500
400
300
200
100
0
-100
-200
-300
-400
Microstrain
0
0.2
0.4
0.6
0.8
1
1.2
1.4
1.6
1.8
Distance along bolt (m)
Stage 2
Stage 2 Model

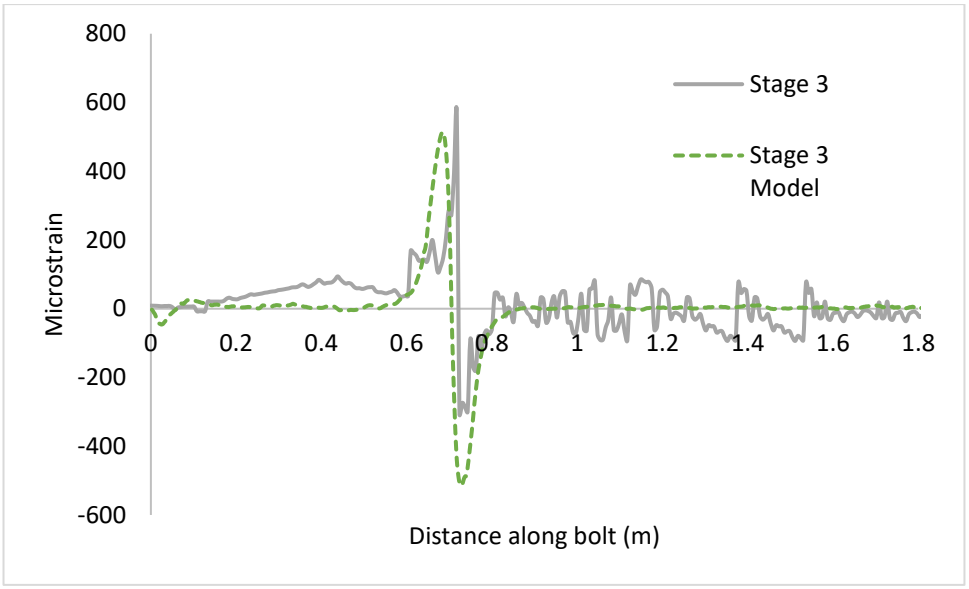
800
600
400
200
0
-200
-400
-600
Microstrain
0
0.2
0.4
0.6
0.8
1
1.2
1.4
1.6
1.8
Distance along bolt (m)
Stage 3
Stage 3 Model

a)

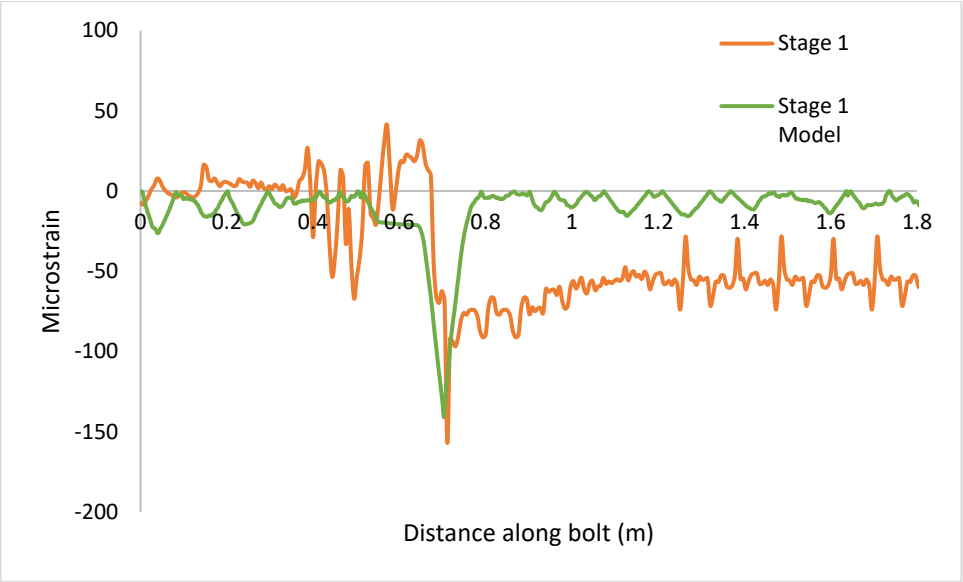
100
50
0
-50
-100
-150
-200
0
0.2
0.4
0.6
0.8
1
1.2
1.4
1.6
1.8
Microstrain
Distance along bolt (m)
Stage 1
Stage 1 Model

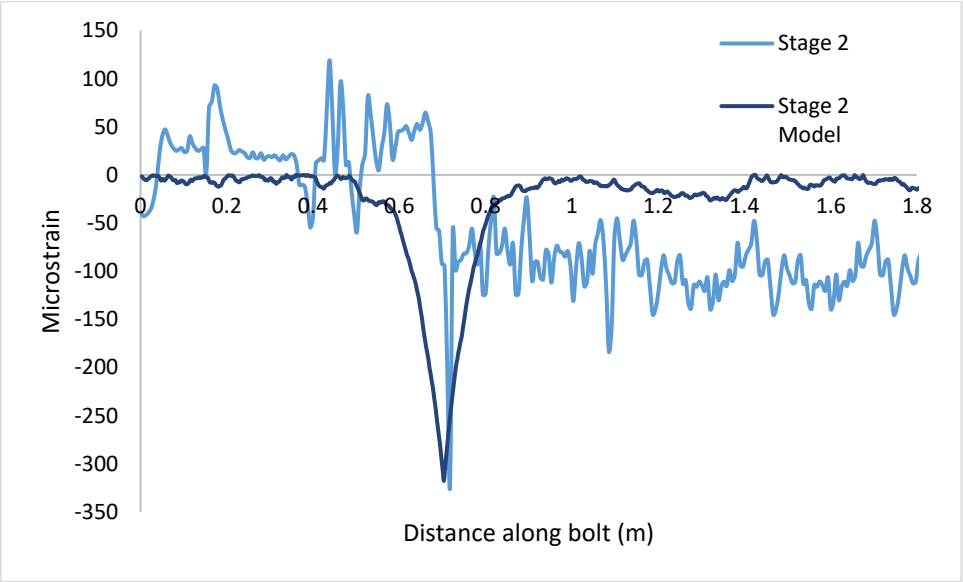
150
100
50
0
-50
-100
-150
-200
-250
-300
-350
0
0.2
0.4
0.6
0.8
1
1.2
1.4
1.6
1.8
Microstrain
Distance along bolt (m)
Stage 2
Stage 2 Model

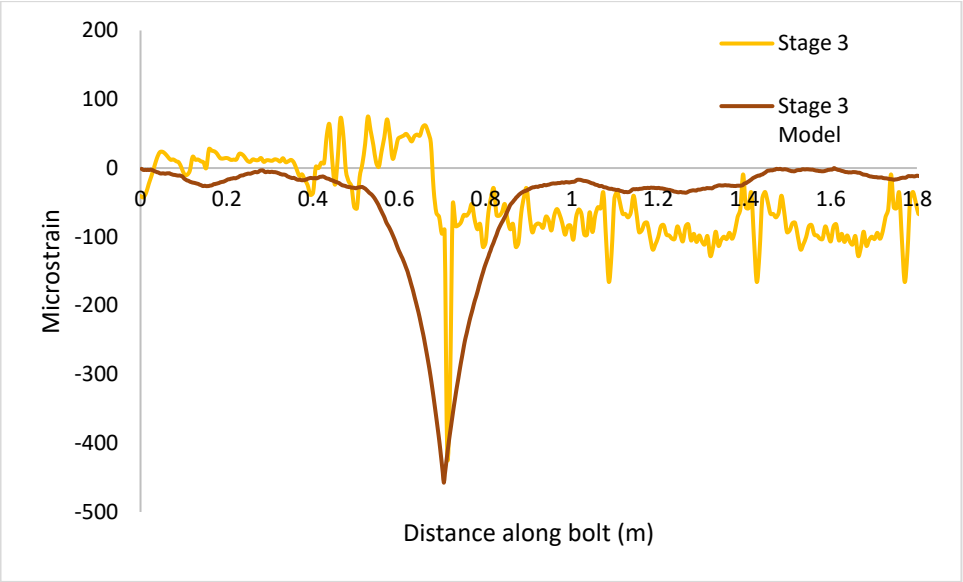

b)

Fig. 6.20 Calibrated bolt 7 model vs in-situ a) Bending strain b) Axial strain

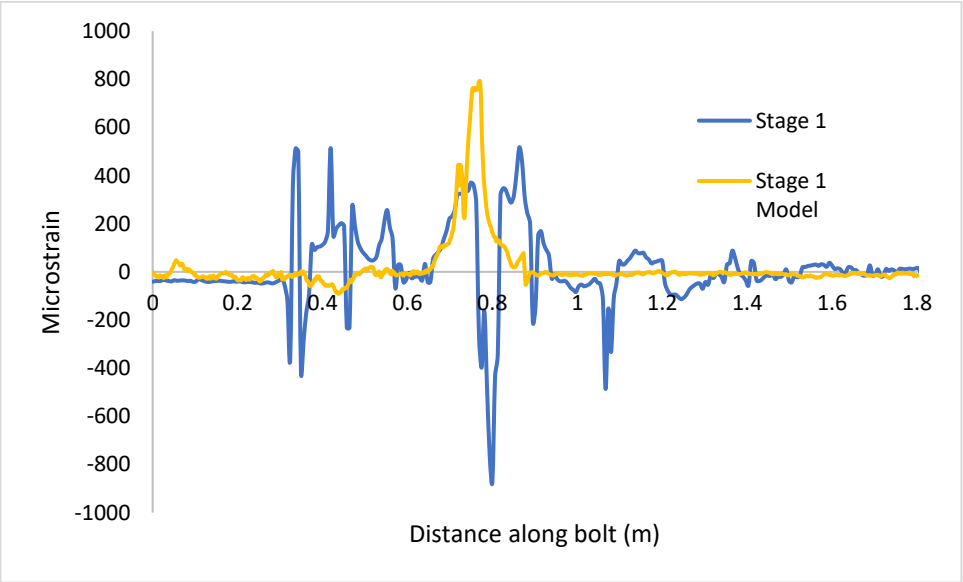

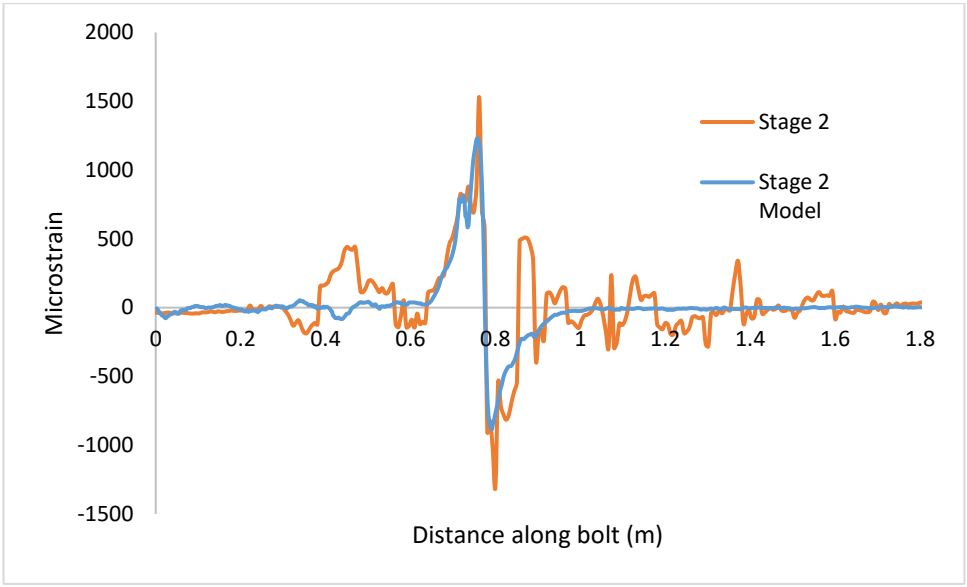
2000
1500
1000
500
0
-500
-1000
-1500
Microstrain
0
0.2
0.4
0.6
0.8
1
1.2
1.4
1.6
1.8
Distance along bolt (m)
Stage 2
Stage 2 Model

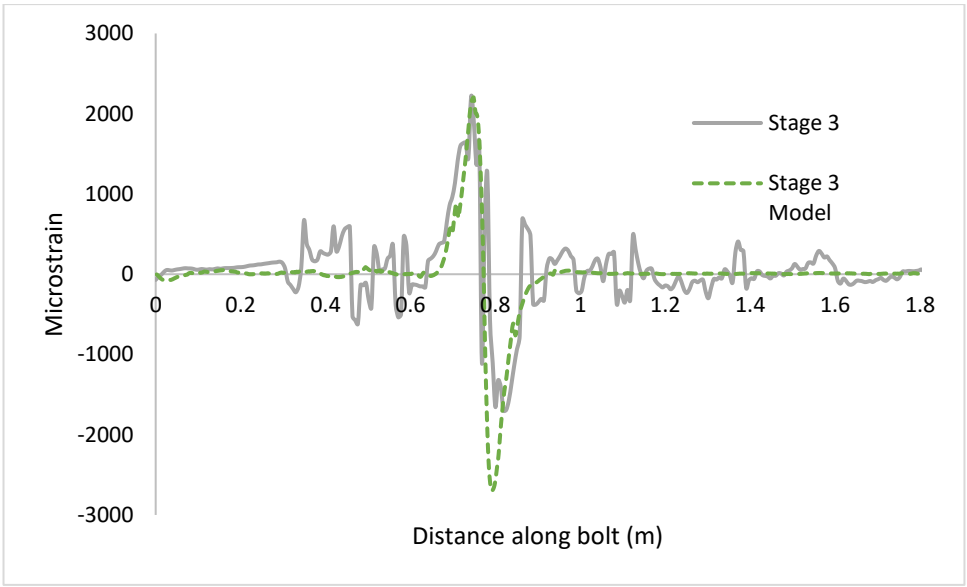
3000
2000
1000
0
-1000
-2000
-3000
Microstrain
0
0.2
0.4
0.6
0.8
1
1.2
1.4
1.6
1.8
Distance along bolt (m)
Stage 3
Stage 3 Model

a)

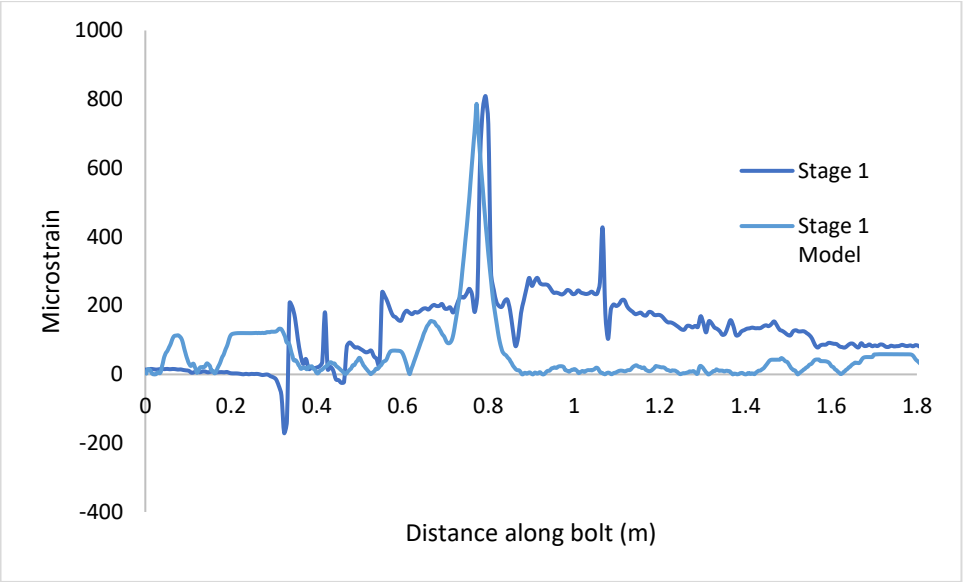
1000
800
600
400
200
0
-200
-400
Microstrain
0
0.2
0.4
0.6
0.8
1
1.2
1.4
1.6
1.8
Distance along bolt (m)
Stage 1
Stage 1 Model

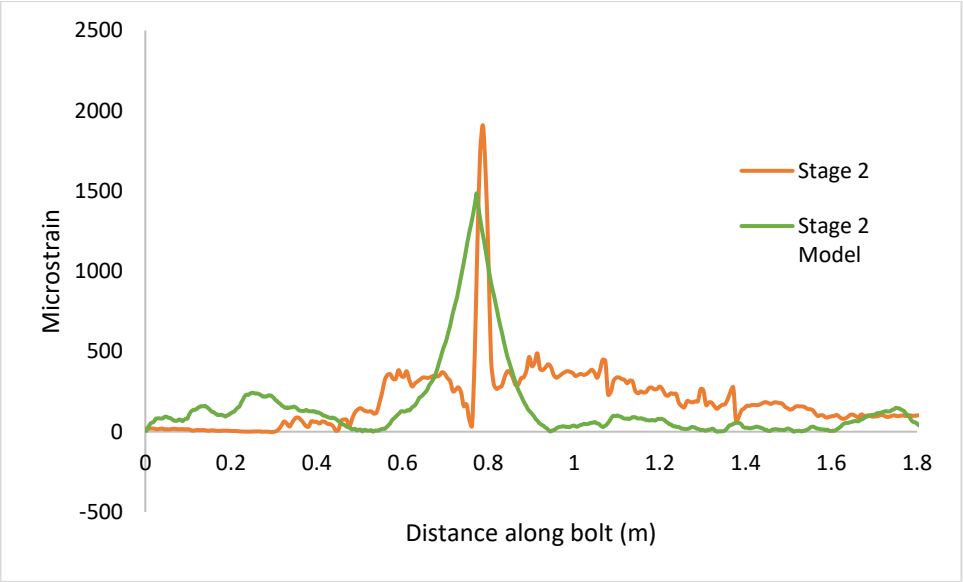
2500
2000
1500
1000
500
0
-500
Microstrain
0
0.2
0.4
0.6
0.8
1
1.2
1.4
1.6
1.8
Distance along bolt (m)
Stage 2
Stage 2 Model

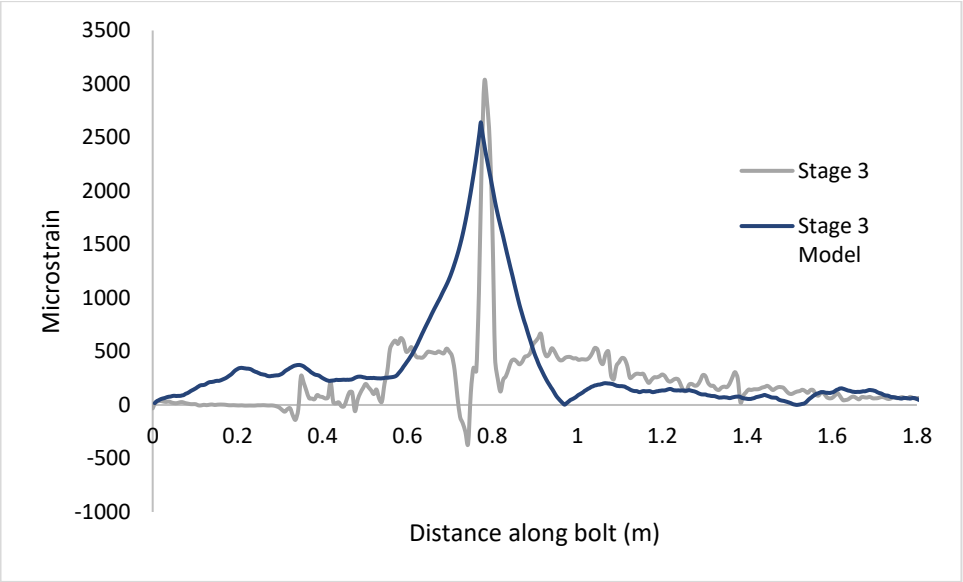

b)

Fig. 6.21 Calibrated bolt 10 model vs in-situ a) Bending strain b) Axial strain

6.6 Conclusions

Optical instrumented rock bolts have been used to study rock bolt behaviour under shear loading in laboratory test and in in-situ. In this paper analytical methods have been proposed to process the strain data from instrumented rock bolts. Bolt-discontinuity angle has been calculated using strain data and the FLAC3D pile element parameters have been calibrated to model the shear behaviour of rock bolt. The results have been validated with laboratory tests and numerical modelling. To demonstrate the methods outlined in the work an in-situ rock bolt model is created in FLAC3D and calibrated with the data from in-situ instrumented rock bolts. The following conclusions can be made from the work done in this paper –

1. New optical instrumented rock bolts provide a very high-resolution strain profile of the rock bolt installed in-situ. This is especially important in the case of a localised loading of rock bolt such as produced by a discontinuity. The instrumentation is capable of capturing the bending strain of the rock bolt due to the shear loading from a discontinuity. The bending strain data can be used for identifying structures and determining their orientation in the rock mass.

2. The strain data from instrumented rock bolt can be used to calculate the load-displacement plot for a rock bolt undergoing shear loading in-situ. This plot can be used to calibrate the shear behaviour of an in-situ rock bolt model. This calibration process provides a better representation of rock bolt's in-situ behaviour compared to the existing method of calibrating the rock bolt model with laboratory shear tests where it is difficult to reproduce the exact in-situ conditions. The calibrated rock bolt model can then be used for designing rock bolt reinforcement for underground excavations using numerical modelling.

Acknowledgement

This work was supported by the Minerals Research Institute of Western Australia (MRIWA); Mining3, Curtin University, Minova Australia and Peabody Energy.

Appendix

Laboratory double shear test strain plots –

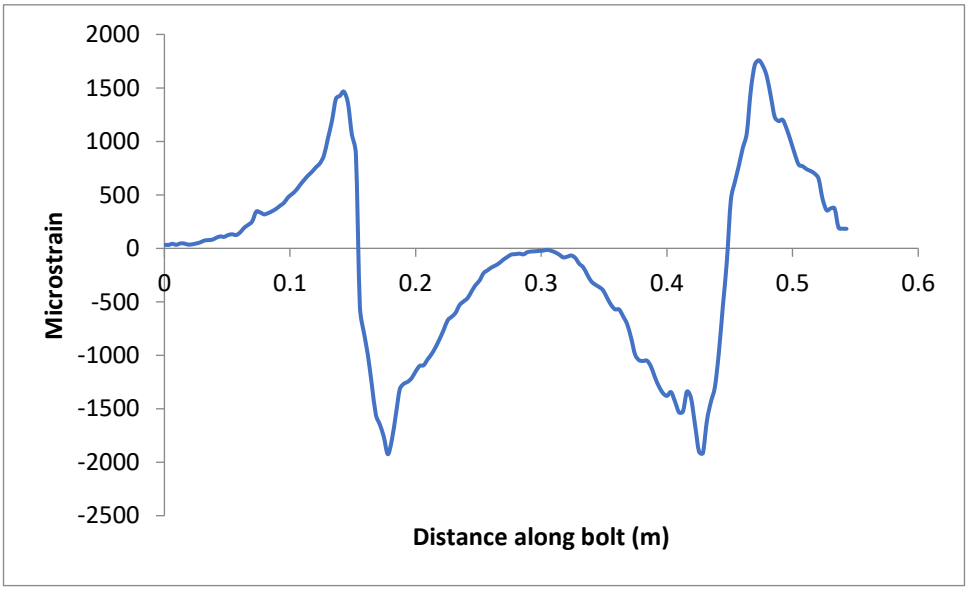

a)

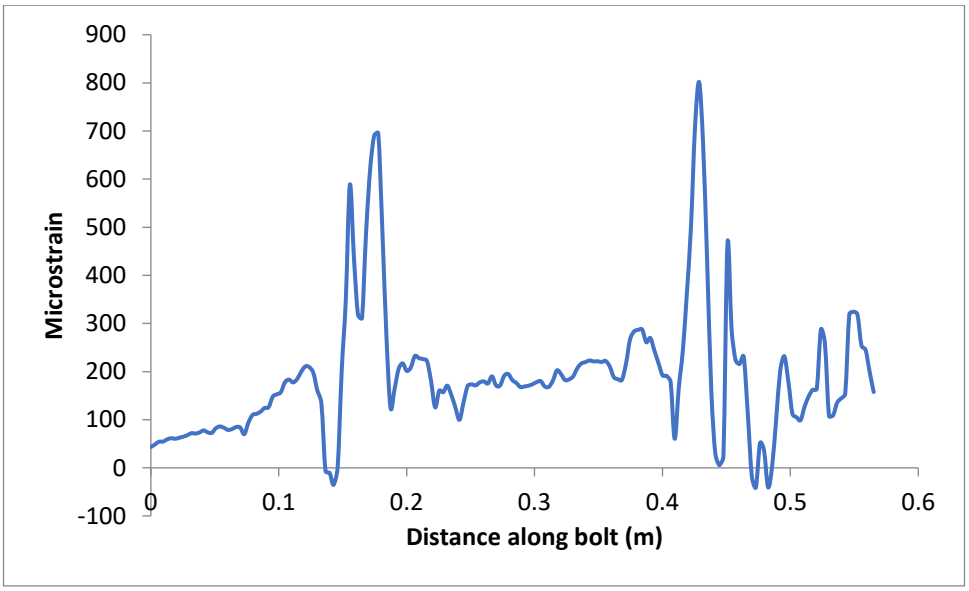

b)

Fig. A1 Strain plots Double shear test 1 a) Bending Strain b) Axial strain

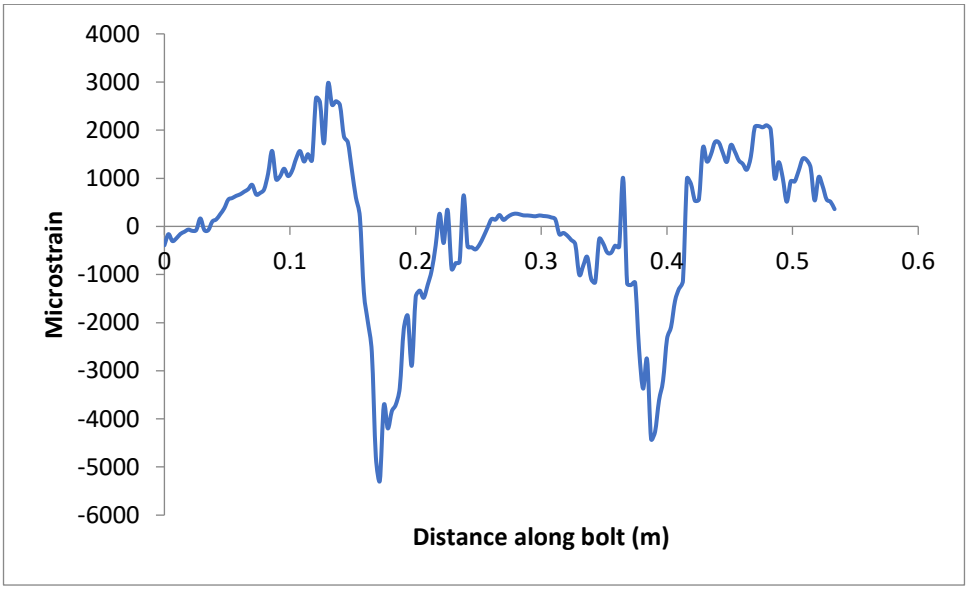

a)

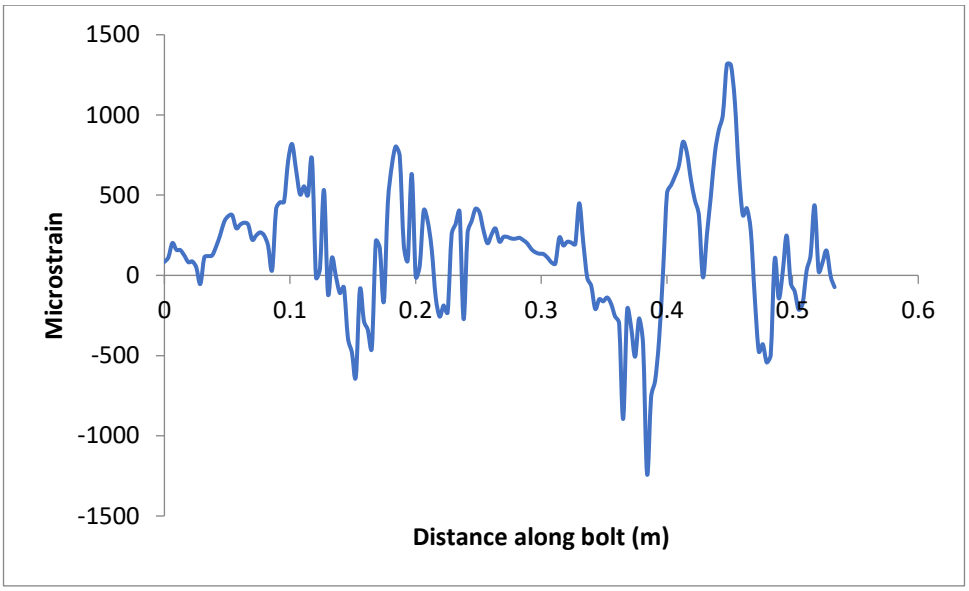

b)

Fig. A2 Strain plots Double shear test 2 a) Bending Strain b) Axial strain

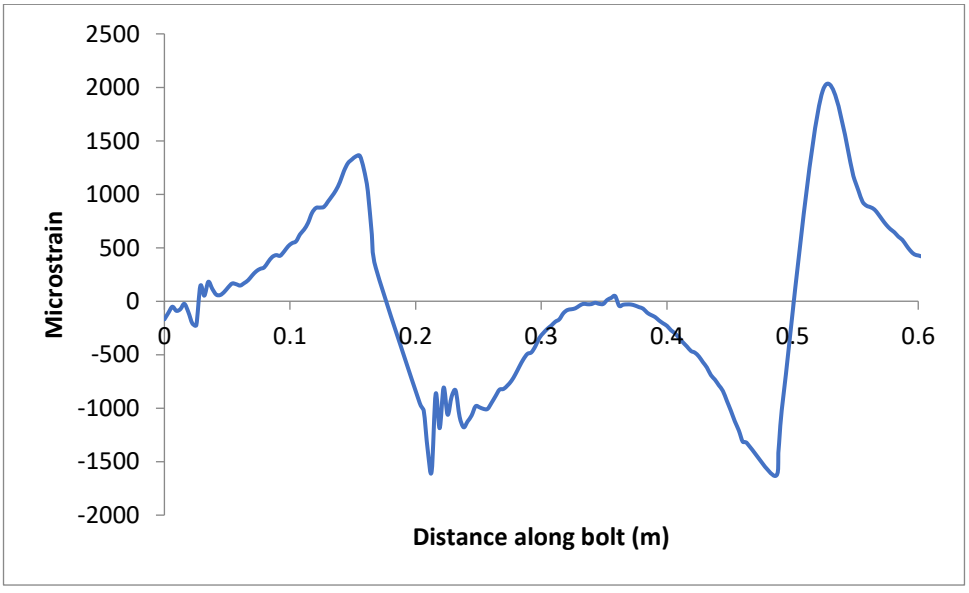

a)

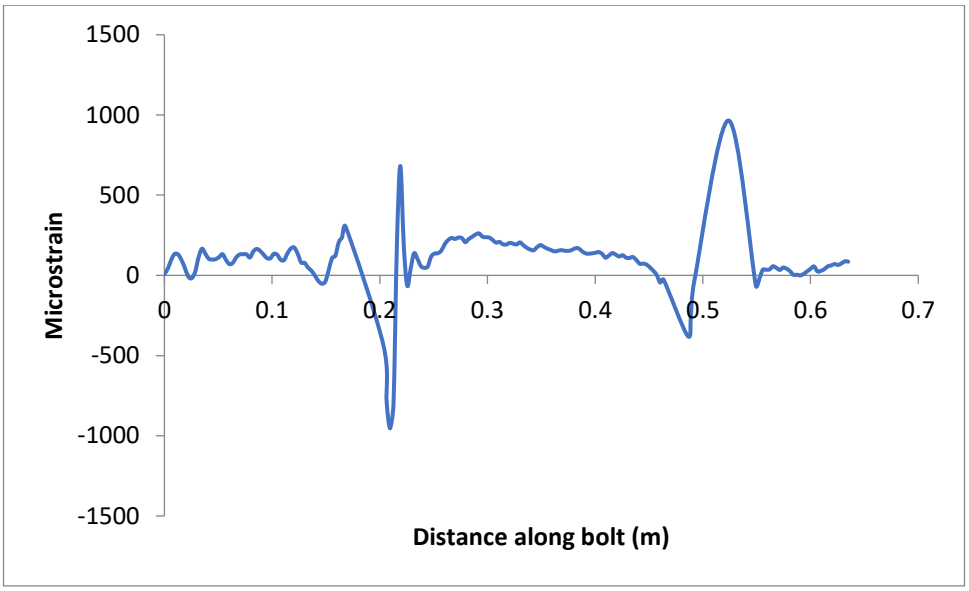

b)

Fig. A3 Strain plots Double shear test 3 a) Bending Strain b) Axial strain

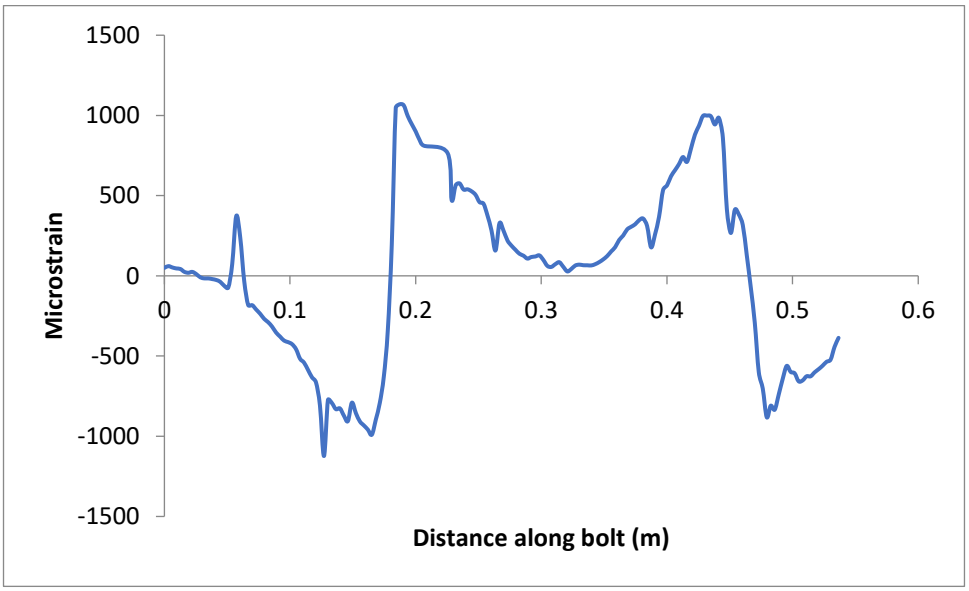

a)

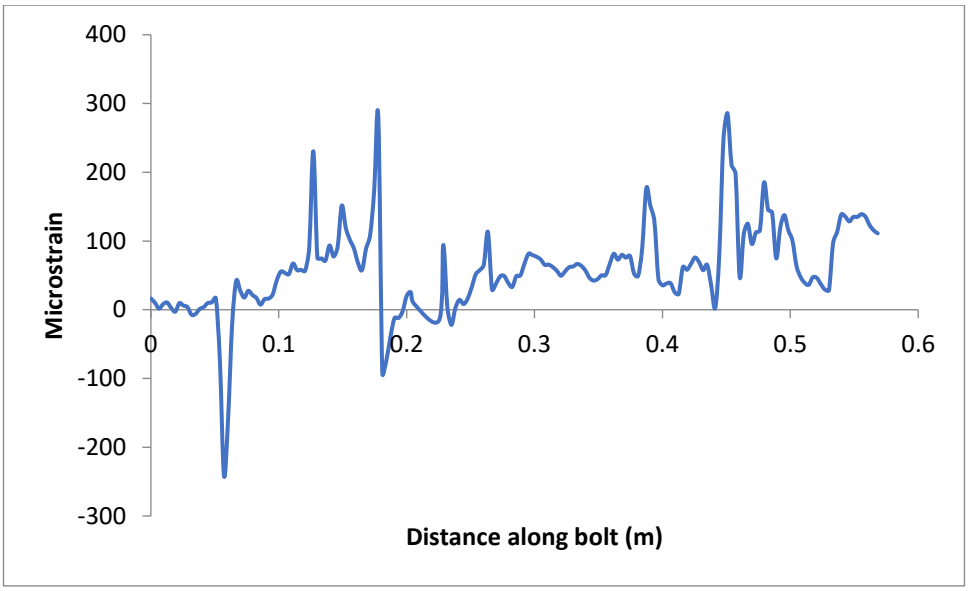

b)

Fig. A4 Strain plots Double shear test 4 a) Bending Strain b) Axial strain

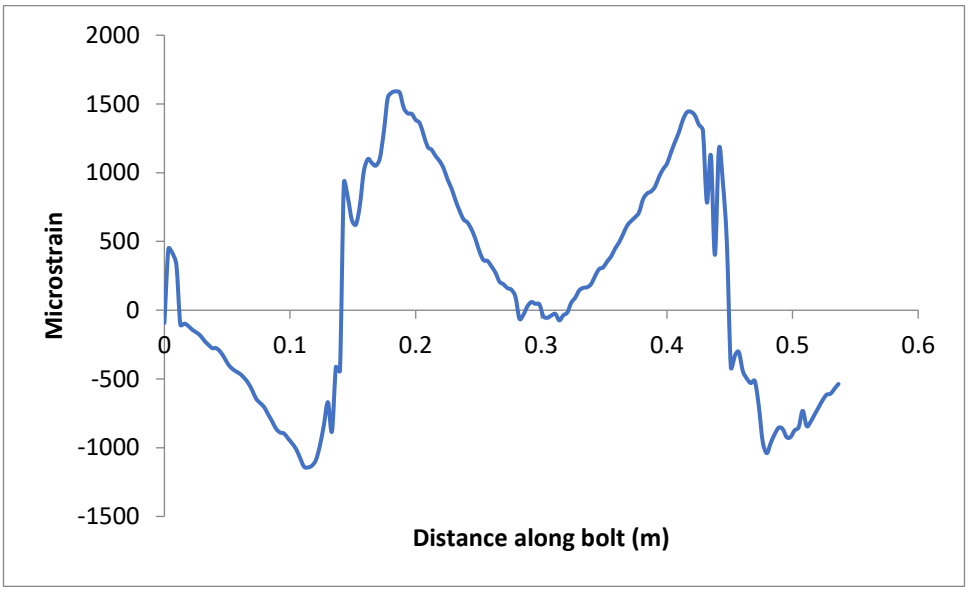

a)

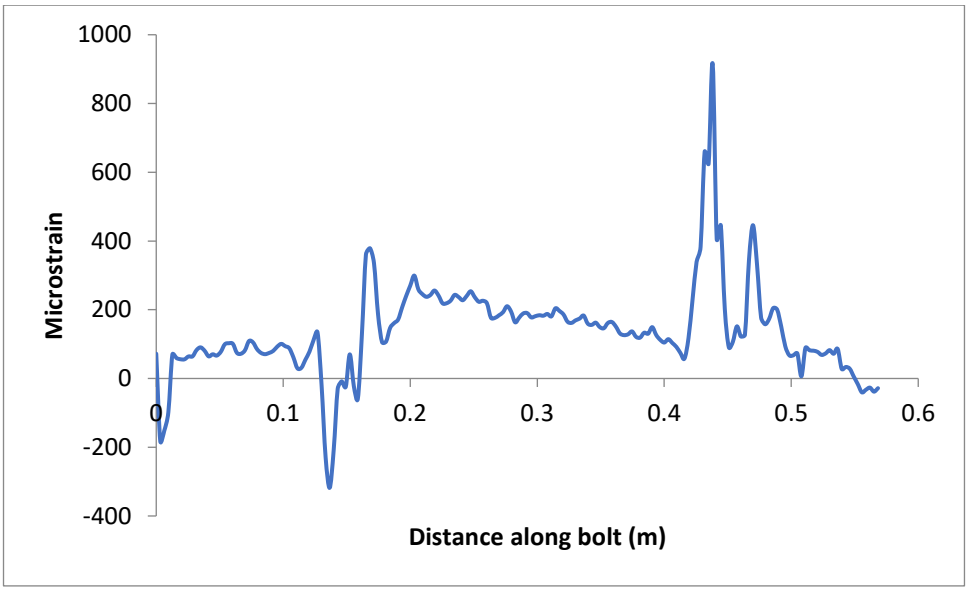

b)

Fig. A5 Strain plots Double shear test 5 a) Bending Strain b) Axial strain

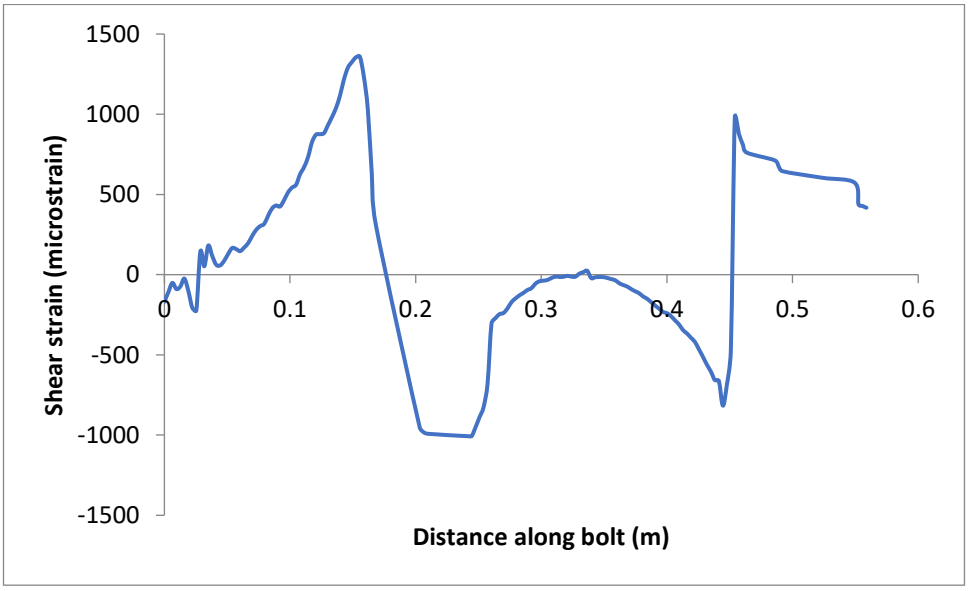

a)

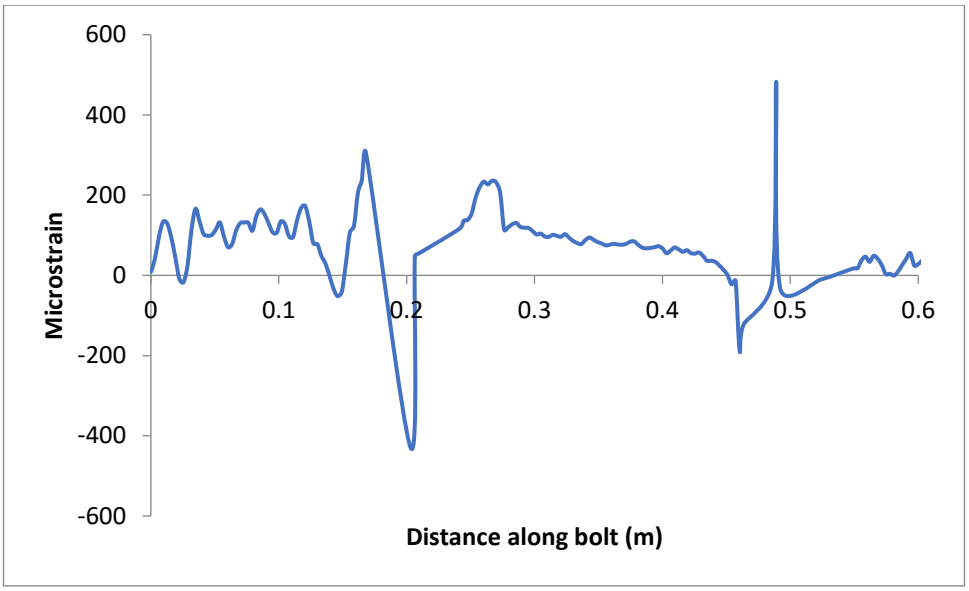

b)

Fig. A6 Strain plots Double shear test 6 a) Bending Strain b) Axial strain

Double shear test numerical model results –

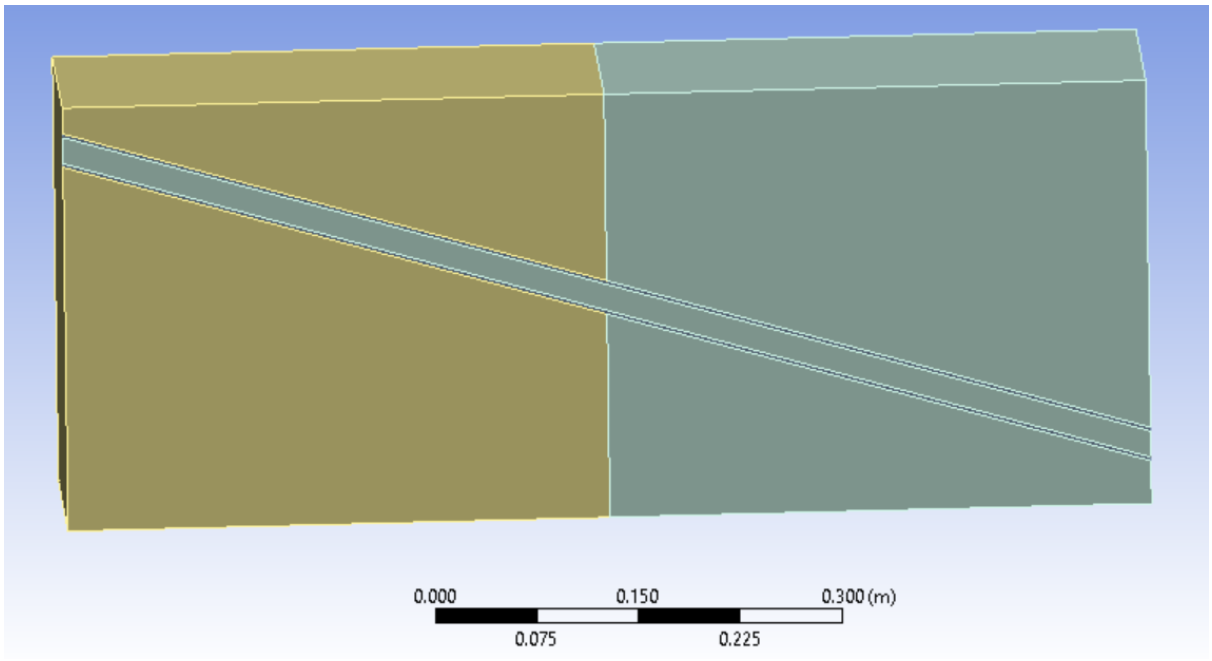

Fig. A7 Shear test model 60^0 bolt

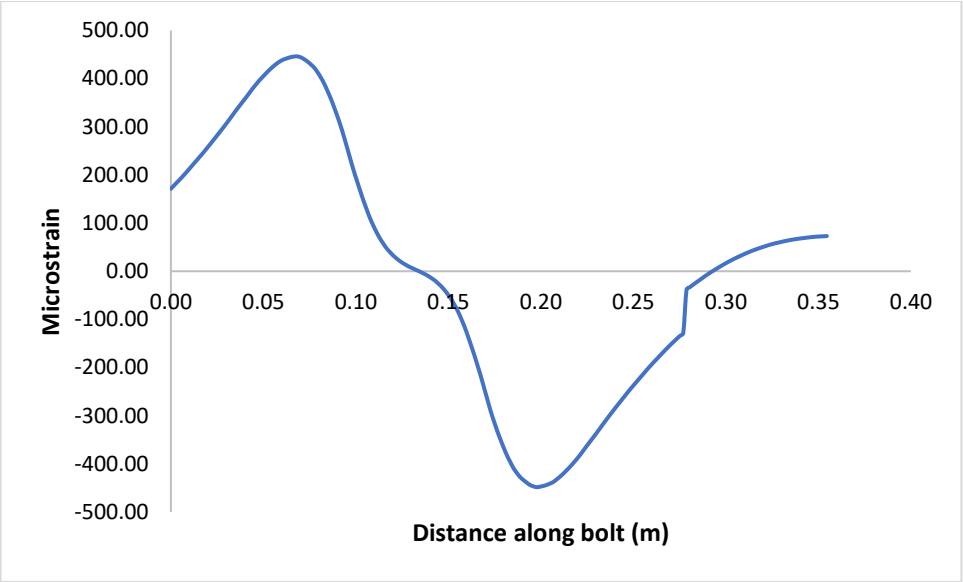

a)

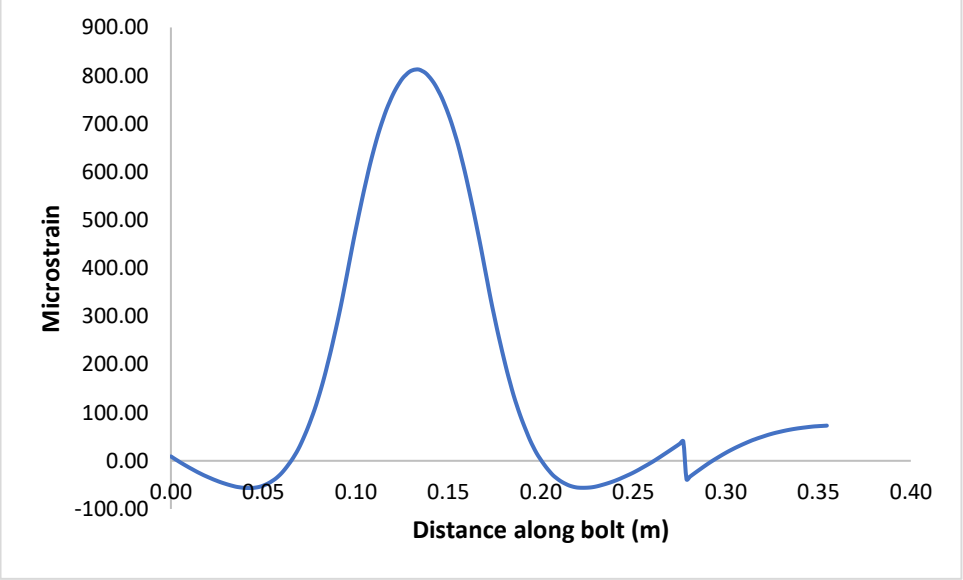

b)

Fig. A8 Strain plots 60^0 shear test model a) Bending Strain b) Axial strain

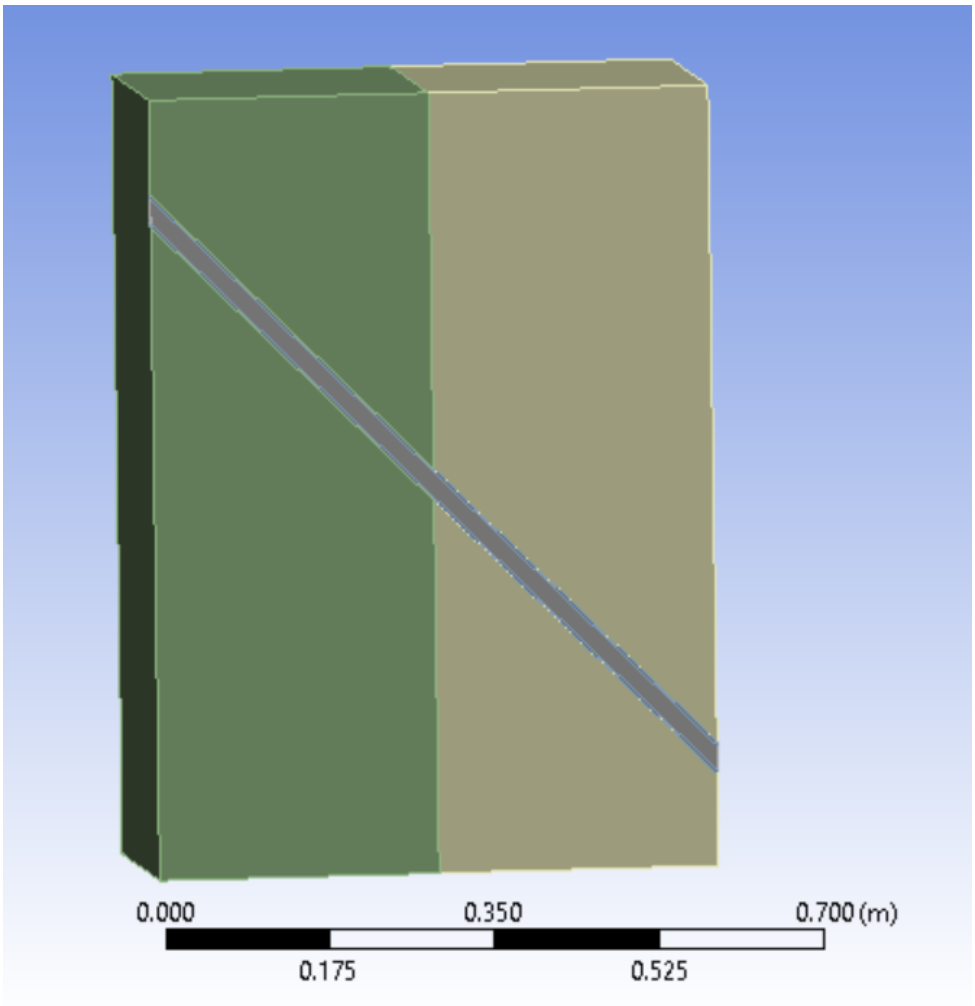

Fig. A9 Shear test model 45^0 bolt

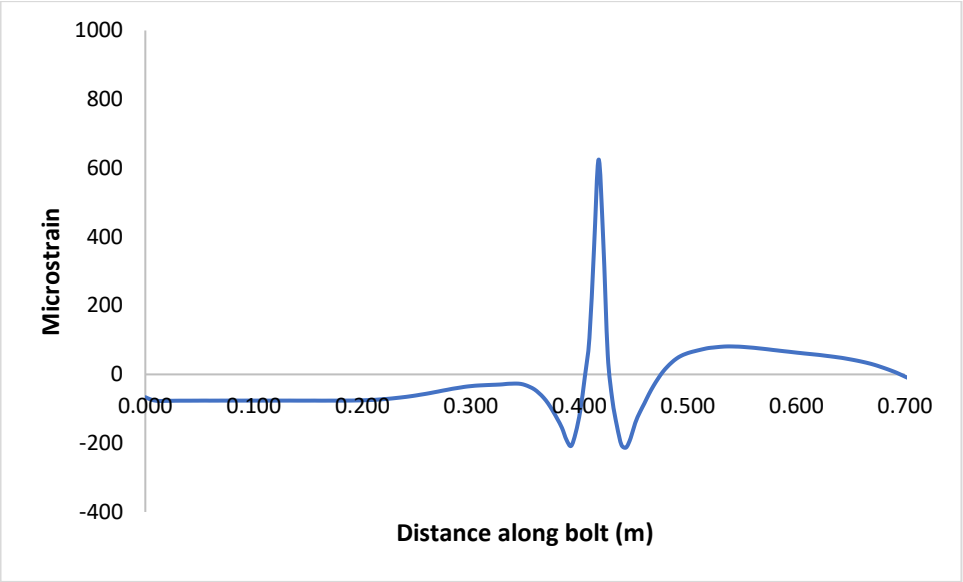

a)

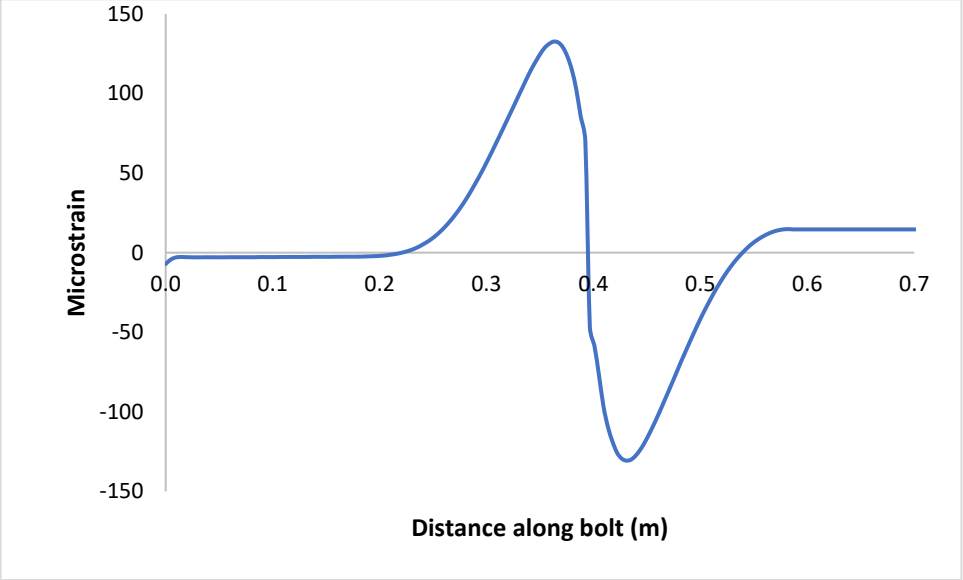

b)

Fig. A10 Strain plots 45^0 shear test model a) Bending Strain b) Axial strain

Instrumented rock bolt in-situ strain plots –

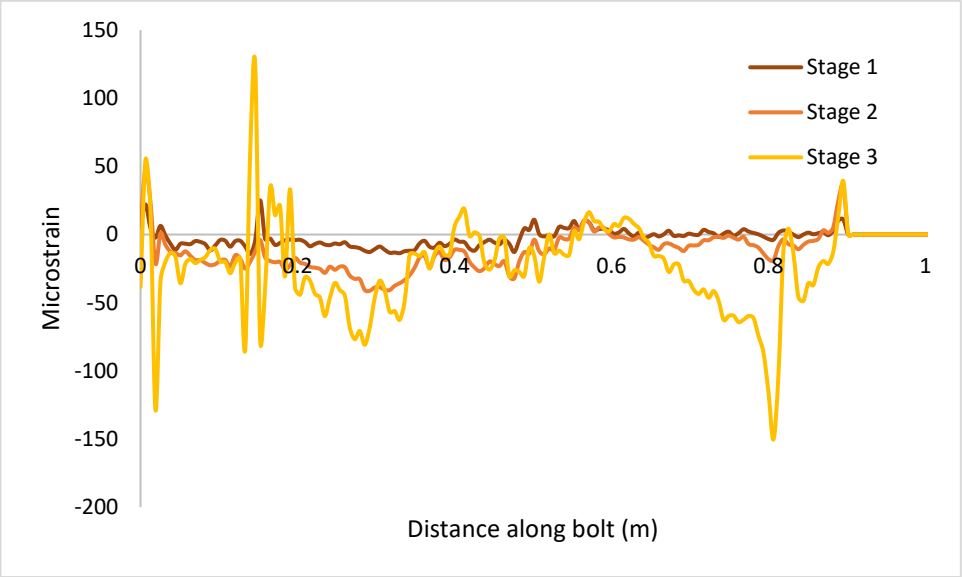

a)

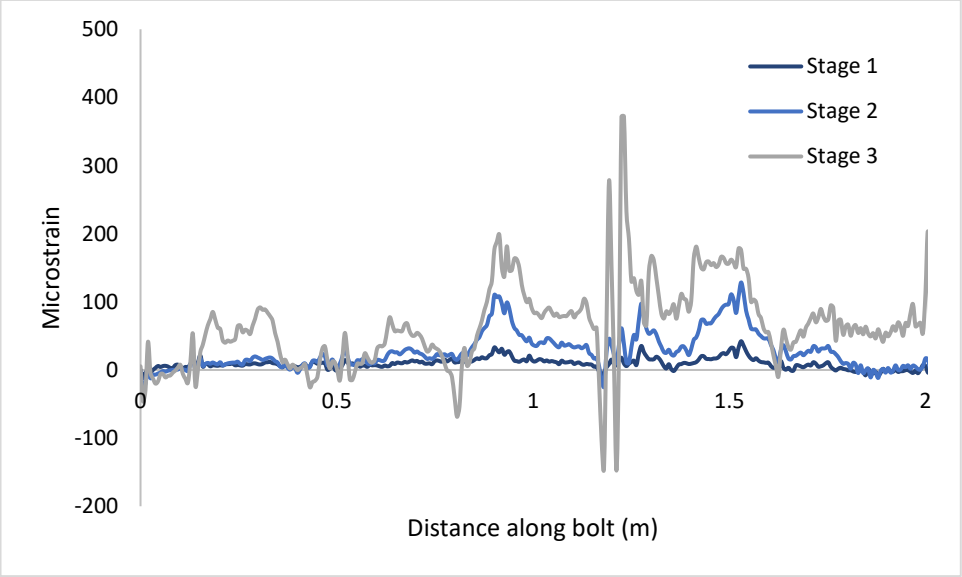

b)

Fig. A11 Bolt 4 in-situ strain a) Bending Strain b) Axial strain

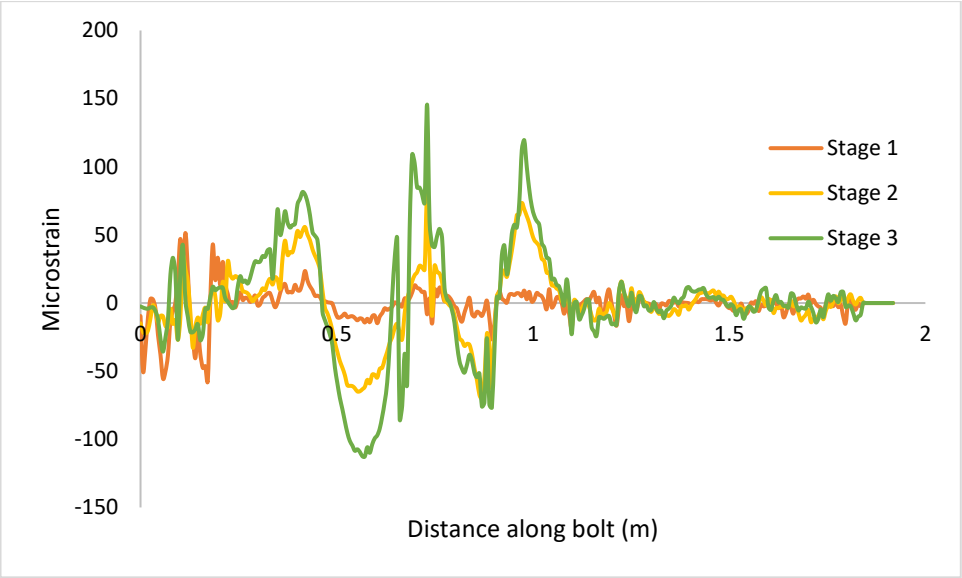

a)

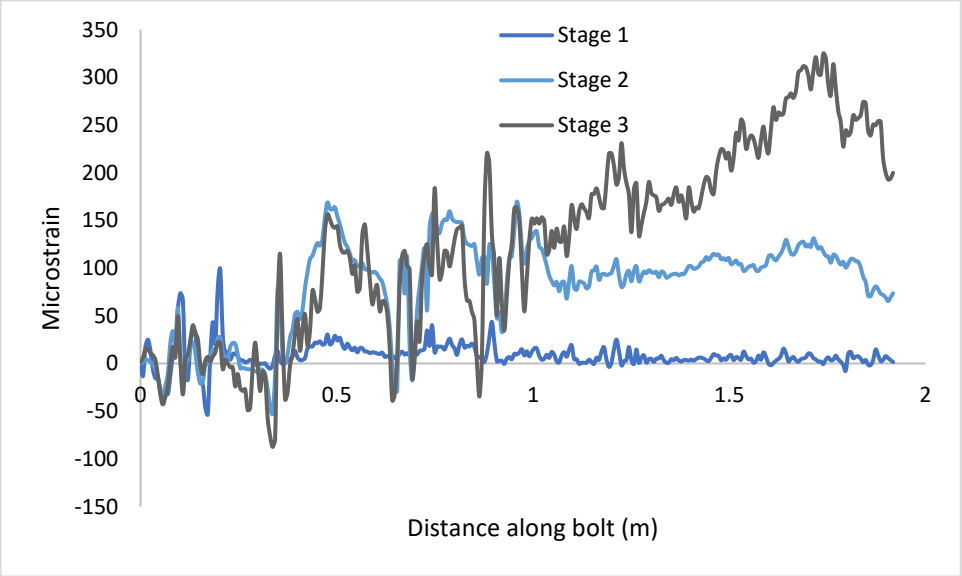

b)

Fig. A12 Bolt 12 in-situ strain a) Bending Strain b) Axial strain

References

Mark, C. Design of roof bolt systems. In: New Technology for Coal Mine Roof Support, Proceedings, NIOSH Open Industry Briefing; 2000;vol. 9453, p. 111-132.

Obert L, Duvall WI. Rock mechanics and the design of structures in rock. New York: Wiley; 1967.

Potvin Y. Empirical open stope design in Canada: University of British Columbia; 1988.

Esterhuizen GS. Extending empirical evidence through numerical modelling in rock engineering design. Journal of the Southern African Institute of Mining and Metallurgy. 2014;114:755-64.

Kostecki TR. Design Methods For Rock Bolts Using In-Situ Measurement From Underground Coal Mines [dissertation]. Carbondale, Southern Illinois: Southern Illinois University Carbondale; 2019.

Freeman T. The behaviour of fully-bonded rock bolts in the Kielder experimental tunnel. Tunnels & Tunnelling International. 1978;10(5).

Serbousek MO, Signer SP. Linear load-transfer mechanics of fully grouted roof bolts: US Department of the Interior, Bureau of Mines; 1987.

Signer SP. Field verification of load transfer mechanics of fully grouted roof bolts: Bureau of Mines, US Department of the Interior; 1990.

Signer S. Load behaviour of grouted bolts in sedimentary rock. New technology for coal mine roof support. In: Proceedings of the NIOSH open industry briefing, NIOSH IC 9453. 2000. p. 73–80.

Johnson JC. Brady T. Larson M. Langston R. and H Kirsten. Use of strain-gauged rock bolts to measure rock mass strain during drift development. The 37th U.S. Symposium on Rock Mechanics (USRMS), Vail, Colorado; 1999.

Signer SP, Cox D, Johnston J. A Method For The Selection Of Rock Support Based On Bolt Loading Measurements. Proceedings of the 16th International Conference on Ground Control in Mining, Morgantown: West Virginia University; 1997:183-190

Spearing A, Gadde M, Ray A, Reisterer J, Lee S. The initial performance of commonly used primary support on US coal mines. Proceedings, 30th International Conference on Ground Control in Mining; 2011.

Spearing AJS, Hyett AJ, Kostecki T, Gadde M. New technology for measuring the in situ performance of rock bolts. International Journal of Rock Mechanics and Mining Sciences. 2013;57:153-66.

Spearing A, Gadde M. Final report on NISOH funded project Improving underground safety by understanding the interaction between primary rock bolts and the immediate roof strata. NIOSH Project, BAA. 2011(2008-N):10989.

Hyett A, Forbes B, Spearing S. Enlightening bolts: using distributed optical sensing to measure the strain profile along fully grouted rock bolts. Proceedings of the 32nd international conference on ground control in mining; 2013.

Kostecki T, Spearing A, Forbes B, Hyett A. New instrumented method to measure the true loading profile along grouted rockbolts. SME transactions; 2015.

Vlachopoulos N, Forbes B, Cruz D. The Use of Distributed Fiber Optic Strain Sensing in Order to Conduct Quality Assurance and Quality Control for Ground Support. Proceedings of the 71st Annual Conference of the Canadian Geotechnical Society; 2018.

Jessu KV, Kostecki T, Spearing S. Measuring roof-bolt response to axial and shear stresses: Laboratory and first in-situ analyses. The CIM Journal. 2016;7(1):62-70.

Forbes B, Vlachopoulos N, Hyett AJ, Valsangkar A. The application of distributed optical strain sensing to measure the strain distribution of ground support members. FACETS. 2018;3(1):195-226.

Hoehn K, Spearing AJS, Jessu KV, Singh P, Pinazzi PC. The Design of Improved Optical Fibre Instrumented Rockbolts. Geotechnical and Geological Engineering. 2020;38(4):4349-59.

Pellet F, Egger P. Analytical model for the mechanical behaviour of bolted rock joints subjected to shearing. Rock mechanics and rock engineering. 1996;29(2):73-97.

Singh P, Spearing A. An Improved Analytical Model for the Elastic and Plastic Strain-hardening Shear Behaviour of Fully Grouted Rockbolts. Rock Mechanics and Rock Engineering. 2021:1-17.

Hyett A, Moosavi M, Bawden W. Load distribution along fully grouted bolts, with emphasis on cable bolt reinforcement. International Journal for Numerical and Analytical Methods in Geomechanics. 1996;20(7):517-44.

Li C, Stillborg B. Analytical models for rock bolts. International Journal of Rock Mechanics and Mining Sciences. 1999;36(8):1013-29.

Spang K, Egger P. Action of fully-grouted bolts in jointed rock and factors of influence. Rock Mechanics and Rock Engineering. 1990;23(3):201-29.

Ren FF, Yang ZJ, Chen JF, Chen WW. An analytical analysis of the full-range behaviour of grouted rockbolts based on a tri-linear bond-slip model. Construction and Building Materials. 2010;24(3):361-70.

Cai Y, Esaki T, Jiang Y. A rock bolt and rock mass interaction model. International Journal of Rock Mechanics and Mining Sciences. 2004;41(7):1055-67.

Ghadimi M, Shahriar K, Jalalifar H. A new analytical solution for the displacement of fully grouted rock bolt in rock joints and experimental and numerical verifications. Tunnelling and Underground Space Technology. 2015;50:143-51.

Ma S, Nemcik J, Aziz N. An analytical model of fully grouted rock bolts subjected to tensile load. Construction and Building Materials. 2013;49:519-26.

Jalalifar H, Aziz N. Analytical behaviour of bolt–joint intersection under lateral loading conditions. Rock mechanics and rock engineering. 2010;43(1):89-94.

Zhang W, Huang L, Juang CH. An analytical model for estimating the force and displacement of fully grouted rock bolts. Computers and Geotechnics. 2020;117:103222.

Spearing AJS, Hyett A. In situ monitoring of primary roofbolts at underground coal mines in the USA. Journal of the Southern African Institute of Mining and Metallurgy. 2014;114(10):791-800.

FLAC3D — Fast Lagrangian Analysis of Continua in Three-Dimensions. 6.0 ed. Minneapolis: Itasca: Itasca Consulting Group, Inc.; 2017.

Nemcik J, Ma S, Aziz N, Ren T, Geng X. Numerical modelling of failure propagation in fully grouted rock bolts subjected to tensile load. International Journal of Rock Mechanics and Mining Sciences. 2014;71:293-300.

Bin L, Taiyue Q, Wang Z, Longwei Y. Back analysis of grouted rock bolt pullout strength parameters from field tests. Tunnelling and Underground Space Technology. 2012;28:345-9.

Tulu I, Esterhuizen G, Heasley K. Calibration of FLAC3D to simulate the shear resistance of fully grouted rock bolts. 46th US Rock Mechanics/Geomechanics Symposium; 2012.

Bjurstrom S. Shear strength of hard rock joints reinforced by grouted untensioned bolts. Proc 3rd Cong ISRM, Denver. 1974;2:1194-9.

Haas CJ. Analysis of rock bolting to prevent shear movement in fractured ground. Min Eng (Littleton, Colo); (United States). 1981: 698-704.

Dight PM. Improvements to the Stability of Rock Walls in Open Pit Mines [dissertation]. Melbourne (VIC): Monash University; 1983.

Grasselli G. 3D behaviour of bolted rock joints: Experimental and numerical study. International Journal of Rock Mechanics and Mining Sciences. 2005;42(1):13-24.

Haas CJ. Shear resistance of rock bolts. Trans Soc Min Eng AIME. 1976;260(1).

Li X, Nemcik J, Mirzaghorbanali A, Aziz N, Rasekh H. Analytical model of shear behaviour of a fully grouted cable bolt subjected to shearing. International Journal of Rock Mechanics and Mining Sciences. 2015;80:31-9.

Lin H, Xiong Z, Liu T, Cao R, Cao P. Numerical simulations of the effect of bolt inclination on the shear strength of rock joints. International Journal of Rock Mechanics and Mining Sciences. 2014;66:49-56.

Ma S, Zhao Z, Shang J. An analytical model for shear behaviour of bolted rock joints. International Journal of Rock Mechanics and Mining Sciences. 2019;121:104019.

Ansys® Academic Research Mechanical, Release 2021 R2.

Bandis S, Lumsden A, Barton N. Fundamentals of rock joint deformation. International Journal of Rock Mechanics and Mining Sciences & Geomechanics Abstracts. 1983;20(6):248-268.

Hoek E, Kaiser PK, Bawden WF. Support of underground excavations in hard rock. 4th ed. Rotterdam (Netherlands): A.A. Balkema Publishers; 1995;232

Sitharam T, Maji V, Verma A. Practical equivalent continuum model for simulation of jointed rock mass using FLAC3D. International Journal of Geomechanics. 2007;7(5):389-95.

Chapter 7. Discussion and Conclusion

7.1 Discussion

Rock bolt reinforcement design in an underground mine should take into consideration the in-situ stresses, rock mass properties, effect of nearby excavations, local and major discontinuities, shape and size of excavation, useful life of excavation etc. These parameters control the deformation of rock mass around an excavation and determine the loading on the rock bolt. In addition to understanding the rock mass load demand, the rock bolt's response to the loading is an important factor to be considered. Empirical methods do not adequately address all the parameters affecting excavation stability. These methods also only account for the axial load demand on the rock bolt. Numerical modelling of rock bolt reinforcement design has become popular in recent years to overcome these shortcomings. The work in this thesis aimed to improve the numerical modelling of rock bolt reinforcement by understanding the rock bolt behaviour under lateral loads and provide a procedure for implementing it in numerical models.

In the presence of a discontinuity in the rock mass such as a joint or a bedding plane, the rock bolt would be subjected to a combination of axial and shear load Figure 7.1. In such a condition it becomes important to design the rock bolt reinforcement for both axial and shear loads. Using empirical approaches to design rock bolt reinforcement based on only axial loading would lead to unsafe design. The work done in this thesis aims to gain a better understanding of rock bolt behaviour and improve the numerical modelling of rock bolt using instrumentation. The thesis objective was to use instrumented rock bolts to improve the numerical modelling of rock bolts by:

- Analysing the effect of combined axial and lateral loading on rock bolt reinforcement and understanding the actual rock bolt response under lateral loading.
- Improve the analytical model for rock bolt response under lateral loading.
- Use instrumented rock bolts to improve the numerical modelling of rock bolt reinforcement under lateral loads in-situ.

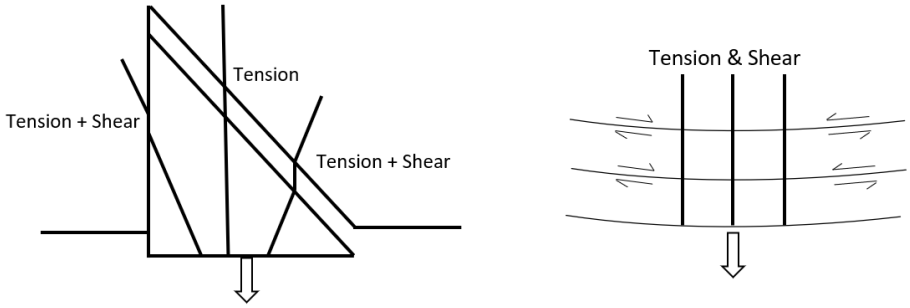

Figure 7.1 - Effect of discontinuity on rock bolt loading.

Current methods of rock bolt reinforcement design calculate only the axial load demand on rock bolts. As such the required load capacity of the rock bolt only takes into account the axial strain on the rock bolt. A discontinuity in the rock mass would subject the rock bolt to a lateral load in addition to the axial load the ultimate axial load that the rock bolt is able to withstand decreases. This decrease in the ultimate capacity of the rock bolt would result in a reduction in the designed safety factor of the rock bolt reinforcement. To analyse the effect of combined axial and shear loading on rock bolt physical and numerical modelling of an excavation with laminated roof was undertaken.

Laboratory tests on a physical model of excavation with a laminated roof showed that there is inter-bed shear displacement which would subject the rock bolts to a combined axial and shear loading. The magnitude of the shear displacement at a location in the roof depends on the factors like roof vertical displacement, bed thickness, height above the roof surface and distance from the centre of the roof. The effect of these parameters on shear displacement were analysed and are shown in Figure 7.2 and Figure 7.3.

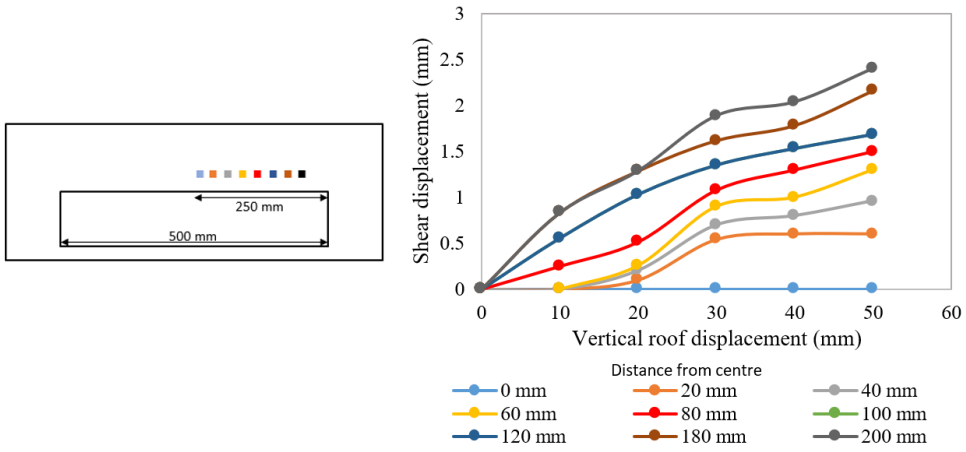

Figure 7.2 - a) Plot lines position in model b) Shear Displacement (12 mm above roof) vs vertical displacement of roof.

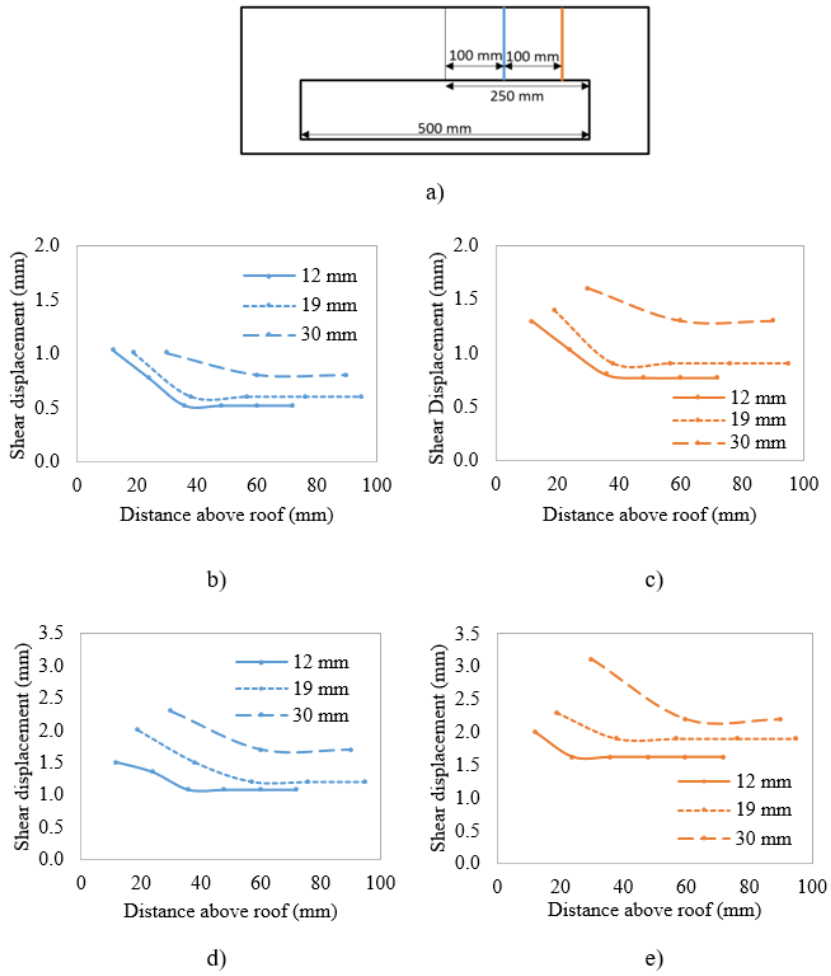

Figure 7.3 - a) Location of Plot lines in the model. Comparison of shear displacement in beds with different thicknesses at b) 100 mm line at 2 cm roof vertical displacement c) 200 mm line at 2 cm roof vertical displacement d) 100 mm line at 3 cm roof vertical displacement.

Numerical modelling was used to analyse the effect of combined loading on rock bolt. Rock bolt reinforcement design with only axial load demand of rock to design rock bolt reinforcement can lead to overestimation of rock bolt reinforcement of the designed safety factor in ground conditions where the rock bolt is subjected to combined axial and shear loads. Numerical modelling of suspension and beam building design methodologies considering only a single model of loading was shown to result in a reduction of safety factor from 3.5 to 2.0 and 2.0 to 1.36 respectively in each case. The results show a significant reduction in the rock reinforcement capacity of rock bolt under combined loading. Numerical models can be used to determine the magnitude of axial and shear load on the rock bolt.

Numerical modelling can be used to simulate the complex geological conditions in-situ for analysing the rock load demand on the rock bolt reinforcement. However, current numerical models are not capable of simulating the true behaviour of rock bolts under those exhibited in situ. The numerical models implement rock bolts as simplified elements whose load-deformation behaviour is calculated using an analytical model. Strain and load data from instrumented rock bolt double shear lab tests was used to calibrate numerical model and analyse the rock bolt behaviour. The magnitude of shear loading on a rock bolt installed across a discontinuity was found to vary with the strength of the host material. A parametric study using numerical modelling of the double shear test showed increasing shear load in higher strength concrete while the bending moment at hinge point remained almost the same. This behaviour was attributed to the change in the location of a hinge point in different strength concretes. The shear load Q, bending moment M and hinge point length L are related by the following equation –

$$M = \frac{QL}{2} \tag{7.1}$$

As the hinge point location decreases with an increase in the concrete strength the shear load on the rock bolt increases while the bending moment remained constant as shown in Figure 7.4 and Figure 7.5.

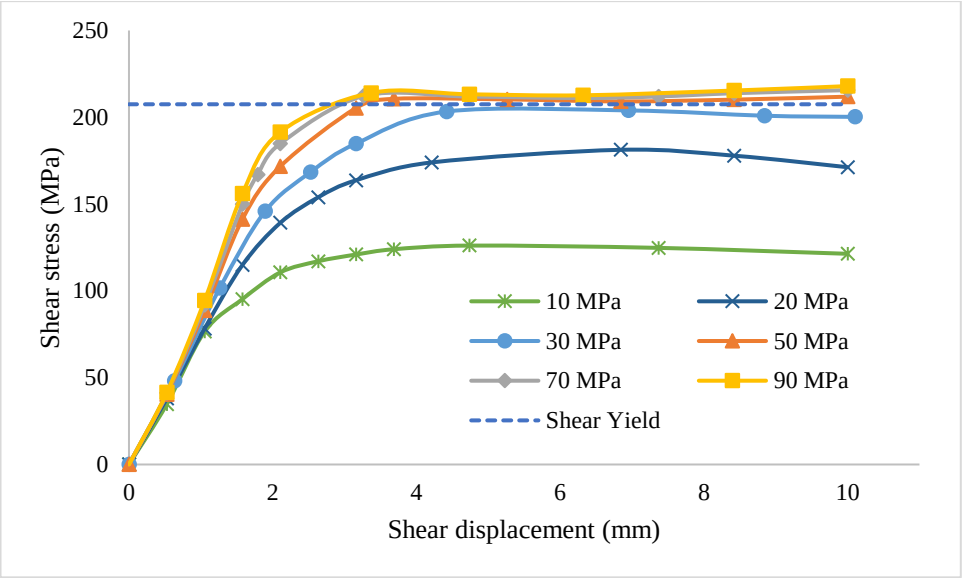

a)

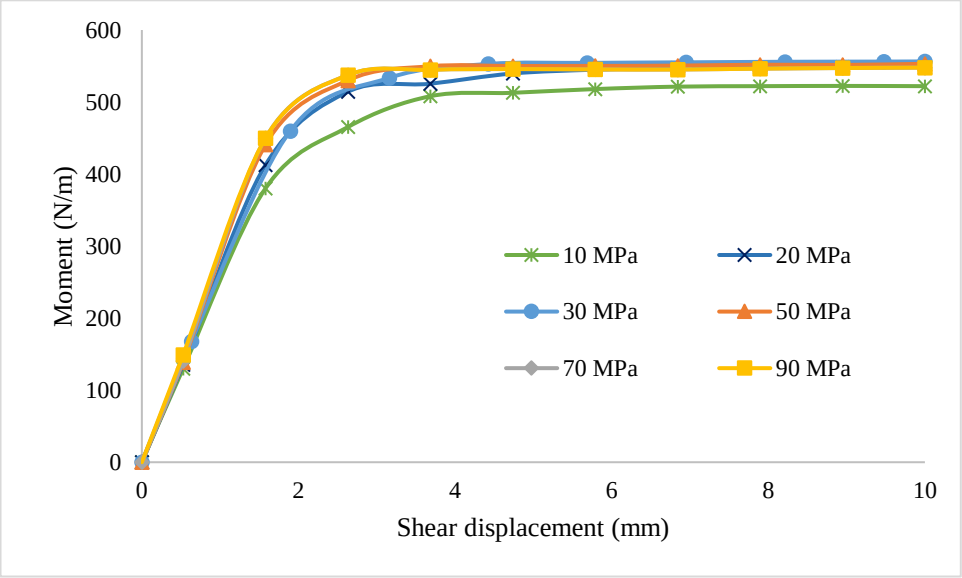

b)

Figure 7.4 – a) Shear stress in the rock bolt for different concrete strengths. b) Bending moment in the rock bolt for different concrete strengths.

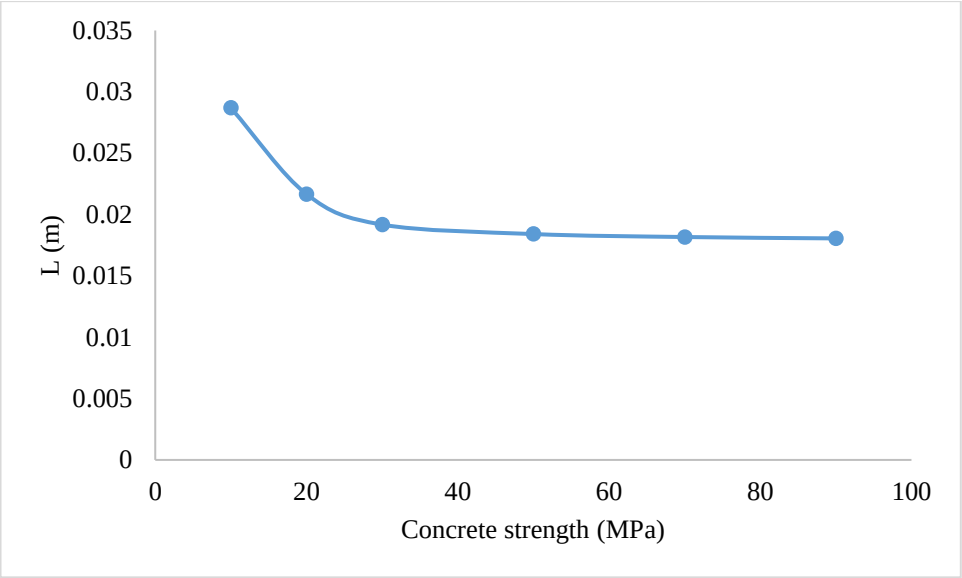

Figure 7.5 -Change in hinge point location at different concrete strengths.

Comparison of the results of the numerical model to the predictions of the analytical model showed that the shear load on the rock bolt was being underestimated in the analytical model. The analytical model was underestimating the shear loads in the post yield-state of the rock bolt. It was proposed that the analytical model underestimated the shear force because the rock bolt was assumed to undergo perfectly plastic bending after the yield stage. This assumption results in the rock bolt model behaving like a truss at the hinge point after yield point. Any further bending deformation happens without any resistance and therefore without any increase in shear load on the rock bolt resulting in underestimation of shear load on rock bolt. The shear force predicted by an analytical model was found to be underestimated by almost 50% compared to the numerical modelling results of the double shear test (Figure 7.5). As the analytical model underestimates the shear load on the rock bolt it will predict a stiffer load-displacement response of the rock bolt under lateral loads. The model will also predict a higher failure load for the rock bolt. Similar results were found when simulating double shear tests with the pile element in FLAC3D.

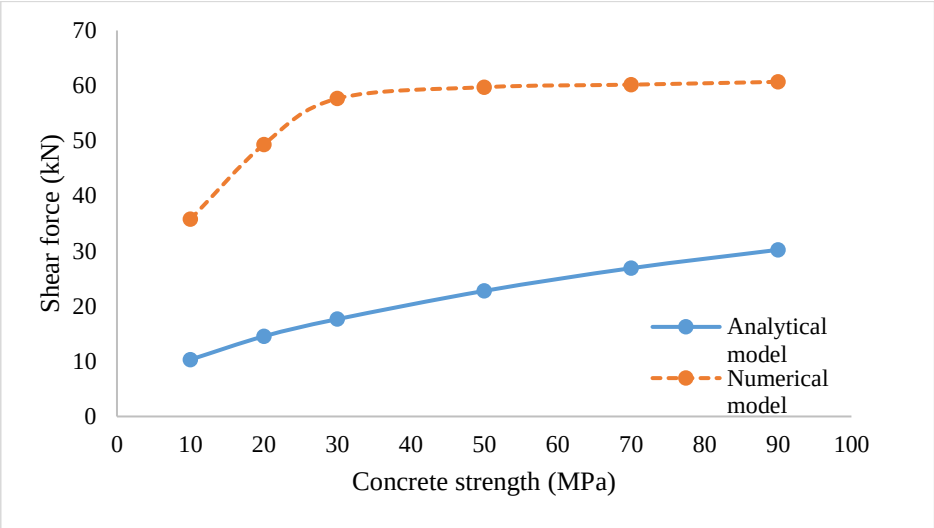

Figure 7.6 - Shear force in rock bolt analytical vs. numerical model.

The FLAC3D pile element used for modelling rock bolts in underground excavation support modelling was modified to estimate the correct response of the rock bolt under shear loading by changing the properties of the normal spring which govern its lateral loading behaviour. The un-modified pile element overestimated the failure load in a numerical model of laboratory shear test by 25% compared to the test results while the pile with modified normal spring behaviour predicted the correct failure load. The modified pile element is capable of correctly estimating the load-displacement response and the failure load of the rock bolt.

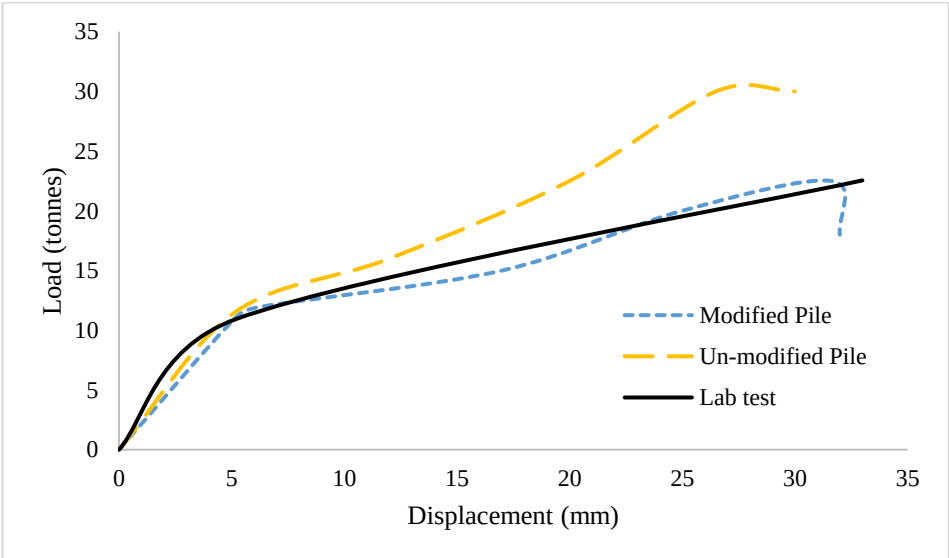

Figure 7.7 - Comparison of shear response of modified pile with laboratory test data.

Structural element models like the pile element in FLAC3D are based on analytical models which describe their load-displacement response. An analytical model capable of accurately predicting the rock bolt response can help in developing better numerical models for rock bolts. Rock bolts exhibit strain-hardening after the yield-stage. This behaviour of post-yield strain hardening is not considered in current analytical models. Load-deformation behaviour of rock bolt under lateral loading was derived using the virtual force method and the equations describing the state of shear load and bending moment along the length of the rock bolt. The existing analytical model for lateral loading response of rock bolt was improved by incorporating the post-yield strain hardening behaviour of steel. The post-yield strain hardening behaviour of steel was included into the model using the concept of reduced bending modulus. A reduced elastic modulus E_r was calculated for the yielding section of the rock bolt using the equation –

$$E_r = \frac{256}{\pi D_b \Delta^3} \int_{\varepsilon_2}^{\varepsilon_1} \sigma\varepsilon \sqrt{\frac{D_b^2}{4} - \frac{D_b^2 \varepsilon^2}{\Delta^2}} d\varepsilon \qquad (7.2)$$

Where, D_b is the diameter of a bolt, Δ is the sum of the absolute values of maximum elongation and contraction strain on the bolt ε_1 and ε_2 respectively, σ is the stress calculated from the stress-strain plot of steel. Comparison with laboratory shear tests showed that with post-yield strain hardening behaviour the model was able to estimate correct rock bolt behaviour while Pellet and Egger (1996) analytical model predicted the failure load to be twice the failure load in laboratory test (Figure 7.8). This result is identical to the earlier findings where the existing analytical models were shown to underestimate the shear load on the rock bolt and predict a higher failure load compared to actual rock bolt behaviour in laboratory testing.

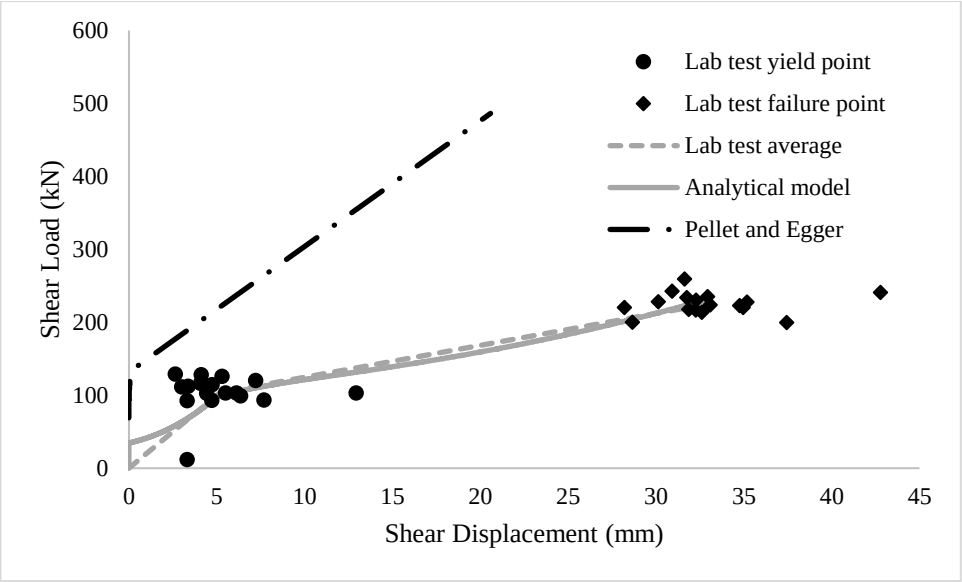

Figure 7.8 - Shear lab test vs analytical model with strain hardening.

A parametric study using the analytical model showed that the post-yield strain hardening effect on rock bolt shear response depends on the rock bolt and host material properties. Larger diameter rock bolts showed a greater strain-hardening effect than smaller diameter rock bolts. The thicker rock bolts can undergo a considerable amount of bending before the inner fibres in the bolt start yielding. The strength of the host material also influences the post-yield behaviour of rock bolts. The change in ultimate shear displacement of rock bolt due to strain-hardening was 10-20% higher in higher strength host media compared to ultimate shear displacement in lower strength host media. This effect of host media strength on shear response of rock bolt matches with the findings discussed above. The results demonstrate that the new analytical model is capable of taking into account the effect of host media strength on the rock bolt behaviour under lateral loading. Analytical models capable of accurately describing the rock bolt response can also be used to analyse the loads and deformation of a rock bolt using strain plots obtained from in-situ instrumentation data.

Numerical models need to be calibrated or validated before they can be used for quantitative analysis of the rock bolt reinforcement system. Current practice is to use visual inspection, in-situ stress measurements, pull tests such as short encapsulation tests and measurements from geotechnical monitoring devices like extensometers to calibrate the rock deformation in the

model. The axial behaviour of the rock bolt can be calibrated using in-situ pull test data. The shear behaviour of a rock bolt is calibrated using laboratory shear tests which do not replicate the actual in-situ conditions. The models need to be calibrated using actual in-situ measurements in order to use the numerical model for optimizing the rock bolt reinforcement design. The strain data from instrumented rock bolts was used to detect the location of discontinuity along the rock bolt length. The orientation of the identified discontinuity with respect to the rock bolt was calculated from the axial strain, bending strain and hinge point location obtained from the instrumented rock bolt strain profile.

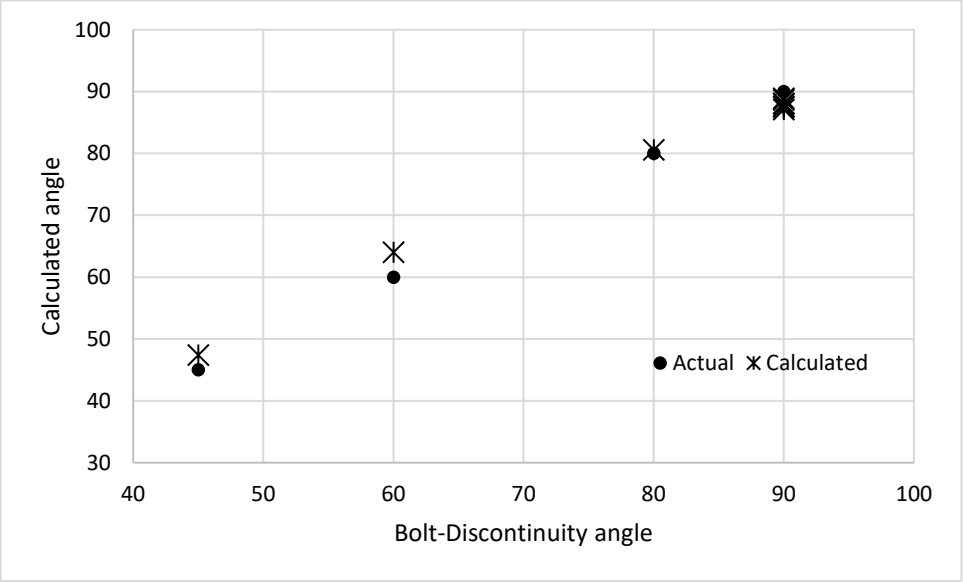

Figure 7.9 - Calculated discontinuity orientation w.r.t rock bolt compared to actual orientation.

Shear-load displacement plot for a rock bolt installed in-situ was calculated from the axial and bending strain plots obtained from the instrumented rock bolts Figure 10. The shear load on the rock bolt was calculated using the bending strain plot. The axial load was calculated from the axial strain plot. The shear displacement was calculated from the shear load using the constitutive equations described in the analytical model for lateral loading of the rock bolt. FLAC3D software was used to model the underground excavation and calibrate the model using the load-displacement plot. FLAC3D software was chosen for the numerical modelling

rather than a discontinuum modelling software like UDEC as the scope of study was limited to understanding and verifying the effect of single joint on rock bolt. In such a condition FLAC3D was sufficient as only single discontinuity was needed to be modelled. Majority of past research works on modelling rock bolt have been done using FLAC3D software. The work done in this thesis builds upon and improves on these past research works.

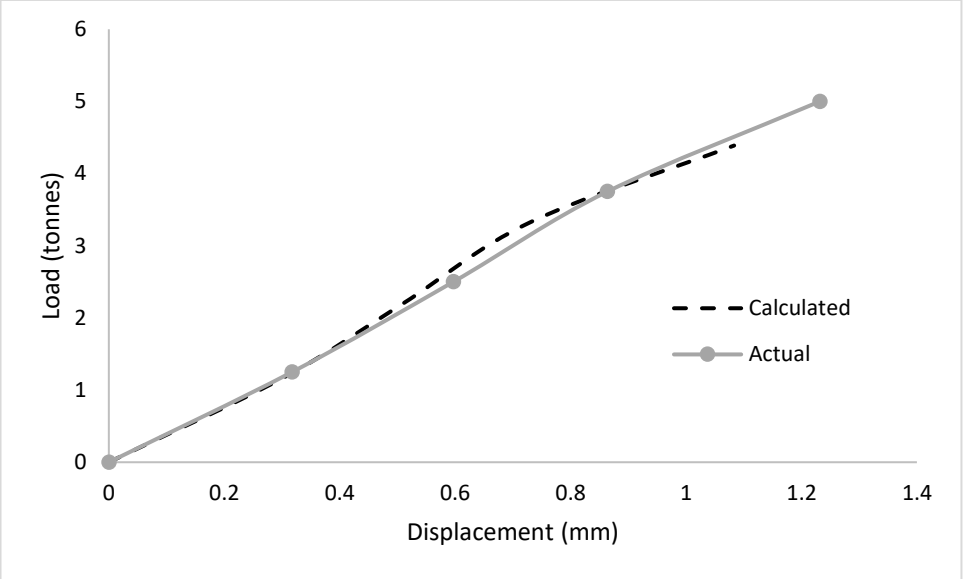

Figure 7.10 - Shear Load vs Displacement plot: Actual vs Calculated.

7.2 Conclusions

Based on the research undertaken and the discussion of the results in the previous section the following conclusions can be made:

- Rock reinforcement design with the required rock bolt capacity calculated for only axial load demand of the rock will lead to an under designed ground reinforcement due to the reduction of the total capacity of the rock bolt when subjected to shear loads in-situ. The safety factor of the designed reinforcement for the particular case considered in the physical and numerical modelling study showed a decrease of 35-40% compared to the designed values.
- Current analytical and numerical model for lateral loading do not represent the true behaviour of fully grouted rock bolt. The models underestimated the shear load on the

rock bolt due to the assumption of perfectly plastic deformation of rock bolt after yield point. In case of shear tests analysed in the study the models estimated the failure load of the rock bolt to be 25% higher than the laboratory results. The models were also not capable of capturing the true load-deformation response of the rock bolt. Using the models in reinforcement design can lead to overestimation of the rock bolt capacity and unsafe rock reinforcement. It is recommended to modify the rock bolt models available in numerical modelling software like the pile element in FLAC3D to simulate the actual rock bolt behaviour. Comparison with laboratory shear tests showed that by modifying the properties of the interface links of the pile element it can simulate the correct constitutive and failure behaviour of rock bolt under lateral loading.

- The effect post-yield strain hardening of the rock bolt under lateral load was analysed in this work. An analytical model was proposed to incorporate the effect of strain-hardening. Modelling the rock bolt without strain-hardening estimated 25% higher displacements at failure loads. The model can be used in evaluating the reinforcement system where the lateral loading of rock bolt has progressed beyond the yield stage. The model can predict the post-yield behaviour of the rock bolt accurately which is critical as the shear yield load of rock bolt is generally between 50-60% of the axial yield load.
- In-situ optical instrumented rock bolts provide high resolution strain data capable of capturing localised lateral loading caused due to discontinuities in the rock mass. The processed using the analytical model for lateral loading of rock bolt can provide accurate information about the location and orientation of local discontinuities causing shear load on the rock bolt. This information is useful for generating accurate local discontinuities in in-situ numerical models.
- Calibrating a numerical model with in-situ measurement is very important in order to produce quantifiable predictions for use in reinforcement design. The strain data from the instrumented rock bolts can be processed to obtain the lateral load-deformation

plot for a rock bolt. The plot can be used for calibrating the rock bolt response in an in-situ numerical model.

Procedure for using instrumented rock bolts for calibrating in-situ numerical models and optimizing rock bolt reinforcement in underground excavations.

The rock bolt reinforcement design process starts with choosing an appropriate numerical modelling method depending on the type of loading expected on the rock bolt. The next step is acquiring the data required for creating the model such as excavation dimensions, in-situ stress conditions, material properties and geological discontinuities. The model is then calibrated with in-situ measurements and the rock bolt reinforcement optimized for the required safety factor. A step-by-step procedure of the rock bolt reinforcement design process using Numerical modelling is shown in Figure 7.11.

The process of numerical modelling starts with identifying the major loading modes that the rock bolt will be subjected to in-situ. The rock bolt strain data from in-situ instrumented rock bolts can be analysed to identify localised shear loading such as caused by a discontinuity. If shear loading is identified, then the next step is to identify the location and orientation of the discontinuity causing the shear loading. The location of discontinuity can be estimated by locating the point on the rock bolt where the discontinuity intersects the rock bolt. Figure 7.12 shows the strain plot of an instrumented rock bolt with localised loading due to a discontinuity.

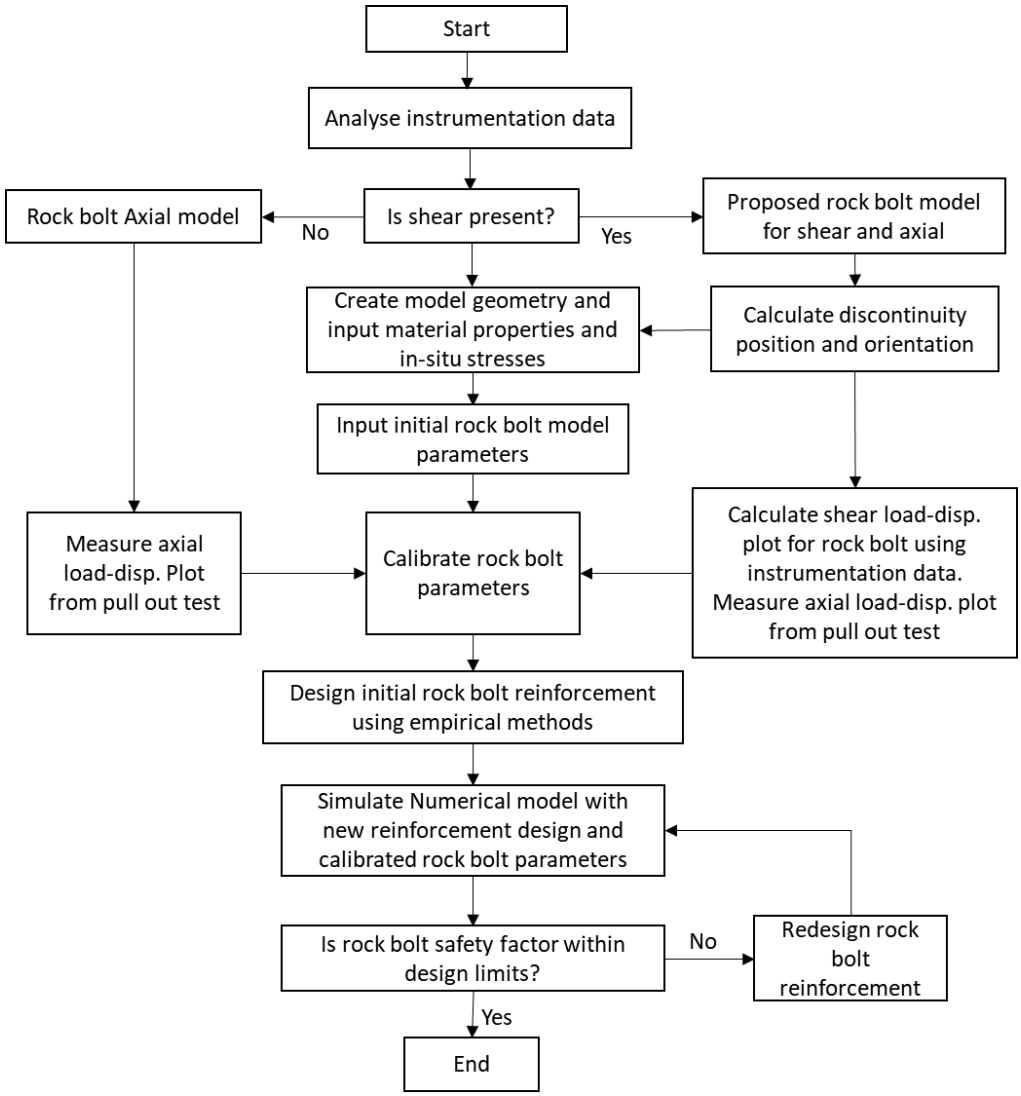

Figure 7.11 - Rock bolt reinforcement modelling procedure.

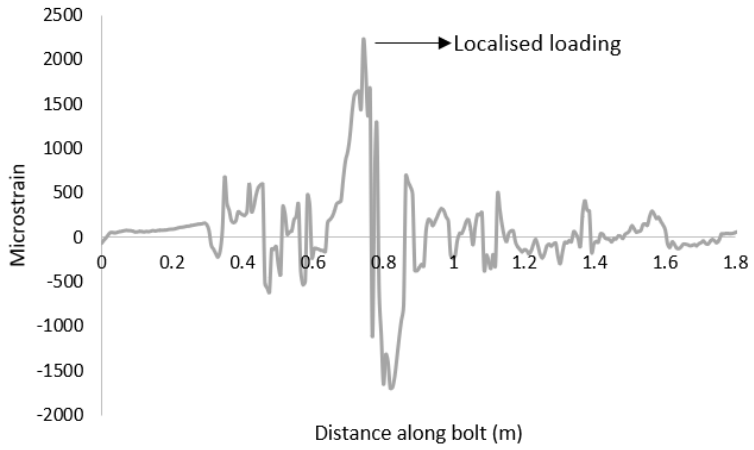

Figure 7.12 - Instrumented rock bolt strain plot with localised loading.

The orientation of the discontinuity α can be calculated from the axial strain, bending strain and hinge point length obtained from the instrumented rock bolt strain profile using the equation –

$$\alpha = \tan^{-1}\left[\frac{1}{\cos\theta}\left(\frac{\Delta_{ext}}{u_y} - \sin\theta\right)\right] \tag{7.3}$$

Where, θ is the bolt deflection, u_y is the bolt lateral displacement and Δ_{ext} is the axial extension of bolt calculated using the analytical model for lateral loading behaviour of rock bolt.

The model geometry with geological discontinuities can now be generated and the material properties and in-situ stress initialised. The instrumented rock bolts to be used for calibration are generated in the model. If lateral loading is identified, then the rock bolt model needs to be modified to simulate the correct shear response of rock bolt. If FLAC3D software is used for modelling then the normal spring properties of the pile element can be modified to get the correct shear response (Singh et al., 2020).

For calibrating the rock bolt response, the load-displacement plots for axial and shear loading are required. The axial load-displacement plot can be measured using a in-situ pull test. For calculating the shear load-displacement plot, the total lateral load and displacement are calculated at different loading stages from the instrumented rock bolt strain data using the analytical model. The rock bolt parameters are first initialised with recommended values in literature (Tulu et al., 2012; Zipf, 2006). The numerical model is executed, and the rock bolt's load-displacement response is compared with the measured load-displacement response of the instrumented rock bolt. The rock bolt parameters are adjusted to calibrate the response of rock bolt model with the instrumented rock bolt.

The calibrated model can then be used for optimizing new rock bolt reinforcement designs. The model is executed with an initial rock bolt reinforcement design calculated using empirical methods(Cording & Mahar, 1978; Grimstad, 1993; Obert & Duvall, 1967) . The axial load T

and shear load S on the rock bolt can be measured from the model. The reduced safety factor for failure due to combined loading can be calculated using the equation –

$$SF_r = \frac{1}{\sqrt{\left(\frac{T}{T_f}\right)^2 + 3\left(\frac{S}{T_f}\right)^2}} \tag{7.4}$$

Where, T_f is the ultimate tensile load of rock bolt. If the reduced safety factor is not within an acceptable range, then the reinforcement design is adjusted, and the procedure is repeated until a satisfactory safety factor is achieved.

7.3 Limitations and Future Work

- The effect of joint opening and block rotation needs to be included in the analytical model for lateral loading of rock bolt.
- The analytical model can be implemented in a numerical code to be verified with in-situ observations. The rock bolts can be over cored to further verify the predictions of the analytical model.
- Instrumented rock bolts in the in-situ test were installed as secondary supports. The rock bolts should be installed as primary support to capture the actual rock load demand.
- Further in-situ testing is required in mines with different geological conditions to test the calibration method for the rock bolt model.

References

Cording, E. J., & Mahar, J. W. (1978). Index properties and observations for design of chambers in rock. Engineering Geology, 12, 113-142.

Grimstad, E. (1993). Updating the Q-system for NMT. Paper presented at the Proceedings of the International Symposium on Sprayed Concrete-Modern use of wet mix sprayed concrete for underground support, Fagemes, Oslo, Norwegian Concrete Association, 1993.

Obert, L., & Duvall, W. I. (1967). Rock mechanics and the design of structures in rock (Vol. 650): Wiley New York.

Singh, P., Spearing, A. J. S., Jessu, K. V., & Caroline Pinazzi da Silva Ribeiro, P. (2020). Establishing the need to model the actual state of stress along rock bolts. International Journal of Mining Science and Technology, 30(3), 279-286.

Tulu, I., Esterhuizen, G., & Heasley, K. (2012). Calibration of FLAC3D to simulate the shear resistance of fully grouted rock bolts. Paper presented at the 46th US Rock Mechanics/Geomechanics Symposium.

Zipf, K. (2006). Numerical modeling procedures for practical coal mine design. Paper presented at the Golden Rocks 2006, The 41st US Symposium on Rock Mechanics (USRMS).

Appendix A

Declaration of Authorship

Declaration of Authorship

Paper – Establishing the need to model the actual state of stress along rock bolts. International Journal of Mining Science and Technology, 2020, 30(3), 279-286.

Author contribution by field of activity

	Conception and Design	**Acquisition of Data and Method**	**Data Conditioning and Manipulation**	**Analysis and Statistical Method**	**Interpretation and Discussion**	**Final Approval**	**Total % contribution**
Prasoon Singh	x	x	x	x	x	x	80%
A.J.S. (Sam) Spearing	x	x			x	x	10%
K.V. Jessu		x				x	5%
P. C. P. da Silva Ribeiro		x				x	5%

Prasoon Singh

Date:11/10/21

I endorse that this level of contribution by the candidate indicated above is appropriate.

Prof. A.J.S. (Sam) Spearing

Associate supervisor and Co-author

K.V. Jessu

Co-author

P. C. P. da Silva Ribeiro

Co-author

Paper – Analysis of the combined load behaviour of rock bolt installed across discontinuity and its modelling using FLAC3D. Geotechnical and Geological Engineering, 2020, 38, 5867-5883.

Author contribution by field of activity

	Conception and Design	**Acquisition of Data and Method**	**Data Conditioning and Manipulation**	**Analysis and Statistical Method**	**Interpretation and Discussion**	**Final Approval**	**Total % contribution**
Prasoon Singh	x	x	x	x	x	x	85%
A.J.S. (Sam) Spearing	x	x			x	x	10%
K.V. Jessu		x				x	5%

Prasoon Singh

Date:11/10/21

I endorse that this level of contribution by the candidate indicated above is appropriate.

Prof. A.J.S. (Sam) Spearing

Associate supervisor and Co-author

K.V. Jessu

Co-author

Paper – An Improved Analytical Model for the Elastic and Plastic Strain-hardening Shear Behaviour of Fully Grouted Rockbolts. Rock Mechanics and Rock Engineering, 2021, 1-17.

Author contribution by field of activity

	Conception and Design	**Acquisition of Data and Method**	**Data Conditioning and Manipulation**	**Analysis and Statistical Method**	**Interpretation and Discussion**	**Final Approval**	**Total % contribution**
Prasoon Singh	x	x	x	x	x	x	85%
A.J.S. (Sam) Spearing	x				x	x	15%

Prasoon Singh

Date:11/10/21

I endorse that this level of contribution by the candidate indicated above is appropriate.

Prof. A.J.S. (Sam) Spearing

Associate supervisor and Co-author

Paper – Improving the Numerical Modelling of In-Situ Rock Bolts Using Axial and Bending Strain Data from Instrumented Bolts. Geotechnical and Geological Engineering, 1-25.

Author contribution by field of activity

	Conception and Design	**Acquisition of Data and Method**	**Data Conditioning and Manipulation**	**Analysis and Statistical Method**	**Interpretation and Discussion**	**Final Approval**	**Total % contribution**
Prasoon Singh	x	x	x	x	x	x	80%
A.J.S. (Sam) Spearing	x	x			x	x	10%
Hyongdoo Jang	x				x	x	10%

Prasoon Singh

Date:11/10/21

I endorse that this level of contribution by the candidate indicated above is appropriate.

Hyongdoo Jang

Supervisor and Co-author

Prof. A.J.S. (Sam) Spearing

Associate supervisor and Co-author

Appendix B

Copyright Permissions

SPRINGER NATURE LICENSE
TERMS AND CONDITIONS

Apr 06, 2022

This Agreement between Mr. Prasoon Singh ("You") and Springer Nature ("Springer Nature") consists of your license details and the terms and conditions provided by Springer Nature and Copyright Clearance Center.

License Number	5219320000834
License date	Dec 31, 2021
Licensed Content Publisher	Springer Nature
Licensed Content Publication	Geotechnical and Geological Engineering
Licensed Content Title	Analysis of the Combined Load Behaviour of Rock Bolt Installed Across Discontinuity and Its Modelling Using FLAC3D
Licensed Content Author	Prasoon Singh et al
Licensed Content Date	Jun 7, 2020
Type of Use	Thesis/Dissertation
Requestor type	academic/university or research institute
Format	print and electronic
Portion	full article/chapter
Will you be translating?	no
Circulation/distribution	200 - 499
Author of this Springer Nature content	yes
Title	Integration of Instrumentation and Computer Modelling to Understand and therefore Better Design and Represent the Rock bolt Support Behavior
Institution name	Curtin University
Expected presentation date	Mar 2022
Order reference number	123
Requestor Location	Mr. Prasoon Singh

SPRINGER NATURE LICENSE
TERMS AND CONDITIONS

Apr 06, 2022

This Agreement between Mr. Prasoon Singh ("You") and Springer Nature ("Springer Nature") consists of your license details and the terms and conditions provided by Springer Nature and Copyright Clearance Center.

License Number	5282971148650
License date	Apr 06, 2022
Licensed Content Publisher	Springer Nature
Licensed Content Publication	Rock Mechanics and Rock Engineering
Licensed Content Title	An Improved Analytical Model for the Elastic and Plastic Strain-hardening Shear Behaviour of Fully Grouted Rockbolts
Licensed Content Author	Prasoon Singh et al
Licensed Content Date	Apr 27, 2021
Type of Use	Thesis/Dissertation
Requestor type	academic/university or research institute
Format	print and electronic
Portion	full article/chapter
Will you be translating?	no
Circulation/distribution	500 - 999
Author of this Springer Nature content	yes
Title	Integration of Instrumentation and Computer Modelling to Understand and therefore Better Design and Represent the Rock bolt Support Behavior
Institution name	Curtin University